

# 7th International Workshop on Concrete Spalling due to Fire Exposure



## Proceedings

**FIRE**  
**SPALLING** 2022  
7th International Workshop  
12-14 October, Berlin

Organized by:



Supported by:



## Preface and dedication

The fire-induced spalling behaviour of concretes has a huge effect on the fire resistance of concrete components. Therefore, fire performance must be taken into account in the design and dimensioning of concrete structures. The use of new types of concrete and different types of cement or binder must also be considered. Despite decades of research, the mechanisms underlying the spalling phenomenon are not yet fully understood. However, knowledge about these mechanisms is the prerequisite for predicting the spalling behaviour as accurately as possible.

Experimental research from material characterisation on the micro scale up to full-sized fire tests as well as the simulation and modelling of fire-induced damage processes offer the opportunity to investigate the spalling behaviour of concrete. Thereby, a variety of influencing parameters must be regarded. Against this background, the effect of avoidance strategies can be evaluated.

Since 2009, the International Workshop on Concrete Spalling due to Fire Exposure (IWCS) offers a platform to get in touch with researchers and practitioners, exchange the latest research results and newly acquired data from real fire scenarios, and discuss current developments in the field of concrete spalling. After the successful workshops in Leipzig (Germany), Delft (Netherlands), Paris (France), Borås (Sweden) and Sheffield (United Kingdom), the 7th International Workshop IWCS will now take place in Berlin at BAM. It will provide insights into the work of two RILEM Technical Committees. Based on this, various results of screening tests and large scale tests for the assessment of the fire-induced spalling behaviour of concretes will be presented, taking into account a large number of influencing parameters. Further topics of the workshop are the analysis of the mechanisms for the spalling phenomenon as well as the modelling and simulation of the spalling processes. A large part of the workshop will be devoted to the high-temperature behaviour of various types of concrete.

The workshop is dedicated to Prof. Diederichs, who passed away on 20 January 2022. With his death, the spalling community lost an internationally renowned expert in the field of fire behaviour of concrete and reinforced concrete components. He played a decisive role in the design of all previous RILEM TCs on the high temperature and fire behaviour of concretes and reinforced concrete components. The spectrum ranges from the first RILEM TC 044-PHT to TC's 129-MHT, 200 HTC, 227-HPB and TC 256 SPF, which ended in 2020.

Prof. Diederichs acquired his expertise in the field of fire protection primarily during his more than 20 years at the Technical University of Braunschweig from 1977 to 1998. He was also active in the field of high temperature behaviour of concrete during his subsequent position as Professor of Building Materials at the University of Rostock from 1998 to 2013. Despite his emigration in 2013, he continued to pass on his knowledge to students at the University of Applied Sciences Wismar and the TU Vienna until 2021. In addition, he worked as an advisor for the promotion of young scientists at the University of Technology Brno in the Czech Republic until 2021.

In his professional career, Prof. Diederichs has published around 85 articles on the high-temperature and fire behaviour of a wide variety of concretes and reinforced concrete components. The spectrum of content is very broad. For example, he investigated the bond behaviour of concrete and steel, the strength and deformation behaviour of different types of concrete, as well as the influence of the concrete composition and the moisture content on the spalling behaviour of the concretes due to fire exposure or at high temperatures. A further object of research was the development and investigation of strategies to avoid spalling of concrete using PP fibres as well as through a deliberate heat treatment of existing concrete structures.

In addition to his professional expertise, we will also greatly miss Prof. Diederichs' very outgoing and open-minded nature.

Finally, we warmly welcome all participants of the 7th workshop and wish them an exciting time with many new insights and contacts.

Dr.-Ing. Frank Weise  
(BAM)

Dr.-Ing. Ludwig Stelzner  
(BAM)

Prof. Frank Dehn  
(KIT)

## Scientific Committees

- Australia:
  - Dr. Vinh Dao
  - Dr. Cristian Maluk
- China:
  - Prof. Yiming Zhang
- France:
  - Prof. H el ene Carr e
  - Prof. Stefano Dal Pont
  - Dr. Dorjan Dauti
  - Dr. Maxime Lion
  - Prof. Fekri Meftah
  - Dr. Alain Millard
  - Dr. Jean-Christoph Mindeguia
  - Dr. Duc Toan Pham
  - Dr. Pierre Pimienta (chairman of RILEM TC CFR)
  - Dr. Fabienne Robert
- Germany:
  - Prof. Steffen Anders
  - Dr. Josipa Bosnjak
  - Prof. Frank Dehn
  - Andr e Klimek
  - Hitesh Lakhani
  - Prof. Klaus Pistol
  - Dr. Ludwig Stelzner
  - Dr. Frank Weise
  - Dr. Matthias Zeiml
- Greece:
  - Prof. Kosmas Sideris
- India:
  - Prof. Umesh Kumar Sharma
- Italy:
  - Prof. Roberto Felicetti
  - Dr. Francesco Pesavento
- Japan:
  - Prof. Mitsuo Ozawa
- Poland:
  - Prof. Izabela Hager
  - Dr. Katarzyna Mr oz
- Portugal:
  - Prof. Jo o Paulo Correia Rodrigues
- Sweden:
  - Dr. Robert McNamee (vice chairman of RILEM TC CFR)
- Switzerland:
  - Dr. Fariza Sultangaliyeva
  - Dr. Benedikt Weber
- United Kingdom:
  - Prof. Luke Bisby
  - Dr. Shan-Shan Huang
  - Dr. Asif Hussain Shah
  - Dr. Giacomo Torelli



# Contents

Development of a new method based on intentional heat treatment (IHT) for fire resistance enhancement of existing concrete structures.....	7
<i>Iveta Nováková, Ulrich Diederichs, Lenka Bodnárová</i>	
Concrete spalling due to fire exposure – overview of its consideration in pre-normative guidelines, existing standards and future codes.....	8
<i>Frank Dehn, Moritz Boxheimer</i>	
Development of the spalling section in the new Eurocode prEN 1992-1-2.....	9
<i>Fabienne Robert, Robert McNamee, Walter Borgogno, Sergio Carrascon, Franz Ehrlich, Jochen Reiners</i>	
Screening-tests on the susceptibility to spalling of two ordinary concretes .....	15
<i>André Klimek, Ludwig Stelzner, Sascha Hothan, Jochen Zehfuß</i>	
Spalling Screening Tests Under Different Loading Conditions.....	25
<i>Katarzyna Mróz, Izabela Hager</i>	
Spalling screening tests for tunnel linings and the impact of the main influence parameters .....	36
<i>Siyimane Mohaine, Bérénice Moreau, Laetitia D'Aloia, Sébastien Bouteille, François Cussigh, Philippe Gotteland, Fabienne Robert</i>	
Experimental investigation on the effect of water content profile on fire spalling.....	48
<i>Bruno Fernandes, Hélène Carré, Jean-Christophe Mindeguia, Céline Perlot, Christian La Borderie</i>	
Comparative study of concrete spalling of Large-scale test with a Mobile furnace test .....	58
<i>Kamakshi Parwani, Jos Bienefeld, Tomas Rakovec</i>	
Port said Suez Canal tunnel segments – Laboratory fire spalling testing.....	68
<i>Pierre Pimienta, Roberto Felicetti, Dimitrios Rizos, Philippe Rivillon, Stéphane Charuel, Tarek Amin</i>	
Scale effect on spalling of high performance self-compacting fiber reinforced concrete .....	79
<i>Fariza Sultangaliyeva, Hélène Carré, Christian La Borderie, Fabienne Robert, Siyimane Mohaine, Pierre Pimienta</i>	
Spalling behaviour of ultra-high performance concrete columns exposed to natural fires .....	88
<i>Jan Lyzwa, Jochen Zehfuß</i>	
A critical review of the moisture clog theory.....	97
<i>Benedikt Weber</i>	
The role of moisture on crack instability of spalling concrete .....	108
<i>Ramin Yarmohammadian, Roberto Felicetti, Fabienne Robert, Laurent Izoret</i>	
Dehydration model of cement paste for predicting the material properties at elevated temperatures.....	120
<i>Simon Peters, Günther Meschke</i>	

Underlying Factors Controlling Experimental Test Outputs for Concrete Samples Subjected to Elevated Temperatures.....	130
<i>Abbas M. Abubaker, Colin T. Davie</i>	
Systematic mapping studies on the impact of spalling on punching shear strength of RC slabs exposed to fire .....	141
<i>Andreia Romero Fanton, Luiz Carlos de Almeida, Leandro Mouta Trautwein</i>	
Numerical studies on the effect of spalling on the concrete cone capacity of single headed stud during fire.....	153
<i>Hitesh Lakhani, Jan Hofmann</i>	
The influence of the physical and chemical properties of hardened cement paste on the fire-induced spalling of concrete .....	164
<i>Jochen Reiners, Christoph Müller, Jochen Zehfuß, Frank Dehn</i>	
An Experimental Study into the Behaviour of Self-Prestressing, Self-Compacting Concrete at Elevated Temperatures.....	179
<i>Hussein Mohammed, Fariza Sultangaliyeva, Mateusz Wyrzykowski, Giovanni Pietro Terrasi, Luke Bisby</i>	
Investigation of the Thermo-Hydral Behaviour of Concrete with Recycled Fibres via Neutron and X-Ray Tomographies.....	193
<i>Yifan Li, Stefano Dal Pont, Alessandro Tengattini, Shan-Shan Huang</i>	
Performance of metakaolin-based alkali activated concrete at elevated temperatures .....	205
<i>Jitong Zhao, Alena Bartsch, Marco Liebscher, Thomas Köberle, Viktor Mechtcherine</i>	
Concrete drying kinetics: development of an accelerated drying protocol for fire testing .....	215
<i>T. Sayari, T. Honorio, S. Mohaine, F. Robert, J.-L. Adia, M. Lion, P. Gotteland, C. Clergue, L. d'Aloia, F. Benboudjema</i>	
Investigation of the fire behaviour of small-format ceiling-type building components .....	226
<i>Peter Harsányi, Martin Schneider, Lukas Treffner</i>	
Influence of elevated temperature and different cooling regimes on mechanical and transport properties on High Strength Self-Compacting concrete .....	236
<i>Pavan Kumar, Umesh Kumar Sharma, A. B. Danie Roy</i>	
Performance of limestone calcined clay cement (LC <sup>3</sup> ) at high temperatures.....	248
<i>Akshay Sharma, Danie Roy A.B., Prem Pal Bansal</i>	

# Development of a new method based on intentional heat treatment (IHT) for fire resistance enhancement of existing concrete structures

Iveta Nováková<sup>1</sup>, Ulrich Diederichs<sup>†</sup>, Lenka Bodnárová<sup>2</sup>

<sup>1</sup>The Arctic University of Norway, Narvik, Norway; iveta.novakova@uit.no

<sup>2</sup>Brno University of Technology, Brno, Czech Republic

**Keywords:** Fire resistance of concrete, Initial heat treatment (IHT) method, porous structure modification, modified ISO834

**Topic:** Protective Measures

Fire resistance is becoming increasingly important along with the development of new concrete types with high strength and dense structure with reduced porosity. Such concrete types are susceptible to fire spalling and extensive crack formation. At the moment, there are a limited number of methods for enhancing of fire resistance of existing structures, which could be applied on underground structures with restricted space and limited air exchange, such as tunnels, underground garages or nuclear power plants.

This work is focused on the development of a new method based on porous structure modification due to the intentional heat treatment (IHT), therefore IHT method. Used analyses investigated the change in pore structure, chemical and mineralogical properties and mechanical properties of various cementitious binders. Furthermore, the theory of “moisture clog,” which contributes to explosive spalling and extensive cracking was verified. The efficiency of the developed method was verified by large-scale testing of one side heated uniaxially loaded samples according to the modified ISO834 (m-ISO) curve.

No extensive crack formation or explosive spalling was observed during the exposure period during the large-scale testing of slabs with the applied IHT method. The total thickness of the IHT method with configuration IHT200/2, composed of IHT zone and IHT transition zone, penetrated to the depth of 25.5 to 43.0 mm depending on the concrete type. Moisture clog in was more significant on samples without IHT than in the case of slabs with applied IHT method, and it could be concluded that the IHT method enhances fire resistance of concrete exposed to elevated temperatures without influencing its compressive strength. Further development is required in the area of the durability of concrete structures treated by IHT method.

# Concrete spalling due to fire exposure – overview of its consideration in pre-normative guidelines, existing standards and future codes

Frank Dehn<sup>1,\*</sup> & Moritz Boxheimer<sup>1</sup>

<sup>1</sup> Karlsruhe Institute of Technology (KIT) Karlsruhe, Germany

\* Corresponding author (frank.dehn@kit.edu)

**Keywords:** Concrete spalling, guidelines, codes, normative obstacles, innovation

**Topic:** Pre-normative research and standardization

The spalling behavior of concrete - because of high thermal impacts - has been the subject of intensive research efforts over the last years. In addition to experimental investigations into the phenomenological description of concrete spalling due to fire exposure, the provision of scientifically based knowledge about the material and constructive influencing factors, as well as those from the relevant test boundary conditions, multi-scale prognosis and simulation models based on corresponding constitutive material laws are increasingly being used. What all efforts have in common is that, in the best-case scenario, strategies can be derived to help to reduce or even completely avoid spalling of concrete in the event of a fire.

Unfortunately, the reliable knowledge gained in recent years is only reflected to an insufficient extent in guidelines and codes. The consequence of this is that concrete structures on one hand are sometimes insufficiently dimensioned for the exceptional case of "fire" or on the other hand are taken with "measures" that are too much on the safe side, which lead to uneconomical results as well as technically questionable ones. It is therefore fundamentally important in terms of updating concrete construction to put findings into practice as quickly as possible and to take them into account when setting code-type regulations.

This article is intended to provide an overview of the current regulatory status with regard to concrete spalling as a result of exposure to fire, but at the same time should be understood as a plea to make innovation usable more quickly for those involved in concrete construction.

# Development of the spalling section in the new Eurocode prEN 1992-1-2

Fabienne Robert<sup>1,8</sup>, Robert McNamee<sup>2,3,8</sup>, Walter Borgogno<sup>4,8</sup>,  
Sergio Carrascon<sup>5,8</sup>, Franz Ehrlich<sup>6,8</sup> & Jochen Reiners<sup>7,8</sup>

<sup>1</sup> CERIB Fire Testing Centre, Epernon, France, f.robert@cerib.com

<sup>2</sup> RISE research Institutes of Sweden, Lund, Sweden, robert.mcnamee@ri.se

<sup>3</sup> Division of Fire Safety Engineering, Lund University, Lund, Sweden

<sup>4</sup> Borgogno Eggenberger + Partner AG, St. Gallen, Switzerland

<sup>5</sup> IECA, Barcelona, Spain

<sup>6</sup> Baumeister und Zivilingenieur für Bauwesen, Wien, Austria

<sup>7</sup> VDZ Technology gGmbH, Düsseldorf, Germany

<sup>8</sup> members of the sub-task group “spalling” from the CEN TC 250/SC2/WG1/TG05  
(WG105)

## ABSTRACT

Feedback from national mirror committees during the systematic review of EN 1992-1-2 1 launched in 2014 highlighted the need to improve the design rules for spalling. Extensive discussions have taken place within the standard committee CEN TC 250/SC2/WG1/TG5 (WG105) and especially within the sub-task group in order to establish new rules consistent with the state of the art. The present article describes the main changes and gives an insight into the reasons for changes.

**KEYWORD:** Concrete spalling, design rules, moisture content

## INTRODUCTION

The revision of the Eurocode EN 1992-1-2 published in 2004 is in its final phase. Detailed technical and editorial comments on the draft for enquiry 2 were collected from the member states during autumn 2021 and a final version has been prepared by the members of CEN TC 250/SC2/WG1/TG5. This final version will be sent out to CEN Formal vote in 2023. In the Formal vote, the standard as a whole can be accepted or rejected.

The new draft includes a new chapter 10 dedicated to “rules for spalling”. Indeed, feedback from national mirror committees during the systematic review of EN 1992-1-2 launched in 2014 highlighted the need to improve the design rules for spalling requirements (see clauses 4.5.1 and 6.2 of 1). During the spalling workshop in Borås (2017) several open questions regarding the chapter on spalling in the Eurocode were discussed 3. Some of these questions were “Is there too much focus on moisture content as a risk factor for spalling?”, “How representative are experimental results?”. In May 2018, the dedicated sub-task group of CEN TC 250/SC2/WG1/TG5, in charge of the new chapter 10, launched a call for contribution among all the Member States 4 in order to take into account fire resistance tests or research results which were not publicly available and which could contribute to design rules for the potential modifications identified by the sub-task group listed below.

1. Moisture content: deletion of moisture content as a criterion to assess whether spalling is unlikely to occur, because generally, the moisture content and the moisture distribution of concrete members cannot be predicted at the design stage;
2. Thermal exposure: provisions will be valid for the standard temperature/time curve or any curve with equivalent or lower temperature-time gradient; experimental evidence should be provided for hydrocarbon curve;
3. Concrete Strength: the maximum concrete strength for which no verification (or no provision) is needed may be reduced from C80 to a concrete with lower strength (for example C70);
4. Risk analysis for certain structural members based on their concrete strength, slenderness, load ratio, section geometry (thin web for example) may be introduced for spalling design;
5. Self compacting concrete: specific requirements may be introduced for SCC;
6. Minimum provisions: some minimum provisions (i.e. minimum PP fibres content) may be introduced as an alternative to a specific spalling assessment.

Finally, after an extensive review of all available research results and the different feedback from mirror committees during the different stages of the elaboration of the new standard, some new rules have been established whose justification has been reported in the background document of the new standard 5.

The new rules mainly focus on the following items:

1. Justification for the new threshold C60 ( $f_{ck} < 70$  MPa) instead of C80 for spalling verification which may be omitted;
2. Deletion of the moisture content criteria;
3. Assessment of lightweight aggregate concrete;
4. Requirements for isolated members exposed on three sides;
5. Guidance on test methodology to determine the performance of concrete with respect to spalling;
6. Deletion of Method A (mesh) for severe spalling.

These new rules related to the spalling section of the Eurocode are here discussed based on the latest draft and background document 5 by the members of the sub-task group “spalling” from the CEN TC 250/SC2/WG1/TG5 (WG105).

## **VALIDITY OF THE NEW SPALLING SECTION 10**

A change in the new draft is that the term “explosive” in “explosive spalling” is not used anymore as there is no clear definition of what it is. It may also be a misleading terminology as continuous progressive spalling of small pieces starting early during the fire exposure have the potential to be as severe for the load bearing capacity as a loss of large parts of the concrete cover in one event later in the exposure (the loss of larger pieces is often associated with explosive spalling). A definition has been included related to spalling in 2 “fire induced spalling of concrete consists of the breaking off of layers or fragments of concrete from the surface of a structural element. Depending on the severity of the phenomenon, it may or may not influence the performance of the structural member.”

The new section 10 on fire spalling is only valid for thermal exposures equivalent or lower than the standard time temperature curve. For more severe exposures like the hydrocarbon curve or fire exposures used for tunnel design, experimental evidence should be provided.

Experience from fire testing shows a significant difference between standard fire exposure and the more severe exposure used in tunnel fire projects 6.

Moreover, the strength limit for when a spalling assessment is needed has been lowered to  $f_{ck} \geq 70$  MPa (concrete grades  $> C60$ ). Indeed, many tests have been performed on concrete structural elements these last decades however test reports on fire resistance tests on structural elements with detailed concrete mix and characteristic strength are not so well documented or publicly available.

A literature study performed within CEN TC 250/SC2/WG1/TG5 and the call for contributions published in May, 2018 4, gave the following results:

- references 7, 8, 9, 10 show that concretes C60 7, C45 and C65 8, C40 9, C 60 10 exhibit good performances related to spalling.
- on the other hand, concrete without pp fibres C85 and C105 8, C90 9, C90 10, C70 11, C70 and C90 12 exhibit some spalling.

Based on this evaluation, the threshold of concrete strength for which no experimental evidence or addition of polypropylene is asked has been changed from C80 to C60 and consequently the threshold of concrete strength for which experimental evidence or addition of polypropylene is required has been changed from  $> C80$  to  $> C60$ .

## MOISTURE CONTENT CRITERIA

In the present version of the Eurocode 1, a moisture limit was set under with spalling is “unlikely to occur”. During the development of the standard, it was not possible to agree on the value for this parameter so the decision was to make the limit a national choice (with the consequence that it varies between 2-4% for different countries). In the new draft the spalling limit and the national choice is deleted but a general recommendation regarding cases when a high moisture content is expected is given.

There are several reasons for deleting the threshold 5:

- It is controversial below which moisture content spalling is “unlikely to occur”. Since a European agreement for the value of  $k$  could not be reached, the decision was left to national annexes (in the present version of EN 1992-1-2, varies from 2% to 4%)
- Scientific results indicate that spalling may appear from different moisture content values depending on the concrete composition, strength, section geometry, load... At first glance, a general fixed moisture limit for spalling seems like a good idea but this is not supported by the literature as so many inter-dependent factors are involved in the phenomenon.
- Even if the temperature, relative humidity (climate history) and age of concrete are known, it is a very difficult task to specify the moisture content of the concrete.
- While moisture gradients do appear instead of uniform moisture contents, nothing is said about where (at the surface, in depth...) and when (3 months after casting, at equilibrium?) the moisture content should be measured or estimated.
- The designer has difficulties to predict what will be the moisture content in the built element, and cannot influence it.

A more detailed background discussion on the topic is given in the chapter “The moisture level in concrete during fires and fire testing” by Jansson 13.

## LIGHTWEIGHT AGGREGATE CONCRETE

Provisions regarding spalling of lightweight concrete are not clear in EN 1992-1-2:2004 1 and can lead to misunderstanding. Some authors reported contradictory results on the performance of LWC regarding spalling [14][15].

According to the reference [15] the main reason for the poorer fire resistance of LWC compared to normal concrete is more severe spalling due to:

- higher moisture content of lightweight aggregates acting like water reservoirs;
- lower permeability (which may result in a higher vapor pressure);
- lower thermal conductivity (which leads to a steeper temperature gradient);
- lower tensile strength due to the greater porosity of LWC (at similar water/binder ratios).

When using lightweight aggregate concrete, a specific assessment of spalling should be undertaken in the new rules.

## REQUIREMENTS FOR ISOLATED MEMBERS EXPOSED ON THREE SIDES

I-beams have shown a specific behaviour (see references [17] and [18]). For thin webs with only one reinforcement layer in horizontal and one in vertical direction, the risk of collapse in case of spalling of the cover concrete is high as the compression resistance of concrete is lost at the very moment of severe spalling. For webs with two layers in horizontal and vertical direction, the risk of collapse in case of spalling of the cover concrete is smaller. Therefore, the definition of minimum web dimensions (to allow for more than one vertical layer of reinforcement) is a means of providing a more robust design.

For members with thin cross sections a spalling assessment according to Table 1 will be required

*Table 1. Minimum web thickness of isolated members below which specific assessment of spalling should be undertaken or polypropylene fibres should be specified [2].*

Standard fire resistance	Minimum web thickness $b_{w,min}$ (mm)	Minimum web thickness $b_{w,min}$ for a distance of 2h from an intermediate support in continuous isolated members
R30	80	80
R $\geq$ 60	100	120

## GUIDANCE ON TEST METHODOLOGY TO DETERMINE THE PERFORMANCE OF CONCRETE WITH RESPECT TO SPALLING

In the present version of the Eurocode [1] no guidance is provided on how to do an assessment based on experimental evidence.

At the time of the revision of EN 1992-1-2 [1], no standard has yet been published to characterize the spalling propensity of concrete structures. However, RILEM Technical Committee 256-SPF "Spalling of concrete due to fire: testing and modelling" has been working on the subject since 2013 and intends to publish some recommendations in the near future. The state of the art performed in the framework of this TC 256-SPF clearly highlights the importance of the geometry (in terms of impact on the self-stress), the loading and the moisture content of the tested specimen.



Full scale tests are not always necessary if intermediate scale tests can be proven to be sufficiently representative in terms of stress state and spalling results. It should be highlighted that intermediate scale tests differ from the material screening tests which are also defined in some recommendations established by the RILEM TC 256-SPF. The material screening tests are only intended to rank concretes by sensitivity to spalling. They do not aim to provide an absolute value of the spalling behaviour.

Preliminary recommendations are given in the background document [5] based on scientific articles ([19] to [26]) and the spalling assessment has been clarified in [2] by adding the following paragraph *“When assessment based on experimental evidence is required, it should be obtained from tests representative of the conditions of the structural member in terms of geometry, stress and moisture content.”*

### **DELETION OF METHOD A (MESH) IN [1] FOR SEVERE SPALLING**

One of the methods listed for spalling mitigation of concrete grades  $80/95 < C \leq 90/105$  is the addition of a complementary reinforcement mesh [3]. This method is deleted from the new draft as it is not proven to be a reliable method [27].

### **CONCLUSION**

Specific rules for avoiding / controlling spalling have been added in the prEN1992-1-2 [2] taking into account the last research findings and allowing a safer design. The main implications in engineering practice and the building industry are the following:

- enhancement of ease of use with clarification of rules, especially regarding the deletion of moisture content parameter which was not sufficiently defined in the current standard;
- guidance on the parameters to be studied when experimental assessment is required;
- need for specific assessment for concrete grades above C60 (>C60) and possibility at the national level to choose a minimal polypropylene fibres content lower than 2,0 kg/m<sup>3</sup> to avoid an experimental assessment.

### **REFERENCES**

1. Eurocode 2, 1992-1-2: Design of concrete structures—Part 1–2: General rules—Structural fire design, 2004
2. DRAFT prEN 1992-1-2:September 2021 - Eurocode 2: Design of concrete structures - Part 1-2:General rules - Structural fire design
3. Robert F. et al. “Eurocode 1992-1-2: Do we need to change the requirements on spalling?” 5th International Workshop on Concrete Spalling due to Fire Exposure, 12-13 October 2017, Borås, Sweden
4. CALL FOR CONTRIBUTIONS EN 1992-1-2 - Revision of the rules on explosive spalling, CEN/TC 250/SC 2/WG 1/TG 5 N 140, 16<sup>th</sup> May 2018
5. EN 1992-1-2: 2023: Background Document (Not published yet)
6. Robert F., Moreau B. and Bisby L., “Fire spalling of concrete: experimental parametric study and numerical modelling”, 4th International Workshop on Concrete Spalling due to Fire Exposure, 8/9 October 2015, Leipzig
7. Franssen J-M. and Dotreppe J-C. “Fire tests and calculation for circular concrete columns”, Fire Technology, 39, 89-97, 2003

8. Clayton N. and Lennon T., "Effect of polypropylene fibres on performance in fire of high grade concrete" BRE Report, BR 395, 2000
9. Raut N. K. and Kodur V. K. R "Response of High-Strength Concrete Columns under Design Fire Exposure", JOURNAL OF STRUCTURAL ENGINEERING © ASCE / JANUARY 2011
10. Experimental Studies for Evaluating the Fire Endurance of High-Strength Concrete Columns, Kodur, V. R.; Mcgrath, R. C.; Leroux, P.; Latour, J. C., Research Report No. 197, May 2005
11. Fire Test – loaded column C 75 – S2 (Braunschweig, test date 18/02/2011) and Fire Test – loaded column C 75 – S4 (Braunschweig, test date 09/06/2011)
12. BRITE EURAM III, BE-1158/BRPR-CT95-0065, Task 3.-3.1&3.2-High temperature testing, Tests in ISO and HC fire, TASK 3 Final Report
13. Jansson R. "Fire Spalling of Concrete – Theoretical and Experimental Studies" PhD Thesis, KTH Royal Institute of Technology, Stockholm, Sweden, 2013
14. Andiç-Çakir Ö. and Hizal S., "Influence of elevated temperatures on the mechanical properties and microstructure of self-consolidating lightweight aggregate concrete," Construction and Building Materials, vol. 34, pp. 575–583, 2012.
15. Lindgard J. and Hammer A T. "Fire Resistance of Structural Lightweight Aggregate Concrete a Literature Survey with Focus on Spalling". Nordic Conc Res Pub 1998;21(1):64-77.
16. Copier W. J., "The spalling of normal weight and lightweight concrete on exposure to fire," Heron, vol. 24, no. 2, 1979.
17. Jansson R. and Boström L. "Fire tests of loaded beams", 2nd international Rilem workshop "concrete spalling due to fire exposure" 5-7 October 2011, Delft, The Netherlands
18. "Two case studies on the influence of explosive spalling in real structures, Fire in a warehouse on April 6, 2018 near Milan", Roberto Felicetti
19. Mohaine S., Robert F., Boström L., Lion M., and McNamee R., "Cross-comparison of screening tests for concrete spalling", Interflam Conference, 1-3 July 2019, Windsor, UK
20. Jansson R. and Boström L., "Factors influencing fire spalling of self compacting concrete," Materials and Structures, vol. 46, pp. 1683-1694, 2013
21. Lo Monte F., Felicetti R., Alberto M. and Bortolussi A., "Assessment of concrete sensitivity to fire spalling: A multi-scale experimental approach," Construction and Building Materials, vol. 212, pp. 476-485, 2019
22. Carré H., Pimienta P., La Borderie C., Pereira F. and Mindeguia J.-C., "Effect of compressive loading on the risk of spalling," MATEC Web of Conferences, vol. 6, 2013.
23. Lo Monte F. and Felicetti R., "Heated slabs under biaxial compressive loading: a test setup for the assessment of concrete sensitivity to spalling," Materials and Structures, vol. 50, no. 192, 2017.
24. Robert F., Labetoulle C., Tessier C. and Collignon C., "Thermo-mechanical modelling to define a screening test for building application under the standard temperature time curve," in 5-<sup>th</sup> International Workshop of Concrete Spalling due to Fire exposure, Boras, 2017.
25. Boström L., McNamee R, Albrektsson J. and Johansson P., "Screening test methods for determination of fire spalling of concrete," RISE Report 2018:05, 2018
26. Boström L., Wickström U. and Adl-Zarrabi B., "Effect of specimen size and spalling conditions on spalling of concrete," Fire and Materials, vol. 31, pp. 173-186, 2007.
27. Schneider U. "Fire resistance of high performance concrete" International RILEM Workshop on Durability of High Performance Concrete, 1994

# Screening-tests on the susceptibility to spalling of two ordinary concretes

André Klimek<sup>1</sup>, Ludwig Stelzner<sup>1,\*</sup>, Sascha Hothan<sup>1</sup> & Jochen Zehfuß<sup>2</sup>

<sup>1</sup>Bundesanstalt für Materialforschung und -prüfung, Berlin, Germany

<sup>2</sup>Technische Universität Braunschweig, Braunschweig, Germany

\*Corresponding author (ludwig.stelzner@bam.de, Unter den Eichen 87, 12205 Berlin, Germany)

## ABSTRACT

Investigating the spalling behaviour of a concrete mixture using large scale members is complex and expensive. Thus, the susceptibility of concrete to spalling is investigated by means of fire tests on small scale specimens. However, the reduction of the fire exposed surface increases the influence of boundary effects. Macrocracking and the water loss via the lateral surfaces reduce the impact of the thermomechanical and thermohydraulic damage mechanisms and therefore, lower the risk of spalling. Thus, the influence of different restrains on the spalling behaviour of intermediate scaled specimens ( $\varnothing 0.47$  m;  $h=0.29$  m) was investigated for two ordinary concrete mixtures. Both mixtures had the same composition except the type of aggregate. One mixture contained only quartzitic aggregates, whereas the other mixture was made with basalt grit as coarse aggregates. Applied steel rings restrained the thermal expansion of the specimen and prevented the loss of water, whereas applied steel sheet primarily reduced the loss of water during the fire test. Additionally, the fire exposed surface of one specimen of each mixture was pre-dried under controlled climate conditions and fire tested with applied steel rings. The results show a higher spalling volume for the ring restrained specimens compared to the other covering types. Further, the pre-dried boundary zone leads to delayed and decreased occurrence of spalling compared to the non-dried specimens for the concrete with quartzitic aggregates and to a prevention of spalling for the mixture with basalt aggregates. Additionally, the results show that the influence of the thermomechanical behaviour of the coarse aggregates increases with increasing restraint are comparable to the conditions in the centre of a large scale member. This test series is a further step for possible concept of steel ring restraint concrete specimens as "screening-tests" in upcoming projects.

**KEYWORD:** Spalling, fire test, ordinary concrete, restraint, steel ring

## INTRODUCTION

Investigating the spalling behaviour of a concrete mixture using large scale members is complex and expensive. Thus, the susceptibility of concrete to spalling was investigated by means of fire tests on small scale specimens. Previous research at Bundesanstalt für Materialforschung und -prüfung (BAM) compared the spalling behaviour for unrestrained large scale members (1.8 m x 1.2 m x 0.3 m), intermediate scale specimens (0.6 m x 0.6 m x 0.3 m) and small scale specimens ( $\varnothing 0.15$  m;  $h=0.3$  m) [1]. The results showed that spalling depends on the size of the fire exposed surface. The intermediate scale specimens spalled less in comparison to the large scale members. For the small scale specimens, no spalling was observed. Thus, the reduction of the specimen size to investigate the spalling behaviour is limited. A decreasing of the fire exposed surface results in an increasing influence of boundary effects. For example, macro cracks occur the fire

exposed surface and at side of the specimen. The increase of connected pores leads to an enhanced moisture transport [2] and water loss at the surface of the specimen. The decreasing water volume inside the concrete results in a reduction of the pore pressure and therefore, reduced tensile stresses [3]. Additionally, the accumulation of the thermal induced stresses depends on the size of the fire exposed surface, too. A smaller specimen leads to reduced thermomechanical induced compression stresses and reduced transverse tensile stresses in the centre of the surface. This lowers the risk of spalling compared to large scale members [4]. To counteract this effect, an experimental setup with passive constraint based on [5] was developed. This contribution shows the spalling behaviour of intermediate scale specimens with different types of restraint for two similar concrete mixtures.

## MATERIALS

### Specimens and methodology

Figure 1 shows an overview of the fire test setup. For each fire test, one specimen was placed vertically in front of the opening on one side of the furnace while closing walls were placed at the remaining openings during the fire test. By means of two controllable oil burners, one vertical and one horizontal, the standard temperature time curve (ISO 834) is applied during the fire test. Thereby, the furnace temperature is determined by the mean value of the two thermocouples that are placed at a distance 10 cm from the inner edge of the furnace openings. To ensure comparable sizes of the fire exposed surface for all specimens, an insulation with a circular opening is used. Thus, the steel rings and steel sheet are shaded off the direct impingement of the flames.

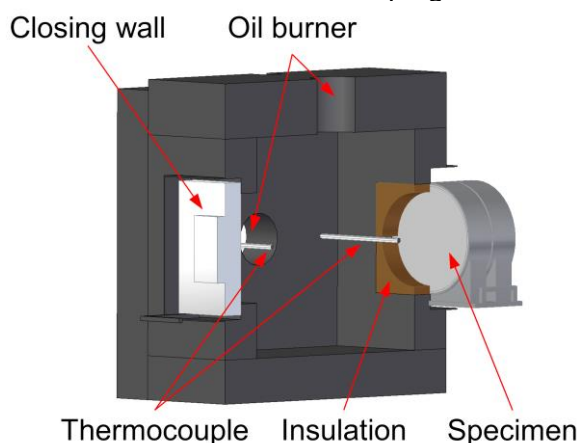


Figure 1 Cutaway model of the test setup

The spalling behaviour of two similar ordinary concrete mixtures was investigated in these test series. Table 1 shows an overview of the compositions. The only difference between both mixtures is the type of coarse aggregates. Ordinary concrete Q (OCQ) includes quartzitic gravel and ordinary concrete B (OCB) is made with basalt grit. For each mixture, four different specimens with different restrains and varying curing conditions were tested. This results in a number of 8 specimens in total. The basis for all tests is an unreinforced specimen with the dimensions of  $\varnothing 0.47$  m;  $h=0.29$  m. Figure 2 shows the setup for the specimen with different coatings. Two steel rings [5] with a gap of 1 cm were applied to restrain the thermal expansion of the concrete as well as the water loss at the shell surface. Therefore, boundary effects are minimised and the test conditions in the centre of a large scale member are replicated. Additionally, one specimen for each mixture was covered by a continuous steel sheet to limit the water loss at the shell surface with neglectable mechanical restraint. Thus, potential spalling of this specimen type is mainly caused by thermohydraulic stresses. All three prior described specimen types remained in the formwork for one day after casting.

Table 1 Overview of the two concrete mixtures

Type of material	Ordinary Concrete Q (OCQ)	Ordinary Concrete B (OCB)
Amount of components [kg/m <sup>3</sup> ]		
Cement (CEM I 42.R)	270	270
Water	175	175
Fly ash	80	80
Superplasticizer	2.7	2.7
Aggregates		
Sand (quartzitic)		
0 / 2 mm	536	536
Coarse aggregates		
2 / 4 mm	Quartzitic gravel	Basalt grit
4 / 8 mm	285	513
8 / 16 mm	339	158
8 / 16 mm	624	711
28 d cube compressive strength [MPa]	50	56
Fire curve	ISO 834	

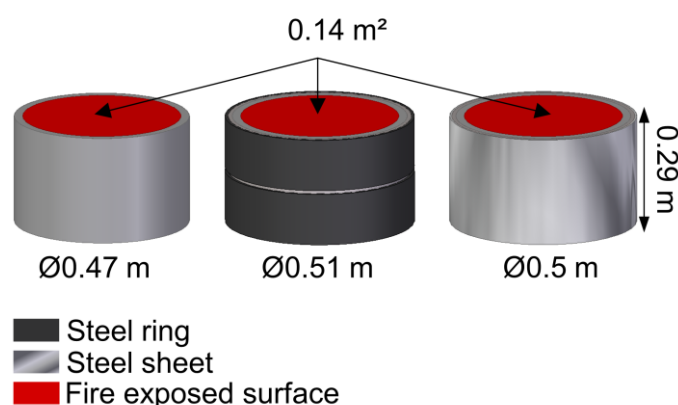


Figure 2 Sketches of the concrete specimens with an unrestrained surface, steel rings and steel sheet restrain

Afterwards, the specimens were sealed in plastic foil and cured wet until two weeks before the fire test. In contrast to the other specimens, the fourth specimen type was unwrapped from the foil after one week of wet curing. Then, the shell surface was sealed, and the specimen cured in a climate chamber with 23 °C and 50 % relative humidity [6] until two weeks before the fire test. Within the two weeks, the steel rings and the steel sheet were applied with expanding mortar and the specimens were stored unsealed at laboratory climate. All specimens cured for at least 98 days before the fire test.

The moisture content of the fire exposed surface is an important factor to interpret the spalling behaviour of a specimen. Therefore, a benchtop Nuclear magnetic resonance (NMR) measuring device examined the relative humidity of all specimens during the curing in the climate chamber and within the last two weeks before the fire test. For this purpose, the device with a measuring area of 4 cm x 4 cm and a maximum measuring depth of 2.5 cm is placed on top of the fire exposed surface. The NMR device uses magnetic fields to affect the spin of the hydrogen within the water inside the concrete to determine the moisture content (see [7] for more detailed information). Additionally, the surface of all specimens was scanned with a 3D scan before and after the fire test. Fixed target points ensure a good

alignment of both scans to examine the spalling depth and spalling volume. During the fire test, the temperature inside the specimen was measured by five embedded thermocouples in depths of 5 mm, 15 mm, 30 mm, 50 mm, and 100 mm from the fire exposed. Four thermocouples were applied on the steel ring surface with a distance of 1 cm to the fire exposed surface (see sketch in Figure 9). These thermocouples measure the steel ring temperature.

## RESULTS

### NMR

The results of the NMR measurements for the pre-dried specimens are shown in Figure 3. The first measurement was carried out on the day of switching the storage conditions from wet to pre-drying. The last measurement took place one day before the fire test. The diagrams show a significant change of the moisture content of the specimen boundary zone within the first two weeks. Afterwards, the moisture content reduces hardly until the day of the fire test. Both mixtures lost more than half of the detectable water within the measuring volume compared to the initial state. All in all, the specimens with basalt (OCB) tend to slightly higher moisture contents. It is assumed that this results from some chemical bound water inside the basalt grit. Figure 4 shows the results of the NMR measurements one day before the fire test for the specimens with unrestrained shell surface, the pre-dried specimens with applied steel rings and the specimens with applied steel sheet. The pre-dried specimens have a significantly lower water content compared to the wet cured specimens. The specimens with steel sheet coating tend to higher moisture values. It's assumed that this results from the application of the coating with expanding mortar. Thus, the amplitude of the specimen with steel sheet is slightly higher than the unrestrained specimen without later additions.

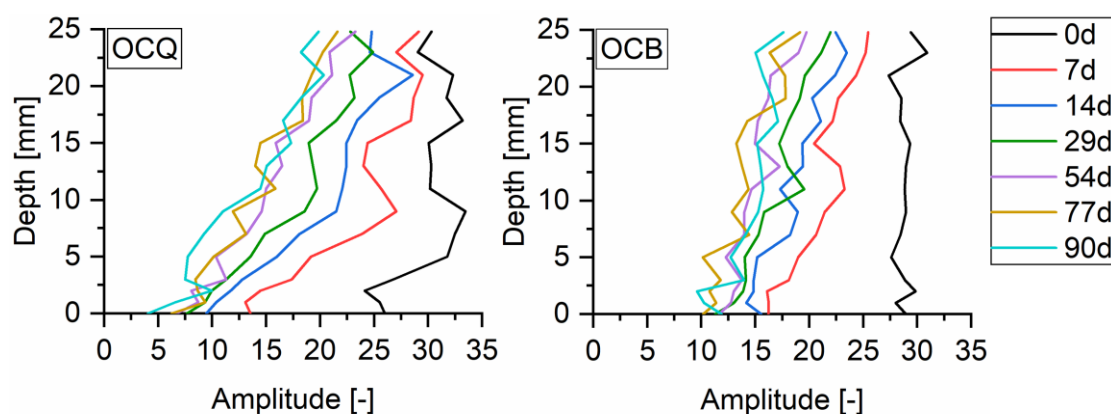


Figure 3 Results of the nuclear magnetic resonance (NMR) measurements for the pre-dried specimens with quartzitic aggregates (OCQ) and coarse basalt grit (OCB)

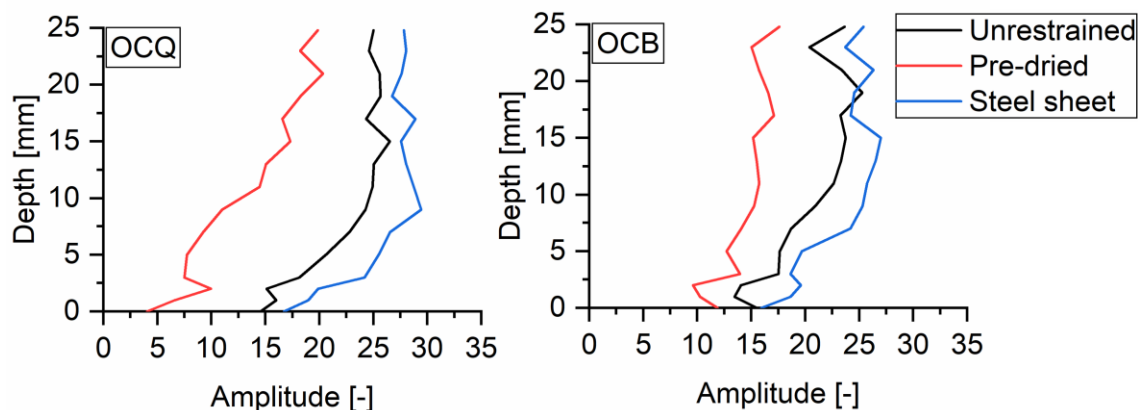


Figure 4 Results of the nuclear magnetic resonance (NMR) measurements of the fire exposed surface one day before the fire test for all specimens with quartzitic aggregates (OCQ) and coarse basalt grit (OCB)

### 3D Scans

The results of the 3D Scans for the concrete with quartzitic aggregates are presented in Figure 5, whereas Figure 6 shows the results of the 3D Scans for the concrete with coarse basalt grit. Comparing the specimens of OCQ and OCB without coating of the shell surface, the spalling behaviour is equal. Applying steel rings and steel sheet to the specimens increase the spalling behaviour of the specimens significantly. Due to the experimental setup, the steel rings expand less than the specimens. This leads to a restraint of the thermal expansion and compression stresses as well as induced transversal tensile stresses inside the concrete. Additionally, the restraint water loss at the shell surface leads to increased pore pressure and tensile stresses as well. The application of the steel rings to the quartzitic specimen results in a spalling volume of 12.1 % and a maximum spalling depth of 6.3 cm, whereas the spalling volume of the specimen with coarse basalt aggregates is 6.8 % with a maximum spalling depth of 4.5 cm. Thus, the spalling volume is almost doubled due to the variation of the type of aggregate. This result is mainly caused by the different expansion of the coarse aggregates in both mixtures. Due to the thermal induced conversion of quartz, the volume increase of the quartzitic aggregates [8] leads to significantly higher stresses inside the OCQ specimen and results in a larger spalling volume compared to the specimen OCB. In comparison to the unrestrained specimens, the spalling volume of the ring restraint specimen is 15 times larger for OCQ and 7.6 times for OCB (Table 2). Covering the shell surface with steel sheet reduces the water loss of the concrete with a low influence on the expansion of the specimen. Thus, thermohydraulic induced tensile stresses mainly influence the spalling behaviour of these specimens. The results show that less spalling occurs for both specimens with steel sheet compared to the ring restraint specimens. For mixture OCQ the spalling volume is 2.9 %, whereas for mixture OCB the spalling volume is 2.1 %. Additionally, the differences in the spalling behaviour of both mixtures are mainly influenced by the limitation of the thermal expansion of the specimens. The pre-dried specimens confirm the larger influence of thermomechanical induced stresses compared to the thermohydraulic induced stresses for this setup. Here, the spalling volume of the specimen with quartzitic aggregates is 10.7 % with a maximum spalling depth of 5.9 cm, whereas the specimen with coarse basalt aggregates showed no spalling. All results show a higher spalling volume for the mixture OCQ compared to mixture OCB under comparable restraint conditions (Table 2).



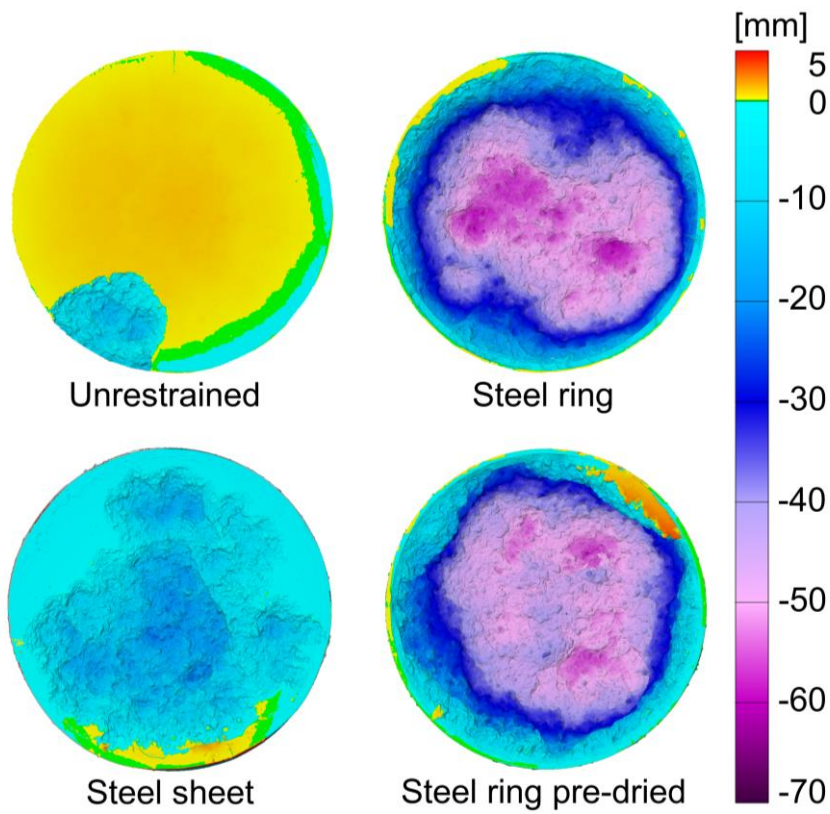


Figure 5 Results of the 3D Scans for the specimens with quartzitic aggregates (OCQ)

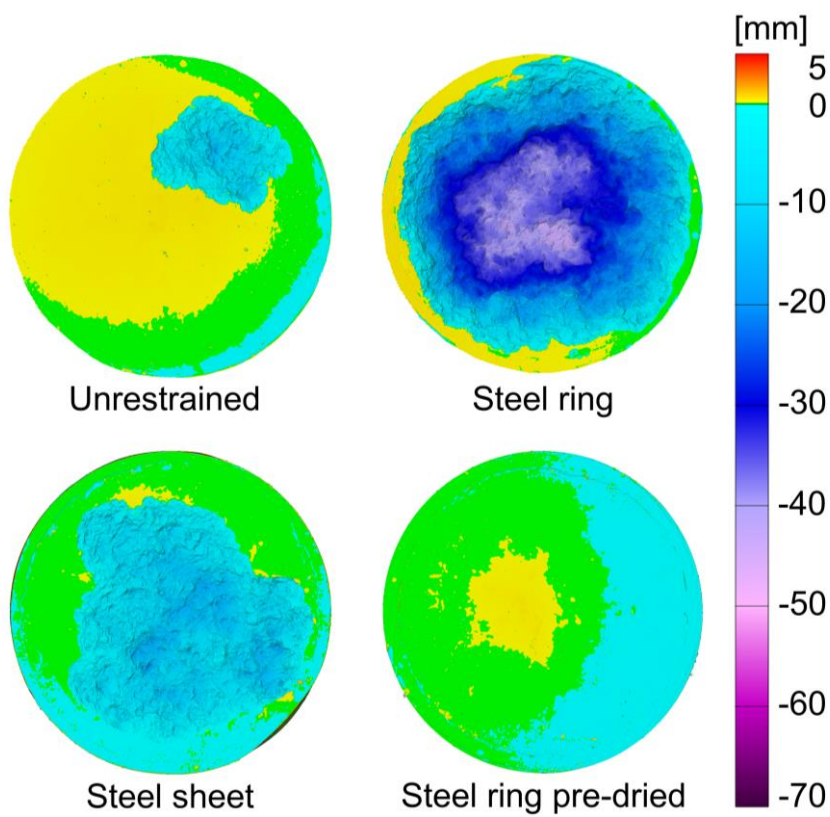


Figure 6 Results of the 3D Scans for the specimens with coarse basaltic aggregates (OCB)



Table 2 Spalling volume and maximum spalling depth for all fire exposed specimens

Specimens		Age [d]	Spalling volume		Maximum spalling depth [mm]
			[dm <sup>3</sup> /m <sup>2</sup> ]	[%]	
Ordinary Concrete Quartz	unrestrained	128	2.3	0.8	15
	steel ring	98	35.1	12.1	63
	steel sheet	98	8.4	2.9	23
	pre-dried	98	31.1	10.7	59
Ordinary Concrete Basalt	unrestrained	121	2.5	0.9	16
	steel ring	98	19.7	6.8	45
	steel sheet	100	6.1	2.1	19
	pre-dried	98	-	-	-

### Concrete temperature propagation

Figure 7 and Figure 8 show the temperature distribution for all specimens in five different depths in dependency of spalling during the fire tests. For specimens without spalling (OCQ unrestrained, OCB unrestrained and OCB pre-dried), the temperatures rise continuously in dependence of the temperature conductivity of the concrete. As shown in the results of the 3D scans, spalling occurred for the other five specimens. The material loss leads to a decreasing concrete covering and a possible exposure of the thermocouples to the fire. This exposure results in a rapid temperature rise in the diagram. Comparing for specimens OCQ unrestrained and OCB unrestrained, the diagrams show a similar temperature distribution.

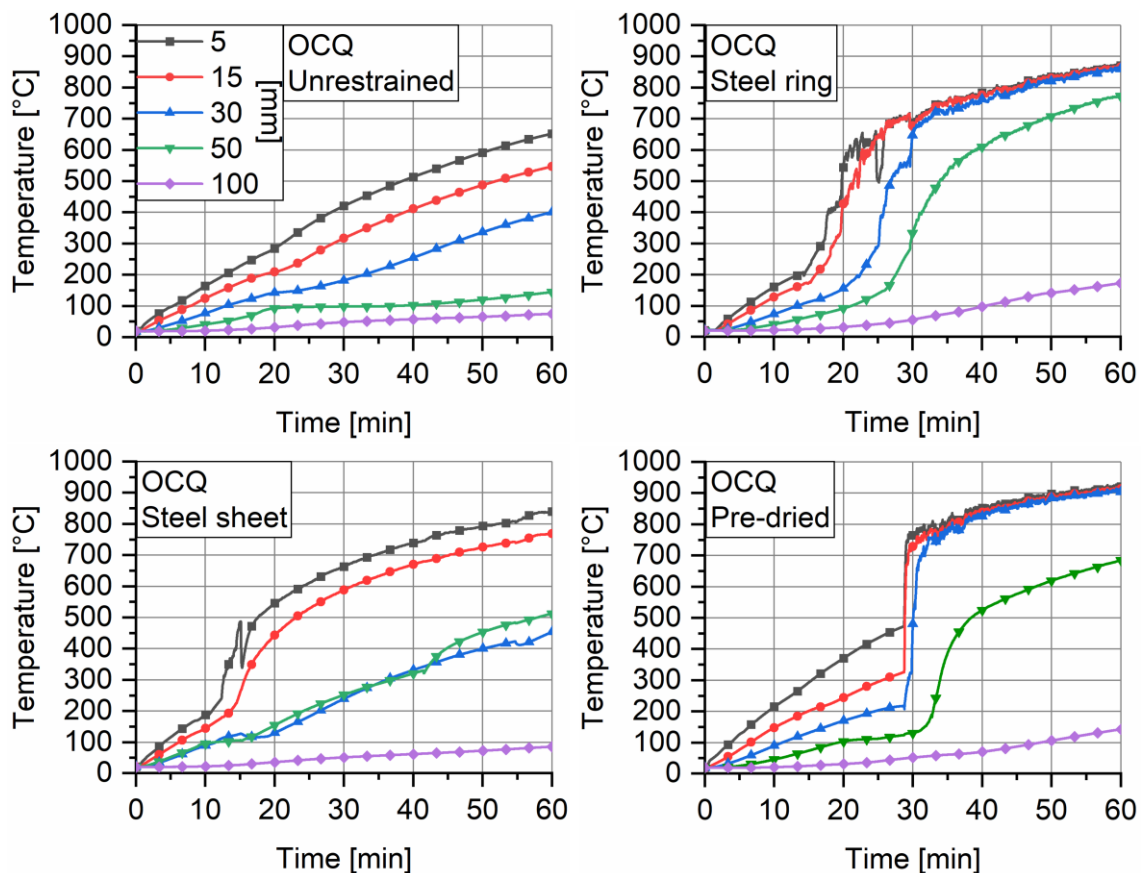


Figure 7 Temperature profiles for all specimens with quartzitic aggregates

Despite the occurrence of spalling, the temperatures increase similar for the specimens OCQ steel sheet and OCB steel sheet, as-well. Thus, the different types of coarse aggregates have no significant influence on the spalling behaviour and therefore, the temperatures of the specimens with the same constraint. On the other hand, the figures of the 3D scans showed larger spalling depths for the steel ring restrained specimens of OCQ in comparison to the steel ring restrained specimens of OCB. The reduced concrete covering leads to a faster increase of ring temperatures and therefore, more damage of deeper parts of the specimen. Thus, only the steel ring covered specimens show a significant increase in the spalling behaviour due to the restrained thermal expansion of the specimen. This result is even more pronounced in the temperature distribution of the specimens with the pre-dried concrete boundary zone. The specimen OCQ spalled and the temperatures increased rapidly in depths up to 50 mm in a short period, whereas for the specimen OCB pre-dried no spalling occurred. Due to the low moisture content, the spalling occurred delayed in comparison to the specimens that cured in a sealed plastic foil. Nevertheless, the temperatures are similar in larger depths at the end of the fire test.

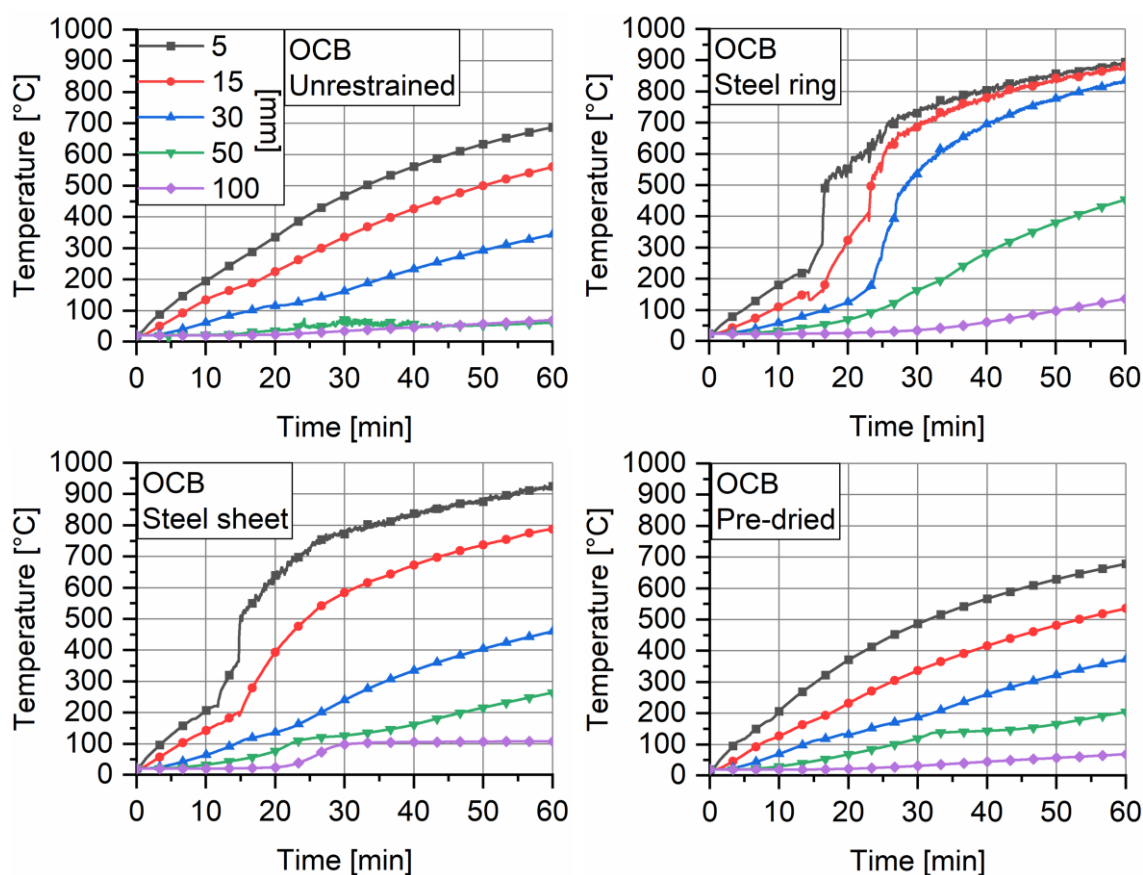


Figure 8 Temperature profiles of all specimens with coarse basalt aggregates

### Steel ring temperature

Four thermocouples were applied to measure the temperature of the steel ring at a distance of 1 cm from the fire exposed surface (Figure 9). The results show that the temperature rise of all four thermocouples on the steel ring is always lower than the temperatures at the embedded thermocouple in 5 mm depth of the specimen. The quicker temperature increase 30 min into the fire test are a result of concrete spalling in this depth. Thus, the thermal expansion of the concrete is always higher compared to the steel during the fire test. This discrepancy increases the compression stresses that lead to transverse tensile stresses inside the specimen and results in the occurrence of spalling. This describes the principle of simulating the conditions in the centre of partially fire exposed larger specimens.

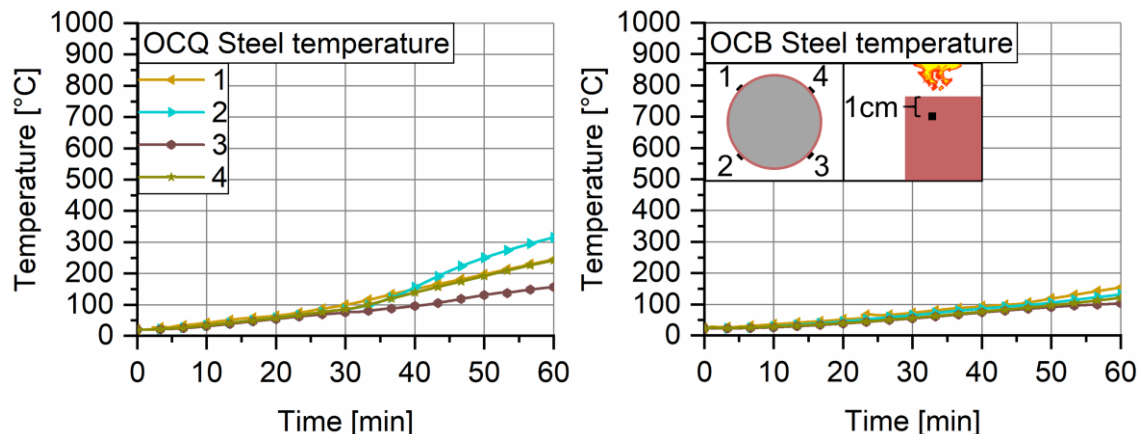


Figure 9 Steel temperature 1 cm from the fire exposed surface for the steel ring covered specimen with quartzitic aggregates and coarse basalt aggregates

## CONCLUSIONS

During this test series, the susceptibility to spalling of two ordinary concrete mixtures with different types of aggregates was investigated. For each mixture four specimens with different types of shell covering were tested. It was the aim to analyse the influence of an external passive restraint on the spalling behaviour. The following results occurred during the fire tests:

- The specimens without covering showed little spalling. The unrestraint expansion of the specimen as well as the water loss at the edge led to minor mechanical stresses and almost no spalling occurred.
- The Steel ring covered specimens spalled the most. The combination of the restraint thermal expansion of the concrete and reduced loss of water at the shell surface increase the stresses and lead to the highest spalling volume and the largest spalling depth in this test series.
- Considering the same covering type, the concrete mixture with quartzitic aggregates has always a higher spalling volume and spalling depth. It is assumed that the higher thermal expansion of the quartzitic aggregates induces larger mechanical stresses compared to basalt.

In case of the pre-dried specimen with steel ring cover, only the one with quartzitic aggregates spalled, whereas the basaltic one did not spall. It is assumed that the reduced moisture content leads to lower thermohydraulic induced stresses and that the stresses induced by the restraint thermal expansion are too low to cause spalling.

## ACKNOWLEDGEMENTS

## REFERENCES

1. Klimek, A., Stelzner, L., Hothan, S., and Rogge, A., "Fire induced concrete spalling in combination with size effects", *Materials and Structures*, submitted, 2022
2. Stelzner, L., Powierza, B., Oesch, T., Dlugosch, R. and Weise, F., „Thermally-induced moisture transport in high-performance concrete studied by X-ray-CT and <sup>1</sup>H-NMR”, *Construction and Building Materials*, **224**, 600-609, 2019

3. Mindeguia, J. C., Carré, H., Pimienta, P and La Borderie, C., “Experimental discussion on the mechanics behind the fire spalling of concrete”, *Fire and Materials*, **39**, 619-635, 2015
4. Hertz, K. D., “Limits of spalling of fire-exposed concrete”, *Fire Safety Journal*, **38**, 103-116, 2003
5. Ozawa, M., Tanibe, T., Kamata, R., Uchida, Y., Rokugo, K., and Parajuli, S. S., “Behaviour of ring-restraint high-performance concrete under extreme heating and development of screening tests”, *Construction and Building Materials*, **162**, 215-228, 2018
6. DIN 50014, “Normklimat für Vorbehandlung und/oder Prüfung-Festlegung“, 2018
7. Nagel, S. M., Strangfeld, C., and Kruschwitz, S., “Application of <sup>1</sup>H proton NMR relaxometry to building materials – A review, *Journal of Magnetic Resonance Open*, **6-7**, 2021
8. Schneider, U., *Behaviour of concrete at high temperatures*, Deutscher Ausschuss für Stahlbeton, 1982

# Spalling Screening Tests Under Different Loading Conditions

Katarzyna Mróz<sup>1,\*</sup> & Izabela Hager<sup>2,\*</sup>

<sup>1</sup> Cracow University of Technology, Faculty of Civil Engineering, Chair of Building Materials Engineering, Kraków, Poland

\* Corresponding author (katarzyna.mroz@pk.edu.pl,  
Warszawska 24 Str., 31-155 Kraków, Poland)

## ABSTRACT

The paper refers to a testing campaign carried out at the Cracow University of Technology for screening the effect of different boundary conditions on the spalling results. The paper presents the novel experimental setup that enables to apply the uniaxial compression, biaxial compression, or no load to the testing element, Figure 1. The presented experiment was carried out to enable the comparison of spalling results and avoid the impact of changes in concrete properties, boundary conditions and other variables that may appear during tests carried out at different testing setups. Concrete slab specimens were made of one concrete mix and cast from one batch. The research was carried out at one universal testing setup and under the same fire load. One high strength concrete (HSC) characterized by initial 28-day compressive strength of  $f_{c,28days} = 63$  MPa was tested. Three types of load conditions were used to test in the laboratory furnace: i) unloaded slabs, ii) slabs under uniaxial compression of 20 % of  $f_{c,28days}$  (13 MPa) and iii) slabs under biaxial compression of 20 % of  $f_{c,28days}$  (13 MPa). The paper compares the spalling events monitored during the tests and the spalling results measured after the test. The results put a clear view on the importance of configuration of testing setup for the spalling screening tests.

**KEYWORD:** Concrete, Uniaxial Compression, Biaxial Compression, Spalling Screening Test

## INTRODUCTION

Fire spalling of concrete is defined as the violent or non-violent breaking off of layer pieces of concrete from the surface of a structural element when it is exposed to high and rapidly rising temperatures as experienced in fire [1]. In literature few natures of spalling are distinguished: aggregate spalling [2], surface spalling [1], corner spalling [3], explosive spalling [4] or peeling of concrete after fire [5]. Spalling may become also the combination of several or, in a certain case, all of the listed types. Each type may be characterized by different forms and intensities and is caused by numerous factors. The most important factors that affect the nature and intensity of concrete spalling in a fire are material-related factors: concrete composition (w/c ratio, presence of mineral additives, aggregate type [6, 7] and maximum grain size [6]), concrete properties (strength [8, 9], gas permeability of concrete and moisture content in concrete [10, 11]), as well as element geometry (the shape [3] and size of the element [12]) and the type of mechanical load and the stresses induced by that load in the element as well as the fire scenario (duration, intensity, how the element is heated [2]).

So far, numerous experimental and numerical research was carried out to describe the fire spalling in concrete. The most common attempt is to indicate experimentally different parameters that may enhance spalling risks, such as the concrete mix composition, heating

scenario, the initial water content, geometry of specimen or mechanical boundary conditions. Testing of concrete spalling in fire is carried out on specimens of different sizes and shapes, moreover, using different testing procedures. Due to the variety of research setups and experimental methods and due to the lack of standardized testing guidance, there is a wide range of approaches to concrete fire spalling assessment and a wide diversity of obtained results [13, 14]. What's more, during the test, different measurements are carried out by the researchers to give a better description of the processes taking place in concrete during heating. Therefore, the comparison of these results is difficult, and it is hard to predict the spalling sensitivity of concrete.

To deliver more input data on reliable methods for assessing the concrete susceptibility to fire spalling, comparative parametric tests of concrete behaviour in a fire have been started. To enable the comparison of results and avoid the impact of changes in boundary conditions and other variables that may appear during tests carried out at different testing setups, the author proposed a universal experimental setup. The author of the paper developed an original frame system enabling fire tests on plate elements under different loading conditions: unloaded and subjected to unilateral and bilateral in-plane compression.

## **NOVEL EXPERIMENTAL SETUP FOR SPALLING SCREENING TEST AT CUT**

### **The furnace**

The Dragon furnace developed in Cracow University of Technology, Figure 1, is made of steel shell and internal lining. The chamber volume is built with hard fireproof ceramic boards and chamotte bricks. The Dragon furnace consists of a furnace opening 600 x 600 mm in size. As a result, such an area can be exposed to direct fire action. The furnace has two ventilation pipes 120 mm in diameter with draft regulators.

During the fire test, the slab specimen of 750 mm x 750 mm x 150 mm is hung on the top of the furnace with the suspension system to ensure the exact position in the opening and the axis of loading (in the case of loaded tests). The specimen placed on the top is set horizontally. The temperature development in the furnace chamber refers to a standard fire scenario ISO 834-1, but also more severe scenario can be reached (ex. RABT). The temperature development is driven by manual control of the 140 kW capacity gas burner. To provide the loading condition the Dragon furnace is additionally equipped with a loading frame that enables the uniaxial and biaxial in-plane compression in slab-like testing elements.

### **The loading frame**

To provide the external load, the original steel loading frame is designed. The proper engineer structural calculations according to Eurocode 3: Design of steel structures - Part 1-1: General rules and rules for buildings are carried out to design the frame that can withstand both the uniaxial and biaxial tension caused by the horizontal forces. The steel frame is made of hot-rolled S235 steel elements. In Figure 1 the scheme of the designed loading frame and the workshop drawing with global dimensions are given, while in Figure 2 the complex setup with the Dragon furnace is presented.

The stress conditions by external loading are provided with the use of four – (in case of biaxial loading) or two (in case of uniaxial loading) flat jacks with the capacity of 750 kN each. The load is distributed in one or two directions by the loading shoes fitted with steel Hilsdorf's brushes to reduce friction between loading shoes and concrete surface and to obtain pure compression, Figure 3b. Twelve steel brushes are located at boundaries – 3 brushes per each of four sides, Figure 3a. Every single brush is made of 1692 (36 x 47) steel bars of diameter 4 mm and a length of 132 mm, Figure 3c. The free unfixed part of bars equals 105 mm. Each bar is welded into a steel pillow of dimensions 200 x 155 x 8 mm equipped with roller support.

It enables the load distribution between flat jacks and a set of brushes. The brushes are adopted from the experimental setup developed previously at CUT [15].

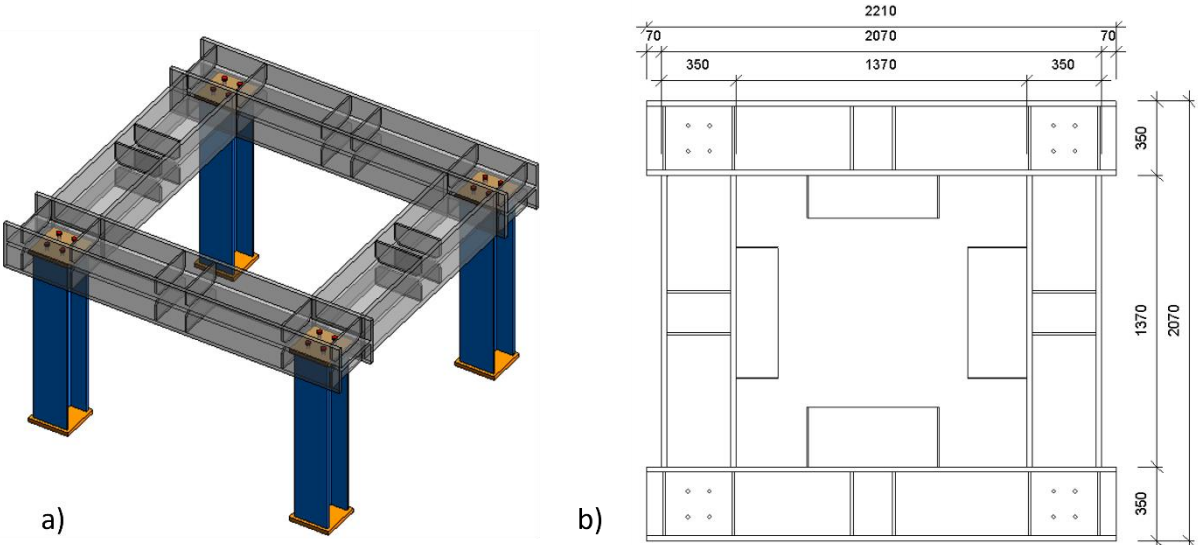


Figure 1. a): A 3D sketch of the original loading frame designed by the author., b) Workshop drawing of loading frame with global dimensions (top view).

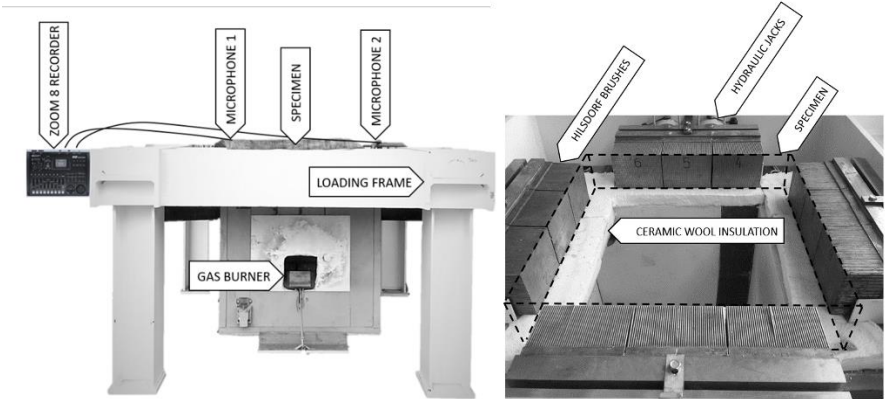


Figure 2. Complex experimental setup for screening tests with the Dragon furnace at CUT

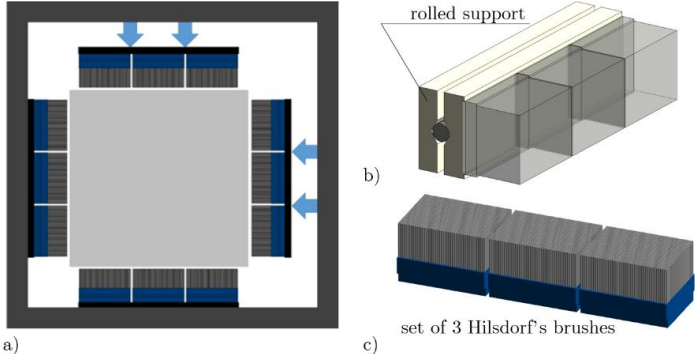


Figure 3. a) External loading frame fitted with flat jacks and brushed shoes, b) rolled support between loading frame and brushed shoes, c) set of three brushes

As a result, the load is distributed from flat jacks through Hilsdorf’s brushes to the concrete slab. The area of the applied load is 600 mm x 150 mm. The maximum stress that can be applied using the original loading frame in one direction is 15.95 MPa. The final experimental setup equipped with hydraulic jacks and Hilsdorf’s brushes is presented in Figure 4.



## MATERIAL AND METHOD

### Material and specimens

One concrete mix is selected to manufacture all the specimens tested in this campaign. The choice of the mix has been based done by preliminary spalling tests carried out for 8 mixes. The results have been presented at IWCS 2015 [9]. The mix composition is presented in Table 1. For determining the initial properties of concrete and the moisture content, standard specimens are manufactured. For fire spalling tests, slab specimens of 750 mm x 750 mm x 150 mm in size are produced. The summary of tested elements along with their dimensions and assigned purposes is presented in Table 2. Each test configuration consisted of 2 specimens.

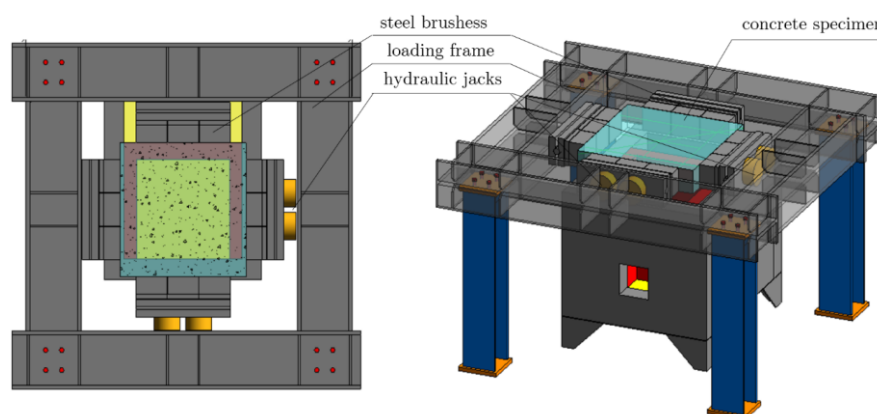


Figure 4. Complete experimental setup for fire tests under compressive load

Table 1 Mix components for tested concrete

Component	Origin	Unit	Amount
CEM III A 42.5 N LH/HSR/NA	Góraždze	kg/m <sup>3</sup>	400
Sand 0/2	Borzecin	kg/m <sup>3</sup>	640
Riverbed gravel 2/8	Tar-Krusz	kg/m <sup>3</sup>	460
Riverbed gravel 8/16	Tar-Krusz	kg/m <sup>3</sup>	690
Water	-	kg/m <sup>3</sup>	150
Admixture Primo LM-131	Atlas	%mc	0.7
Admixture AddiCRET PT20	Hufgard	%mc	0.6

Table 2 Summary of manufactured elements

Loading conditions	Dimensions of specimens (mm)			No. of specimens
	785	785	150	
no load	785	785	150	2
uniaxial compression	785	785	150	2
biaxial compression	785	785	150	2

All the specimens are moulded from one batch (concrete ordered from the concrete plant). After moulding, the specimens are covered with geotextile and watered every day for 14 days. After 14 days, the specimens are demoulded but in the case of each element to be tested in a fire test, the bottom (fire exposed) side is demoulded 14 days before running the particular fire test to prevent air drying. The specimens are kept in the storage chamber with a relative humidity of 50±5 % until the day of the test. The age of concrete specimens at the time of the fire test is between 300 and 330 days.

The concrete compressive strength at 28-days was 61 MPa and moisture content determined by drying of the reference sealed cylinders was ca. 4%.



## Testing procedure

To observe the effect of different loading conditions, three configurations of the slab are used:

- Unloaded
- In-plane loaded with uniaxial compression
- In-plane loaded with biaxial compression

External load is applied by flat jacks and distributed to the specimen through the steel Hilsdorf's brushes described before. The slab is loaded unilaterally or bi-laterally in a plane of concrete slab with a stress level of 15 MPa in each direction (650 bars from each hydraulic jack). Before running the fire test, the load of a target level of 15 MPa is applied to the concrete slab and kept for one hour to homogenize the conditions in the concrete inert. After one hour, when the fire tests start, the pressure in cylinders is not changed by hand if it changes its value.

The slab is exposed to ISO 834 fire scenario on the bottom surface in the area of 600 x 600 mm. The test duration in this study is set at 60 minutes. In the case of shortening the experiment time, the authors present the reasons for this derogation.

## Measurements were taken during and after the fire test

During the test, the observation concerning the nature and intensity of spalling is observed: the spalling event is recorded by a voice recorder and characterised by its frequency and type of sound (ex. pop-corn, explosion), according to the method developed for this purposes presented in [16]. The time of spalling initiation ( $t_0$ ) and its end ( $t_1$ ) are reported. In particular, the time of occurrence and the duration of water release through developed cracks to connect it with spalling observations. The temperature ( $T$ ) is measured in the furnace chamber with the use of a plate thermocouple.

After heating, the specimens are freely cooled down. Before taking measurements, the fire-damaged surface is not brushed or cleaned. The spalling propensity is assessed by investigation of the fire-exposed area and spalled material. When the specimen is removed from the furnace, the pieces of spalled material are inventoried – their dimensions, amount, and diversity is assessed. On the spalled surface, the spalling topography is developed. Measurements of spalling depth are taken manually in a grid with a mesh of 25 mm. Having the data gathered, the maximum spalling depth ( $d_{max}$ ), the volume of spalled material ( $V_s$ ) and volume  $V_s$  related to the initial volume of the slab ( $V_{rel}$ ) are indicated.

## RESULTS

### Spalling events – observations during a fire test

The first spalling event takes place between 1<sup>st</sup> and 2<sup>nd</sup> minute of fire exposure at temperature 230 - 600 °C. It is probably most associated with the temperature difference between the outer surface and inner layers of concrete. In such spalling events, the short, two-three events occur, with the sound being similar to this taking place while stone flaming. This kind of spalling, called aggregate spalling, is present only in tests without load. In the loading cases, it is noticed but less frequently.

From the 3<sup>rd</sup> minute and temperature close to 580 °C ± 30 °C, the spalling recalling the sound of making pop-corn takes place. The surface spalling is observed in all tested cases. In unloaded slabs, this kind of spalling can be easily distinguished from the earlier spalling events, while in the case of the loaded slabs, the spalling events start with this kind of spalling. As the temperature of occurrence is close to the temperature of the phase  $\beta - \alpha$  change of quartz at

573°C, it is assumed that this transformation is mostly responsible for the occurrence of this kind of spalling. It is more frequent and louder than the previous one and continues up to the 5th - 7th minute of fire exposure. In the case of unloaded slabs, the spalling continues and in the 7th - 8th minute of fire exposure, the pop-corn spalling continues and starts to be accompanied by the explosive spalling. It is observed that the intensity and frequency of explosive spalling depend strongly on the extent of load. In the case of unloaded slabs, two events of explosive spalling occur in the 7th - 10th minutes of fire exposure and after 10 minutes of the test, the spalling events stop entirely. In the slabs loaded with uniaxial and biaxial compression, the spalling events are more frequent. The spalling events stop after 20 minutes in the case of uniaxial compression. In the case of biaxial compression, spalling continues and does not stop before the termination of the test in the 30th minute of fire exposure. The termination of the test after 30 minutes of fire exposure was required to keep the safety of the tests and not lead to collapsing of the slab. While applying the biaxial compression to a concrete slab, a few (2 - 3) spalling events remind in sound a very severe explosion.

As was expected, the most severe test for spalling occurrence is the slab tested in biaxial compression. The summary of the time of the first spalling event, the temperature in the furnace at first spalling and its duration are indicated in Table 3 for every individual testing case.

The recognition of the nature of spalling events taking place in different moments of fire tests is in line with the inventory of spalled particles after the fire tests. In the unloaded slabs, only small elements have been found that correspond to the aggregate and surface spalling, while the bi particles were found in the loaded cases, as the explosive spalling dominated, Figure 7.

*Table 3 The summary of information of spalling events*

	time of the first spalling event (min' sec")	temp. in the furnace at first spalling (°C)	spalling duration (min' sec")	max spalling depth (mm)	spalling volume (cm <sup>3</sup> )	spalled / total volume (%)	spalled / fire exposed volume (%)
unloaded	1' 22"	484	10' 23"	16	1711	2	3
	1' 17"	232	08' 42"	18	1545	2	3
uniaxial load	3' 33"	561	18' 38"	32	6783	7	12
	3' 31"	606	20' 32"	49	5967	6	11
biaxial load	3' 19"	603	nonstop	130	26376	28	48
	2' 54"	545	nonstop	136	31093	34	58

### **Cracking development during fire test and spalling topography**

During fire exposure, it is observed that the inert part of concrete that experiences thermal expansion causes the cracking of the external part of a concrete slab. The cracks are observed in unloaded slabs and the uniaxially loaded slabs (only in the unloaded axis). As soon as cracks occur, the water starts to evaporate through the gaps – the spalling continues during the fire test as long as the water starts to flow out as boiling streams, Figure 5. At the time of appearing the liquid water escaping from the cross-section, the spalling terminates.

Moreover, the scheme of crack development differs according to the loading scheme. In the unloaded slab, the cold rim cracks in both directions as the inner part expands in both directions. In the case of the uniaxially loaded slab, the main cracks appear in the direction of load application, which is because the concrete is more prone to expand in the unloaded axis.

Finally, the biaxially loaded slab does not crack, which is due to acting forces in both directions, that keep the cracks closed and seal the concrete cross-section in both directions. The spalling results and the water transport processes during the fire test, have hence a clear connection. The comparison of the crack pattern and the spalling topography is presented in Figure 6.

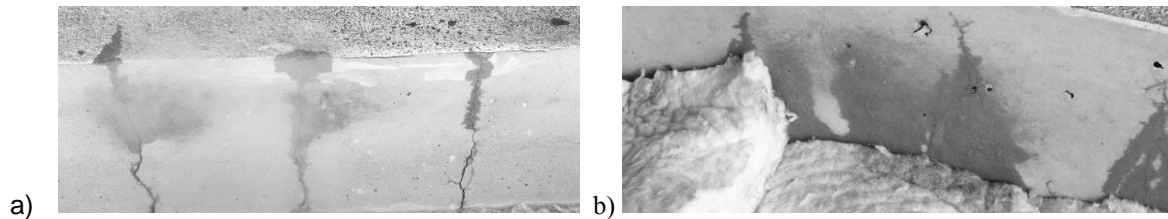


Figure 5. a) the water evaporating through cracks created at the sides of the slab – spalling continues; b) water flowing out of cracks as boiling liquid – spalling stops.

After specimens are cooled down, the topography of spalled regions is performed. The maximum spalling depth and the spalling volume are measured and the maps of topography are performed for each case, Figure 6.

The maximum spalling depth within all the tested cases is measured for slab loaded in biaxial compression and was equal to 136 mm (test terminated manually). To facilitate the comparison of the spalling extents, the spalling topography is presented for each configuration in one global colour scale, Figure 6. The dark grey colour indicates the regions without spalling while the white colour shows the maximum measured spalling depth of 136 mm.

As can be seen, the lowest spalling extent is observed for the unloaded test. As described before, in these tests the popcorn spalling is observed but after 10 minutes of fire exposure, the spalling events are terminated. In the unloaded slab, the cracks are created very quickly enabling water evaporation and leakage.

While the concrete slab is loaded in uniaxial compression, the load and decreased mechanical properties of concrete at elevated temperatures cause the creation of cracks across the specimen in the direction parallel to the load application. Nevertheless, the spalling continues, and water evaporates by the cracks created in the load direction or is extruded in the form of small drops on the unheated surface. Spalling is terminated after ca. 20 minutes when the water continuously escapes from the slab in the form of boiling liquid.

Finally, the biaxial compression of concrete slabs provides results that are incomparable to others. Both, the intensity of spalling and its length are much greater than in any other tested case. The maximum spalling depth is over three-fold greater than the one measured for slabs loaded in uniaxial compression. It is worth noticing, that this testing case when carried out as a trial test (third slab), was not terminated manually. In that case, the spalling continued until the extensive explosion of the slab that resulted in the formation of a great opening, Figure 7. Moreover, during the test, the spalling events do not terminate before turning off the fire. Considering the development of the crack, only a few small cracks that are visible by the naked eye are created on the unexposed surface. The slabs are extensively cracked, which can be seen only by measurement of deformation tracked by the DIC method (presented in [17]). Also, nor evaporated neither boiling liquid water is observed to escape during the tests of biaxial loading.

The comparison of obtained results of maximum spalling depth and calculated spalling volume are presented in Figure 8.

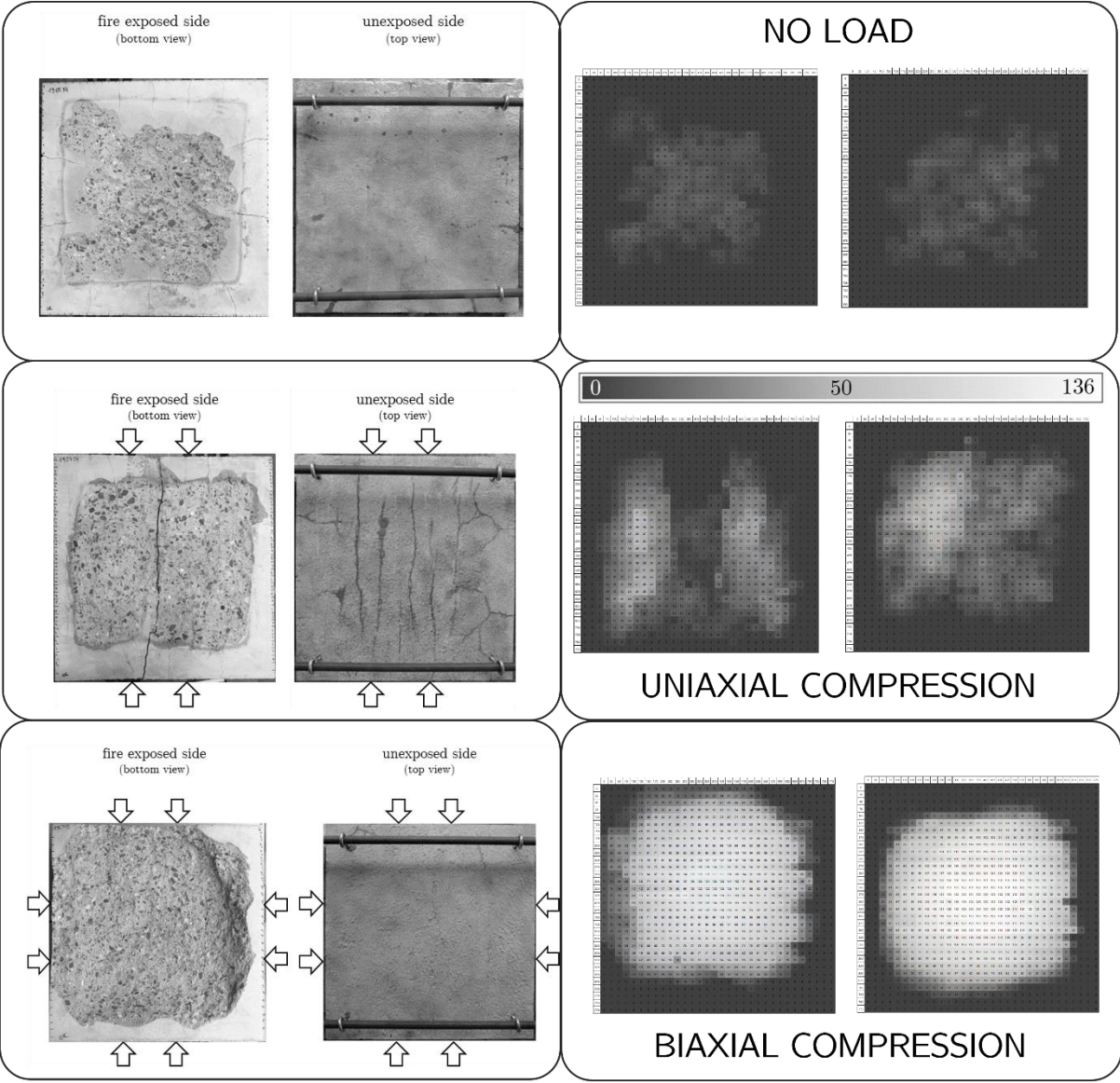


Figure 6. The pictures of the fire exposed side after tests.



Figure 7. The result of an extensive explosion that took place while testing the loaded concrete slab in biaxial compression.

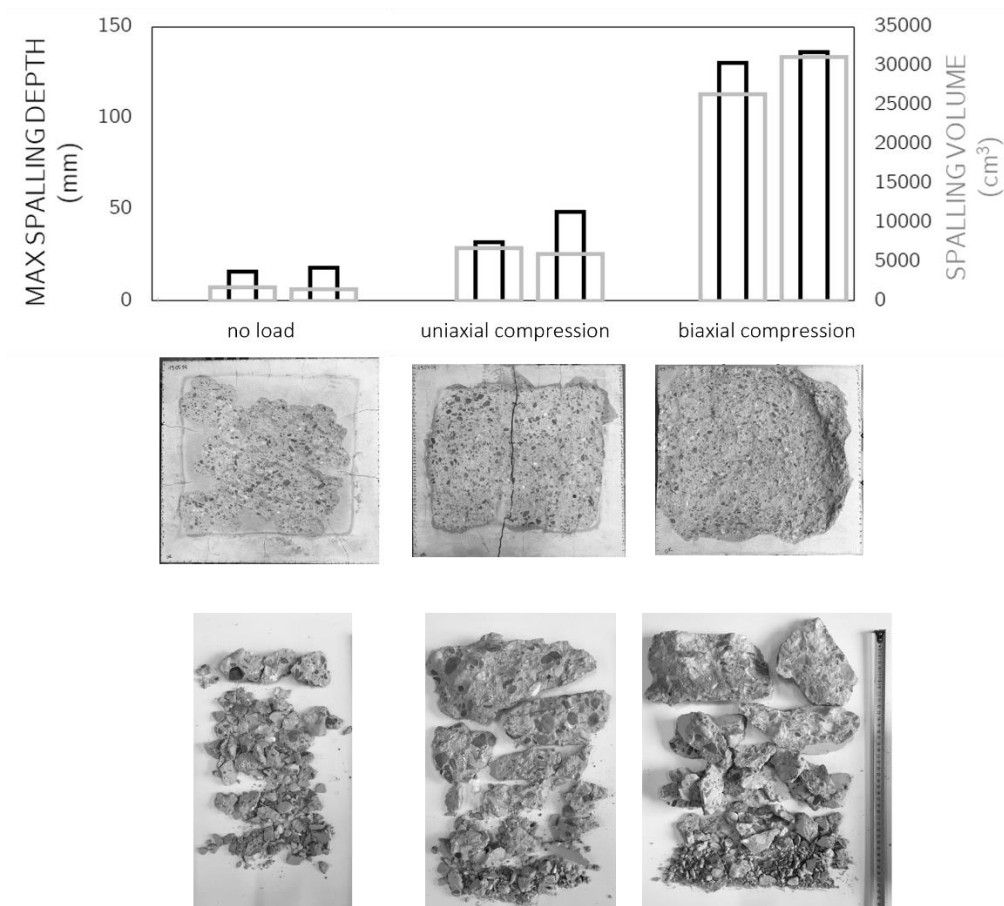


Figure 8. The result of an extensive explosion that took place while testing the loaded concrete slab in biaxial compression.

## DISCUSSION OF RESULTS AND CONCLUSIONS

1. The uniaxial compression results in the splitting of the concrete slab in the unloaded direction. The applied load generates cracks in its direction and facilitates water migration. In the opposite to all the tests without external load, evaporation is not observed. Instead, at first, the drop of liquid water appears on the top of the surface in the 9<sup>th</sup> minute of fire exposure, but spalling continues.
2. The biaxial compression of concrete slab exposed to fire delivers the results that stand out from the others tested within this experimental program. The active restraint to thermal dilation of concrete acting from both directions effectively contributes to closing the cracks and limits any deformation of concrete during fire exposure. As a result, the water that goes toward the colder sides of the concrete element migrates into sealed material that promotes a build-up of high pressure of water/water vapour in the pores of the material. When spalling takes place, the amount of water that cumulated in the layer near to spalled depth evaporates and the further migration of water toward the deeper part is continued. While testing the spalling propensity, one shall be aware that the element of any class of concrete under investigation may spall under biaxial compression.
3. The higher restraint level induces fire spalling in high-strength concrete exposed to fire.
4. The level of restraint affects the nature of spalling. It has been recently confirmed that the type of spalling can be distinguished based on its well-defined frequency. As a result, in unloaded test cases, explosive spalling occurs rarely, while aggregate spalling occurs most frequently. In the case of external compression,

most of the spalling events are described as explosive spalling. The aggregate spalling is less prone to occur.

5. It is possible to propose a unified testing procedure to study the influence of stress state on spalling propensity in concrete. To study the influence of stress state on spalling propensity in concrete, it is possible to define one recommended testing procedure.
6. Spalling is directly linked to stresses induced by water that cannot escape from the concrete inert. When the evaporation is hindered by active or passive restraint the spalling is more intense and its extent increases proportionally to the restraint ratio. If water can find a way to escape, the spalling is limited. However, spalling stops only if the water can escape fast enough. Therefore spalling stops only when the liquid water appears on the specimen's external side. This is the only case in which the water can easily migrate out of the specimen and does not build up pressure in concrete inert.

## REFERENCES

1. Debicki G., Haniche R., Delhomme F., "An experimental method for assessing the spalling sensitivity of concrete mixture submitted to high temperature", *Cement and Concrete Composites*, **34**, 958-963, 2012.
2. Khoury, G. A., Anderberg, Y., *Concrete Spalling Review*, Fire Safety Design, 2000.
3. Willam, K., Lee, K.K., Xi, Y., Xotta, G., Salomoniet, V., "Explosive spalling of concrete materials under extreme environments", Proceedings of 2nd International RILEM Workshop on Concrete Spalling due to Fire Exposure, Delft, The Netherlands, 2011.
4. Gary, M., "Fire tests on reinforced concrete buildings (in German)", Heft 11, Verlag Wilhelm Ernst und Sohn, Germany 1916.
5. Hager, I., Tracz, T., Śliwiński, J., Krzemień, K., "The influence of aggregate type on the physical and mechanical properties of high-performance concrete subjected to high temperature", *Fire and Materials*, **40**, 668–682, 2016,
6. Connolly, R., *The spalling of concrete in fires*. The University of Aston in Birmingham 1995.
7. Khoury, G. A., Anderberg, Y., Both, K., Fellingner, J., Høj, N.P., *Majorana, C., Fire design of concrete structures - materials, structures and modelling*, Fib Bulletin. Stuttgart: Sprint-Digital-Druck, vol. 38(1), 6245. 2007
8. Phan, L., "Spalling and mechanical properties of high strength concrete at high temperature", *Concrete Under Severe Conditions: Environmental & Loading (CONSEC '07)*, 1595–1608, 2007
9. Hager, I., Tracz, T., "Parameters influencing concrete spalling severity - intermediate scale tests results", Proceedings of 4th International RILEM Workshop on Concrete Spalling due to Fire Exposure, 294–300, 2015.
10. Hertz, K. D., "Limits of spalling of fire-exposed concrete", *Fire Safety Journal*, **38**(2), 103–116, 2003.
11. EN 1992-1-2, Eurocode 2: Design of concrete structures - Part 1-2: General rules - Structural fire design, Authority: The European Union Per Regulation 305/2011, Directive 98/34/EC, Directive 2004/18/EC, 2004.
12. Jansson, R., *Spalling of concrete exposed to fire*. SP Report 2008:52, Borås 2008.
13. Jansson R., *Fire spalling of concrete: theoretical and experimental studies*. KTH, Stockholm 2013.
14. Taillefer N., Pimienta P., Dhima D., "Spalling of concrete: A synthesis of experimental tests on slabs", *MATEC Web of Conferences*, vol. 6(1), 01008, 2013.

15. Ligęza W., Redystrybucja sił wewnętrznych we wzmacnianych betonowych elementach tarczowych, Wydawnictwo Politechniki Krakowskiej, Kraków 2000.
16. Mróz, K., Hager, I., "Evaluation of nature and intensity of fire concrete spalling by frequency analysis of sound records", *Cement and Concrete Research*, **148**, 106539, 2021.
17. Mróz, K., Tekieli, M., Hager, I., „Measurement of strains and crack propagation by Digital image correlation method in fire exposed concrete slab”, Applications of Structural Fire Engineering, Ljubljana, Slovenia, 9-11, June, 2021.

# Spalling screening tests for tunnel linings and the impact of the main influence parameters

Siyimane Mohaine<sup>1,\*</sup>, Bérénice Moreau<sup>1,2</sup>, Laetitia D'Aloia<sup>2</sup>, Sébastien Bouteille<sup>2</sup>, François Cussigh<sup>3</sup>, Philippe Gotteland<sup>3</sup> & Fabienne Robert<sup>1</sup>

<sup>1</sup> Fire Testing Centre, CERIB, Épernon, France

<sup>2</sup> CETU, Lyon, France

<sup>3</sup> FNTP, Paris, France

\* Corresponding author (s.mohaine@cerib.com, 1 rue des longs réages, 28230 Épernon, France)

## ABSTRACT

This paper presents the results of two collaborative research programs conducted between CETU (Centre for tunnel studies), FNTP (National Federation of Public Works) and the Fire Testing Centre of CERIB. The objectives of the programs were to (i) contribute to understand the relative impact of the main parameters influencing the spalling of concrete and (ii) attempt to the design of a screening test setup that would be used to select the mix before a full-scale test. The screening test should be sufficiently severe to screen the materials and to be possibly representative of the full-scale test, but it should be also simple, cost efficient and should not be more severe than the full scale test whose stress state is in adequation with the studied tunnel project.

On one hand, a multiscale experimental campaign has been conducted to study the contribution to spalling of three parameters: (i) internal stresses due to the thermal gradient, (ii) indirect actions due to the restrained thermal expansion and (iii) constraints induced by mechanical loading. On the other hand, different intermediate scale test setups have been investigated to define the most representative test setup for spalling. The impact of restraint and load ratio have been studied. The contribution of the internal stresses due to the thermal gradient have been confirmed. The presence of loading in a screening test was discussed.

**KEYWORDS:** Screening tests, Cut-and-Cover Tunnels, Modified Hydrocarbon Fire, Spalling

## INTRODUCTION

Concrete spalling is one of the parameters that is considered when dealing with the fire resistance of concrete tunnel linings. The current French guidelines include a tunnel lining full-scale spalling test for which the stress-state in the tunnel section needs to be calculated prior to the test to define the mechanical load to apply. The stress-states are usually determined using numerical modelling – this allows reproducing the stress profiles linked to the internal stresses due to the thermal gradient and the indirect actions due to the restrained thermal expansion.

Prior to performing a tunnel-lining full-scale test, preliminary tests are often run to select the concrete mix that is less sensitive to spalling. These screening tests are meant to be cost effective and severe enough to be able to screen different concretes. However, they are not meant to be more severe than a tunnel lining full-scale test. Spalling of concrete is both inherent to the material and dependent on the boundary conditions of the test specimen as well as its shape and dimensions.



In that context, two collaborative research programs have been conducted between CETU (Centre for Tunnel Studies), FNTP (National Federation of Public Works) and the Fire Testing Centre of CERIB. Two main objectives were identified. The first one was to investigate the possibility to simplify the test setup that is currently used for tunnel linings by studying the relative impact of three main parameters that influence concrete spalling. The second one was to attempt to define a suitable and representative intermediate scale spalling test that will allow to screen different concrete mixes prior to conducting a tunnel lining full-scale test.

## **CETU RESEARCH PROGRAM**

### **Objectives and approach**

This research program was conducted to contribute to the understanding of the coupling and the relative impact of the main parameters influencing the spalling of concrete. The contribution to spalling of three parameters was studied : (i) internal stresses due to the thermal gradient, (ii) indirect actions due to the restrained thermal expansion and (iii) constraints induced by mechanical loading. The main objective was to study the possibility to simplify the tunnel lining full-scale test by proposing a test setup where only the impact of the internal stresses is considered.

Two main phases of the research program are presented in this paper:

Phase A: assessment of the role of internal stresses due to thermal gradient by testing intermediate scale slabs with different thicknesses (from 10 cm to 60 cm). Two concrete mixes have been used for that purpose (with and without polypropylene fibres).

Phase B: Comparison of the impact on spalling of the three parameters (internal stresses, indirect actions due to the restrained thermal expansion and constraints induced by mechanical loading). The tests have been performed on wall configurations that have been designed based on numerical modelling. The simulations (not presented in this study) were used as a tool to predict the stresses for these configurations compared to a tunnel lining full-scale test. The objective was to evaluate these test configurations and assess their representativity compared to a tunnel lining full-scale test.

Three wall tests were performed with the thickness and concrete selected based on the results of Phase A. A cut and cover tunnel lining full-scale test was also performed on a slab with the same thickness.

For all the fire tests, a modified hydrocarbon curve was used:

$$\theta_g = 20 + 1080 * (1 - 0.325 * e^{-0.167t} - 0.675 * e^{-2.5t})$$

### **Materials and test setups**

Two concrete mixes are used to investigate the internal stresses due to thermal gradient in Phase A: without and with (300 g/m<sup>3</sup>) polypropylene fibres. The dosage of polypropylene fibres was chosen based on previous results, not presented in this paper, where different amounts were tested in order to have a concrete with a lower but still existing sensitivity to spalling. The compressive strength was measured on 12 specimens at 28 days and 6 specimens at the day of the test (15 x 15 x 15 cm<sup>3</sup> cubic specimens) that were stored in similar conditions as the fire test specimens. For phase B, only one concrete mix was used (based on the results of phase A). Details are presented in Table 1.

Table 1 Concrete mixes details used during the CETU research program

		Concrete mix #1	Concrete mix #2
Components	Silico-calcareous aggregate 0/4	840 kg/m <sup>3</sup>	
	Calcareous aggregate 4/20	870 kg/m <sup>3</sup>	
	Cement CEM I	385 kg/m <sup>3</sup>	
	Water	175 kg/m <sup>3</sup>	
	Admixtures (superplasticizer and additive for difficult sands (Mastersuna SBS 3890))	2.9 L	
	Monofilament polypropylene fibres (Ø=22 mm)	-	300 g/m <sup>3</sup>
Compressive strength (Phase A : slabs)	28 days	48 MPa	43 MPa
	Day of the test (90 days)	43 MPa	43 MPa
Compressive strength (Phase B : walls and full-scale test)	28 days	-	64 MPa
	Day of the test (5.5 months approximately)	-	63 MPa

Table 2 presents the different test setups used for Phase A and B, also illustrated in Figure 1. For Phase A, the four intermediate scale slabs have been tested simultaneously in a single fire test. Each slab was simply supported on two ends of top of the furnace (200 mm on each end against the side walls of the furnace). The exposed faces of the slabs correspond to the bottom of the moulds and were exposed to fire through a surface of 1 300 x 980 mm<sup>2</sup>. A 25 mm thick mineral wool lining was placed on each of the longitudinal sides of the slabs. The temperature in the furnace was controlled with plate thermometers in order to follow the temperature/time curve. Two plate thermometers were placed below each slab.

Table 2 Test setups and configurations studied during the CETU research program

	Specimens	Specificities
Phase A	Intermediate scale slabs 1.7 x 0.98 x 'e' m <sup>3</sup>	Thickness e = 10 cm
		Thickness e = 25 cm
		Thickness e = 40 cm
		Thickness e = 60 cm
Phase B	Walls 4.42 x 1.3 x 0.4 m <sup>3</sup>	Wall A – free expansion
		Wall B – mechanical load of 150 T on top of the wall (equivalent stress 3 MPa)
		Wall C – Restraint (use of pretensioned bars opposite to the expansion)
Phase B	Full-scale test for tunnel linings 8 x 1.6 x 0.4 m <sup>3</sup>	30 T on each edge, which corresponds at t=0 to : *5.9 MPa on the underneath face of the slab at its middle *7.2 MPa on the underneath face of the slab close to the supports

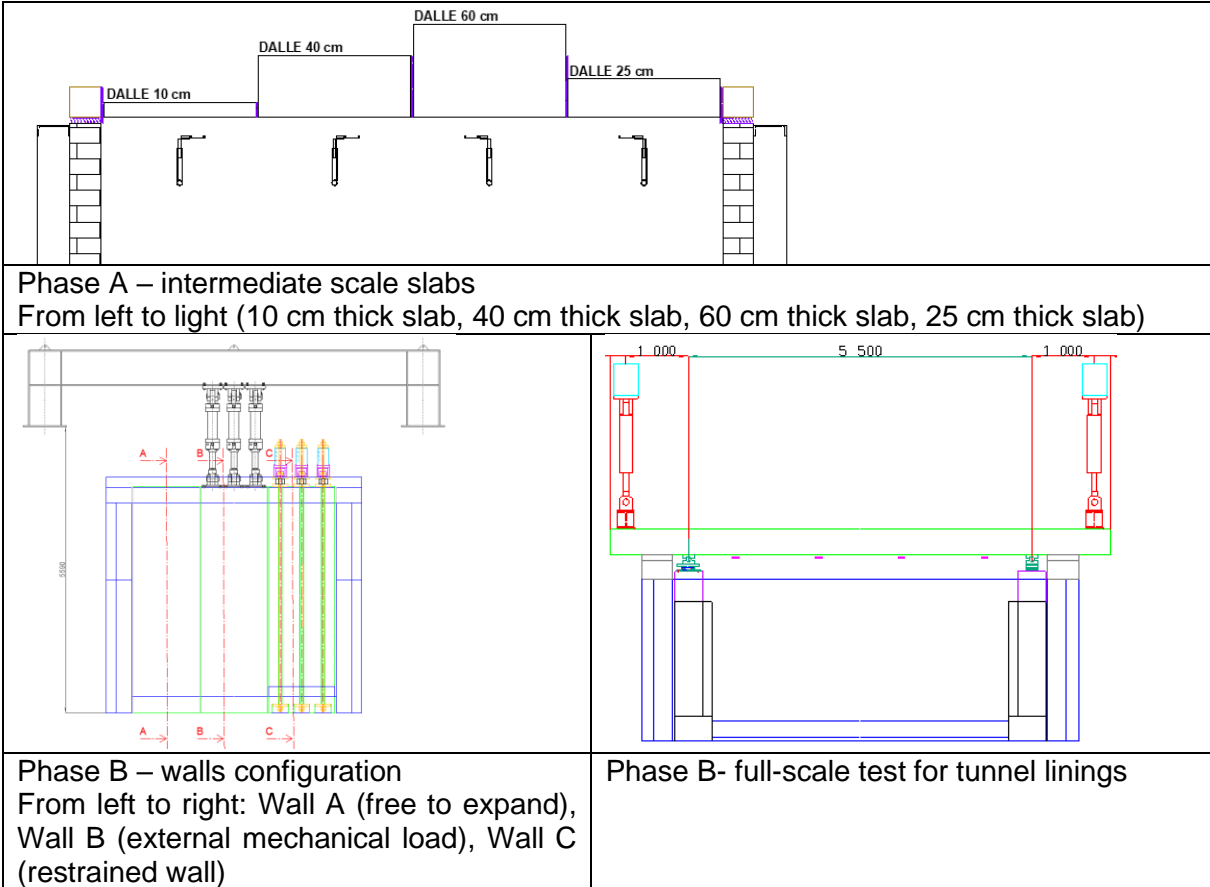


Figure 1 Test setups used for the CETU research program

**Results**

**Phase A**

Table 3 shows the spalling results obtained after 60 minutes and the representative moisture content of each slab. Moisture content was measured on samples that have a length corresponding to the thickness of the fire specimens they aim to represent. No spalling was observed for the 10 cm thick slab, which confirmed the results obtained in the preliminary study [1]. For the higher thicknesses, both concretes spalled: a slab thickness threshold at 25 cm was observed for the concrete without fibres, above which spalling did not increase significantly. For the concrete with fibres, this threshold was at 40 cm thickness (Figure 2). For Phase B, the concrete mix with fibres was chosen in order not to experience too much spalling during the full-scale tests. Along with this concrete, the thickness threshold regarding spalling was also chosen for the full-scale tests (40 cm).

Table 3 Spalling results of the slabs tested in Phase A (CETU research program)

Slab thickness	Start/end of spalling		Average/maximum spalling in spalled area		Spalled area*		Moisture content at 0-2.5 cm/2.5-5 cm	
	Without fibres	300 g/m <sup>3</sup>	Without fibres	300 g/m <sup>3</sup>	Without fibres	300 g/m <sup>3</sup>	Without fibres	300 g/m <sup>3</sup>
10 cm	-	-	-	-	-	-	3.2%/4.5%	3.8%/5.1%
25 cm	2 min/	2 min/9 min	50 mm/85 mm	25 mm/65 mm	90.7 %	57.6%	3.7%/5.7%	4%/5.7%
40 cm	1 min/	3 min/	60 mm/110 mm	50 mm/95 mm	90.1%	87.5%	4%/6.1%	3.8%/5.4%
60 cm	1 min/	3 min/	NM**	53 mm/140 mm	NM	84.6%	3.9%/6%	4%/6.1%

\*Non spalled surfaces were not considered to calculate the average spalled area

\*\* not measured because of the collapse of the slab after the end of the test

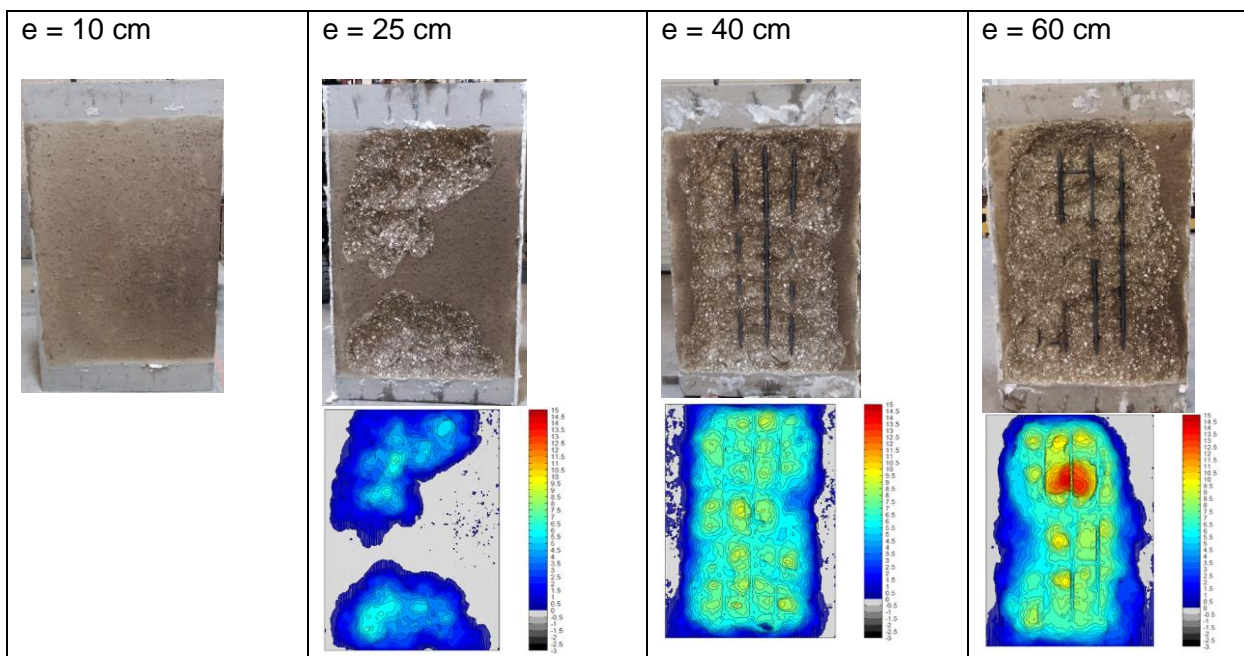


Figure 2 Exposed face of the slabs at the end of the fire test for the second concrete mix (with 300 g/m<sup>3</sup>) for the CETU research program

### Phase B

The wall configurations and their boundary conditions were defined based on numerical modelling using St1-feu software developed by CETU. The stress profiles were compared based on the maximum value of the stress peak at a given time as well as their shape. For the maximum value of the stress peak, the loaded wall (Wall B) had a very similar stress profile to the full-scale test at 1 min – after that, all the proposed configurations had similar profiles. However, the shape of the stress peak of the tunnel lining full-scale test was higher than for the wall configurations.

Table 4 and Figure 3 show the results obtained on the walls and the tunnel lining full-scale test. The tests had to be terminated at different times depending on the evolution of the spalling to guarantee a post-test safety. The results of the full-scale tests are therefore not directly

comparable to the intermediate scale slabs. However, a comparison is still possible between the wall configurations and the full-scale tunnel lining test.

*Table 4 Spalling results on the wall configurations and the tunnel lining full-scale test (CETU research program)*

Test	Duration of the test	Start/end of spalling	Average/max spalling in spalled area	Spalled area	Moisture content at 0-2.5 cm/2.5-5 cm
Wall A	19 min	2 min/ 13 min	20 mm/ 80 mm	38 %	4.8%/ 6.3%
Wall B	12 min	2 min/ -	45 mm/ 75 mm	76 %	4.8%/ 6.3%
Wall C	19 min	2 min/ 13 min	50 mm/ 100 mm	95 %	3.9%/ 5.4%
Full-scale test	16 min	2 min/ 6 min	77 mm / 100 mm	100 %	4.5%/ 5.5%



*Figure 3 Exposed face of the walls and tunnel lining full-scale test at the end of the fire tests for the CETU research program*

## FNTP RESEARCH PROGRAM

### Objectives and approach

The main objective of this research program was an attempt to define a screening test configuration that would be representative of a tunnel lining full-scale test. The screening test should be sufficiently severe to screen different concrete mixes but at the same time should not be more severe than the full scale test whose stress state is in adequation with the studied tunnel project.

Two series of screening tests were run to verify their representativity compared to a full-scale test using a new concrete mix that is sensitive to spalling.

The first series consisted of three categories of test setups: non-loaded slabs, loaded slabs (using pretensioned bars) and restrained slabs (using metallic frames). A tunnel-lining full-scale test was also performed.

The second series consisted of loaded slab configurations with different load levels to investigate the effect of the load level on spalling. Reproducibility tests were also performed to compare the results from the first and second series.

All the fire tests were performed using the modified hydrocarbon curve:

$$\theta_g = 20 + 1080 * (1 - 0.325 * e^{-0.167t} - 0.675 * e^{-2.5t})$$

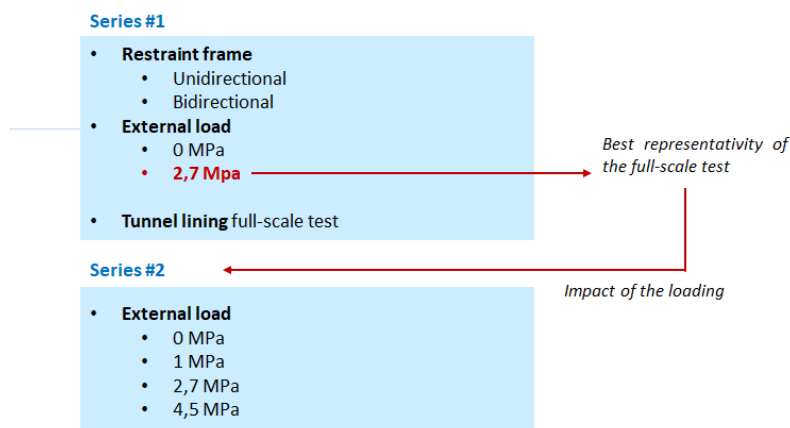


Figure 4 Overview of the FNTP research program

### Materials and test setups

The concrete mix used for the FNTP research programme has a compressive strength class of C30/37 and contains silico-calcareous aggregates. 0.6 kg/m<sup>3</sup> of polypropylene fibres were incorporated. This concrete mix, for which the details are not given in this paper, was chosen based on its sensitivity to spalling that was observed in previous private testing.

Table 7 and Table 8 summarise the test setups for the two test series. Each intermediate scale slab was simply supported on two ends of top of the furnace. The exposed faces of the slabs correspond to the bottom of the moulds.

The average compressive strength at 90 days for each cast is indicated in the tables. The measures were performed on cubic samples 15 x 15 x 15 cm<sup>3</sup> that were stored next to the fire specimens.



Table 7 Test setups of the FNTF research program – first series

1 <sup>st</sup> series (2017)				
Scale	Load?	Restraint?	Geometry	$f_{c90}$ (MPa)
Intermediate scale test	-	Unidirectional	With metallic frame: 2.05 x 2.4 x 0.3 m <sup>3</sup> Within the frame: 1.8 x 1.4 x 0.3 m <sup>3</sup> Exposed surface: 1.3 x 0.95 m <sup>2</sup>	44.5 MPa
	-	Bidirectional	With metallic frame: 2.05 x 2.4 x 0.3 m <sup>3</sup> Within the frame: 1.8 x 1.4 x 0.3 m <sup>3</sup> Exposed surface: 1.3 x 1.04 m <sup>2</sup>	
	-	-	1.7 x 0.98 x 0.3 m <sup>3</sup> Exposed surface : 1.3 x 0.98 m <sup>2</sup>	
	2 * 400 kN applied at t=0 (2.7 MPa) Loading applied using 2 bars that are pretensioned with jacks before the test (Figure 5)	-	1.7 x 0.98 x 0.3 m <sup>3</sup> Exposed surface : 1.3 x 0.98 m <sup>2</sup>	
Full-scale test	950 kN on each edge : 14 MPa on the underneath side of the slab at t=0	-	8 x 1.6 x 0.5 m <sup>3</sup>	43 MPa

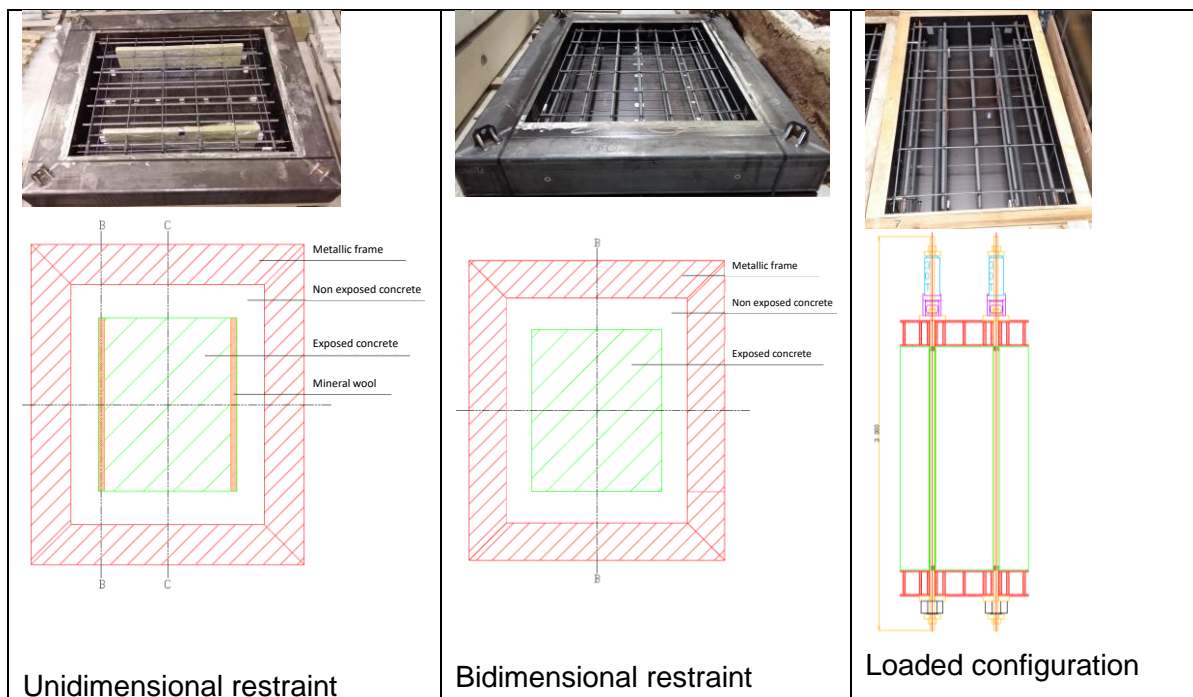


Figure 5 Illustration of the restraint frames and loaded slabs

Table 8 Load levels of the loaded slabs – FNTF research programme

Specimens	Load	1 <sup>st</sup> series (2017)	2 <sup>nd</sup> series (2019) f <sub>c90</sub> =33.3 MPa
Intermediate scale slabs 1.7 x 0.98 x 0.3 m <sup>3</sup>	0 MPa	x	x
	1 MPa	-	x
	2.7 MPa	x	x
	4.5 MPa	-	x
Full-scale slab 8 x 1.6 x 0.5 m <sup>3</sup>	950 kN on each edge : 14 MPa on the underneath side of the slab at t=0	x	-

## Results

Table 9 shows the results of the first test series (screening tests and tunnel-lining full-scale test). The tests were run for 60 minutes. All the slabs spalled to a different degree: the non-loaded slab had the lowest maximum spalling depth while the loaded slab (2.7 MPa) had the highest one. This slab was the most representative compared to the tunnel lining full-scale slab with regards to the maximum spalling depth. Therefore, for the second test series, this screening test setup is selected to investigate in more depth the influence of the load level and identify a threshold for spalling propensity.

Table 9 Test results of the 1<sup>st</sup> test series FNTF research program

Test specimen	Start/end of spalling	Max spalling in spalled area	Representative moisture content at the surface
Unidirectional restraint	3 min/ 18 min	6 cm	3.9%
Bidirectional restraint	4 min/ 13 min	5 cm	3.9%
Non-loaded	4 min / 7 min	3 cm	3.9%
Loaded (2.7 MPa)	3 min / 17 min	7 cm	3.9%
Full-scale test specimen	2 min/ 40 min	7.5 cm	3.6%

The evolution of the average and maximum spalling depth as well as and estimation of the spalled area are given in Table 10 for the loaded slab configurations. Data obtained on the tunnel lining full-scale test are also presented for comparison. The exposed face of the elements after being tested are presented in Figure 5.

The impact of the loading is clearly shown in the spalled area of the second series: more than 90 % of the surface of the loaded slabs spalled while only 25% of the surface did for the non-loaded configuration.

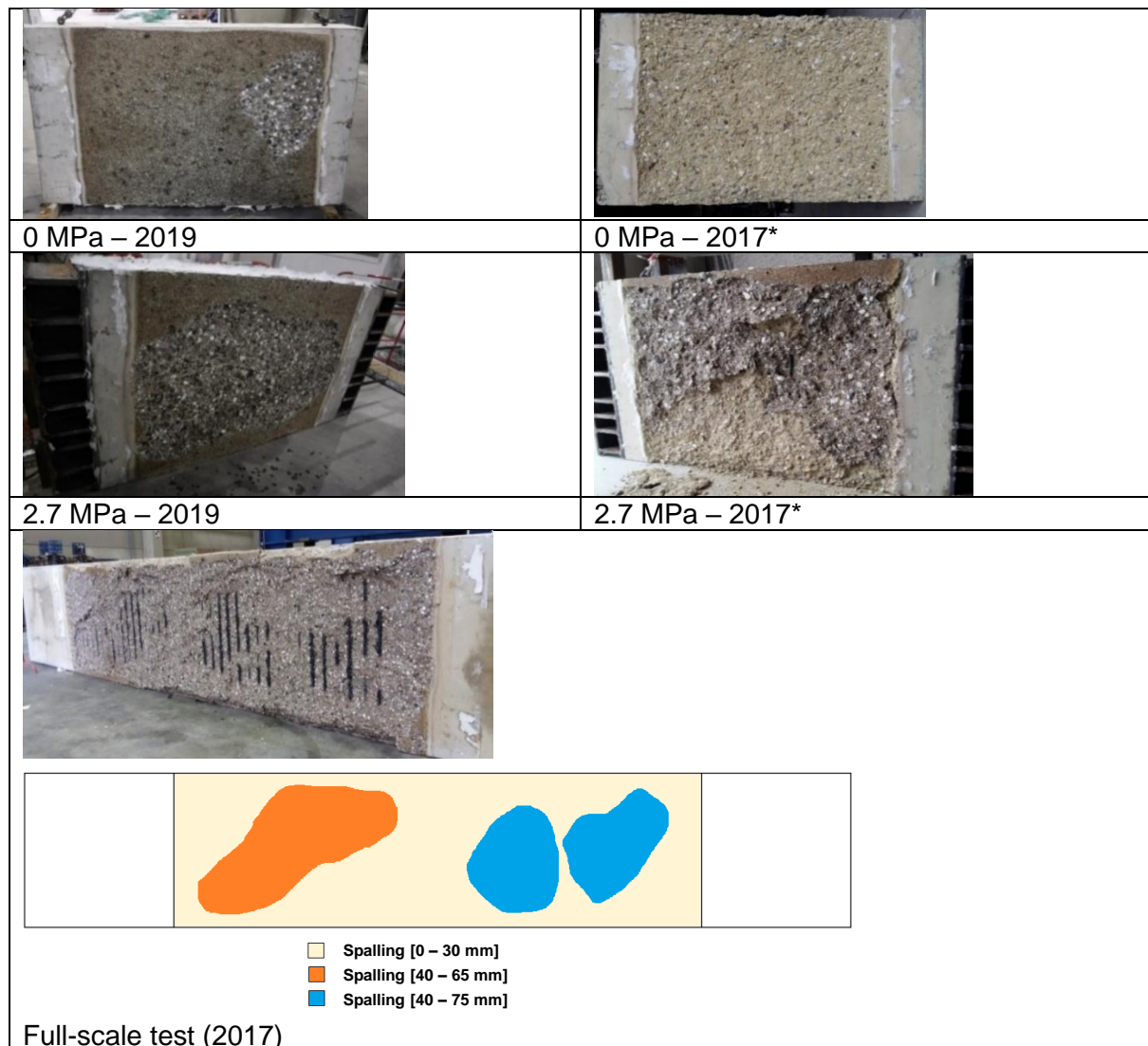
Regarding the reproducibility, the spalled surfaces are comparable between the two series – however the spalled depths are lower in the second series, which is probably partly due to the lower compressive strengths obtained for this cast (average strength lower by 10 MPa).



Table 10 Spalling results of the loaded slabs tested in FNTF research program

		Start/end of spalling		Average/max spalling in spalled area		Spalled area		Moisture content at the surface	
		2017	2019	2017	2019	2017	2019	2017	2019
Loaded slabs	0 MPa	4 min/ 7 min	3 min/ 4 min	NE*/ 30mm	15mm/ 20 mm	60%	25%	3.9%	4.1%
	1 MPa	-	1 min/ 3 min	-	19mm/ 32mm	-	98%	-	4.1%
	2.7 MPa	3 min/ 17 min	2min/ 3min	NE/ 70 mm	15mm/ 21 mm	82%	92%	3.9%	4.1%
	4.5 MPa	-	2 min/ 3 min	-	24mm/ 51mm	-	95%	-	4.1%
Full-scale test		2min/ 40 min	-	Fig 5/ 75 mm	-	100 %	-	3.6%	-

\*NE : not evaluated



\*Pictures have been taken after additional concrete fall-off due to rehydration of concrete

Figure 6 Exposed face of the specimens tested within the FNTF research program

## DISCUSSION

Based on the tests conducted in the two research programs, the following observations were drawn:

- Internal stresses:

Intermediate scale slabs with thicknesses ranging from 10 cm to 60 cm were tested (free expansion) in the framework of the CETU research program. The existence of a threshold above which the impact of internal stresses on spalling becomes less prominent was confirmed. The threshold was situated between 25 cm and 40 cm depending on the spalling sensitivity of the tested mixes. This confirms that a sufficiently thick slab is necessary for concrete spalling tests.

The results obtained on intermediate scale slabs can not be directly compared to the full-scale tests as the duration on the tests were not comparable (60 minutes versus less than 20 minutes).

- Restrained thermal expansion and constraints induced by mechanical loading:

Three 40 cm wall configurations were tested to evaluate the contribution of each parameter:

- without loading and free to expand,
- with external mechanical loading (approximately 3 MPa),
- with restraint using pretensioned bars opposite to the expansion,

as well as a tunnel lining full-scale test with the same thickness in the CETU research program.

The spalling of the wall that was free to expand was the furthest from tunnel lining full-scale test. On the other hand, the spalled area and the spalling depths were comparable between (i) the loaded and restraint configurations and (ii) the tunnel lining full-scale test. However, restrained thermal expansion configurations are very dependent on the tested concrete mix and its intrinsic thermal expansion. More tests with this configuration are needed to assess its representativity of a tunnel lining full-scale test. These wall configurations have not been further considered as they present some stability issues during the tests.

Intermediate scale slabs tests with restraint and external loading were also investigated in the FNTF research program. When comparing restraint and loaded configurations to the full-scale test, the best representativity in terms of spalling depths and spalled area was observed for the loaded slab configuration. In this program, tests on differently loaded slabs have shown (i) the importance of the presence of any load with regards to spalling and (ii) the best representativity seems to be around 3 - 4 MPa. The non-loaded slabs were the farthest from the tunnel-lining with regards to spalling.

## CONCLUSIONS

Two research programs have been conducted as an attempt to understand the relative impact of the main parameters influencing the spalling of concrete and to propose a design of a screening test setup that would be used to select the mix before a full-scale test. The screening test should be sufficiently severe to screen the materials and to be possibly representative of the cut-and-cover tunnel lining full-scale test, but it should be also simple, cost efficient and should not be more severe than the full scale test whose stress state is in adequation with the studied tunnel project.

At all the steps of the two projects, the studied test setups were compared to a corresponding tunnel lining full-scale test. The following conclusions can be drawn:

- The impact of the internal stresses due to the thermal gradient on spalling was confirmed, with the existence of a thickness threshold situated between 25 and 40 cm.
- The internal stresses due to the thermal gradient in a full-scale test cannot alone be representative of a tunnel lining full-scale test, however its thickness.
- Different screening tests have been investigated in the two programs: unloaded slabs, restraint slabs and loaded slabs. In the FNTTP program, a loaded 30 cm slab (load of 3 – 4 MPa) was found to yield the closest spalling results to the tunnel lining full-scale slab. The spalling of the non-loaded configuration was the furthest from the full-scale tests.

The question of whether a 40 cm thick non loaded slab is sufficiently representative of a full-scale test is raised and should be further investigated, as the results of the two experimental programs cannot be directly compared (different concrete mixes and testing conditions).

Future work should include comparison of non-loaded 40 cm thick slabs and 30 cm loaded slabs with respect to spalling. These results should also be confirmed and completed by running (i) repeatability and reproducibility tests and (ii) complementary tests with different concrete mixes that have different spalling sensitivities.

## REFERENCES

1. Robert F., Moreau B., and Bisby L., “Fire spalling of concrete: experimental parametric study and numerical modelling” In *International Workshop on Concrete Spalling*, Leipzig, 2015.

# Experimental investigation on the effect of water content profile on fire spalling

Bruno Fernandes<sup>1,\*</sup>, Hélène Carré<sup>1</sup>, Jean-Christophe Mindeguia<sup>2</sup>, Céline Perlot<sup>1,3</sup>, Christian La Borderie<sup>1</sup>

<sup>1</sup> Université de Pau et des Pays de l'Adour, E2S UPPA, SIAME, Anglet, France

<sup>2</sup> Université de Bordeaux, Laboratoire I2M, Talence, France

<sup>3</sup> Institut Universitaire de France (IUF)

\* Corresponding author (bruno.fernandes@univ-pau.fr)

## ABSTRACT

The fire spalling of concrete is a complex phenomenon involving different chemo-thermo-hydro-mechanical mechanisms. It can be influenced by many factors related to material (e.g. permeability, porosity and water content), geometry (e.g. shape and size) and environmental parameters (e.g. place, mechanical load and heating rate). Among these parameters, the water content is known to be a key factor for spalling risk, as many experimental works indicate that spalling risk is higher for concretes with high water content. Even if there is no clear consensus about the exact role of water content, it certainly plays a role in the local build-up of pore pressure. In addition, it affects the mechanical properties of concrete at high temperatures. It is worth noting that the global water content value is a key parameter for spalling and, more probably, the water content profile in the first exposed centimetres. This paper's main objective is to analyse the influence of different water content profiles on the spalling risk of concrete. Saturated concrete prisms were dried at 80°C for different drying periods (from 12 hours to 7 days) to obtain different water content profiles throughout the sample thickness. At the same time, small concrete cylinders underwent the same drying procedure to determine water content at different depths of the samples. After different drying periods, samples were exposed to a standard fire curve (ISO 834-1) with a constant uniaxial compression load. After each test, spalling volume and depth were evaluated through digital photogrammetry. Results allowed to link the spalling intensity according to the water content profile of the samples. As expected, spalling was strongly sensitive to the water content profile. The results provided new data for understanding the fire spalling phenomenon and underlined the importance of the water content measurement method for spalling assessment of concrete.

**KEYWORD:** Spalling, Fire Test, Concrete, Water Content Profile

## INTRODUCTION

The fire spalling of concrete is a complex phenomenon involving different chemo-thermo-hydro-mechanical mechanisms. It can be influenced by many factors related to material (e.g. permeability, porosity and water content), geometry (e.g. shape and size), and environmental parameters (e.g. mechanical load and heating rate) [1]. Among these parameters, the water content is a crucial factor for spalling risk. Previous works indicate that spalling risk is higher for concrete with high water content [2–6].

The effect of water content on concrete spalling is related to the build-up of pore pressure [4] - one of the theories behind the spalling phenomenon. Pore pressure build-up is a thermo-hygral process driven by water vaporisation and transport. During heating, the vapour moves towards the exposed surface and into the inner part of the concrete (nonheated). Its noteworthy that, if concrete is not saturated, the vapour will only move towards the inner part. In any case, owing to thermal gradients, the vapour may condense in the inner core, creating a saturated layer a few centimetres from the exposed side (the so-called 'moisture clog'). This zone blocks further vapour movement, leading to an increase in pore pressure. When stresses resulting from pore pressure exceed the tensile strength of concrete, spalling may occur [3,7–10]. It is noteworthy that other theories have also been studied in previous works, such as spalling due to thermal stresses [3,9,10] and spalling due to thermo-chemical mechanisms [10]. Most likely, spalling may occur as a combination of stresses due to pore pressure and thermal, mechanical and chemical stresses.

In any case, water content and water content profile play a vital role in the spalling risk assessment. This paper aims to analyse the influence of different water content profiles on spalling. To this, fire tests were carried out on concrete made with natural aggregate (NA). Before fire tests, initially saturated concrete prisms were dried at 80°C for different drying periods (from 12 hours to 7 days) to induce different water content profiles throughout the sample thickness, especially along the first centimeters of the exposed surface. After the drying period, concrete prisms were subjected to the ISO 834-1 [11] fire curve and a constant uniaxial compressive stress. Small concrete cylinders underwent the same drying procedure to determine the water content at different depths of the samples. For postfire assessment, spalling volume and depths were evaluated through digital photogrammetry. Lastly, spalling was examined in light of the different water content profiles.

## EXPERIMENTAL PROGRAM

### Concrete mixes

One mix was produced: concrete made with natural aggregates (NA). Cement was CEM II/A-L 42.5R by Eqiom, limestone filler was Betocarb HP-SC by Omya, and superplasticiser was ViscoCrete Tempo-483 by SIKA. Fine aggregate was alluvial sand with a fineness modulus of 3.10. The NA was made from diorite (Genouillac, France). Table 1 lists the material properties.

Table 1 *Material properties.*

Property	Sand	Natural Aggregate	
Grading Size	0/4	4/10	10/20
Density (kg/m <sup>3</sup> )	2650	2820	2840
Water absorption (%)	0.35	0.92	0.81
LA coefficient (%)	-	16	16

Concrete was designed to meet NF EN 206/CN:2014 [12] durability requirements for XD3 exposure class. Table 2 presents the mixture proportions for all mixes. For the mixing procedure, first aggregates and cement were mixed for 2 minutes. Then, water and SP were added and mixed for two minutes.

Fresh and hardened properties are listed in Table 2. For each mix, cylindrical specimens (11 x 22 cm) were cast to determine the compressive strength at 28 days (NF EN 12390-3 [13]). For the fire tests, prisms with dimensions of 20 x 20 x 10 cm (height x length x width) were cast. In addition, prisms of 15 x 15 x 10 cm (height x length x width) were cast for the water

content study. Samples were then kept submerged in water between 70 and 90 days, then subjected to the drying process (later specified).

Table 2 Mix design (in kg/m<sup>3</sup>) and properties.

Material	Mix
Cement	350
Filler	60
Sand	804.3
NA 4/10	331.7
NA 10/20	711.1
Water	175
SP (% of cement)	0.9
Slump (mm)	195
$f_{c28}$ (MPa)	47.0 ( $\pm$ 3.2)

### Water content analysis

A specific workflow was proposed to estimate the water content profile. From the saturated prisms of 15 x 15 x 10 cm, small concrete cylinders of  $\varnothing$  1 x 10 cm were cored (Figure 1a). Then, the curved surface (lateral) of the cylinders was wrapped with aluminium tape and placed in the oven for drying (Figure 1b). They were dried at 80°C and 3% RH for different drying periods (saturated, 12 hours, 1 day, 2 days, 3 days, 4 days and 7 days). Six cylinders per drying condition were evaluated. After this period, cylinders were removed from the oven. Then, they were sliced into small pieces of approximately 1 cm (Figure 1c) using dried sawing.

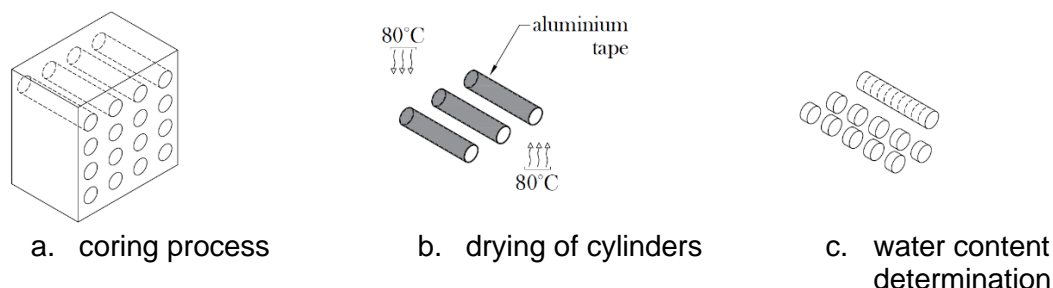


Figure 1 Water content analysis process.

Each small piece was measured and then dried (80°C and 3% RH) until mass stabilisation (mass variation less than 0.05%) to determine the water content in each one of the slices. The position of each slice was calculated based on piece thickness and the total height of the small cylinders. This method was done to take into account the thickness of the saw cut. With these two measures, the water content profile for each mix/condition was estimated. Since drying was symmetrical, half of the cylinder was mirrored to obtain a denser cloud of data, and better estimate the profile. Then, a regression analysis was done for each case to estimate the water profile curve.

Figure 2 presents three examples of the water content profile estimation. It shows the water content profile after 1, 4 and 7 days of drying. The scatter values of each piece were plotted together with a regression line. For this regression, a second-degree polynomial was used for the fit. Some variations from the individual values were observed, but they were expected given the small size of the cylindrical sample. In any case, the method seems to be an appropriate

estimation of the water content profile. The same procedure was done for all the studied conditions.

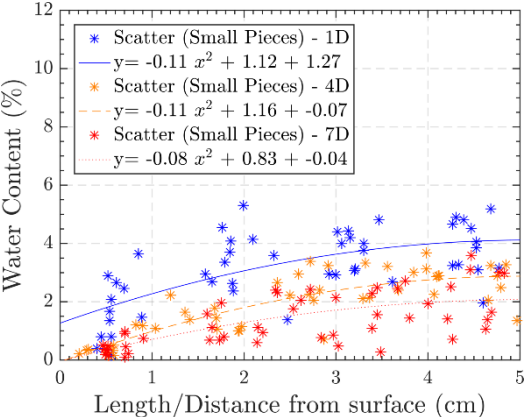


Figure 2 Water content profile after drying.

**Fire tests**

Spalling was evaluated by testing 21 concrete prisms subjected to a standard fire and uniaxial mechanical loading. Three prisms were evaluated for each drying condition. Saturated samples were removed from the water curing and sealed with aluminium foil tape in the four lateral sides (20 x 10 cm). Then, they were placed in the drying oven at the same conditions (80°C and 3% RH) and exposure days as the small cylinders (saturated, 12 hours, 1 day, 2 days, 3 days, 4 days and 7 days). After the referred drying period, samples were removed from the oven and went to spalling tests. The samples were also insulated with 12 cm of rock wool from both sides.

An intermediate-scale furnace was used. It is powered by a linear propane gas burner controlled during the test to follow the ISO 834-1:1999 [11]/NF EN 1363-1:2020 [14] fire curve. The furnace has an opening for an exposure surface of 20 x 20 cm. Three type K jacketed thermocouples were used to measure the heating curve. These thermocouples were placed in front of the furnace at 1cm from the heated face of the sample. This furnace was used in similar experimental studies [15–18]. A hydraulic press was used to apply an uniaxial loading of 5 MPa. The tested specimen was placed between two concrete blocks (top and bottom supports). First, the load was applied, and after stabilisation, the heating process was initiated. After 30 minutes, the heating was turned off, and, after 5 minutes, the sample was discharged. Some details of the test setup, including sample and furnace detail are shown in Figure 3.

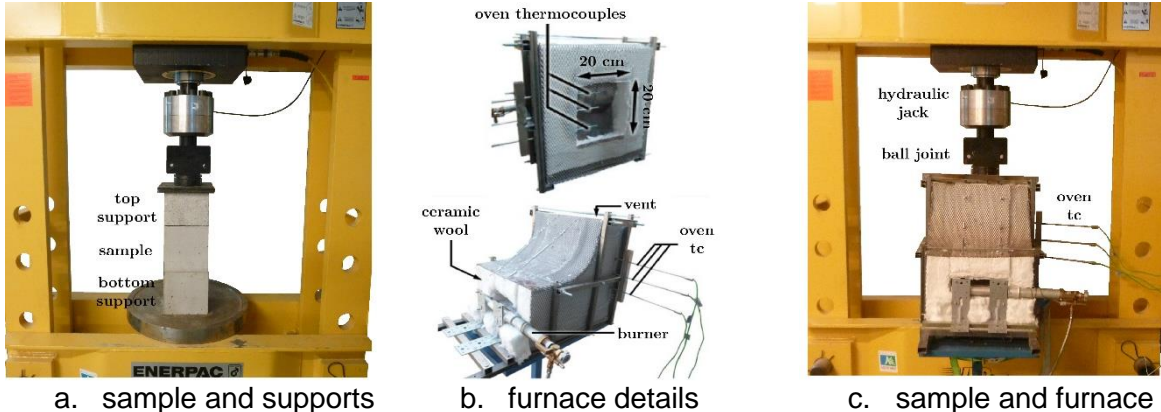


Figure 3 Experimental setup details.

The occurrence of every spalling event was recorded during each test. Figure 4 presents the time-temperature curves from all tests (average of the three thermocouples). The x marks indicate the time of the first spalling event for each sample. After the first spalling event, the temperature recorded distances from the fire curve. The main criterion adopted for test validation was whether the curve followed the tolerances up to the first spalling event. Hence, only one mix (sample 2 from NA-1D) was excluded from further analysis.

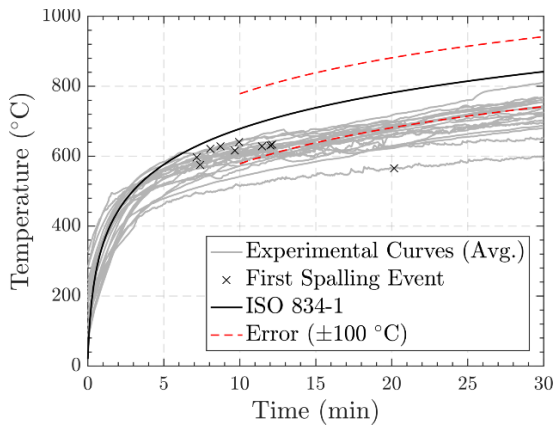


Figure 4 *Developed fire curves.*

Different postfire analyses were done. First, mass measurements were made before and after the fire tests. Digital photogrammetry was used to quantify the spalling (volume and depth). This approach involves image acquisition and processing, 3D reconstruction, mesh generation, and post-processing [19]. Samples were placed in a rotating table to orientate 3D reconstruction successfully. The camera (Panasonic DMC-GX80) was fixed on a tripod, and between each shot, the rotating table was turned 10°. A total of 36 images were obtained for each sample. The image processing and 3D reconstruction were done with Meshroom [20] software. The 3D model of each model was then processed (cleaned and scaled) using CloudCompare software [21]. A binary mesh of the 3D model was imported in a Cast3m [22] algorithm, which post processed the model to obtain the spalling volume and depths. The error between the dimensions measured by photogrammetry analysis and the caliper range from 1.06% to 2.07%, as show in Fernandes et al. [18].

## RESULTS

### Water content profiles

The water content profiles estimated from the measurements of the small pieces are presented in Figure 5. As expected, it shows the progressively drying of the sample. For example, after 2 days of drying, the NA samples showed 1.6% water content at 1cm, while after 7 days of drying, the water content at 1 cm is lower, close to 0.7%.



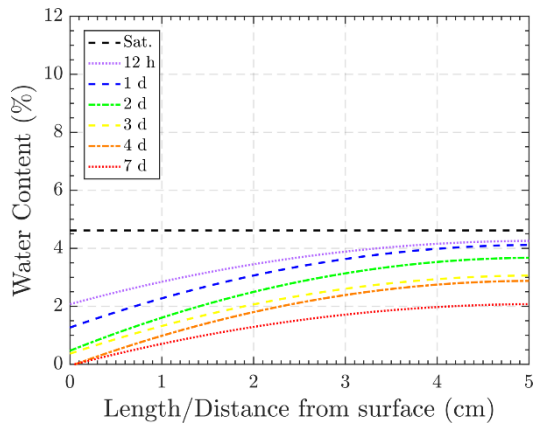


Figure 5 Water content profiles after different drying processes - curves are a regression (second-degree polynomial) of measured points.

### Postfire assessment of spalling

From photogrammetry, two indicators were chosen to evaluate spalling: the mean spalling depth and the spalled volume. Figure 6a shows the variation of spalled volume with drying period. First, at the saturated state, concrete showed a high spalling volume. It is noteworthy that the results are close to the ones obtained in previous works with similar conditions and the same test setup [18].

However, drying changed the observed behaviour. Samples presented higher spalled volume after 12 hours. It went from 2.4% saturation to 4.7% after 12 hours of drying. Further drying led to reduced spalling after 1 and 2 days of drying. The latter already shown relevant variations in spalling risk, given that, out of four samples tested at this drying condition, two did not spall, one presented small located spalling (0.1%), and one had high spalled volume (6.8%). Starting from 3 days of drying, no spalling was registered for all samples. Similar observations can be drawn from the evaluation of mean spalling depth (Figure 6b). Again, similar values from previous works were obtained at a saturated state [18] - 5.5 mm for concrete made with NA. Then, even after 1 day, drying reduces significantly the mean spalling depth.

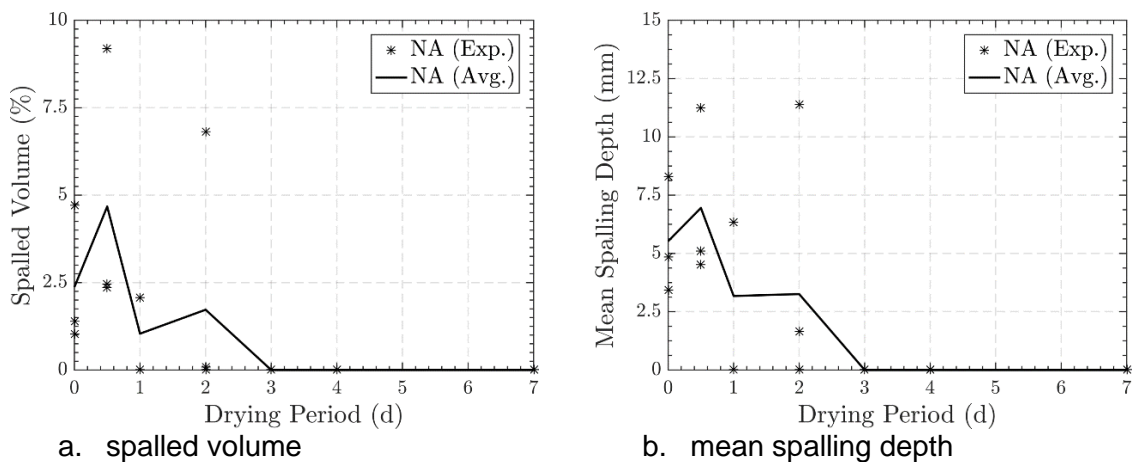


Figure 6 Evolution of spalling indicators for different drying periods.

To further evaluate the effect of the water content on the spalling behaviour, the water content was calculated at different depths using the regression curves. Figure 7 shows mean spalling depth versus water content ( $W_c$ ) at 1, 1.5 and 2cm from the exposed surface. The trends for

all depths indicate the same: an increase of the mean spalling depth with the rise in water content. These graphs also give an idea of the minimal water content needed in the 2 first centimetres for possible trigger spalling. For NA, spalling was observed when water content was higher than 1.3% and 2.1% at 1 cm and 2 cm, respectively.

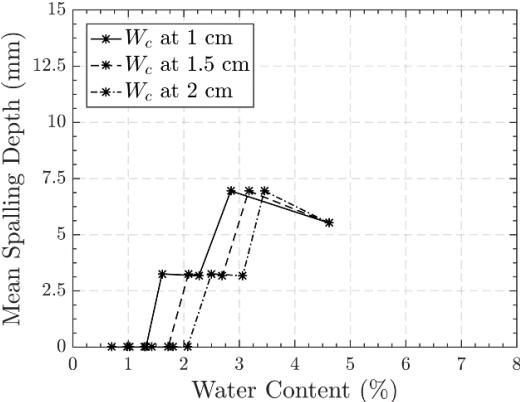


Figure 7 Mean spalling depth versus water content at different depths.

The results herein showed the influence of the water content profile in the spalling risk evaluation. However, evaluating the water content or the amount of water needed to trigger spalling is complex. When analysing the first centimetres, part of the water evaporates, and another moves towards the centre to form the so-called 'moisture clog'. To further investigate the triggering water content, three different graphs are presented in Figure 8.

First, Figure 8a plots the mean spalling depth versus the water content calculated at this mean depth. For this first case, except for one spalled sample (out of 14), water content at the mean spalling depth was higher than 1.5% for NA. Figure 8b plots the mean spalling depth versus the mean of water content between the surface and the mean spalling depth. As expected, this average water content is lower. In this case, the critical water content was around 1%. In the last case, Figure 8c, the mean spalling depth is plotted against the mean water content in all the first 5 centimetres (half cylinder). In this case, the value is dependent on the sample size. For this case, spalling happened with a water content of 2.6%.

It is noteworthy that this analysis shows a difference between the 'triggering' water content. The first two approaches are more conservative. These water contents agree with the ones obtained by Maier et al. [5] They observed that concrete spalling is likely to occur for more than 1% of water content. The last approach indicates a higher water content. It is noteworthy that the value is close to the Eurocode 2 [23] recommendations, which states that explosive spalling is unlikely to happen if the moisture content is lower than 3% by weight.

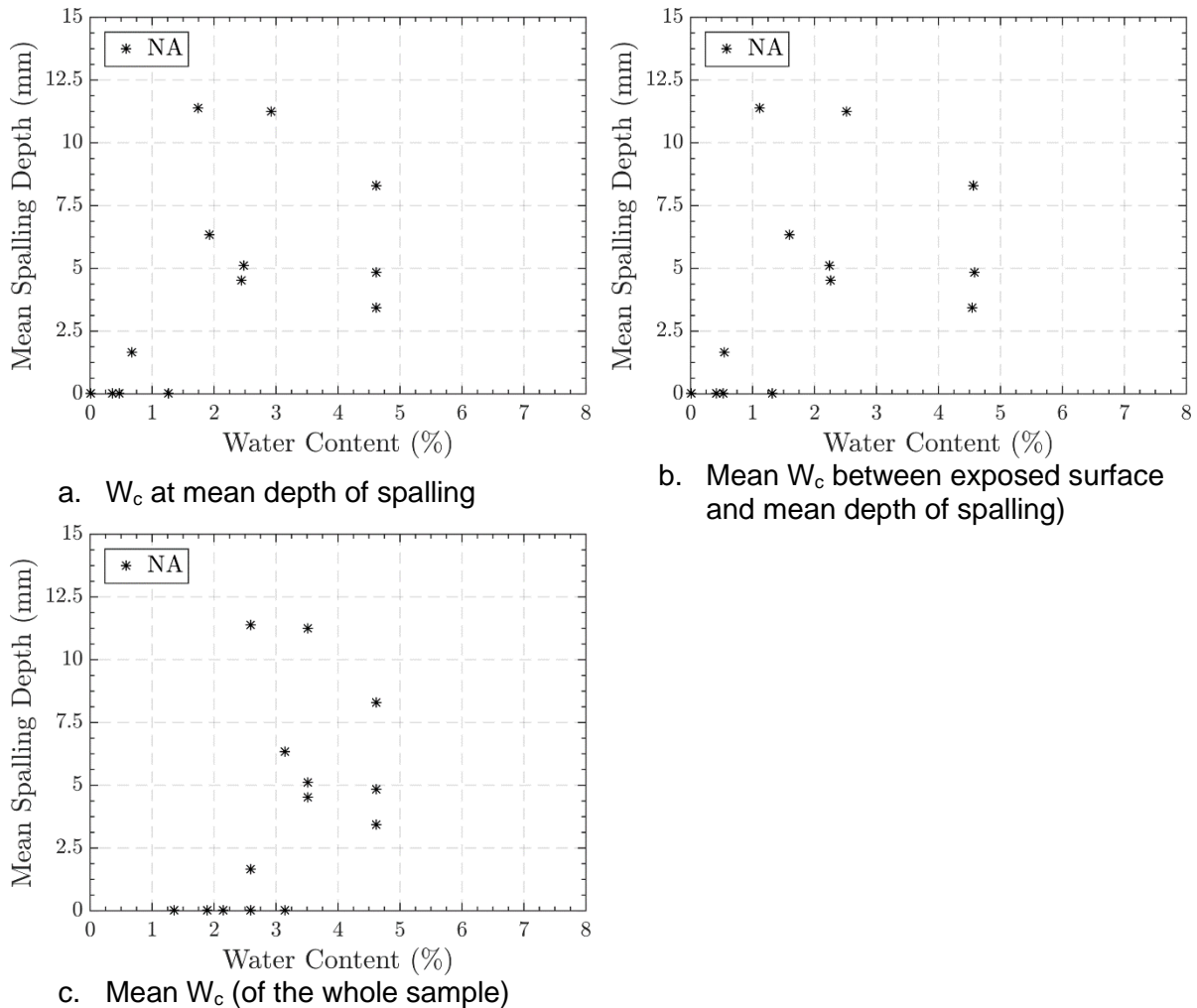


Figure 8 Mean spalling depth versus water content.

## CONCLUSIONS

This paper presented an experimental investigation on the effect of different water content profiles on the spalling sensitivity of concrete. Based on the results, the following conclusions were drawn:

- The water content measurement through a small cylinder showed potential to correctly estimate the water content profile along the thickness of samples before fire test.
- After 7 days of drying, concrete made with NA showed a low water content in the first centimetres (0.7% at 1 cm depth, for example).
- Drying significantly reduced the spalling risk of concrete. After only 3 days of drying at 80°C, no spalling was registered.
- Most of the spalled samples showed a water content higher than 1.5% at the mean spalling depth. This value was even lower in the case of average water content at the first centimetres - between surface and spalling depth. This possible threshold is closer to previous works. At the same time, when evaluating the mean water content through all depth, the critical value is close to 2.6% - value closer to what is currently specified in Eurocode 2 [23].

## REFERENCES

1. Khoury, G.A., "Effect of fire on concrete and concrete structures", *Progress in structural engineering and materials*, **2**, 429–447, 2000.
2. Phan, L. T., " Pore pressure and explosive spalling in concrete", *Materials and structures*, **41**, 1623-1632, 2008.
3. Mindeguia, J.-C., Carré, H., Pimienta, P., La Borderie, C., "Experimental discussion on the mechanisms behind the fire spalling of concrete", *Fire and materials*, **39**, 619-635, 2015.
4. Li, Y., Yang, E., Zhou, A., Liu, T., "Pore pressure build-up and explosive spalling in concrete at elevated temperature: A review", *Construction and Building Materials*, **284**, 122818, 2021.
5. Maier, M., Zeiml, M., Lackner, R., "On the effect of pore-space properties and water saturation on explosive spalling of fire-loaded concrete", *Construction and Building Materials*, **231**, 117150, 2020.
6. Maier, M., Saxer, A., Bergmeister, K., Lackner, R., " An experimental fire-spalling assessment procedure for concrete mixtures", *Construction and Building Materials*, **232**, 117172, 2020.
7. Shorter G. W., Harmathy T. Z., "Discussion on the fire resistance of prestressed concrete beams", *Proceedings, Institute of Civil Engineers*, **20**, 313, 1961.
8. Harmathy T. Z., "Effect of moisture on the fire endurance of building elements", *ASTM Special Technical Publication*, **385**, 74-95, 1965.
9. Ma, Q., Guo, R., Zhao, Z., Lin, Z., He, K., " Mechanical properties of concrete at high temperature-A review", *Construction and Building Materials*, **93**, 371–383, 2015.
10. Liu, J., Hai, K., Yao, Y., "A new perspective on nature of fire-induced spalling in concrete ", *Construction and Building Materials*, **184**, 581–590, 2018.
11. International Organization for Standardization, "ISO 834-1: Fire-resistance tests -- Elements of building construction -- Part 1: General requirements", Geneva, 1999.
12. Comité Européen de Normalisation, "NF EN 206/CN:2014 - Concrete - Specification, performance, production and conformity", Brussels, 2014.
13. Comité Européen de Normalisation, "NF EN 12390-3: Essai pour béton durci - Partie 3 : résistance à la compression des éprouvettes", Brussels, 2003.
14. Comité Européen de Normalisation, "NF EN 1363-1: Essais de résistance au feu - Partie 1 : exigences générales", Brussels, 2020.
15. Carré, H., Perlot, C., Daoud, A., Miah, M.J., Aidi, B., " Durability of ordinary concrete after heating at high temperature ", *Key Engineering Materials*, **711**, 428–435, 2016.
16. Miah, M.J., "The Effect of Compressive Loading and Cement Type on the Fire Spalling Behaviour of Concrete", Université de Pau et des Pays de l'Adour, 2017.
17. Sultangaliyeva, F., "Formulation of fluid fire-resistant fiber reinforced cementitious composite: Application to radioactive waste disposal", Université de Pau et des Pays de l'Adour, 2020.
18. Fernandes, B., Carré, H., Mindeguia, J.-C., Perlot, C., La Borderie, C., "Spalling behaviour of concrete made with recycled concrete aggregates", *Construction and Building Materials*, **344**, 128124, 2022.
19. Cavaco, E., Pimenta, R., Valença, J., "A new method for corrosion assessment of reinforcing bars based on close-range photogrammetry: Experimental validation", *Structural Concrete*, **20**, 996-1009, 2019.
20. AliceVision, "Meshroom: A 3D reconstruction software", <https://github.com/alicevision/meshroom>, 2018.
21. G. Software, "Cloud Compare", <http://www.cloudcompare.org/>, 2021.
22. Commissariat à l'énergie atomique et aux énergies alternatives, "Cast3M", <http://www-cast3m.cea.fr/>, 2020.

23. Comité Européen de Normalisation, “ Eurocode 2: Design of concrete structures - Part 1-2: General rules - Structural fire design”, Brussels, 2004.

# Comparative study of concrete spalling of Large-scale test with a Mobile furnace test

Kamakshi Parwani<sup>1,\*</sup>, Jos Bienefelt<sup>1</sup> & Tomas Rakovec<sup>1</sup>

<sup>1</sup> Efectis Nederland, Bleiswijk, Netherlands

\* Corresponding author

(kamakshi.parwani@gmail.com, +31685055750)

## ABSTRACT

Over the last few years in the Netherlands, there has been a significant amount of research and testing into the behaviour of concrete in tunnels at high temperatures, particularly with the RWS fire curve. This has become of chief interest since it was found that the concrete is not always as fire resistant as it was designed to be. Since many tunnels have been constructed in the Netherlands and around the world, with the expectation that concrete may not "spall; this causes safety concerns in case of fire. The best method to determine the concrete behaviour at high temperatures continues to be through testing. For the new tunnel projects, it is possible to determine the concrete behaviour including its protection system through extensive lab testing prior to construction of the tunnel. However, for existing tunnels that is not possible. In the latter case, a mobile furnace provides an ideal solution, as a part of a tunnel cannot be transported to a laboratory. The furnace can be placed on both the tunnel wall and the ceiling and hence all the other parameters of the tunnel and concrete are automatically considered.

The first prototype of the Efectis mobile furnace (Mobifire<sup>®</sup>) was developed almost 15 years back to bridge the gap between laboratory testing and testing of existing structures. It has been extensively used in tunnel projects worldwide and is regularly improved. However, the challenge with the mobile furnace is the size of the specimen that is exposed to the fire load. With the Efectis mobile furnace, a maximum of 1 m<sup>2</sup> (1 m x 1 m) surface of the specimen can be exposed, while large scale testing in laboratory like the one at Efectis, generally has an exposed surface of at least 8 m<sup>2</sup>. In order to quantify the difference between the large-scale testing and the mobile furnace testing in a tunnel, Efectis decided to perform a comparative study. In this study, two slabs cast in a concrete factory with the same concrete mix were chosen, and the same load and same protection system were applied to both the slabs. One slab was tested on the Efectis large scale furnace, while the other was tested with the mobile furnace. Both these slabs were exposed to the RWS fire curve and tested till the occurrence of spalling. The results of the comparative study show that in this specific case, large scale test was more conservative by a margin than the mobile furnace test. Other parameters such as spalling temperature and time to first spalling are compared and discussed in the report. This study aims to be a starting point in the comparative study between the two methods.

**KEYWORD:** RWS fire curve, Mobile furnace, Fire protection

## INTRODUCTION

Due to the requirements from the government authorities around the world, the new and existing tunnels are being subjected to stricter requirements for performance in a fire scenario. In general, A concrete segment/element, is susceptible to fire-induced spalling when exposed to the RWS fire curve. Due to the findings of spalling sensitivity of even low strength concrete [1], it has been a point of concern in the Netherlands. Recent tunnel projects, such as

Rotterdamsebaan, in Den Haag, the Netherlands, exposed this fact further [2], making it essential to test the spalling sensitivity of concrete prior to finalizing the concrete mix used in the tunnel.

One of the commonly used methods is to protect the concrete with fire protection boards. The boards can be applied to the concrete in a pre-fixed or a post-fixed method. In a pre-fixed method, the boards are applied before the casting of concrete as lost formwork. On the other hand, in post-fixed system, the boards are applied with the help of anchors after the concrete is cast and has a developed microstructure.

The passive fire protection system of boards can be tested with different thicknesses to arrive at the optimal thickness for a specific tunnel project. These fire tests can be performed on concrete slabs cast with the same concrete mix as used in the tunnel and protected with a fire protection system at the fire laboratory prior to testing. However, lab testing is not possible for the existing tunnels due to the sheer logistics involved in cutting part of the tunnel concrete (which in most cases is a safety risk) and transporting it to the laboratory. In the Netherlands, a popular method for assessing the performance of existing tunnels is with the help of a mobile furnace. Efectis has developed a mobile furnace which has an exposed surface area of 1 m<sup>2</sup> [3]. The exposed surface value is much lower than that of a full-scale furnace at the Efectis facility which is typically 8-10 m<sup>2</sup> for a RWS fire curve. The difference in the testing method brings other factors to the forefront that are different, such as the effect of the cold rim in a small-scale test (mobile furnace), which is much higher than in a large-scale test performed in the lab. Another important difference is the effect of joints on the protection system. The size of boards indirectly leads to more joint length, which can impact the spalling behaviour in a fire test.

Due to these underlying differences, it was decided to make a comparison study to see the differences between the two tests. The first step in this regard was taken by CSTB [4], although on an unprotected concrete slab which was not mechanically loaded during the test. With this study, the effect of loading thereby restricted deformation and the corresponding compression in concrete is also considered. This brings the comparison much closer to the actual situation in a tunnel. Also, in the older tunnels, if the concrete is found to be susceptible to spalling, the method used to make the concrete fire-proof is most probably the application of fire protection boards. Hence a comparison method with protection will help in better selection of the fire protection system.

## **TEST SPECIMENS**

Two identical test specimens of size 5 m x 2.4 m x 0.4 m were manufactured simultaneously are chosen for this study. By utilizing an external loading frame, a compressive stress of 10 MPa is applied for both cases in the concrete (uniformly distributed over the cross-section). As the purpose is to compare the two fire tests, only the exposed area plus a few mm was protected for both specimens. For the large-scale test, an area of approx. 4.2 m x 2.4 m was protected with post-fixed fire protection boards. For the mobile furnace test, an area of 1.25 m x 1.25 m was protected with fire protection boards. The exposed area in the large-scale test is about 4.0 m x 2.4 m, whereas the exposed area for the mobile furnace test is 1.0 m x 1.0 m.

### **Concrete mix properties**

The concrete mix properties of both test specimens have been described in Table 1. The average concrete moisture content for the tested slabs was found to be 5.5%

Table 1 Concrete Mixture

Description	Properties	Weight in kg per m <sup>3</sup>
Strength class		
Cement	CEM III/B 42.5 N	310
Aggregate	Limestone	1061
Sand	Riversand 0/1	35.5
	Riversand 0/4	852.5
Plasticizer 1	Cretoplast 35% conc.	0.47
Plasticizer 2	Cugla LR-9400 30% conc.	0.93
Water cement factor	0.499	
Slump class	S3	
DMax	32 mm	
Concrete compressive strength (28 day)	44.1 N/mm <sup>2</sup> (average of 3 cubes)	
Splitting tensile strength	3.7 N/mm <sup>2</sup> (average of 3 cubes)	

### Protection material and thickness

Tunnel grade Calcium Silicate boards of 22 mm thickness were used for the Fire Protection. The main reason for choosing a relatively low material thickness was to initiate spalling in the concrete in order to be able to compare the time and temperature when the spalling occurred between the two tests. Table 2 gives the details of the protection system used in the two tests.

Table 2 Properties of fire protection material

	Large-scale test	Mobile furnace test
Thickness nominal	22 mm	22 mm
Thickness measured (average)	22 mm	22 mm
Density measured	892 kg/m <sup>3</sup>	877 kg/m <sup>3</sup>
Moisture content (on the day of the fire test)	3.94 %	3.79 %

## EXPERIMENTAL SETUP

For the large-scale test, the concrete specimen was placed on top of the furnace and the concrete segment was loaded with the help of an external loading frame. A uniform load of 10 MPa was applied to the segment with hydraulic jacks, as shown in Figure 1 and Figure 2. Figure 3 shows the placement of the specimen in the large furnace before the fire test. Figure 4 shows the boards and the thermocouples applied for the large-scale tests. For the mobile Furnace test, the loading frame was placed on concrete blocks, as shown in Figure 5. Figure 6 shows the mobile furnace specimen just before the fire test. It can be seen that only a part (1.25 m x 1.25 m) of the large slab (5 m x 2.4 m) is protected with fire protection boards. Figure 7 shows the placement of the thermocouples in the test specimen. The two fire tests were both conducted in the horizontal placement as it is the most conservative scenario for the test with protection boards.

### Large-scale test

The protection boards were applied to the concrete specimen according to the test procedure of Efectis and RWS [5]. Here, one full-sized board (2500 mm x 1200 mm) was mounted onto the concrete slab in the centre, surrounded by smaller boards. All types of joints between the boards were included in the test, including T joint and X joint, as prescribed by the test





### Mobile Furnace test

The Fire protection board system was applied according to the test procedure of Efectis and RWS for mobile furnace [5]. Nine thermocouples (TK1-9) were applied to the concrete surface, as shown in Figure 7. A total of three thermocouples were placed behind the joints between the boards and six directly behind the boards.



Figure 5 Experimental set-up for mobile Furnace test

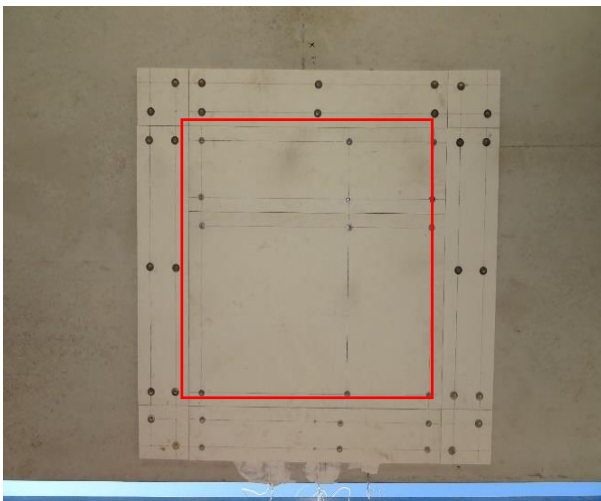


Figure 6 Experimental set-up for mobile Furnace test ( the middle 1m<sup>2</sup> is tested as marked in red)

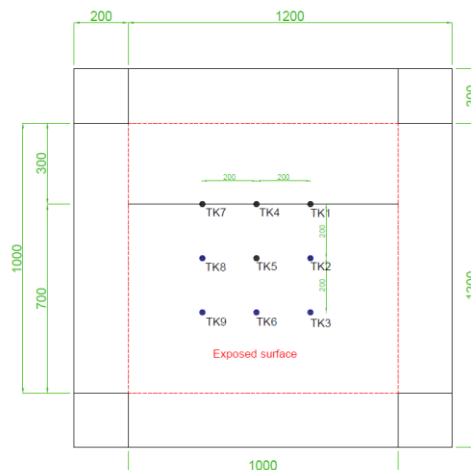


Figure 7 Positioning of the boards and thermocouples (thermocouples TK 1, 4 and 7 are placed at the board joints)

### FURNACE CONDITIONS

The aim of the fire test was to heat the specimen for up to 120 min according to the RWS fire curve. For the large-scale test 10 Inconel sheathed type-K thermocouples were used to measure the furnace temperature. For the mobile furnace test, 4 Inconel sheathed type-K thermocouples were used to measure the furnace temperature., This kind of thermocouples are a better solution for RWS fire curve than the standard plate thermometers used for standard fire curve, as their reaction is very slow to sudden increase in temperature in the

initial phase of the fire curve which can lead to incorrect information about the situation in the furnace.

## OBSERVATIONS

For the large-scale test, the onset of spalling was observed at 66 min. The first spalling during the mobile furnace test occurred at 81 min. The measured temperatures are provided in Figure 8 and Figure 9.

It was noted that the temperatures in the joints during both tests were much higher than the rest of the measurements. This is highlighted in Figure 8 where it can be seen that thermocouples 5, 6, 21 and 22 (all present at T or X joints) recorded highest temperatures before the start of spalling during the large-scale test. The same phenomenon was visible during the mobile furnace test where thermocouples TK1 and TK4 (both present at the joints) recorded the highest temperatures before spalling, see Figure 9. This can also be understood by the scatter in the temperatures recorded. The difference between the maximum and minimum temperatures during the large-scale test at the onset of spalling was around 319 °C as shown in Table 3. The scatter was much lower with the mobile furnace test, with the difference between the maximum and minimum temperatures being around 139 °C. Since the joints in the mobile furnace test have a smaller joint length, and are only between two boards, the difference can be attributed to it. This highlights the fact that in a spalling test, the joints between the fire protection system can be critical to the overall spalling behaviour of the specimen.

In both the fire tests, the furnace was shut down within a few minutes (less than 5 min) of the occurrence of spalling. This can be noted in the temperature measurements. In Figure 10, 11 and 12, the photographs of the specimen of large scale test after the fire test can be seen. The main reason for stopping the test immediately is safety. Another reason for stopping the fire test was to observe the exact location where the spalling started, however, due to damage on almost the entire concrete surface, it is difficult to point out the start location.

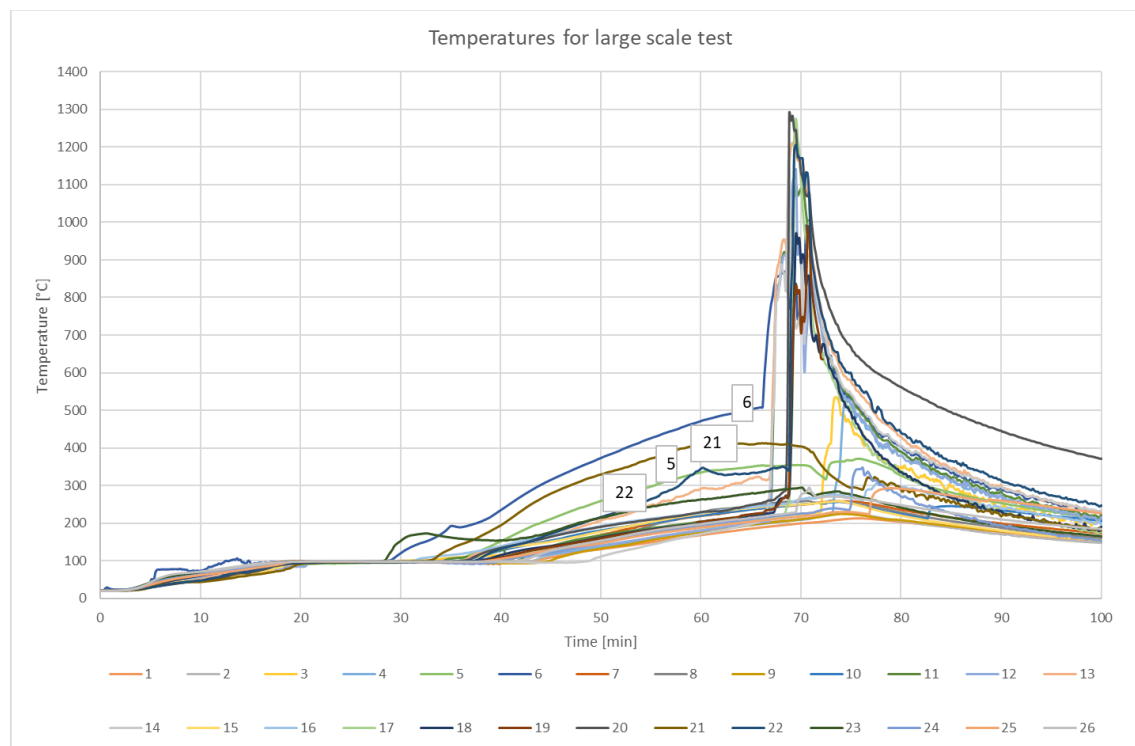


Figure 8 Temperatures for Large Scale test

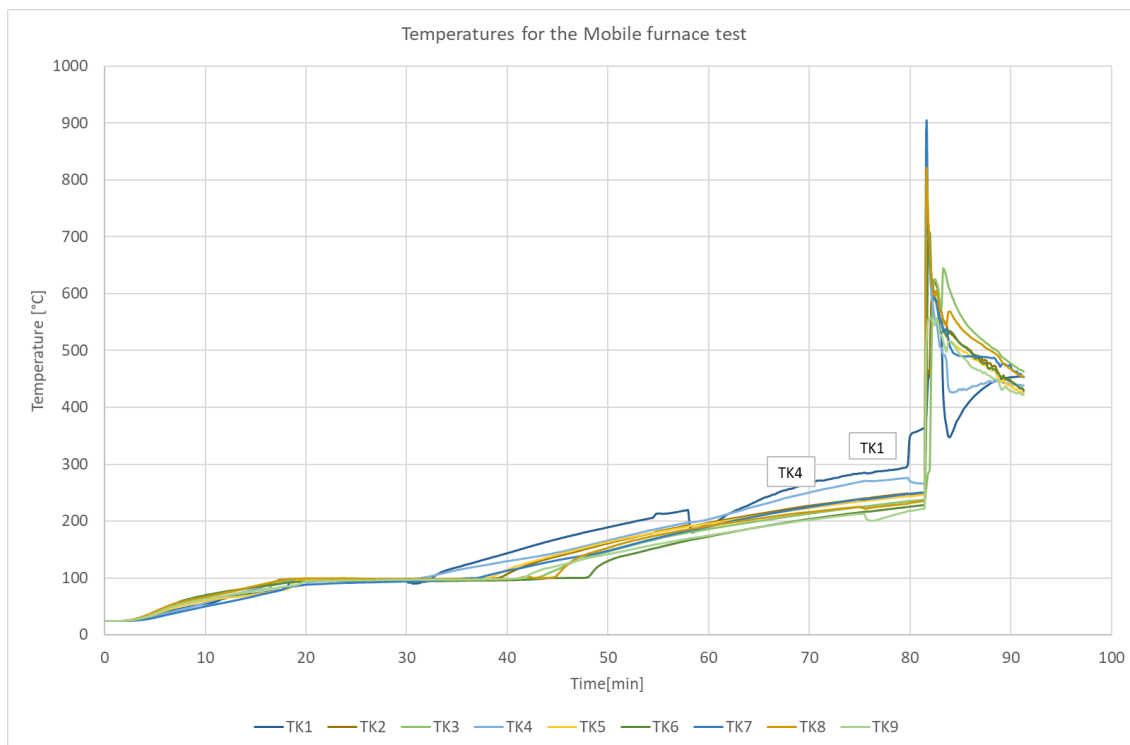


Figure 9 Temperatures for mobile Furnace test

Table 3 Minimum, Maximum and Average temperatures recorded at 61 min and 88 min

<b>66 min</b>	<i>Large scale test</i>	<i>Mobile furnace test</i>
Minimum	188 °C	192 °C
Maximum	507 °C	244 °C
Average	248 °C	212 °C
<b>81 min</b>	<i>Large scale test</i>	<i>Mobile furnace test</i>
Minimum	Not applicable	221 °C
Maximum	Not applicable	360 °C
Average	Not applicable	254 °C



Figure 10 Photograph taken in the furnace 1 day after the fire test (large scale test)



Figure 11 Photograph taken after the specimen was taken out of the furnace (large scale test)





Figure 12 Photograph taken after the specimen was taken out of the furnace day after the fire test (large-scale test)



Figure 13 Photograph of the mobile furnace test specimen immediately after the fire test (mobile furnace test)

## DISCUSSION

### Time of spalling

The time of spalling for the large scale test is 66 min whereas the time of spalling of the mobile furnace test 81 min. The large scale test is more conservative by 15 min.

However, It is often observed in the past that even between two exact specimens of a large-scale test, a slight difference in the spalling time is possible. Hence, given the complex nature of spalling itself, it is considered an acceptable time gap.

### Average temperature

The average temperature between the two fire tests is shown in Figure 14. The temperatures are very similar till they reach the moisture plateau. At the time of the spalling of large scale test specimen at 66 min, the average temperature difference between the two tests is 36 °C. This is also an acceptable temperature difference

### Temperature behind the joints

The temperature scatter in a large-scale fire test is much higher than the mobile furnace test. In Figure 15, the thermocouples are divided in two categories, the one behind the joints and the one behind the boards and their averages are plotted. For the large-scale fire test, the difference between the two sets of temperatures only increases after the end of moisture plateau and continues till the occurrence of spalling.

However, for the mobile furnace test, the difference is about 38 °C at the occurrence of spalling. This is attributed to the large size boards and the more vulnerable joint types such as T and X joints present in the large-scale test. This requires further investigation.

In Figure 15, all temperature lines have similar temperature development except the temperature behind joints for large-scale tests. This is expected due to the shrinkage of the boards, thereby exposing the joints during the duration of fire as also seen in [2].

Since the joint behaviour is a strong determining factor in this study, other parameters, such as the effect of the cold rim is expected to be limited. Additionally, as concrete is protected by the boards, the concrete surface temperatures are much lower. The cold rim effect could however be different in case of an unprotected concrete element test where the surface temperatures of exposed concrete will be much higher.

It is therefore difficult to make a definitive conclusion about the two methods. However, the fact that the two test results are close from a global perspective, gives the opportunity to further investigate this.

### Chronology of failure

In both fire tests, it is expected that spalling of concrete led to board failure, which in turn probably led to more spalling. Although it is impossible to prove this without a footage of a furnace camera. It is known to the authors based on previous experience that this concrete is sensitive to spalling. And the fire protection with a sufficient thickness, if tested with a concrete mix which performs well in fire (such as mix with pp-fibres) maintains usually its integrity for the whole test period.

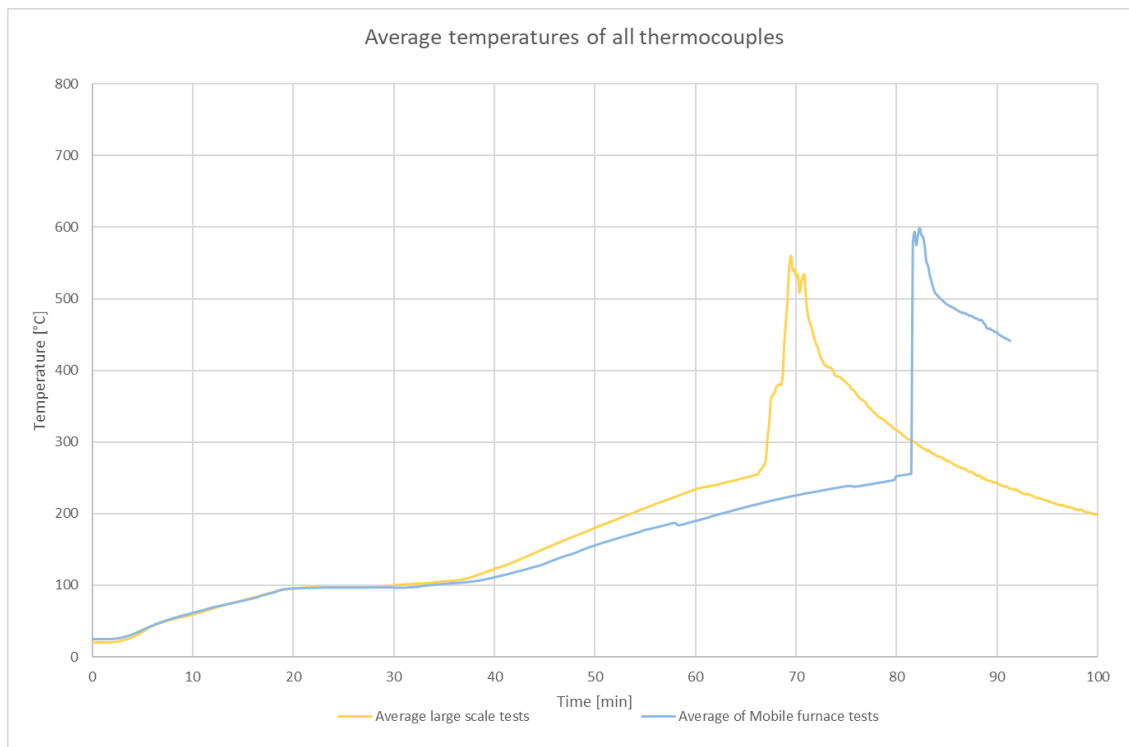


Figure 14 Average Temperatures for fire tests

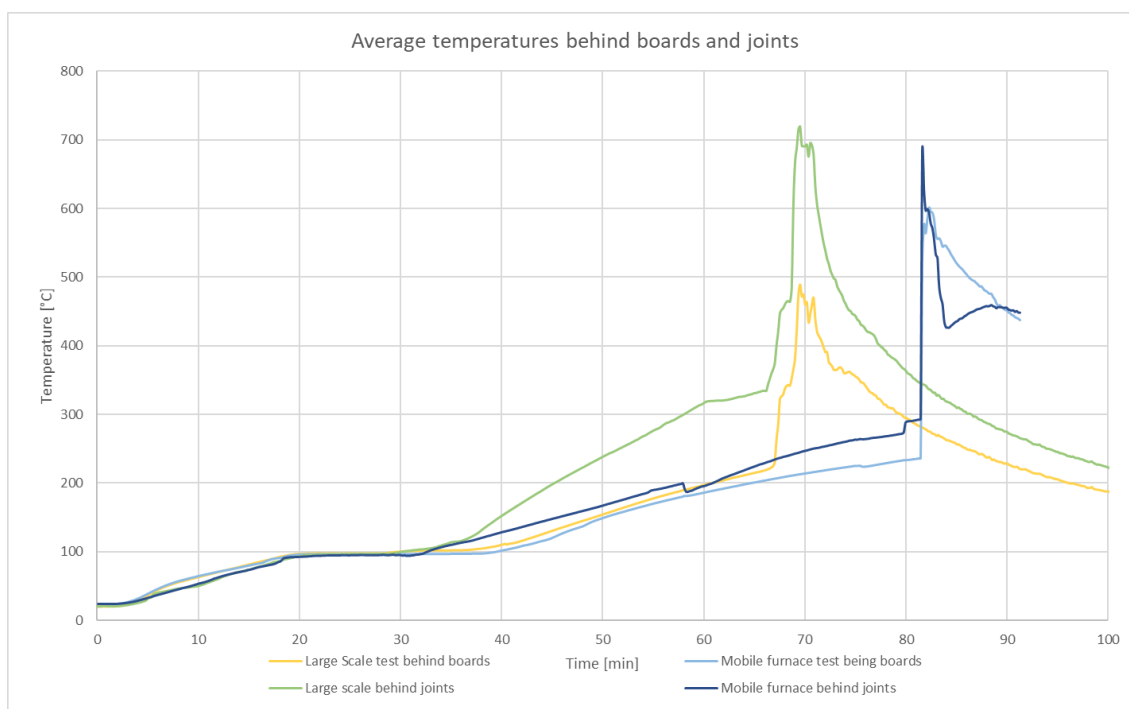


Figure 15 Average Temperatures for fire tests behind joints and behind boards

## CONCLUSIONS

The aim of this study was to draw a comparison between the large scale furnace tests performed in the laboratory to the mobile furnace tests which are used on-site. The results help in understanding the closeness of the two types of testing methods and also shed light on the differences. Two tests' specimens with the same concrete mix were protected with tunnel grade fire protections boards of 22 mm nominal thickness and loaded with a uniform compressive stress of 10 MPa and subjected to the RWS fire curve.

It was noted that the temperatures at the concrete interface of a large-scale test and a mobile furnace test can be comparable if no joint behaviour of the fire protection system is considered as shown in Figure 14 and Figure 15. If the temperatures behind the joints are considered, there is a large scatter between the temperatures observed even within a single specimen. Based on the data, it is observed that the joint behaviour in the fire protection system can be an important factor affecting the spalling behaviour of the test specimen.

In this study, the large-scale test is more conservative (as it spalled earlier at 66 min) and hence lab testing continues to be good method for the design of fire protection system for new tunnels. For the existing tunnels, as it is not a possibility to perform large-scale laboratory testing, mobile furnace offers a good solution.

With this comparison study, it is difficult to draw strong conclusions about the two test methods, hence it is recommended to continue the comparison study with more specimens to draw a better conclusion about the testing methods.

## REFERENCES

1. Waart, van der, T., Breunese, A.J., Jansson, R., Bostrom, L., Annerel, E., "Spalling behaviour of a non-spalling qualified concrete", Proceedings of the 4<sup>th</sup> International Workshop on Concrete Spalling due to Fire exposure, Leipzig, Germany, 8-9 October 2015.
2. Parwani, K., Bienefeld, J., Rakovec, T., Haring, F., "Fire behaviour of large scale loaded tunnel segment tests for project Rotterdamsebaan, the Netherlands", IABSE Congress Ghent 2021 – Structural Engineering for Future Societal Needs, 22-24 September 2021
3. Vermeer, M., Pieters, B., Breunese, A., "Mobile furnace for determining spalling sensitivity of existing concrete tunnel linings", Proceedings of the 2nd RILEM International Workshop on Concrete Spalling due to Fire Exposure, 385-392, Delft, The Netherlands, 05-07 September 2011
4. D. Pardon et al., "In situ concrete spalling risk assessment in tunnel by means of a mobile oil-fired furnace," presented at the 6th International Workshop on Concrete Spalling due to Fire Exposure, Sheffield, United Kingdom, 19–20 September 2019.
5. Efectis, "Fire testing procedure for concrete tunnel linings and other tunnel components," Efectis Netherland BV, Netherland 2020, vol. R0695:2020.

# Port said Suez Canal tunnel segments – Laboratory fire spalling testing

Pierre Pimienta<sup>1,\*</sup>, Roberto Felicetti<sup>2</sup>, Dimitrios Rizos<sup>3</sup>, Philippe Rivillon<sup>1</sup>,  
Stéphane Charuel<sup>1</sup>, Tarek Amin<sup>3</sup>

<sup>1</sup>Centre Scientifique et Technique du Bâtiment, CSTB, Marne la Vallée, France

<sup>2</sup>DICA - Politecnico di Milano, Milano, Italy

<sup>3</sup>Orascom Constructions, Cairo, Egypt

\* Corresponding author (pierre.pimienta@cstb.fr  
84, avenue Jean Jaurès, 77447 Marne-la-Vallée Cedex 2, France)

## ABSTRACT

Two twin tunnels have been constructed to cross the Suez Canal, one at Port Said near the North entrance of the Suez Canal and one at Ismailia city in the midst of the Canal. In order to assess the fire behavior of the segmental lining, large scale fire resistance tests were carried out in CSTB. Tests were performed at full scale on the segments manufactured in the 2 construction factories.

This paper will focus on the results of 3 tests carried out on the segments from the Port Said tunnel.

Mechanical stresses on the segments were applied as a combination of vertical and horizontal loads to simulate the maximum in situ stresses exerted on the tunnel lining due to earth and water pressure. Concrete segment samples were subjected to the well-known RWS temperature curve (with a maximum temperature = 1350 °C) for a duration of 2 hours. Temperatures, loads and displacements at different locations were recorded, during the heating and the cooling phases. The main aim of the test was to assess the sacrificed thickness of concrete and quantify the spalling phenomena during fire testing.

Two tests were carried out on full segments at the age of 5 and 23 months. Spalling depth on this second segment was much lower.

A new non-destructive technic has been employed during the last test: ultrasonic Pulse Echo (UPE). This technic was adapted by Politecnico di Milano to monitor concrete damage and spalling progression during a fire test. Findings from this innovative method are presented.

**KEYWORD:** Full-scale tests, Tunnel Segments, Monitoring, Non-destructive Technic, Ageing

## INTRODUCTION

As part of the “The Suez Canal Corridor Area Project” – crossing mainland Egypt to Sinai - two twin road tunnels projects have been constructed. The dual-carriageway tunnels projects aim to connect Sinai with other Egyptian provinces, providing a gateway for investment opportunities, accelerating the development of the North Sinai province and populating the region to increase security. The tunnels’ external lining diameter is 12.60 m with segment thickness of 60 cm.



Fire safety and structural integrity, in case of fire hazard, are amongst the main concerns in case of road tunnels where heavy trucks and dangerous goods are allowed to enter the tunnels. In order to assess the fire behaviour of the segmental lining, large scale fire tests have been carried out on full-scale segments under mechanical stress. The segments have been produced at the construction factories of the project under the actual project conditions.

The CSTB center, located close to Paris in France, was appointed to carry out the fire load tests on full-size segments for the tunnel projects under the Suez Canal. Samples size was 4.5 meters long, 2 meters wide and 60 cm thick. Part of the tests results were presented by Pimienta et al [1].

Compressive mechanical stresses at the intrados are one of the main parameters influencing the risk of spalling. During the test process, a combination of horizontal and vertical loads with the appropriate eccentricity have been applied on the segments. Applied horizontal and vertical loads were respectively 7300 kN and 1750 kN in order to simulate the 12 MPa anticipated in situ stress, due to earth and water pressure.

Samples were subjected to the RWS temperature curve - developed in the Netherlands (temperature higher than 1300 °C) - for a duration of 2 hours followed by an almost linear cooling phase of 2 supplementary hours.

In addition to the tests carried out on the full segments, several tests have been carried out on couples of two half segments. The latter is also essential since the tunnel ring consists of an assembly of precast reinforced concrete segments with joints between the segments. Consequently, it is possible to assess the fire resistance and the response of the lining at the joint locations during the fire incident, where the mechanical stresses are expected to be higher due to the stress concentration at the reduced contact area between the adjacent segments. Tests on two half segments have been presented by the authors in a previous paper [1].

This paper presents a new test carried out in 2019 on a full segment at the age of 23 months old and the obtained results. In many cases, in order to avoid the thermal shock of the furnace walls and because of the difficulty to determine the spalling depth fields on hot samples, samples are removed from the furnace and spalling depth measurements are carried out one day after the fire test. For this test, spalling depth fields have been determined about 2 hours after the end of the test with a 3D laser scanner. The influence of measuring depth quickly after testing when severe temperature curves are applied to concrete samples will be discussed.

The paper presents also the test results from the fire tests carried out on segments during the project execution when the samples' age was only 5 months.

In order to allow the real-time monitoring of spalling progression during fire tests, the Ultrasonic Pulse Echo (UPE) technique was also implemented by Felicetti and Lo Monte [2]. Description of the developed technic, main results and comparison with the spalling depths values will be presented.

## **TEST EQUIPMENT AND PROCEDURES**

### **Test specimens**

The segments have been prepared and cast in the segmental lining factory. Their geometry is the following:

- dimensions of the reinforced concrete segment: 4524 mm x 2000 mm x 600 mm,
- curvature radius R: 5600 mm.

The concrete mix design is given in Table 1. Due to the aggressive groundwater conditions containing a high percentage of sulphates and chlorides the cement type was CEM III-A. In addition, the concrete contained silica fume (8.5 % by weight of cement content). In order to reduce the risk of concrete spalling in the event of fire, 2 kg/m<sup>3</sup> of monofilament polypropylene fibres were added (length = 6 mm and diameter = 18 microns). Water/cement ratio was 0.33. The concrete cover of the steel reinforcements on the intrados (the exposed side) was 50 mm.

Table 1 *Mix design of the concrete.*

Constituent type	Constituent designation and characteristics	Content
Cement	Cement CEM III A from CEMEX Factory	470 kg/m <sup>3</sup>
Silica fume	Micro Silica from Russia	40 kg/m <sup>3</sup>
Total water	-	172 kg/m <sup>3</sup>
Sand	0-5 mm sand from Abo Shalaby Ismailia	772 kg/m <sup>3</sup>
Aggregates	Crushed stone aggregates size 5-14 mm from Ataka crushers in West side (dolomite)	900 kg/m <sup>3</sup>
Admixtures	Pantrahit PC180 from Ha Be.	6.2 kg/m <sup>3</sup>
Polypropylene fibres	PP Fiber from BASF length 6 mm	2 kg/m <sup>3</sup>

Small cylindrical samples were prepared with the same concrete as the segments for the determination of concrete compressive strength at the time of test execution. This was determined according to the European standard NF EN 12390-3. Mean value determined at the time of testing was 64.8 MPa. Mean water content determined on concrete pieces taken from the segment concrete edges was between 2.0 and 2.5 %.

The segments were equipped by CSTB personnel with the assistance of the producer company with more than 40 thermocouples (Figure 1). Six lines of 1 mm glass silk K type thermocouples were installed at different heights. In each line, thermocouples were positioned at 25, 50, 75, 100, 150, 200, 250 and 300 mm depths from the exposed surface. The series of 8 thermocouples were beforehand assembled along a thin metal rod. Additional thermocouples were installed on the upper side of the longitudinal reinforcing bars in the segments.

After a period exceeding 1 month, segments were transported with the small cylindrical samples by trucks and boat to CSTB in France. In CSTB, the samples were stored in the laboratory hall until the tests date. The fire resistance test presented in this paper was carried after a period of 23 months.

Tests were carried out in the extensively large and modular gas furnace "Vulcain"; allowing experimentation on 7 m long samples in the horizontal direction and on samples of 9 m in height. Gas burners total power can be as high as 13.5 MW. During the test phase, temperatures and displacements were recorded at different locations during the heating and the cooling phases.

#### Load application

An original mechanical loading equipment was designed and produced in CSTB. It is represented in Figures 2 and 3. It consists in:

- one horizontal frame with one 2400 kN jack and two 4500 kN jacks;
- one vertical frame with two vertical 2000 kN jacks.

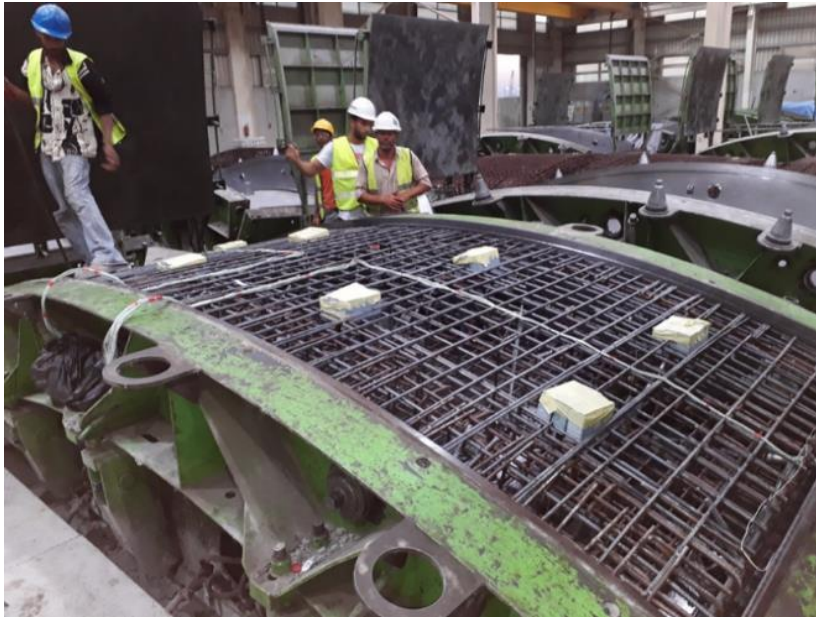


Figure 1 Steel reinforcement cages in the mould and thermocouples.

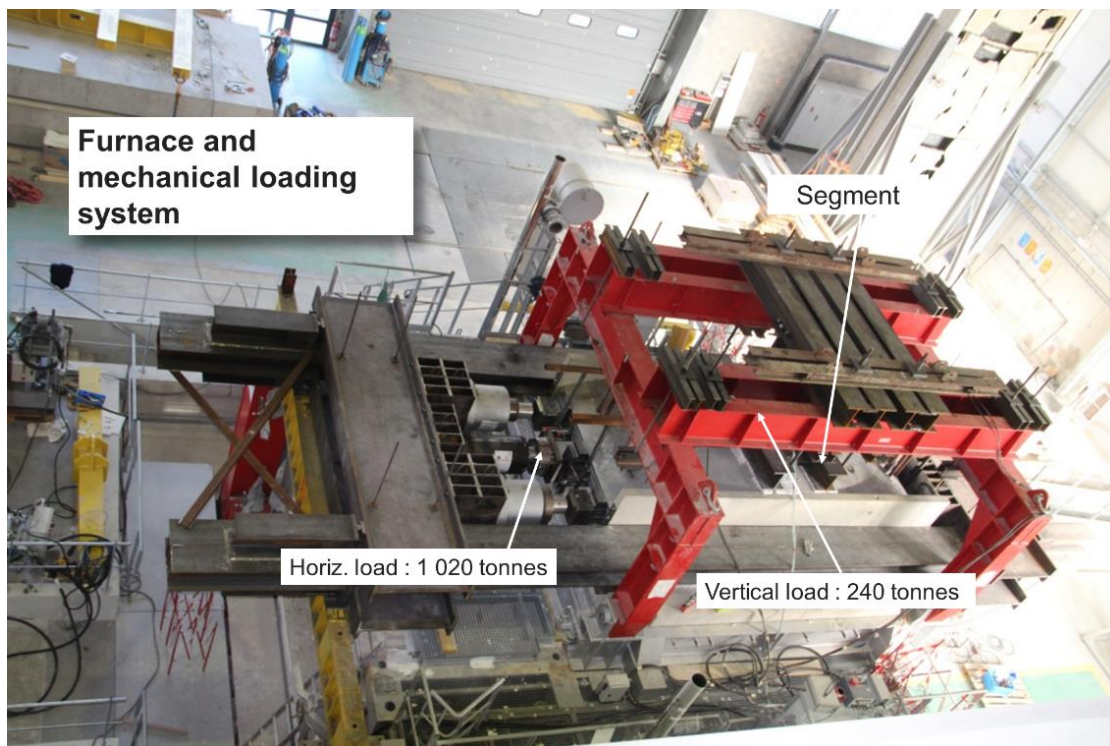
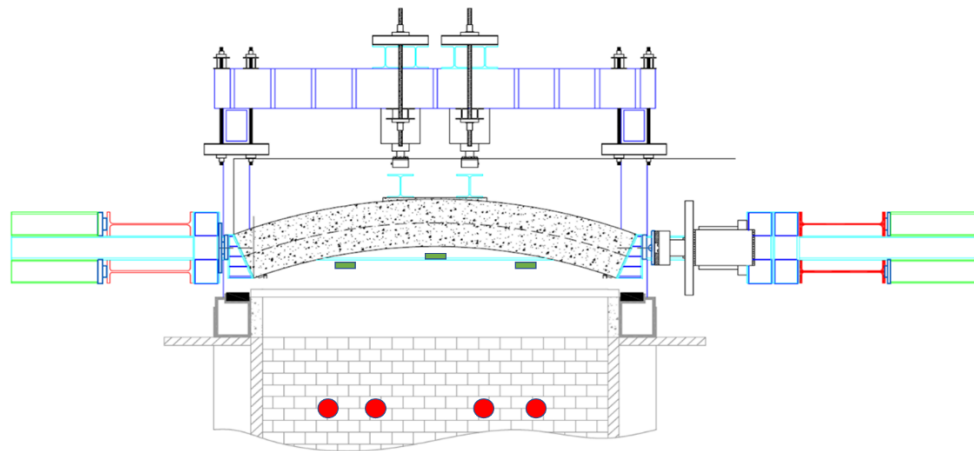


Figure 2 Top view of the furnace, the mechanical loading system and the segment.

The in situ calculated and monitored stresses at the intrados of the tunnel lining tubes was 12 MPa. In order to reach this value, applied horizontal and vertical loads were respectively 7 300 kN and 1 750 kN. In order to reproduce the desired stresses, the horizontal load was applied with an eccentricity of 105 mm above the segment mid height. A mortar layer was applied on the top of the segment in order to obtain a flat and horizontal surface to vertically load the sample.



*Figure 3 Schematic view of the furnace, the mechanical loading system and the segment. The position of the 8 burners and the 6 furnace plate thermometers are represented respectively in red and green.*

CSTB equipment allows to maintain constant either the load or the position during the fire test, once a target load is reached. It was decided that vertical load be maintained constant during the entire test. Thus, vertical displacements were possible to occur during the test. The position of the horizontal jacks was blocked during the fire test. Thus, the horizontal load change was possible.

It is also to be noted that before commencing the fire test both horizontal and vertical loads had to be increased gradually at the same time and not one after the other in order to avoid cracking the segments by provoking at intermediate states of the loading too high tensile stresses in the intrados or the extrados of the segment.

Horizontal and vertical displacements were measured with Solartron potentiometric sensors and wire sensors: 4 sensors in the horizontal direction and 2 sensors in the vertical direction.

### **Applied temperature curve**

The furnace was heated by means of the 8 burners positioned in this section of the chamber (Figure 3). The first 120 min of the fire exposure (ascending branch and the beginning of the descending branch) complied with the RWS curve. This first stage was followed by an almost linear cooling phase of 2 supplementary hours. The temperature at the end of this second stage was approximately 200 °C.

The temperatures were measured by using six plate thermometers located at 10 cm from the exposed face of the segments and recorded during the test, in accordance with standard NF EN 1363-1. The 6 plate thermometers were positioned on each side evenly distributed along the furnace 4 m length and at 50 cm from the sides (Figure 3).

The main aim of the tests was to assess and quantify the spalling phenomena during the fire tests and the affected concrete thickness due to its exposure to the very high temperature. Two endoscopic cameras allowed to display in real-time the behaviour of the whole surfaces exposed to the fire and record it.

### **Spalling depths fields determination**

Spalling depths have been measured on the same day and 4 days after the test with a 3D laser scanner, FARO Focus 3D X30. The measurement carried out the same day was performed about 2 hours after the end of the temperature cooling phase and 1 hour after removing the segment from the furnace.

### **Ultra-sonic pulse velocity (UPE) measurements**

In order to allow the real-time monitoring of spalling progression during fire tests, the Ultrasonic Pulse Echo (UPE) technique was implemented by Felicetti and Lo Monte [2]. The principle is to trigger very short ultrasonic pulses (1.5 cycles at 50 kHz) at the segment extrados and to detect the returning signal after complete back-reflection at the fire-exposed intrados (Figure 6). The total time of flight is governed by the combined effect of the element thickness and the material quality (pulse velocity). Concrete damage due to heating translates into a gradual increase, while spalling events lead to sharp reductions in propagation time. The method was implemented by means of a dry-point contact shear-wave sensor array (M2502 by ACS) fitted with a square wave pulser, a high gain amplifier and a digital scope. The sensor was installed in the central point of the segment and could monitor about 1 m<sup>2</sup> of the exposed intrados. The shift of propagation time was calculated based on the best cross-correlation between the current and the initial reflected echoes.

## **TEST RESULTS**

### **Thermo-mechanical behaviour**

As it has been described above, the position of the horizontal jacks was blocked during the fire test. Thus, the horizontal load change was possible. It was recorded a low increase of the load during the fire test mostly due to the thermal expansion of the concrete. The maximum determined horizontal load change was lower than 10 %. It is to be noted that the thickness of tested segments was high (60 cm) and temperatures were little affected over about 70 % of the height of the segments. When horizontal jacks are blocked, horizontal load changes should tend to be larger when thinner segments are tested.

Vertical and horizontal displacements have been measured in different locations. Curves versus the time are not given in this paper. Results can be summarized as follows: measured horizontal and vertical displacements were lower than 2 mm. This result can appear contradictory to the previous information on horizontal deformations. However, it is important to specify that the constant horizontal position was maintained by locking the jacks. Thus, the horizontal load change was possible. During the heating up process, the horizontal load increased by about 500 kN due mainly to the thermal dilation of the concrete. The frame, made of very thick steel elements, is very rigid. It is, however, very long too. Then, the load variations during the test led to an elongation of the frame, and thus of the segment, of about 1 mm.

### **Spalling depths**

Spalling was observed very early after the start-up of the furnace, during the first minute. The frequency of the events was quite constant during about 5 min and then decreased. Spalling stopped after 8 min.

Four pictures from the segment taken at different times are given in Figure 4. Figure 4a is a screenshot from the recorded video with one of the endoscopes after 8 min test. We can clearly observe the relief related to the spalling phenomena. Spalling depth is low. The reinforcement



is not visible which means that spalling depth is lower than 50 mm. It is to be noted that, in the pictures from the endoscopes, the relief appears exaggerated at the beginning of the test. Spalling depth is quite homogeneous in Figure 4b taken in the furnace just after the cooling phase. We just can observe the fall of a flake in the upper left corner of the picture. A large number of flakes have fallen down during handling the segment out of the furnace (Figure 4c). The phenomena continued until the 3D laser scanning (Figure 4d). In this picture, most of the visible concrete at the end of the test has disappeared. Fallen concrete pieces are visible at the foot of the segment. The measured thickness of concrete crust pieces was between 8 and 9 mm.

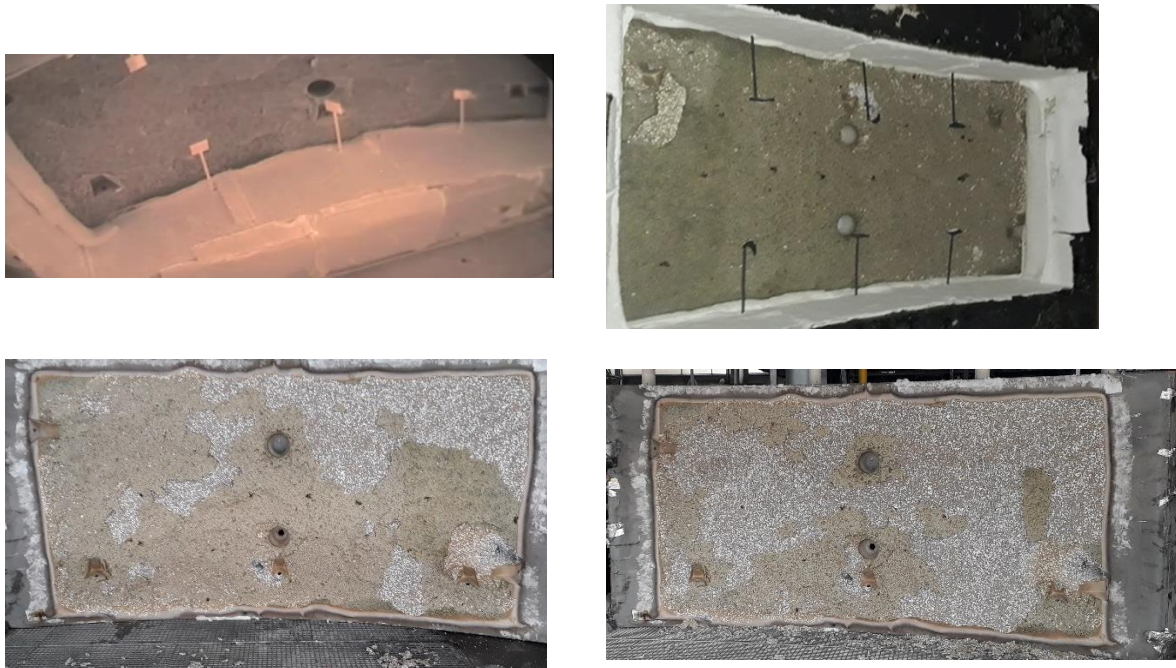


*Figure 4 Four pictures from the segment taken at different times: in the furnace during the fire test after 8 min taken with one of the 2 endoscopes (Figure 4a – up, left), in the furnace after cooling down the temperature (Figure 4b – up, right), just after removing the segment from the furnace (Figure 4c – down left), 1 hour after removing the segment from the furnace during the 3D laser scanning (Figure 4d).*

Spalling depth field determined from 3D laser scanning about 2 hours after the end of the temperature cooling phase and 1 hour after removing the segment from the furnace is given in Figure 5.

The zones corresponding to the remaining crust layers in Figure 4d are visible in Figure 5. Surprisingly, part of the values is positive. This is explained by the fact that in addition to the loss of concrete due to the spalling phenomena (negative values in Figure 5), the material expanded below the surface with partial detachment of concrete layers. We indeed observed bumps on the segment and could hear by hammering the surface that there were voids below. Although the segment was removed after a 4-hour cooling phase and the temperature reached in the furnace was below 200°C, we partly attribute the phenomena observed after removal from the furnace (loss of concrete and partial detachment of concrete layers) to the thermal shock of the direct exposure of the segment to the ambient air of the laboratory.

Spalling depths are higher in 2 zones:

- upper left quarter with depth values between 30 and 38 mm.

- central part with depth values between 20 and 26 mm.

By considering that there was no expansion (no partial detachment) in these 2 areas and that the thickness of the fallen crust before the measurement was 8 mm, the spalling depth at the end of the fire test could have been between 22 and 30 mm and 12 and 18 mm respectively. Spalling depths values to be used in the calculations are the ones during the fire test exposure. From the measured values and the observation, we tend to estimate these values before the crust falls down. Calculated values are given in Table 2. The mean value is estimated to be close to 4 mm and maximum value to be 30 mm.

Determined values after 4 days are given in Table 2 too. During the 4 days period, the few remaining crust pieces and part of the concrete on the surface fell down (spalling depth increase). At the same time, additional expansion with partial detachment of concrete layers has occurred in some locations (spalling depth decrease). The two phenomena tended to compensate each other over the whole area. The mean value was little changed (from  $\approx 12$  mm to 13 mm). On the other hand, the maximum value increased significantly (from 38 mm to 48 mm). The reinforcement bars were visible in a few locations.

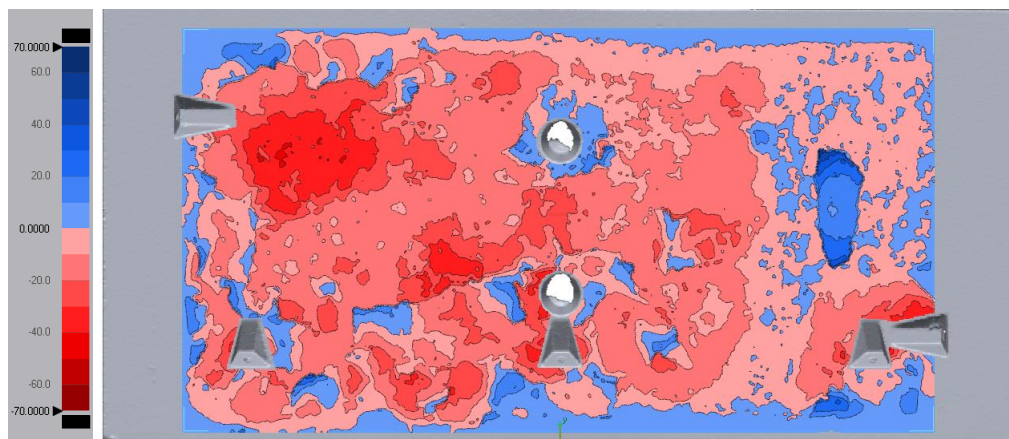


Figure 5 Spalling depth field determined from 3D laser scanning. Values are given in mm.

Table 2 Spalling depth values determined after 2 hours and 4 days.

Spalling depths	Mean value	Maximum value
Determined values from direct measurements after 2 h	$\approx 12$ mm	38 mm
Estimated values after 2 h by taking into account the 8 mm crust fall down	$\approx 4$ mm	30 mm
Determined values from direct measurements after 4 days	13 mm	48 mm

These comparative results show the importance of the timing of spalling depths measurements after the test when severe temperature curves are applied on concrete samples. Spalling depths measurements after 2 hours have shown that too early exposure of the concrete to the ambient temperature can induce too severe thermal shock. In our experiment, this have led to the partial detachment of concrete crusts (with some positive values) and the fall down of concrete pieces. Spalling depths measurements after 4 days are higher and the sample shows additional concrete degradation and fall down.

### Ultra-sonic pulse velocity (UPE) results

As explained before, the sensor was installed in the central point of the segment and could monitor about 1 m<sup>2</sup> of the exposed intrados (Figure 6). The results show that three spalling events occurred in the first 6 minutes, leading to a total reduction of propagation time by 4.5, 10 and 21 microseconds. By considering the initial shear wave velocity (2.7 km/s) and the expected material decay (average temperature in the detaching splinters ranging between 70 and 650°C) the corresponding total depths of spalling are 6, 13 and 21 mm.

The last value is relatively consistent with the estimated result of 3D laser scanning in the central region of the segment (between 12 and 18 mm).

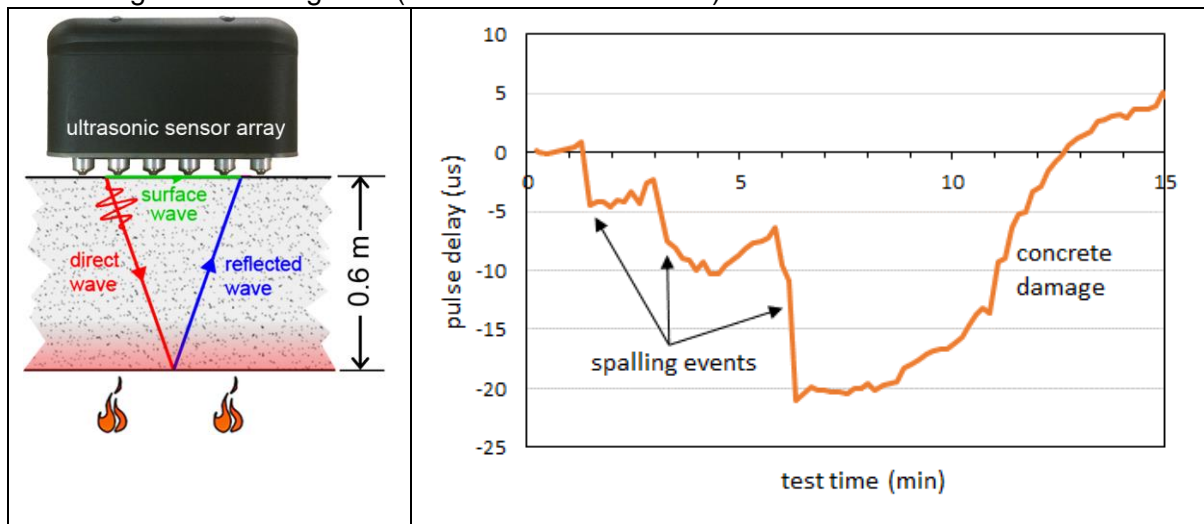


Figure 6 Ultrasonic Pulse Echo (UPE) technique principle (left) and pulse delay versus time (right), showing a sharp decrease at each spalling event and a smooth increase due to cover damage.

## RESULTS ANALYSES

### Results comparison between tests carried out at different age

Two previous tests have been performed on two other segments: one single segment and one two half segment [1]. They were manufactured at the same time and received on the same date at CSTB. Table 3 compares the ages, the determined water content ranges and the spalling depths measurements determined, without a thermal shock exposure, 1 day (age = 5 months) and 4 days (age = 23 months) after the tests.

The 3 tests have been carried out under the same conditions (same mechanical and thermal loads). Results clearly show a drastic reduction of the spalling sensitivity of the concrete segments after 23 months. As written before, moisture content is one of the main influencing parameters on concrete fire spalling [3 – 5]. The water content decrease from 4.2 – 4.8 % (5 months) to 2.0 – 2.5 % (23 months) must then be the main reason for the spalling sensitivity reduction.



*Table 3 Spalling depth determined at 5 months (1 day after the test) and 23 months (4 days after the test).*

	Age	Water content (%)	Mean spalling depth	Maximum spalling depth
Full segment	5 months	4.2 – 4.8	57 mm	103 mm
Two half segments	5 months	4.2 – 4.8	59 mm	110 mm
Full segment	23 months	2.0– 2.5	13 mm	48 mm

### **Spalling concrete behaviour**

Concrete mix included 2 kg/m<sup>3</sup> of monofilament polypropylene fibres. Their length and diameter were 6 mm and 18 microns respectively. It has been shown in many experiments that polypropylene fibres can significantly reduce the risk and the amount of spalling [3 – 5]. However, as presented above, spalling phenomena were observed, in particular during the tests carried out after 5 months. Indeed, the presented test has several characteristics that can increase the risk of spalling. Some of them are:

- the very fast increase of the temperature (RWS) at the beginning of the tests,
- the high water content in the tests carried out after 5 months,
- the medium range concrete compressive strength (64.8 MPa after 23 months),
- the very high applied compressive stress on the exposed face (12 MPa) [6].

### **CONCLUSIONS**

Several full-scale fire resistance tests have been successfully carried out on mega size reinforced concrete segments from two twin tunnels under the Suez Canal. A new and original mechanical loading equipment has been designed and produced in CSTB. Horizontal and vertical loads with appropriate eccentricities were applied to simulate the in-situ tunnel stresses. Samples have been exposed to the RWS temperature curve for 2 hours.

Spalling depth fields have been measured about 2 hours after the end of the test with a 3D laser scanner. The importance of the timing of spalling depths measurements after the test when severe temperature curves are applied on concrete samples has been shown. Too early exposure of the concrete to the ambient temperature can induce a too severe thermal shock. By opposite, measurements after 4 days can be modified (in the great majority of case, increased) as a result of concrete degradation.

The Ultrasonic Pulse Echo (UPE) technique was successfully used in order to monitor the spalling progression. Determined values were relatively consistent with the result of 3D laser scanning ones.

Spalling depths results determined after 5 months and 23 months clearly show a drastic reduction of the spalling sensitivity of the concrete segments in the latter test. Water content reduction is expected to be the main reason of the observed behavior.

From the gained experience and the captured results, the authors would like to emphasize the importance of those tests to be conducted for major projects.

### **ACKNOWLEDGEMENT**

The authors want to acknowledge the contribution of all the CSTB team that was involved in the project. Special acknowledge is addressed to Ménad Chenaf, José Pestana, Léo Gontier, Jean François Moller, Pierre-Jean Degiovanni and Nicolas Pinoteau.

## REFERENCES

1. Pimienta P., Doll M., Rizos D., Shamma M., Marie-Jeanne B-L, Rivillon P., Chenaf M., Bakhoun M., Fouda A., Gewaily A., Hussein Y., Youssef T., Saad S., Amin T., "Laboratory fire testing on tunnel segments: Suez Canal tunnels case". Proceedings of International Conference INTERFLAM, London, 2019, July 1 – 3. pp 1415 – 1426.
2. Felicetti R., Lo Monte F., "Pulse-Echo Monitoring of Concrete Damage and Spalling during Fire", Proceedings of the 9th International Conference Structures in Fire, Princeton (USA), pp. 851-858. June 8-10, 2016.
3. Boström, L., Jansson, R., "Self-compacting concrete exposed to fire" SP Report. SP No. 2008:53, Boras, Sweden. 2008.
4. Taillefer, N., Pimienta, P., Dhima, D., "Spalling of concrete: A synthesis of experimental tests on slabs". Proceedings of the 3rd International Workshop on Concrete Spalling due to Fire Exposure 2013. MATEC Web of Conferences.
5. Mindeguia, J.-C., Carré, H., Pimienta, P., Borderie, C.L., "Experimental discussion on the mechanisms behind the fire spalling of concrete". *Fire and Materials* 39, 619–635, 2014.
6. Miah, M.J., Lo Monte, F., Felicetti, R., Carré, H., Pimienta, P., La Borderie, C., "Fire Spalling Behaviour of Concrete: Role of Mechanical Loading (Uniaxial and Biaxial) and Cement Type". Proceedings of the International Conference on Concrete under Severe Conditions - Environment & Loading. 12 – 14 September 2016.

# Scale effect on spalling of high performance self-compacting fiber reinforced concrete

Fariza Sultangaliyeva<sup>1,\*</sup>, Hélène Carré<sup>1</sup>, Christian La Borderie<sup>1</sup>, Fabienne Robert<sup>2</sup>,  
Siyimane Mohaine<sup>2</sup>, Pierre Pimienta<sup>3</sup>

<sup>1</sup> Université de Pau et des Pays de l'Adour, E2S UPPA, SIAME, Anglet, France

<sup>2</sup> Fire Testing Center, CERIB, Epernon, France

<sup>3</sup> Centre Scientifique et Technique du Bâtiment, Champs-sur-Marne, France

\* Corresponding author (fariza.sultangaliyeva@univ-pau.fr)

## ABSTRACT

A high performance fiber reinforced self-compacting concrete for use in nuclear waste storage containers was tested for fire at different scales. Three specimens subjected to ISO 834-1 fire were prisms of 20 x 20 x 10 cm<sup>3</sup>, slabs of 100 x 170 x 30 cm<sup>3</sup> and two containers of 202 x 202 x 165 cm<sup>3</sup>. Two mixes were tested at three scales with different polypropylene fiber dosages and geometries: one with 1.5 kg/m<sup>3</sup> of 18 mm fibers with a diameter of 34 μm (18/34) and another with 1 kg/m<sup>3</sup> of 24/34 fibers. At the end of the tests, the specimens were examined in terms of mean and maximum depth of spalling. Experimental results were discussed and conclusions on scale effect on spalling were presented.

**KEYWORD:** self-compacting concrete, polypropylene fiber, ISO fire, scale effect, spalling

## INTRODUCTION

Project Cigéo of ANDRA proposes a solution for a problem of storage of radioactive waste in terms of a deep geological disposal (500 meters) of intermediate level and long-lived (ILL) and high-level radioactive waste in the east of France. For ILL radioactive waste, a disposal in precast reinforced concrete containers with a cover is suggested. Two major risks associated with use of these containers are the risk of fall, as containers are stacked and should be available for a surface recovery, and the risk of fire, in case of which the principal role of the container would be to protect primary waste reservations. The type of concrete used for such containers must meet a number of requirements in terms of durability, fluidity and fire resistance imposed by ANDRA [1]. Ensuring a thermal stability of concrete for these containers presents a significant challenge due to variety of factors that influence the phenomenon of concrete spalling. One of these factors is a scale effect which, when increased, is shown to enhance fire spalling [2], [3], [4], [5]. Whilst some progress has been shown in the past, predicting the behaviour of concrete as it transitions from material scale (laboratory small scale prisms) to structural scale (container) remains a complicated task.

The aim of this paper is to study the scale effect of two high performance concrete mixes containing polypropylene fibers for use in radioactive waste disposal containers. Fire tests are performed on prisms, slabs and containers following standard fire curve. Thermo-hydro-mechanical computations have been completed on tested geometries with a purpose of providing an additional information on obtained state of stresses and strains. Analysis of experimental results coupled with simulations has confirmed scale effect, which is not

solemnly related to size, but to significant thermo-mechanical stresses induced by testing conditions as well.

## EXPERIMENTAL STUDY

### Materials and methods

Cement CEM III/A 52.5 L (Eqiom, Heming) with 35 % clinker and 61 % granulated ground blast furnace slag is used (density: 2990 kg/m<sup>3</sup>, Blaine surface: 5350 cm<sup>2</sup>/g). Siliceous filler (Sibelco) is used (density: 2650 kg/m<sup>3</sup>, Blaine surface: 2879 cm<sup>2</sup>/g). Calcareous aggregates (Calin) are sand 0/4 and gravels 4/6 and 6/10 (densities: 2540, 2610, and 2620 kg/m<sup>3</sup>, water absorption coefficients: 1.94, 1.09, and 1.01 %). Polypropylene fibers (Eurofiber, Baumhüter) with length of 18 and 24 mm and diameter of 34 µm at 1.5 and 1 kg/m<sup>3</sup> (marked as 18/34-1.5 and 24/34-1) are used. Optima 145 and Plast V90 (Chryso) are chosen as superplasticizer and viscosity agent (dry extract: 31.5 ± 1.5 % and 5.3 ± 0.5 %). The composition of two concrete mixes is given in Table 1.

Table 1 Composition of concrete mixes in kg/m<sup>3</sup>.

	C-18/34-1.5	C-24/34-1
Cement	400	400
Water	160	160
Filler	368	342
Sand 0/4	868	883
Gravel 4/6	297	302
Gravel 6/10	297	302
SP	16.90	14.10
VA	0.45	0.25
PP fibres	1.5	1

Table 2 Fresh and hardened properties of mixes for three types of samples.

	Thickness (cm)	Load (MPa)	Spread (cm)	Compressive strength (MPa)		Tensile strength (MPa)		Water content (%)	
				28 d	Test	28 d	Test	1 <sup>st</sup> cm	Mean
<b>C-18/34-1.5</b>									
Prism	10	20	68	90.3-92.4 <sup>a</sup>	93.7-98.2 <sup>a</sup>	5.5-6.2 <sup>a</sup>	-	-	4.3
Slab	30	0	72	83.9	87	-	-	4.1	5.0
	30	2.5	72	92.9	95	-	-	3.6	4.8
	30	7	73	87.5	98	-	-	3.8	4.7
Container		0	72	86.2	97	6.85	4.6-5.1	-	4.9
<b>C-24/34-1</b>									
Prism	10	20	70	90.3-92.4 <sup>a</sup>	93.7-98.2 <sup>a</sup>	5.5-6.2 <sup>a</sup>	-	-	4.5
Slab	30	0	77	90.5	105	-	-	3.8	5.0
	30	2.5	76	80.7	90.5	-	-	2.7	4.3
	30	7	78	88.2	86	-	-	3.2	4.5
Container		0	73	87.2	102	6.7	4.6-5.1	-	3.3

<sup>a</sup> No measurements are available for these mixes, values present a range for similar mixes studied in [6].

Fresh and hardened state properties of the mixes have been determined and are presented in Table 2. Compressive strength is measured as following:

- Prisms: two cylinders (D=11 cm, H=22 cm) stored in water for both 28 and 90 days (test);
- Slabs: three cubes (a=15 cm) stored in water for 28 days and those for 90 days (test) in climatic chamber (T=23 °C, RH=50 %) from the moment of demolding;
- Container: three cylinders (D=11 cm, H=22 cm) stored near container for 28 and 100 days (test).

Tensile strength is determined via splitting test on cylinders (D=11 cm, H=22 cm) stored similarly as the ones for compressive strength. Water content in the first centimeters and global water content are found using slices from cylinders dried at 105 °C for slabs and containers and at 80 °C for prisms.

Fire tests have been performed on three different scales:

- Prisms 20 x 20 x 10 cm<sup>3</sup> per mix in Université de Pau et des Pays de l'Adour: mobile gas furnace and hydraulic press [6] with compressive load of 20 MPa (from preliminary numerical simulation of containers). Prisms were stored 7 days in water and 81 days in relative humidity of 75 %. During 30 min standard fire, one face was heated, another exposed to laboratory environmental and four lateral sides are insulated from thermal and hydral losses.
- Slabs 100 x 170 x 30 cm<sup>3</sup> in CERIB: in Atlas furnace tested under unloaded and loaded conditions (2.5 and 7 MPa). The information on reinforcement, pretensioning and furnace can be found in [7],[8]. Slabs were stored in climatic chamber (T=23 °C, RH=50 %). The bottom face of slabs was heated for 30 min standard fire.
- Containers 202 x 202 x 165 cm<sup>3</sup> in CSTB: Vulcain furnace [9] tested in unloaded condition for 1h in standard fire. Position of container in the furnace is presented in Figure 1. To allow placing thermocouples, container is placed on concrete supports of 60 cm height.

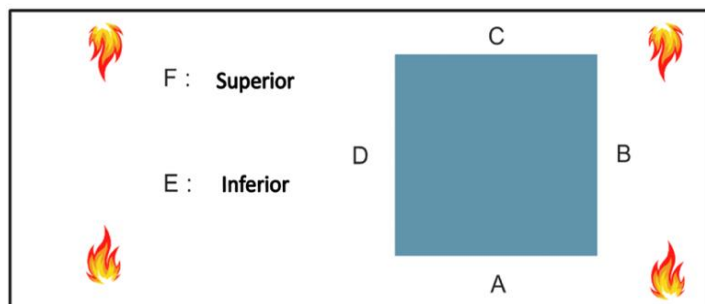


Figure 1 Position of container in the furnace: view from the top.

## Fire test results

The surfaces of prisms exposed to fire for 30 minutes under 20 MPa uniaxial loading are shown in Figure 2. Mixes with 18 mm fibers have not spalled while mixes with 24 mm fibers have spalled. Despite the fact that longer fiber are more efficient than shorter ones in terms of spalling reduction [6], [10]-[12], due to a higher dosage of fibers, 18 mm fibers were efficient in spalling prevention.

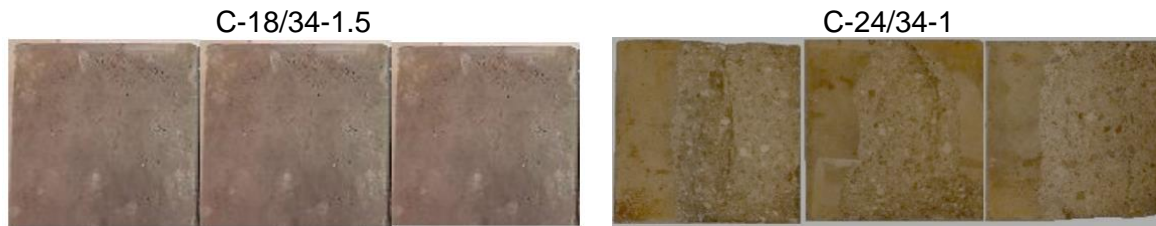


Figure 2 Spalled surfaces of prisms C-18/34-1.5 (no spalling) and C-24/34-1.

Figure 3 shows the spalled surfaces for slabs tested under three different loadings for 30 min standard fire scenario. A slight spalling is observed for mix C-18/34-1.5 with no loading, which happened at 21 minutes. No spalling is observed for intermediate loading of 2.5 MPa for both mixes. For 7 MPa loading, both mixes present significant spalling that expose reinforcement, 24 mm fiber mix having more severe spalling. Results indicate a major influence of loading when passing from 2.5 to 7 MPa. It was observed that increase of loading level increases spalling [13]-[15].

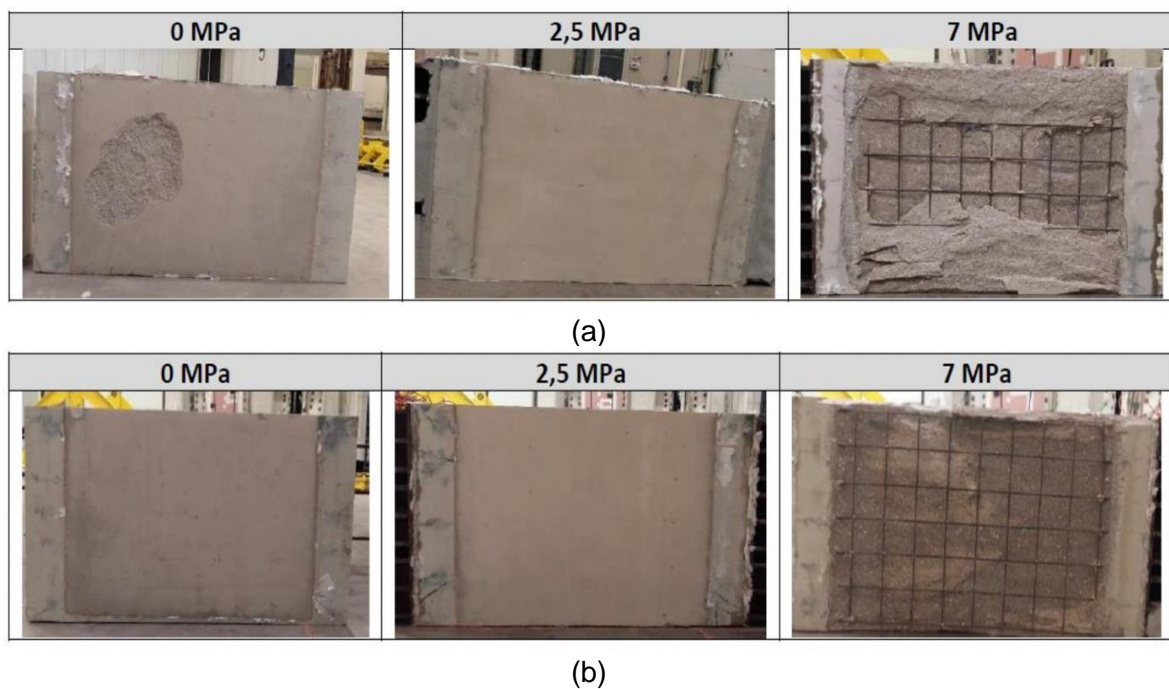


Figure 3 Spalled surfaces for 0, 2.5, 7 MPa load for slabs: a) C-18/34-1.5, b) C-24/34-1.

Figures 4 and 5 present the images of spalled surfaces of container with mixes C-18/34-1.5 and C-24/34-1 after 1 hour standard fire curve heating. In general, container with 18 mm fibers has spalled less than the one with 24 mm ones due to higher dosage of fibers. Temperatures registered by thermocouples (see Figure 6) installed on surfaces have showed a presence of temperature gradients. The sides B and D located along longitudinal direction (Figure 1) were heated the most for both containers. The lowest temperatures were for sides A and E for container C-18/34-1.5 ( $\Delta T \approx 200$  °C) and sides A and C for container C-24/34-1 ( $\Delta T \approx 100$  °C). Unfortunately, not all the sides could be observed during heating, but from what was available for observation, first spall was noted on the side D: 5 minutes after start of fire test with spalling continuing until 25 minutes. The sides B and D with the severest heating have spalled more than sides A and C with a difference in a mean spalling depth of 20-33 mm for C-18/34-1.5 and 10-15 mm for C-24/34-1. Side F (cover) was free to deform and has not spalled in



comparison to rest of the container. Sides B and D are approaching the case of slabs loaded to 7MPa, while side F without spalling is closer to case of slabs with 0 and 2.5 MPa loading. This shows a presence of significant thermo-mechanical stresses due to the influence of thermal gradients.

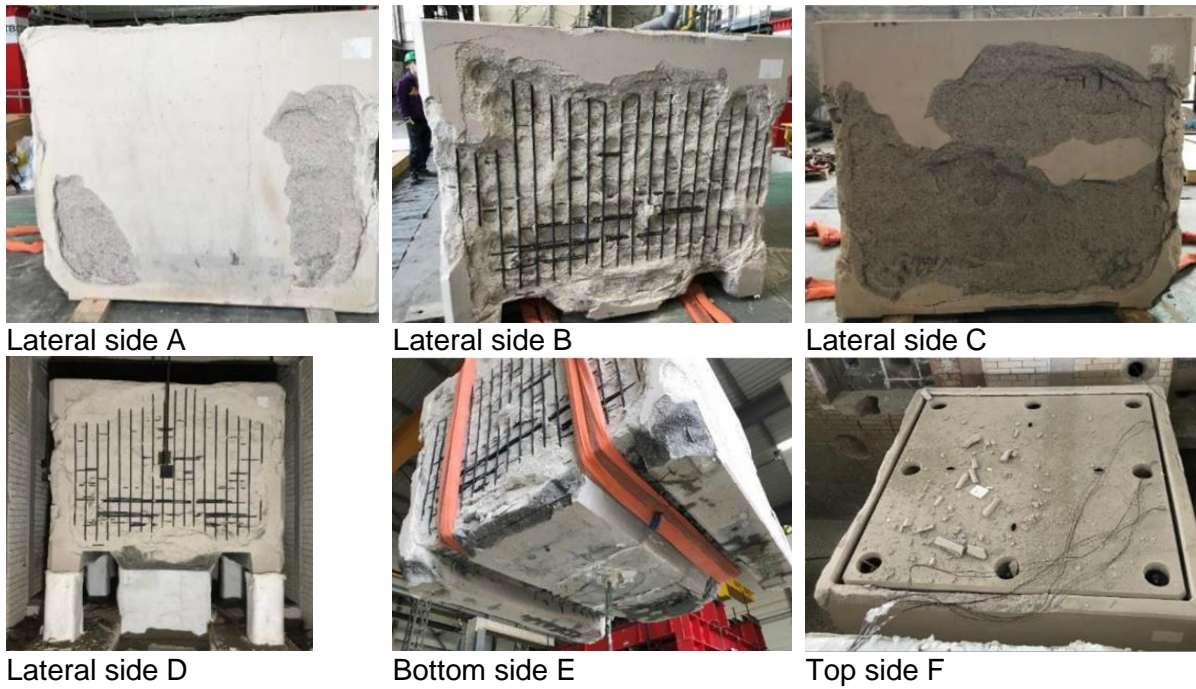


Figure 4 Spalled surfaces of container C-18/34-1.5.

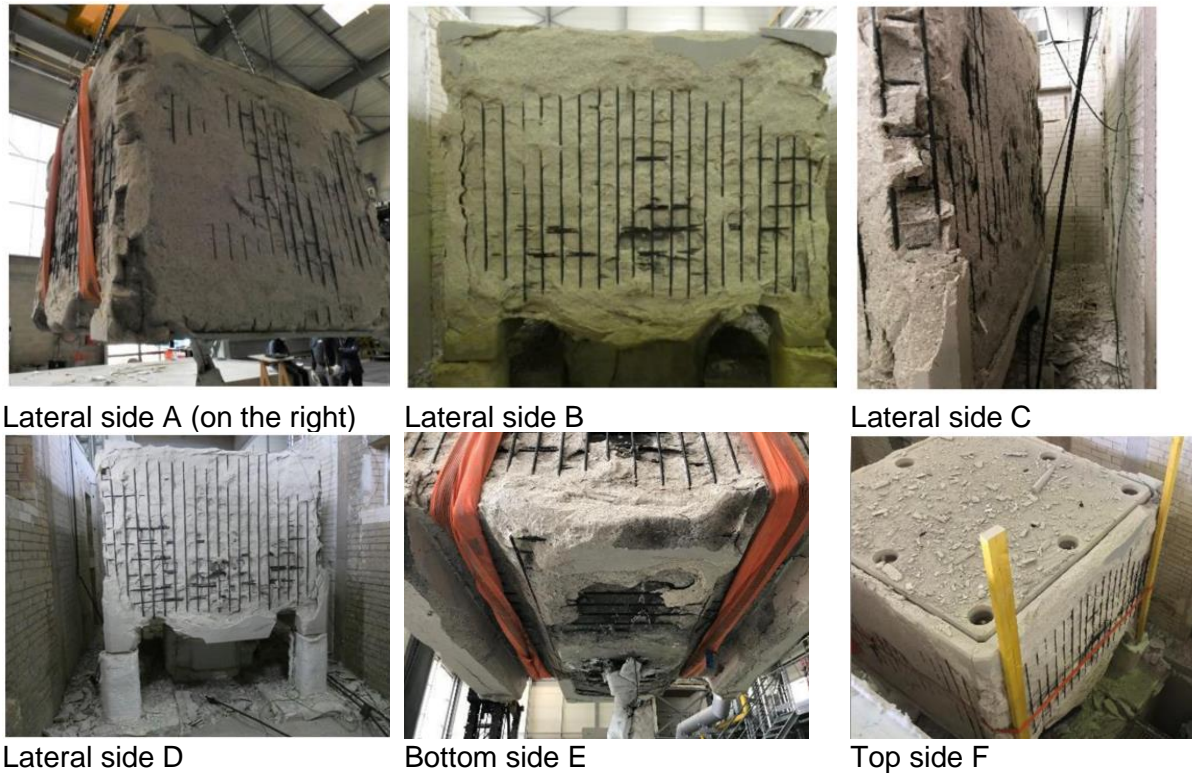
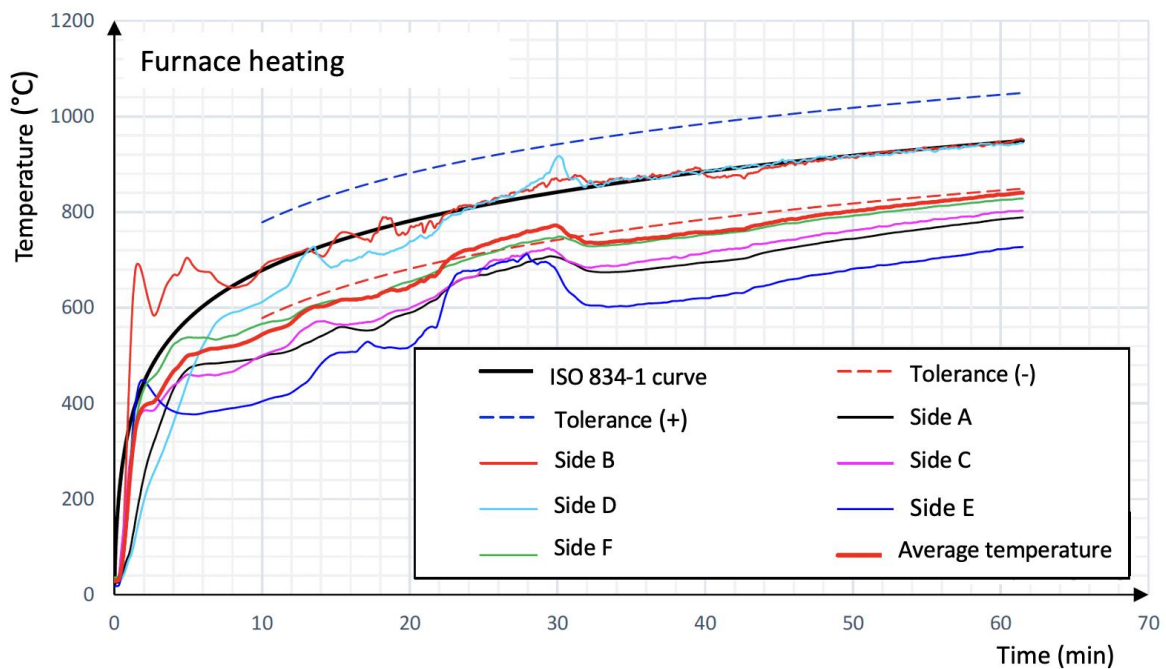
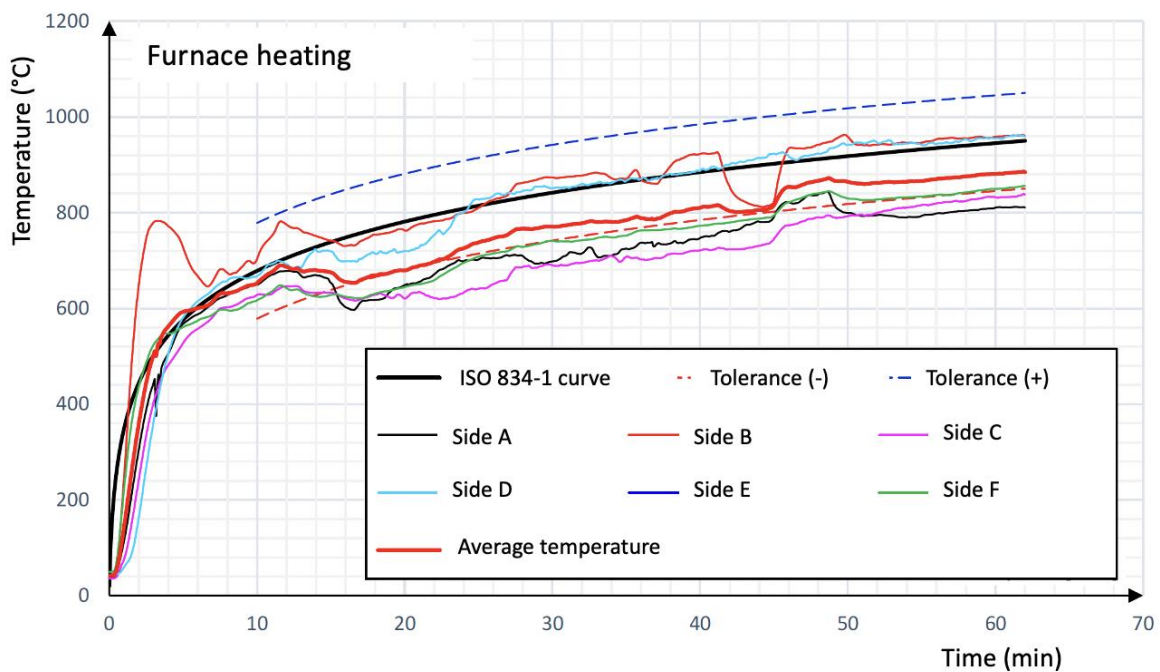


Figure 5 Spalled surfaces of container C-24/34-1.



(a)



(b)

Figure 6 Thermocouple recordings for heating of container surfaces: a) C-18/34-1.5 and b) C-24/34-1.

Figure 7 presents values of mean and maximum spalling depth excluding edges for two concrete mixes tested in three scales: prisms, slabs, containers. Overall, mixes with 24 mm polypropylene fibers at 1 kg/m<sup>3</sup> have spalled more than concrete with 18 mm and 1.5 kg/m<sup>3</sup> due to lower fiber dosage. The results show that both mean/maximum spalling depth has increased with increase of scale: for C-18/34-1.5 from no spalling (prism) to 22 mm/50 mm (slab, 7 MPa) and 50 mm/85 mm (container). For C-24/34-1, these values go from 4 mm/16



mm to 71 mm/94 mm (slab, 7 MPa) and 50 mm/117 mm (container). Summary of these results can be found in Table 3.

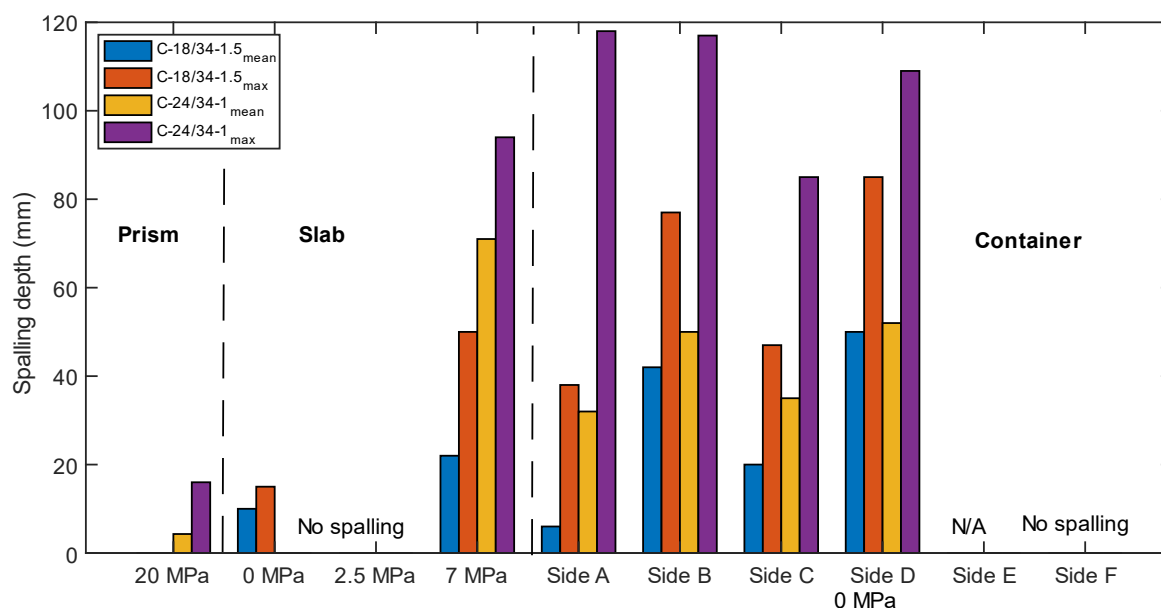


Figure 7 Mean and maximum spalling depth for two mixes tested in three scales (for each configuration 3 prisms, 1 slab and 1 container were tested).

Table 3 Summary of results of fire tests for three types of samples.

	Side	Load (MPa)	Spalling (Yes/No)	Spalling start (min)	Spalling depth (mm)		Spalled surface (%)	
					Mean	Max		
C-18/34-1.5	Prisms	20	No	-	0	0	0	
	Slabs	0	Yes <sup>a</sup>	21	10	15	15	
		2.5	No	-	0	0	0	
	Container	7	Yes	16	22	50	100	
		A	0	Yes	N/A	6	38	28
		B	0	Yes	13	42	77	94
		C	0	Yes	13	20	47	47
D		0	Yes	5	50	85	100	
E <sup>b</sup>	0	Yes	N/A	N/A	N/A	N/A		
F <sup>c</sup>	0	No	-	0	0	0		
C-24/34-1	Prisms	20	Yes	17	4.3	16	N/A	
	Slabs	0	No	-	0	0	0	
		2.5	No	-	0	0	0	
	Container	7	Yes	10	71	94	100	
		A	0	Yes	N/A	32	118	92
		B	0	Yes	N/A	50	117	100
		C	0	Yes	N/A	35	85	89
D		0	Yes	5	52	109	97	
E <sup>b</sup>	0	Yes	N/A	N/A	N/A	N/A		
F <sup>c</sup>	0	No	-	0	0	0		

<sup>a</sup> Only one spalling event has occurred

<sup>b</sup> Spalling is not characterized for this side of container (side E is the container bottom)

<sup>c</sup> No spalling for side F (cover of the container).

## CONCLUSIONS

This paper has investigated the scale effect of high performance self-compacting polypropylene fiber reinforced concrete in terms of spalling due to fire. Fire tests following standard fire curve were performed on three different scales: a) prisms under uniaxial loading of 20 MPa, b) slabs in unloaded and loaded conditions (2.5 and 7 MPa), c) container without loading. Experimental results show existence of scale effect as spalling depth has increased passing from small to full scale. Significant increase in spalling was observed between loading of 2.5 to 7 MPa in case of slabs. In container, faces have experienced different heating curves, thus, different spalling degrees due to more complex experimental conditions (position in the furnace, position of the burners, convection, etc.). Although the containers were tested in unloaded conditions, the sides which were exposed to the faces exposed to the ISO 834-1 fire showed spalling depths relatively close to those of the 7 MPa loaded slabs. In addition, the covers on the upper sides did not spall as the unloaded slabs.

## ACKNOWLEDGMENTS

The authors would like to acknowledge that this work is carried out using the financial assistance from the program of the Investments for the Future of the French government managed by ANDRA.

## REFERENCES

1. ANDRA, "Cahier des charges - Développement d'une formulation béton pour conteneur de stockage MAVL et réalisation de prototypes", 2012.
2. Klimek, A., Hothan, S., and Rogge, A., "Investigation of Size Effects in Concrete Spalling", Proceedings of the 6<sup>th</sup> International Workshop on Concrete Spalling due to Fire Exposure, 61-70, Sheffield, United Kingdom, 19-20, September, 2019.
3. Taillefer, N., Pimienta, P., and Dhima, D., "Spalling of concrete: A synthesis of experimental tests on slabs", Proceedings of the 3<sup>rd</sup> International Workshop on Concrete Spalling due to Fire Exposure, Paris, France, 25-27, September, 2013.
4. Mindeguia, J.-C., Contribution expérimentale à la compréhension des risques d'instabilité thermique des bétons, PhD Thesis, Université de Pau et des Pays de l'Adour, 2009.
5. Kanéma, M., Influence des paramètres de formulation sur le comportement à haute température des bétons, PhD Thesis, Université de Cergy Pontoise, 2007.
6. Sultangaliyeva, F., Formulation of fluid fire-resistant fiber-reinforced cementitious composite: Application to radioactive waste disposal, PhD Thesis, Université de Pau et des Pays de l'Adour, 2020.
7. Robert, F., Labetoulle, C. Tessier, C., and Collignon C., Thermo-mechanical modelling to define a screening test for building application under the standard temperature time curve, Proceedings of the 5<sup>th</sup> International Workshop on Concrete Spalling due to Fire Exposure, Boras, Sweden, 12-13, October, 2017.
8. Mohaine, S., Boström, L., Lion, M., McNamee, R., and Robert, F., "Cross-comparison of screening tests for fire spalling of concrete", *Fire and Materials*, 1-14, 2021.
9. Lahour, M., Pinoteau, N., Caron, J.-F., Forêt, G., and Rivillon, P., "Fire design of post-installed bonded rebars: Full-scale validation test on a 2.94 x 2 x 0.15 cm<sup>3</sup> concrete slab subjected to ISO 834-1 fire", *Engineering Structures*, **174**, 81-94, 2018.
10. Bilodeau, A., Kodur, V.K.R., and Hoff, G.C., "Optimization of the type and amount of polypropylene fibres for preventing the spalling of lightweight concrete subjected to hydrocarbon fire", *Cement and Concrete Composites*, **26**, 163- 174, 2004.

11. Heo, Y.-S., Sanjayan, J.G., Han, C.-G., and Han, M.-C., "Relationship between inter-aggregate spacing and the optimum fiber length for spalling protection of concrete in fire", *Cement and Concrete Research*, **42**, 549-557, 2012.
12. Knack, I., New pp-fibre with exceptional melting characteristics for improved fire protection in concrete building, Proceedings of 1<sup>st</sup> International Workshop on Concrete Spalling due to Fire Exposure, Leipzig, Germany, 3-5, September, 2009.
13. Jansson, R. and Boström, L., "Factors Influencing Fire Spalling of Self Compacting Concrete", *Materials and Structures*, **46**, 1683-1694, 2013.
14. Boström, L., Wickström, U., and Adl-Zarrabi, B., "Effect of Specimen Size and Loading Conditions on Spalling of Concrete", *Fire and Materials*, **31**, 173-186, 2007.
15. Kodur, V. K. R., and Phan, L., "Critical Factors Governing the Fire Performance of High Strength Concrete Systems", *Fire Safety Journal*, **42**, 482-488, 2007.

# Spalling behaviour of ultra-high performance concrete columns exposed to natural fires

Jan Lyzwa<sup>1,\*</sup>, Jochen Zehfuß<sup>1</sup>

<sup>1</sup> Technische Universität Braunschweig, Institute of Building Materials, Concrete Construction and Fire Safety (iBMB), Division of Fire Safety, Braunschweig, Germany

\* Corresponding author (j.lyzwa@ibmb.tu-bs.de)

## ABSTRACT

In this paper the thermo-mechanical material properties of UHPC based on both the thermal exposure of the ISO 834 standard fire and a natural fire exposure, including a cooling phase are depicted. These material properties were derived from steady-state and transient creep tests on concrete cylinders at the iBMB. Furthermore the spalling behaviour of two equal ultra-high performance concrete columns stressed by the same mechanical load and exposed to the standard fire and a natural fire is presented and compared to each other. The spalling affected the temperature development in the cross-section of the columns. For simulating the heating behaviour a simplified numerical approach to consider spalling is applied.

Regarding the thermal exposure, the experimental results have shown that compared to the ISO 834 standard fire a natural fire can have a negative effect on the strength as well as on the spalling behaviour of UHPC.

**KEYWORD:** UHPC, thermo-mechanical material properties, natural fire models, column fire tests, numerical simulation

## INTRODUCTION

Concrete with compressive strengths  $f_{ck} > C100/115$  is usually referred as ultra-high performance concrete (UHPC). UHPC can achieve compressive strengths of up to 250 N/mm<sup>2</sup>. This makes it possible to construct the components significantly sligher and lighter compared to structures of normal-strength or high-strength concrete. Due to the smaller cross-sectional dimensions thermal exposures lead to a faster heating of the components.

The high density of the cement matrix is a main reason for explosive spalling of UHPC when exposed to fire. Due to the very dense structure there are rarely any possible transport routes for evaporation. This microstructure, which is almost free of capillary pores, represents a decisive disadvantage in the event of fire, since it can lead to structural damage and explosive spalling due to the high pore pressure at rising temperatures  $T > 100$  °C [1].

Extensive research has been carried out on ultra-high performance concrete (UHPC). However, UHPC has not been standardized in prEN 1992-1-2 [2]. In order to avoid spalling usually an appropriate amount of polypropylene fibres (PP-fibres) is included in the UHPC recipes.

In [3] investigations of the fire behaviour of UHPC for increasing temperatures regarding the common ISO 834 standard fire for fire safety design were carried out. In addition to the determination of the thermal and thermo-mechanical material properties, the spalling

behaviour of UHPC was examined. Here, a certain PP fibre content in the concrete recipe was obligatory. For the investigated concrete composition in [3] a minimum content of 2.25 kg/m<sup>3</sup> was determined.

Although the main factors are the moisture content of the components and the density of the concrete, the heating rate is another relevant factor for spalling. The application of natural fire models is provided in prEN 1992-1-2 [2] as an alternative to the common ISO 834 standard fire for fire safety design. In Figure 1 it is shown that in natural fires the heating rate as well as the maximum temperature can exceed the standard fire during the first minutes of thermal exposure. Another general difference between the temperature-time curves is, that the ISO 834 standard fire is only characterized by a heating phase, while natural fire models are composed of a heating and a cooling phase.

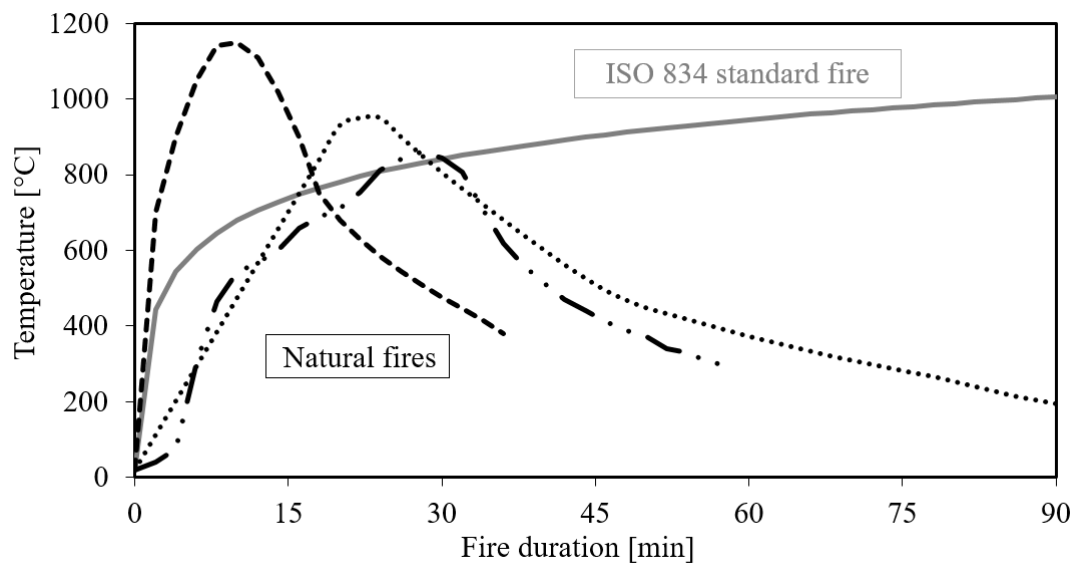


Figure 1 Temperature-time curves of ISO 834 standard fire and different natural fires [4]

The thermal inertia of concrete components can lead to a delayed heating or high tensile forces in the cooling phase. The pressure of the evaporating free and bound water causes spalling because it can lead to high tensile stresses that can exceed the tensile strength of concrete. Thus, compared to the standard fire, natural fires with large heating rates might cause a more critical spalling behaviour.

## EXPERIMENTAL INVESTIGATIONS

### General

In the research project [5] the material behaviour of normal, high and ultra-high performance concrete, considering natural fires, including a heating and a cooling phase, was investigated. Here, temperature-dependent thermal and thermo-mechanical material properties for the different concrete strengths were determined with small and midsize scale experiments. For validation purpose two real-scale fire tests on columns were carried out for each concrete strength.

In this paper the experimental results in [5] are reprocessed regarding the spalling behaviour of UHPC.

In Table 1 the components of the concrete composition of the UHPC are shown that has been analysed within the research project.

Within the research project concrete cylinders with a diameter of 80 mm and a height of approximately 240 mm and columns with a cross-section of 300 mm x 300 mm and a length of 3.7 m were assembled.

A detailed description of the experimental investigations are included in [5] and [6].

*Table 1 Components of the investigated ultra-high performance concrete*

Components of the concrete	Mass [kg/m <sup>3</sup> ]
Water	161
CEM 52,5 R-SR3/NA (Holcim®)	650
Silica fume Silikoll P uncompacted (Sika®)	177
Superplasticizer ViskoCrete 2810 (Sika®)	21
Quartz powder Millisil W12 (Quarzwerte®)	325
Quartz powder Millisil W 3 (Quarzwerte®)	132
Quartz sand H33 0.125mm/0.5mm (Quarzwerte®)	354
Basalt 2/5	298
Basalt 5/8	298
Steel fibers, WEIDACON FM 0,19 mm x 13 mm (Stratec®)	79
Polypropylene fibers FKSPM512, plastic fiber 12 mm 19,8 µm (Stratec®)	2.25
Total	2497.25
water/cement ratio	0.248

### Results of the experiments for determining thermo-mechanical material properties

For the determination of the thermo-mechanical material properties of UHPC steady-state and transient creep tests were carried out in [3] and [5]. In the steady-state tests the specimen are investigated at a constant temperature with an increasing mechanical load until failure, while the deformation is measured. These tests enable to determine the temperature dependent concrete strength. Since the steady-state tests do not take transient creep into account, additional transient creep tests have to be performed in order to investigate the deformation behaviour of the concrete in case of fire. Generally, in the transient creep tests the specimen are heated until mechanical failure under a constant load, while the deformation of the specimen is measured. In [3] the thermo-mechanical material properties were determined based on the thermal exposure to the ISO 834 standard fire. Hereby, the reduction of strength of UHPC at maximum temperature were derived. In [5] five different temperature testing programs were defined in order to determine thermo-mechanical material properties for natural fire exposures, which include a heating and a cooling phase. Here, the specimen were heated to a maximum temperature and subsequently cooled to a lower temperature level. Thus, these specimen were tested at the lower (cooler) level after reaching a maximum temperature.

In Table 2 the reduction of the strength of UHPC for elevated temperatures at maximum temperature [3] and for natural fires including a cooling phase [5] are compared to the values at maximum temperature for high performance concrete with a strength  $f_{ck} \geq 70$  N/mm<sup>2</sup> according to prEN 1992-1-2 [2].

The drop and regain in strength during the heating phase does normally not apply for conventional concrete. However, in [5] for UHPC as well as for normal and high performance concrete the experimental investigations have clearly shown that the strength during the cooling phase is always below the strength at the maximum temperature. Thus, a general statement for concrete seems to be that a delayed heating or high tensile forces in the cooling phase cause a further reduction in strength.

In [3] it has been shown that for temperatures up to 300 °C, a decrease of the strength can be observed for the UHPC. This loss is followed by an increase of the compression strength at

higher temperatures up to 500 °C. After these temperatures a relatively slow decrease of the compression strength begins yielding to about 79 % of the compression strength at 20 °C at 700 °C. However, in [5] has been shown that the compression strength in the cooling phase is significantly below the compression strength at maximum temperature. Thus, the drop in strength between 100°C and 300 °C in the heating phase does not occur again in the cooling phase. Compared to the values in prEN 1992-1-2 [2] the decrease in strength at maximum temperature [3] and during the cooling phase [5] is lower for the investigated UHPC.

*Table 2 Reduction of strength of UHPC for elevated temperatures at maximum temperature (left) [3], including a cooling phase (middle) [5] and according to prEN 1992-1-2 [2] (right)*

Temperature	$f_{c,\theta}/f_{ck}$ [3]	Temperature testing program	$f_{c,\theta}/f_{ck}$ [5]	Temperature	$f_{c,\theta}/f_{ck}$ [2]
20 °C	1.0	20 °C	1.0	20 °C	1.0
100 °C	0.85	100 °C – 20 °C	0.92	100 °C	1.0
300 °C	1.15	300 °C – 200 °C	0.82	300 °C	0.75
500 °C	1.07	500 °C – 200 °C	0.67	500 °C	0.60
700 °C	0.79	700 °C – 500 °C	0.68	700 °C	0.30
700 °C	0.79	700 °C – 300 °C	0.59	700 °C	0.30

Concerning the deformation behaviour of heated UHPC in [3] it has been indicated that UHPC shows a stiffer stress-strain-relation at ambient temperature and with increasing temperature compared to normal concrete. Furthermore in prEN 1992-1-2 [2] for concrete strengths  $f_{ck} < 70$  N/mm<sup>2</sup> as well as for  $f_{ck} \geq 70$  N/mm<sup>2</sup> the same strain values ( $\epsilon_{c1,\theta}$  and  $\epsilon_{cu1,\theta}$ ) are used for the derivation of the stress-strain-curves.

In [5] the evaluation of the transient creep tests has shown that the stress-strain-relation of UHPC between the heating phase and the cooling phase only slightly differ for maximum temperatures up to 500 °C.

However, since low heating rates of 4 K/min were chosen in [3] and [5] no spalling occurred during the investigation of the thermo-mechanical material properties of the UHPC concrete cylinders.

### Column fire tests

Within the research project [5] two UHPC column fire tests were conducted. The columns with a cross-section of 300 mm x 300 mm consisted of 8 longitudinal reinforcement bars of steel B 500 B with a diameter of 20 mm and an axis distance of 5.5 cm. Also a total of 22 stirrups, each with a diameter of 10 mm were installed. For the measurement of the cross-sectional temperatures, thermocouples in different depths and heights provided in the columns.

Two different temperature-time curves were chosen for the column fire tests as shown in Figure 2.

The columns were clamped with a force of 35 kN into the testing facility. Subsequently, the mechanical load was increased path-controlled to 4.930 kN which equalled approximately 65 % of the load bearing capacity at ambient temperature. This load was kept constant over the entire column fire tests. In a next step, all four faces of the columns were exposed to the temperature-time curves *T1* and *T2*, utilizing six oil burners.

For the first 90 minutes the temperature-time curve *T1* corresponds to the ISO 834 standard fire and is followed by a cooling phase with a bi-linear course. Although, within the first 11 minutes in the test the fire curve is below the boundary of the standard fire. A reason for this is the occurred spalling, which leads to a drop in the temperature of the fire curve. Due to the spalled (cooler) surfaces, the column absorbs more energy.

The temperature-time curve  $T_2$  represents a natural fire in a 53 m<sup>2</sup> office building with a fire load density of 584 MJ/m<sup>2</sup>.

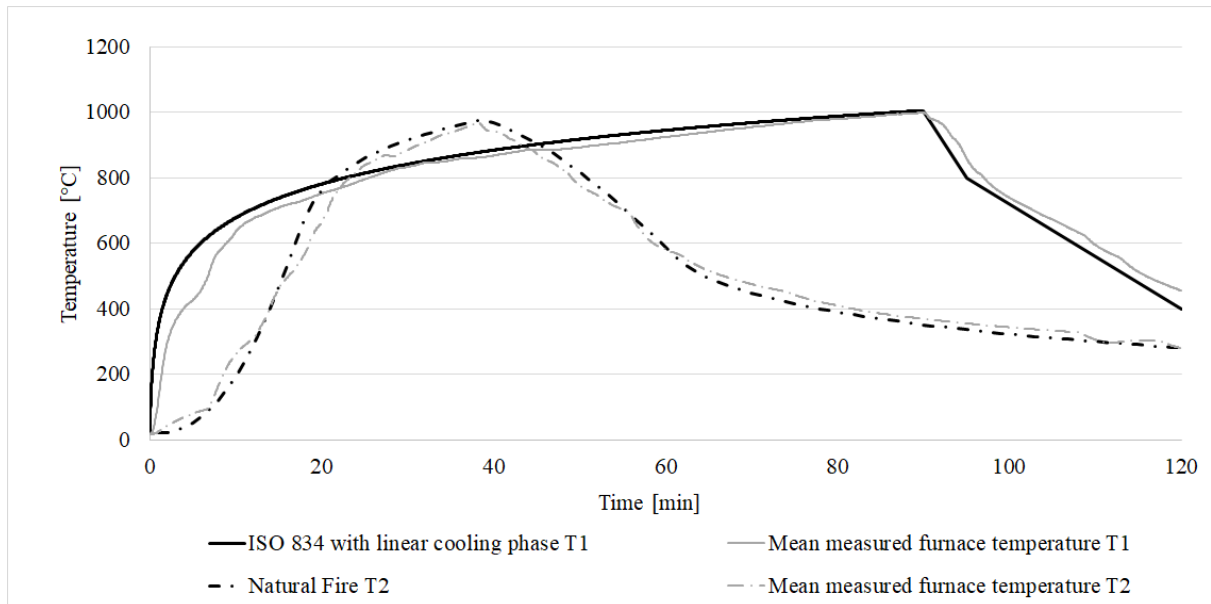


Figure 2 Temperature-time curves  $T_1$  and  $T_2$  of the column fire tests [6]

The two columns have been produced 9 months before the fire tests and were stored inside the testing halls of the institute at ambient conditions for the entire time. The moisture content of the UHPC exposed to  $T_1$  was 2.02 % and of the UHPC exposed to  $T_2$  was 1.93 % at the day of the column fire test.

In Figures 3 and 4 the two columns are shown at different times during the fire test.

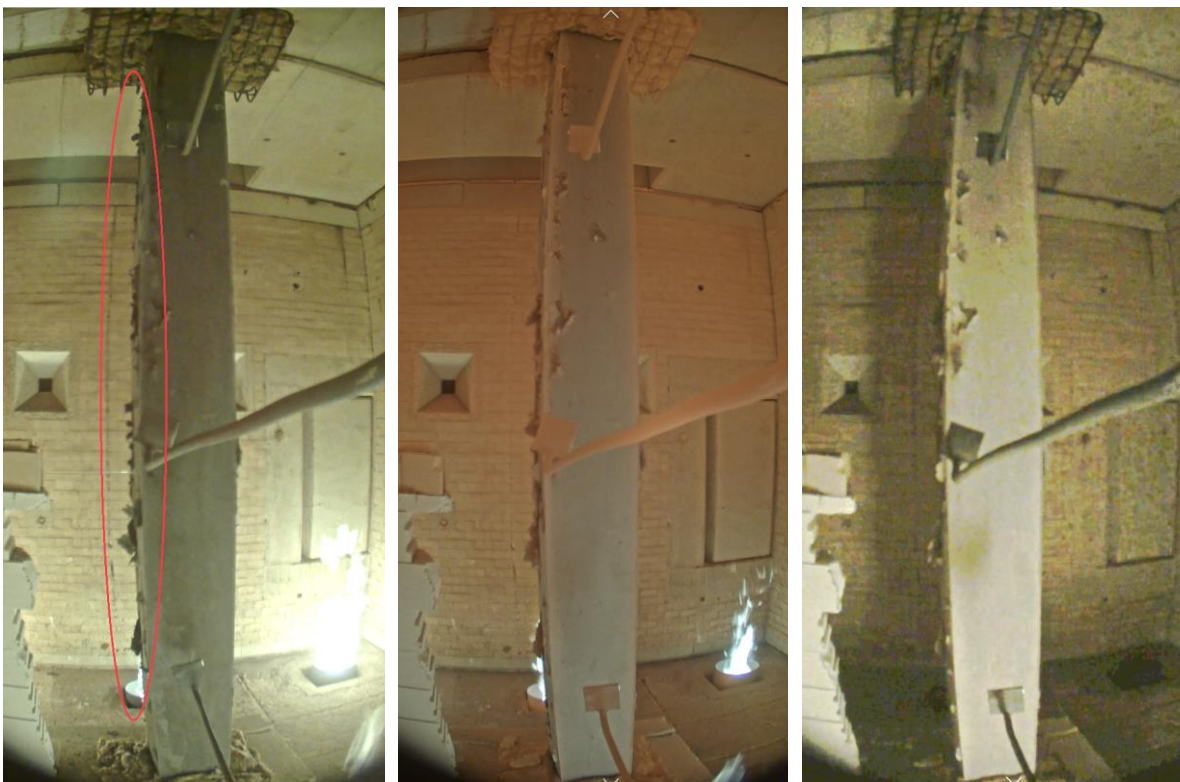


Figure 3 UHPC column during thermal exposure according to temperature-time curve  $T_1$  after 15 (left), 20 (middle) and 110 (right) minutes



Although a PP-fibre content of  $2.25 \text{ kg/m}^3$  was contained in the concrete recipe, spalling occurred in both column fire tests. While only local spalling could be observed for the ISO 834 based temperature-time curve ( $T1$ ), massive spalling at all 4 surfaces and the entire length of the column appeared for the temperature-time curve  $T2$ . Compared to  $T1$ , the temperature gradient above  $500 \text{ }^\circ\text{C}$  and the possible resulting higher pressure of the water vapour during the heating phase of the temperature-time  $T2$  might be a reason for this massive spalling behaviour. In [7] the spalling behaviour of UHPC was investigated, where the complete avoidance of explosive spalling could not be achieved by adding PP fibres. The reason for this was constituted by the insufficient distribution of the fibres, which results from the stickiness of the fresh concrete.

However, in both fire tests the columns resisted the entire fire exposure of 120 minutes.



Figure 4 UHPC column during thermal exposure according to temperature-time curve  $T2$  after 19 (left), 34 (middle) and 120 (right) minutes

## NUMERICAL SIMULATIONS

A simple way to consider spalling is to reduce the cross-section during the thermal analysis of the component. For this purpose the cross-section can be divided into different layers where single layers are removed after a certain time in order to take into account the faster heating and thus the faster decrease in strength of the remained cross-sectional area during the fire exposure. Here, a simplification is that the occurring spalling is regarded as a linear removing of the layers. In fact in reality spalling occurs crater like. For the simulation the point in time spalling occurs as well as the deepness of the spalling can only be approximated according to the visual observations in the fire tests.

For the thermal analysis the temperature dependent material properties (density  $\rho$ , thermal conductivity  $\lambda$  and the specific heat capacity  $c_p$ ) have to be taken into account. These material properties were implemented into the FE-Software ANSYS according to the given functions in

prEN 1992-1-2 [2]. Regarding experimental measurements the density  $\rho$  of the UHPC at ambient temperature was set to 2500 kg/m<sup>3</sup> and the moisture content to 2 %.

In prEN 1992-1-2 [2] a new approach for the thermal conductivity function is included. The new function combines the two limit functions from the current Eurocode (EN 1992-1-2). In this new function, the thermal conductivity follows the upper limit function in the temperature range up to 140 °C. In the temperature range between 140 °C and 160 °C, the thermal conductivity drops linearly and follows the lower limit function in the temperature range between 160 °C and 1200 °C. Although, it is well known that the thermal conductivity increases with an increasing strength of the concrete (due to an increasing density) prEN 1992-1-2 [2] allows the application of the same functions for concrete strengths  $f_{ck} \geq 70$  N/mm<sup>2</sup>.

According to [3] the specific heat capacity  $c_p$  only slightly differs between normal concrete and UHPC at elevated temperatures.

Since the material properties of concrete differ between the heating and the cooling phase in [8] it is recommended to assume constant values for the thermal material properties for the entire cooling phase depending on maximum temperature.

For the approximation of the occurred spalling in the column fire test exposed to the temperature-time curve *T1* a 1 cm thick layer of the cross-section was removed during the simulation. For the UHPC column exposed to the temperature-time curve *T2* a 2 cm thick layer was removed after 18 minutes and another 1 cm thick layer after 36 minutes. This principle is shown in Figure 5. This simplified assumption is based on the time-dependent visual observations the spalling occurred as well as on the measured temperatures in the fire tests.

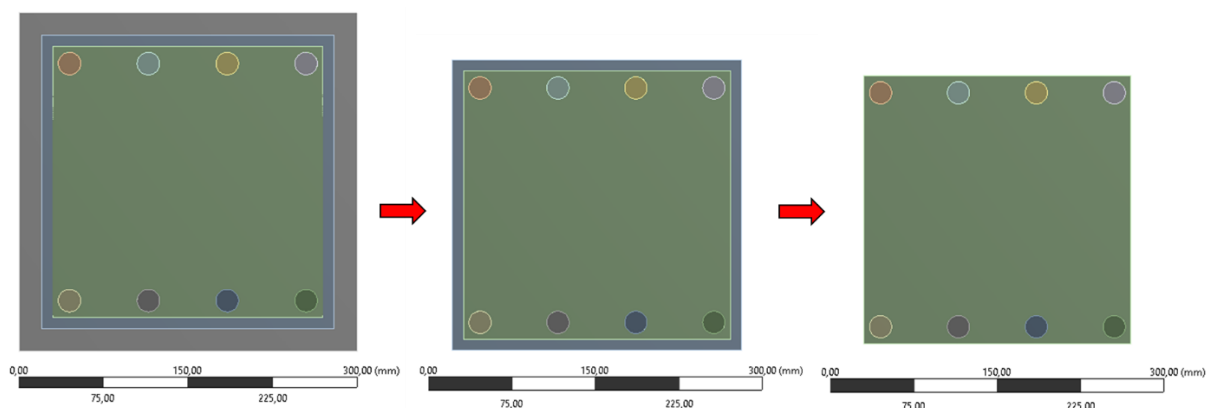


**Figure 5** *Modelling of the spalling for the UHPC column exposed to the temperature-time curve T2 at the beginning (left), after 18 minutes (middle) and after 36 minutes (right)*

In Figure 6 the measured temperatures ( $M$ ) in the column fire tests in depths of 40 mm and 150 mm (centre of the column) from the fire exposed surface are compared to the numerical simulations. Here, two cases were analysed. In case 1 (*C1*) no spalling was considered in the simulation. Thus, no reduction of the cross-section due to spalling was taken into account. In case 2 (*C2*) the above described reduction of the cross-section was carried out.

Indeed the results show deviations between the experimental measurements and the numerical simulations. In fact a disregard of the spalling in the simulations leads to an underestimation of the temperature development in the cross-section and thus to an overestimation of the load bearing capacity in case of fire.

The UHPC column exposed to the temperature-time curve *T1* exhibited only local spalling. Thus, compared to case 2 in the simulations case 1 shows a good accordance to the measured temperatures in a depth of 40 mm for the heating phase (first 90 minutes). However, in the

centre (150 mm) the calculated temperatures are nearly identical for both cases (C1 and C2) regarding T1.

The UHPC column exposed to the temperature-time curve T2 exhibited massive spalling. Thus, compared to case 1 in the simulations case 2 shows a better accordance to the measured temperatures. Without the consideration of spalling in the simulation (case 1) the calculated temperatures highly underestimate the measured temperatures in a depth of 40 mm as well as in the centre (150 mm).

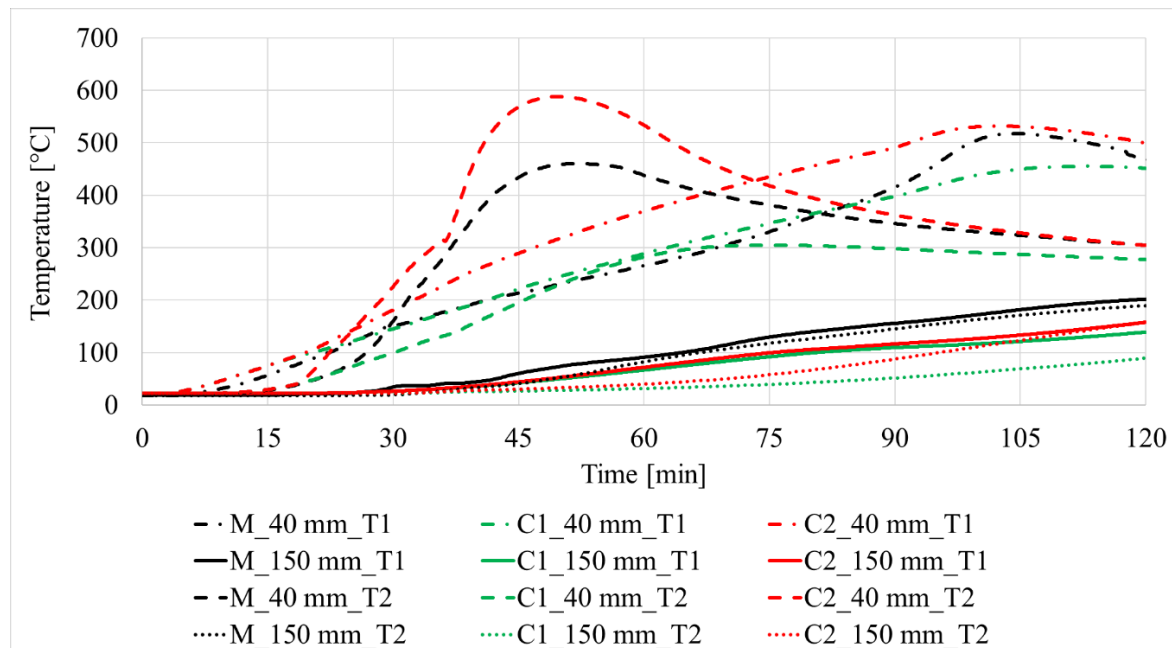


Figure 6 Comparison of the temperature development between the measured temperatures in the column fire test (black), the simulation without consideration of spalling (green) and with consideration of spalling (red) in the cross-section in depths of 40 mm and 150 mm exposed to the temperature-time curves T1 and T2

The comparison of the measured temperatures and the simulations highlights following statements:

- The consideration of massive spalling leads to a better prediction of the temperature development in the cross-section of the columns compared to the simulation without consideration of spalling. However, the simulated temperatures underestimate the temperature in the centre (150 mm) in both cases (C1 and C2).
- For the simulations the thermal material functions according to prEN 1992-1-2 [2] were chosen. These functions can be utilized for concrete strengths  $f_{ck} \geq 70 \text{ N/mm}^2$ . Indeed the thermal conductivity of UHPC at ambient temperature and at elevated temperatures differs to normal and high performance concrete.
- Based on extensive investigations on heated concrete in [8], for the cooling phase it is recommended to assume constant values for the entire cooling phase depending on maximum temperature. However, present investigations have shown that a modification of the thermal material properties in the cooling phase should be taken into account for a better compliance between numerical simulations and experimental results [5].

## CONCLUSIONS & OUTLOOK

In this paper the results of the experimental investigations of the thermo-mechanical material properties of ultra-high performance concrete exposed to the ISO 834 standard fire and natural fires, including a cooling phase are compared to each other. The focus is on the spalling behaviour of UHPC columns exposed to fire and their modelling for the examination of the temperature develop within a thermal analysis.

Thus, so far no well-established and standardized model for the spalling behaviour of concrete in case of fire is available. However, spalling reduces the cross-section of concrete building components and thus leads to faster heating and reduction in strength of the UHPC. For UHPC exposed to the ISO 834 standard fire the decrease in compression strength for temperature > 300 °C is lower compared to standardized normal concrete. Regarding natural fires, compared to the heating phase the compression strength of UHPC significantly drops in the cooling phase. Furthermore it has to be taken into account for natural fires that the heating rate, as well as the maximum can exceed the ISO 834 standard fire during the first minutes of thermal exposure. Especially a high temperature gradient in the temperature-time curve has a negative influence on the spalling behaviour of concrete components. Therefore, numerical models have to be developed for the spalling behaviour of concrete that take into account the modelling of PP-fibres, the different densities of the concretes as well as the moisture content and the mechanical load. Beside these elementary factors other parameters as the aggregate type or the amount of reinforcement influences the spalling behaviour of concrete components.

## REFERENCES

1. Schmidt, M., *Nachhaltiges Bauen mit ultra-hochfestem Beton*, Ergebnisse des Schwerpunktprogrammes 1182, Gefördert durch die Deutsche Forschungsgemeinschaft (DFG). Universität Kassel: kassel university press, 2014.
2. Eurocode 2: Design of concrete structures - Part 1-2: General rules - Structural fire design, prEN 1992-1-2: 2021.
3. Hosser, D. et al., "Theoretical and experimental determination of the high temperature behavior of ultra high performance concrete (UHPC)", Final Report: SPP 1182, 2013.
4. Zehfuß, J., *Bemessung von Tragsystemen mehrgeschossiger Gebäude in Stahlbauweise für realistische Brandbeanspruchung*, Dissertation TU Braunschweig Hrsg. Braunschweig: Institut für Baustoffe, Massivbau und Brandschutz iBMB – Materialprüfanstalt für das Bauwesen MPA; H. 175, 2004.
5. Zehfuß, J.; Lyzwa, J., "Theoretische und experimentelle Untersuchungen zur Erweiterung der Berechnungsgrundlagen unterschiedlicher Betone bei Naturbrandbeanspruchung", Schlussbericht DFG-Forschungsvorhaben ZE 1053/1-1, 2019.
6. Lyzwa, J., Zehfuss, J., "Experimental investigations of ultra-high performance concrete exposed to natural fires", *Fire Safety Journal*, Volume 125, 2021.
7. Schneider, U., Diederichs, U. & Horvath, J., "Verhalten von Ultrahochfesten Betonen (UHPC) unter Brandbeanspruchung", *Beton- und Stahlbetonbau*, 98 (7), pp. 408-417, 2003.
8. Schneider, U., "Concrete at High Temperatures - A General Review", *Fire Safety Journal*, Volume 13, 1988.

# A critical review of the moisture clog theory

Benedikt Weber <sup>1,\*</sup>

<sup>1</sup> Empa, Dübendorf, Switzerland

\* Corresponding author (benweber@bluewin.ch, Empa, Swiss Federal Laboratories for Materials Science and Technology, 8600 Dübendorf, Switzerland)

## ABSTRACT

The moisture clog theory suggested by Shorter and Harmathy is one of the oldest and most cited spalling theories. The original version is a qualitative explanation of a mechanism leading to a pressure build-up during heating of concrete and finally to spalling. Later, Harmathy published a simple model to derive a quantitative criterion for spalling. The concepts of the theory are important for understanding spalling, but the details have hardly been evaluated or developed further in the literature. A detailed analysis is missing even in modelling papers.

In this paper, we critically review the moisture clog theory. Especially, when looking at the simple quantitative model, it becomes clear that some of the underlying assumption do not correspond to the actual physics. Nevertheless, the principle ideas are still valid and can be used to formulate a revised model. Although this model still does not explain the spalling mechanism, it clearly illustrates the relationship between temperature, permeability, and pressure at the drying front and is useful for interpreting the results of a more sophisticated finite element simulation.

**KEYWORD:** spalling theory, moisture accumulation, drying front.

## INTRODUCTION

In 1961, Shorter and Harmathy published a "probable mechanism of spalling" [1]. This was originally only a discussion on an experimental paper about the fire endurance of prestressed concrete beams, but became later known as the "moisture clog theory". In a follow-up paper, Harmathy developed a more quantitative version of the moisture clog theory [2]. Using simple approximations, he developed a spalling criterion based on moisture content and permeability. While the criterion looks reasonable, the model contains several assumptions that are difficult to justify on physical principles.

The moisture clog theory has become very popular over the years. It is usually used to explain the mechanism of pressure build-up during heating in an intuitive way, often accompanied by elaborate illustrations. Some of these illustrations were reproduced many times, with or without reference to the originals, which are hard to trace back. Some of the early figures are due to Connolly [3] and to Consolazio [4]. Although some details of the theory have been repeated again and again, it remained basically an unproven hypothesis. Despite its widespread acceptance, the moisture clog theory has not been able to provide a generally accepted explanation of the spalling mechanism.

One step towards proof seems to be the observations made in some experiments. For instance, water accumulation has been observed in X-ray tomography [5] and in neutron tomography [6]. Water accumulation has even been observed visually by splitting a concrete slab in a fire test [7]. However, the existence of a moisture clog in itself does not constitute a proof of the theory. The question remains as to how a moisture clog is related to a pressure build-up and to spalling.

If experiments cannot prove the theory, one would expect that at least numerical models could explain how a moisture accumulation triggers a pressure build-up and spalling. However, no attempts in this direction have been found in the literature. Although many publications on numerical models present Harmathy's theory in the introduction, they do not use their model to validate this theory. In the best case, numerical models reproduce an increase of saturation in the cold zone and confirm this part of the theory. However, they do not explain how a saturated zone causes a pressure build-up.

In this paper, we critically review the moisture clog theory and show that some of the underlying assumptions have to be revised. However, while retaining the general ideas, it has been possible to develop a new view of the drying mechanism and the pressure build-up.

## **MOISTURE CLOG THEORY**

A qualitative description of the theory has first been suggested by Shorter and Harmathy [1]. The theory has then been stated more precisely in a follow-up paper by Harmathy [2], in which he also presented a simple quantitative model.

### **Qualitative theory**

The qualitative description is presented first. It comprises the following steps (Figure 1a):

- As the temperature in a thin layer near the exposed surface exceeds the boiling temperature, capillary water evaporates and vapour moves into the interior, where the temperature is lower. There it condenses and fills the pores with liquid, generating a fully saturated layer called the moisture clog.
- In the meantime, the temperature at the exposed surface keeps rising, while the temperature at the drying front is not much higher than the boiling temperature. A steep temperature gradient thus develops across the still relatively thin dry layer. This results in a high heat flow and a high rate of vaporization.
- As the passage into the colder region is blocked by the saturated layer, the vapour can only move towards the exposed face. However, as the thickness of the dry layer increases, its resistance to vapour flow also increases and hinders the vapour from escaping. This leads to a rapid pressure build-up at the drying front.
- The high pressure and the thermal stresses due to the high temperature gradient finally lead to spalling.

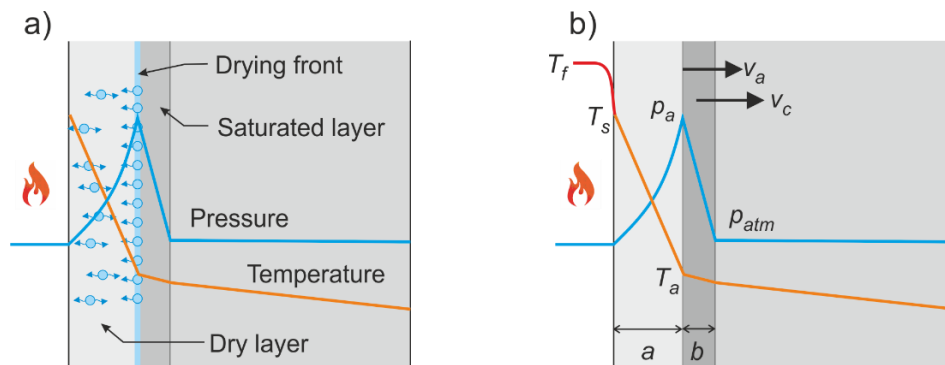


Figure 1: a) Moisture clog theory according to Shorter and Harmathy [1] and b) Model after Harmathy [2].

The moisture clog theory was one of the first attempts to understand the phenomenon of spalling. The general picture with a drying front and a pressure peak has been confirmed by neutron experiments showing that there is indeed a relatively sharp drying front in the interior [8], and in some cases water accumulation has also been observed [6]. The theory thus still contributes to the basic understanding of the process. However, on closer examination of the physics described in the theory, some caveats are in order.

A large part of the theory is devoted to the formation of the saturated zone and the development of the resistance against vapour flow towards the interior and towards the exposed face. These detailed explanations and the name of the theory could give the impression that this part is the essence of Harmathy's theory. However, the other points, the steep temperature gradient and the high vaporization rate are at least as important. Indeed, the explanation of the vapour flow and the formation of a dry and wet zone merely describes the initial phase of the drying process. The essential argument for the pressure build-up is the high vaporization rate due to the steep temperature gradient. Concentrating only on the saturated zone, as is often done in the literature, is thus misleading. In fact, there is no need for full saturation to block the vapour flow towards the interior, since the resistance in this direction is already high due to the large distance to the unexposed face and the partial saturation in this region.

A weak point of the theory is that it assumes a steep temperature gradient because of the small thickness of the dry zone and the relatively low temperature at the drying front "not much above the boiling temperature". The steep gradient implies a large heat flow and in turn a high rate of vaporization. The idea behind these considerations is that most of the heat flow is consumed by vaporization, which in turn prevents a large temperature increase. This would be similar to ice in hot water, where the ice is molten rather than heated. However, the situation is different here. Since the water is only present in the pores, only a fraction of the heat flow is consumed for vaporization, whereas most of it passes through the front by conduction in the solid skeleton. In consequence, the vaporization rate is not as high as anticipated. In addition, the water temperature at the front can be much higher than the boiling temperature due to the high pressure. This would also mean that the temperature gradient would no longer be as steep as expected.



### Quantitative model

In a later paper [2], Harmathy used the ideas of the moisture clog theory in a simple numerical model and derived a spalling criterion. The model is not only the basis of the spalling criterion but also clarifies some details of the original qualitative model.

The model includes a dry and a saturated layer as shown in Figure 1b). Initially, the concrete is partially saturated with a saturation  $S$ . When heated, this water evaporates and moves in both directions. The fraction  $\delta$  that moves to the cold side fills the pores and forms the saturated zone. The thickness of the saturated zone then becomes

$$b = \delta a \frac{S}{1-S} \quad (1)$$

Next, we consider the heat flux. The original version of the model calculates the surface temperature  $T_s$  from the furnace temperature  $T_f$  and from a heat transfer coefficient. Since both have to be estimated, we prefer to use directly the surface temperature. This simplifies the derivation and focuses on the essential ideas. Assuming a linear temperature distribution, the heat flux in the dry layer is

$$q_T = -k \nabla T = k \frac{T_s - T_a}{a} \quad (2)$$

where  $k$  denotes the heat conduction coefficient and  $\nabla T$  the temperature gradient. At the drying front, this heat flux is used for vaporization. The energy balance at the drying front can generally be described by the Stefan condition. A classic example of a Stefan problem is the melting of ice. When heating liquid water in contact with a body of ice, the ice stays at a temperature of zero degree Celsius and all thermal energy is consumed by the melting process. The Stefan condition relates the heat flux to the propagation speed of the drying front. Assuming full saturation and taking into account the porosity, Harmathy uses the condition

$$q_T = v_a \rho_l \phi \Delta h \quad (3)$$

where  $v_a$  is the speed of the drying front,  $\rho_l$  is the liquid density,  $\phi$  is the porosity, and  $\Delta h$  is the specific enthalpy of evaporation. Combining Eq. (2) and (3) results in the speed of the drying front

$$v_a = \frac{k(T_s - T_a)}{a \Delta h \rho_l \phi} \quad (4)$$

The model by Harmathy also takes into account the movement of the saturated zone due to the pressure at the drying front. Assuming a linear pressure distribution in the liquid, the velocity of the moisture clog is described by Darcy's law as

$$v_c = \frac{\kappa_l}{\mu_l} \frac{p_a - p_{atm}}{b} \quad (5)$$

where  $\kappa_l$  is the permeability and  $\mu_l$  the viscosity of the liquid. Harmathy now suggests a spalling criterion by comparing the two velocities  $v_a$  and  $v_c$ . He argues that if the moisture clog moves faster than the evaporation front, this would prevent a further pressure build-up. On the other hand, if the moisture clog moves more slowly than the evaporation front, the pressure build-up would continue until the tensile strength of the concrete is reached and spalling occurs. His spalling condition is thus

$$v_c < v_a \quad (6)$$

Before discussing these arguments further, we show the results obtained by Harmathy. Replacing  $b$  in Eq. (5) by Eq. (1) and setting the pressure difference equal to the tensile strength of the concrete, i.e., setting  $p_a - p_{atm} = \sigma_f$ , the spalling condition becomes

$$S(\kappa_l) > \frac{1}{1 + \frac{\delta\mu_l(T_s - T_a)}{\rho_l\Delta h} \frac{k}{\phi\kappa_l\sigma_f}} \quad (7)$$

Note that this formula expresses the criterion in terms of  $T_s - T_a$ , whereas Harmathy expresses it in terms of  $T_f - T_a$  (there is a typo in Eq. (9) of Harmathy's paper). For his calculations, Harmathy assigned "plausible values" to the variables but did not specify all parameters individually. In Table 1, we provide a set of values consistent with the calculations by Harmathy. Note that the water properties given in the table relate to standard temperature and pressure conditions. In reality, the liquid viscosity at 150°C would be five times lower than at room temperature. However, with this lower value, the numbers by Harmathy cannot be reproduced. Using the values given in Table 1, Eq. (7) generates the curve shown in Figure 2, which is identical to the original curve by Harmathy. This result is consistent with the general observation that a high initial saturation and a low permeability increase the risk of spalling. Note, however, that the permeability here is related to the liquid and not to the gas, as one would normally expect.

Table 1: Parameters used for spalling criterion according to Harmathy

$\delta = 0.3$	$\mu_l = 10^{-3} \text{ Pa} \cdot \text{s}$	$\Delta h = 2.25 \text{ MJ/kg}$
$T_s = 500 \text{ }^\circ\text{C}$	$\rho_l = 10^3 \text{ kg/m}^3$	$\phi = 0.3$
$T_a = 150 \text{ }^\circ\text{C}$	$k = 1 \text{ W/(m} \cdot \text{K)}$	$\sigma_f = 1.7 \text{ MPa}$

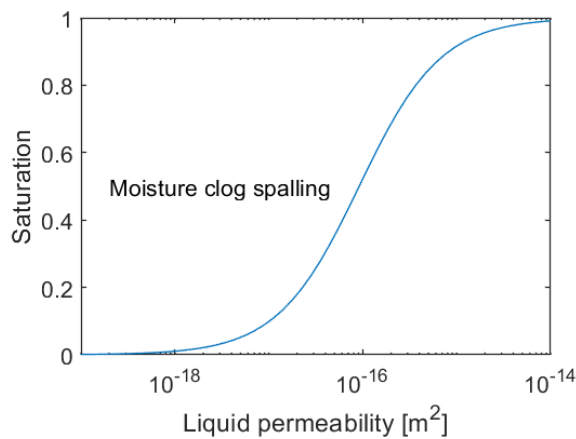


Figure 2: Spalling criterion according to Harmathy [2].

A weak point of the derived model concerns the formulation of the Stefan condition, as already discussed in the qualitative theory. In contrast to the melting ice problem, not the entire heat flux is consumed by drying. A large part of the incoming heat passes through the solid skeleton by conduction and heats up the concrete behind the front. Only the difference in the heat flux drives the evaporation. The full Stefan condition reads

$$k_1\nabla T_1 - k_2\nabla T_2 = v_a\rho_l\phi\Delta h \quad (8)$$

where  $k_1$  and  $k_2$  are the thermal conductivities in the two zones, and  $\nabla T_1$  and  $\nabla T_2$  are the corresponding temperature gradients. As will be shown below in some simulations, the difference in the heat flux is actually only a small fraction of the incoming heat flux.

Another problematic point concerns the movement of the moisture clog due to pressure. According to Harmathy, a pressure build-up is prevented if the moisture clog moves faster than the drying front. This condition seems to be rather questionable. It is more likely that the drying front develops relative to the saturated zone. A moving moisture clog would thus just increase the absolute velocity of the drying front without having a big effect on the pressure. On the other hand, it is not expected that an immobile moisture clog would unconditionally lead to a continuous pressure increase.

In summary, the analysis of the moisture clog theory has revealed a number of assumptions that are not compatible with the underlying physics. In particular, the theory does not explain the pressure build-up in a convincing way.

## REVISED MODEL

### Basic relations

The simple quantitative model by Harmathy can be adapted to better account for the physics of the drying process. Although the revised model does not directly lead to a new spalling criterion, it helps to better understand the mechanism of the pressure build-up and to interpret results from a more sophisticated finite element simulation.

In the revised model, as in the original model, we assume that the vapour is generated exclusively at the drying front and moves only towards the hot face. The vapour flux is thus determined by the peak pressure at the front. Since the vapour is a compressible gas, the transport from the drying front to the free surface has to be formulated based on constant mass flux. For a perfect gas, the pressure follows a square root distribution:

$$\rho_v(x) = \sqrt{\rho_{atm}^2 + \frac{\rho_a^2 - \rho_{atm}^2}{a} x} \quad (9)$$

where the coordinate  $x$  has its origin at the free surface. Employing Darcy's law, the convective mass flux is thus

$$j_{conv} = -\rho_v \frac{\kappa_g}{\mu_g} \nabla p_v = -\frac{M_w}{RT} \frac{\kappa_g}{\mu_g} \frac{\rho_a^2 - \rho_{atm}^2}{2a} \quad (10)$$

where  $\rho_v$ ,  $\kappa_g$ ,  $\mu_g$ , and  $\nabla p_v$  denote the vapour density, the gas permeability, the gas viscosity, and the pressure gradient, respectively. In the second part of Eq. (10), the vapour density has been replaced by the perfect gas law

$$\rho_v = \frac{M_w p_v}{RT} \quad (11)$$

where  $M_w$  and  $R$  are the molar mass of water and the universal gas constant, respectively. Equation (10) is also often used in permeability measurements, where the expression  $M_w/RT$  is replaced by  $\rho_v/p_v$  according to the perfect gas law.

In contrast to Harmathy's model, we do not derive the vapour source from the heat flux. As will be demonstrated in the example below, the temperature profile is not much affected by the energy lost due to vaporization, and the change in the heat flux at the drying front is rather

small. However, we can still use the relation between the propagation speed of the front and the generated vapour flux:

$$j_{evap} = v_a S \phi \rho_l \quad (12)$$

where  $S$  is the liquid saturation, which could be less than one if the medium is not fully saturated. In fact, a fully saturated zone is not demanded in this model. Equation (12) is nothing than a mass conservation relation: The water mass evaporated is removed from the liquid in the pores at the speed of the front. Assuming that all vapour moves to the hot face, we can set the generated vapour flux  $j_{evap}$  equal to the convective heat flux  $j_{conv}$ . The vapour flux determined from the peak pressure can thus be used to estimate the propagation speed of the drying front:

$$v_a = \frac{j_{conv}}{S \phi \rho_l} \quad (13)$$

In summary, to describe the process, we start with the pressure peak, which mainly depends on the temperature at the drying front. The pressure peak determines how much vapour passes through the dry layer. This vapour is produced by removing liquid water from the pores, which defines the speed of the drying front.

### Example

To exemplify the relations derived above, they are applied to a finite element simulation of the Kalifa test [9]. This test has often been used in the literature to validate numerical models. In all known simulations, the permeability used in the model is considerably lower than the measured one [10]. Here, the model described in [11] is used with two different permeabilities: a low permeability, tuned to match the pressures measured in the experiment, and a high permeability corresponding to the measured value. Note that in the simulation most material parameters depend on temperature, whereas the simple formulas given here assume constant parameters. The results are thus only estimates depending on the actual constant parameter values chosen. Also note that the heating in this test was less severe than in a fire and the front thus propagates much more slowly. Nevertheless, the example demonstrates the essential phenomena.

Results with the lower permeability are shown in Figure 3. Several variables with different units and different scaling are plotted in one figure. Figure 3a) shows the mass source, the saturation, and the temperature. After two hours of heating, the drying front is at 3 cm, as indicated by the peak of the mass source. This position separates the dry and the almost saturated regions as confirmed by the saturation curve. The temperature curve exhibits a small kink at the drying front, which is hardly visible and which corresponds to the heat flux consumed by evaporation. Figure 3b) shows the pressure, the mass flux, and the vapour saturation pressure. The pressure in the partially saturated region follows the vapour saturation pressure determined by the temperature and drops to the atmospheric pressure within the dry region. The pressure peak is slightly lower than the vapour saturation pressure due to capillary effects according to the Kelvin equation. The vapour generated at the drying front moves almost entirely to the hot side as confirmed by the positive mass flux.

In the case with higher permeability, shown in Figure 4, the front has moved almost 5 cm in two hours. Although the pressure is lower than in the first case, the increased permeability leads to a larger mass flux and thus to a larger depth of the front at the time of comparison. The temperature curve is barely affected by the drying, but the temperature at the front is

lower, because the front has moved further into the concrete. Finally, the low pressure is due to the lower temperature at the front.

From the two simulations, it becomes clear that the pressure is mainly determined by the temperature at the front. The permeability affects the pressure only indirectly through the propagation speed of the front. The heat flux given by the slope of the temperature curve, or more precisely by its change at the drying front, is very small and cannot be used to estimate the vapour source. Assuming that the total incoming heat flux is consumed by vaporization, as did Harmathy, is certainly not valid.

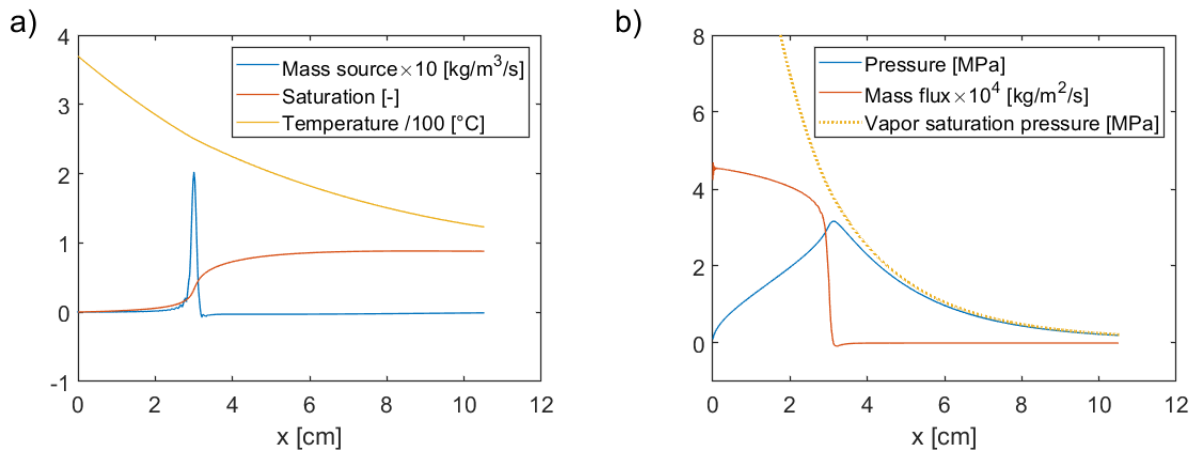


Figure 3: Results from finite element simulation (low permeability).

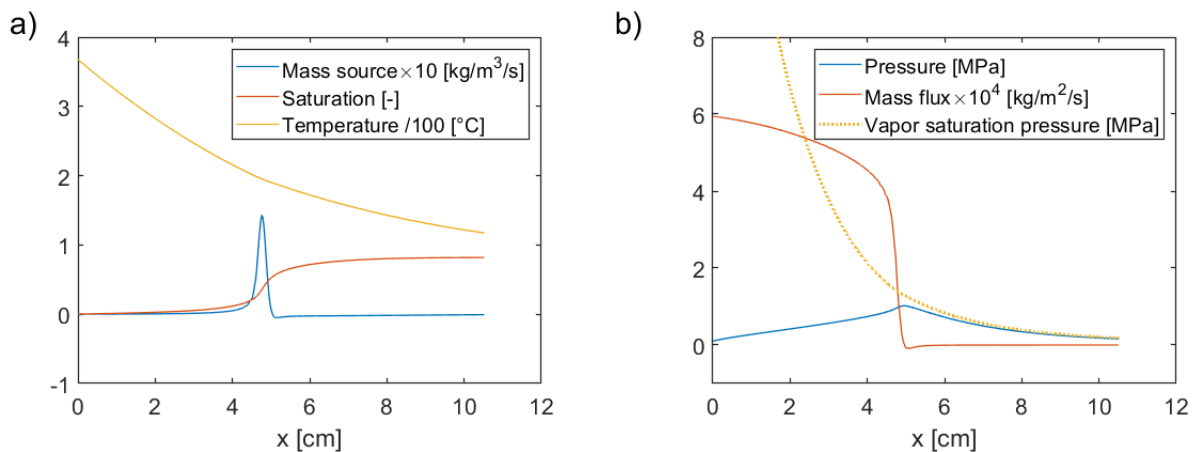


Figure 4: Results from finite element simulation (high permeability).

Table 2: Parameters for revised model

Common	Low permeability	High permeability
$M_w = 0.018 \text{ kg/mol}$	$\kappa_g = 12 \times 10^{-18} \text{ m}^2$	$\kappa_g = 2.1 \times 10^{-16} \text{ m}^2$
$R = 8.3145 \text{ J/(mol} \cdot \text{K)}$	$\rho_a = 3.2 \text{ MPa}$	$\rho_a = 1.0 \text{ MPa}$
$\rho_{atm} = 0.1 \text{ MPa}$	$a = 3.0 \text{ cm}$	$a = 4.8 \text{ cm}$
$\phi = 0.09$	$T_a = 250 \text{ }^\circ\text{C}$	$T_a = 200 \text{ }^\circ\text{C}$
$S_0 = 0.74$		
$m_{hyd} = 55 \text{ kg/m}^3$		
$\rho_l^0 = 1000 \text{ kg/m}^3$		
$\mu_g = 1.8 \times 10^{-5} \text{ Pa} \cdot \text{s}$		

To check the equations of the revised model, some numbers consistent with the simulations are chosen as presented in Table 2. The gas viscosity has been taken at 250°C for both cases. Using Eq. (10) the vapour flux is  $j_{conv} = 4.7 \times 10^{-4} \text{ kg/(m}^2\text{s)}$  for the low permeability and  $j_{conv} = 5.5 \times 10^{-4} \text{ kg/(m}^2\text{s)}$  for the high permeability, which both agree sufficiently well with the simulation results.

The propagation speed of the front can easily be determined from the mass flux according to Eq. (13). This equation just expresses the fact that the front moves as water is removed. For the water mass per volume of concrete, one has to be aware that the saturation at the drying front can be slightly higher than the initial saturation due to vapour condensation, due to thermal expansion of the liquid, and due to dehydration. Dehydration is modelled in the finite elements simulation as a function of temperature. In the example, only part of the initially hydrated water  $m_{hyd}$  is released at the temperature at the front. Taking for the water mass the initial water content and half of the hydration water yields  $m_w = \phi S_0 \rho_l^0 + \frac{1}{2} m_{hyd} = 94 \text{ kg/m}^3$ . The resulting velocities are then 1.8 cm/h and 2.1 cm/h for the low and high permeability, respectively. These velocities are indicated in Figure 5a) where the position of the front is plotted vs. time for both cases. A third case with reduced saturation is mentioned later. Note that it takes some time for front to develop. Also note that in a fire, the heating is more severe and the front moves faster than in this experiment. Different front speeds have been observed directly in neutron experiments, where concrete with fibers showed a faster front movement [12,13].

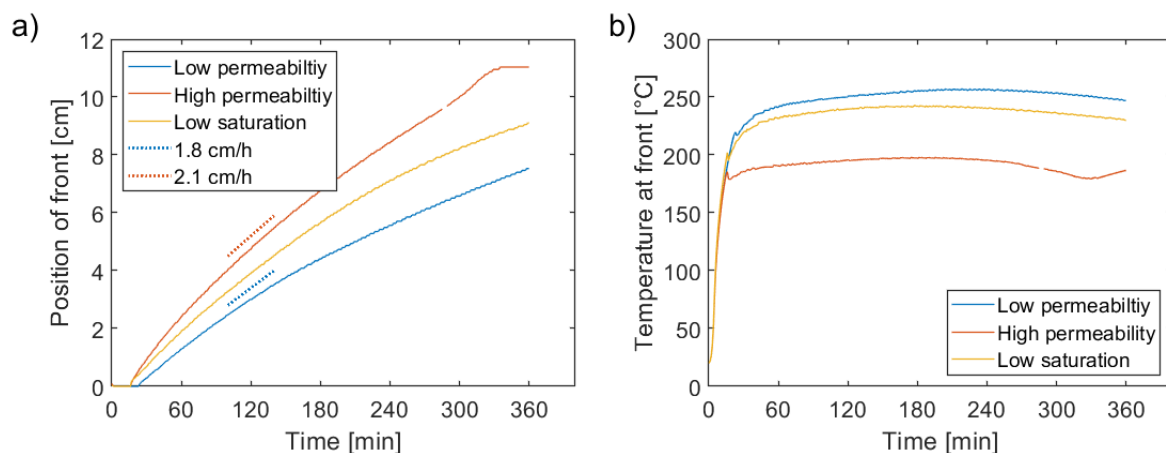


Figure 5: a) Position of the front vs time, b) temperature at the front vs time.

An interesting observation is that the temperature at the front is stable, as shown in Figure 5b). The propagation speed adjusts itself to keep the equilibrium. If the overall temperature increases too fast, the pressure increases as well, which in turn increases the propagation speed until the front has reached a lower temperature. If, on the other hand, the overall temperature increases too slowly, the propagation speed is reduced. It appears thus that both the overall temperature and its gradient play a role in this process. However, an exact stability condition will not be derived here.

The interaction between the temperature at the drying front and the movement of the drying front can also explain the effect of different initial saturations. A smaller saturation increases the speed of the front and moves it to a lower overall temperature, which also leads to a lower pressure. This is shown in Figure 5 for a simulation with the low permeability and an initial saturation reduced to  $S_0 = 0.2$ .

While the moisture clog theory fails to provide a convincing explanation for a pressure build-up, the revised model still predicts a high pressure in case of a low gas permeability and a high liquid saturation. In this case, the front moves slowly and remains close to the hot face, where the temperature is highest. Since the pressure is essentially determined by the temperature at the front, this results in a high vapour pressure.

## **SUMMARY AND CONCLUSIONS**

The moisture clog theory was one of the first attempts to understand the mechanism of spalling. The general concept with a drying front and a pressure peak still contributes to understanding, but some details of the derivation are not consistent with the underlying physics. Despite recent advanced in modelling, the moisture clog theory has not been further analysed or even disputed in the literature.

The first part of the theory describes the formation of the saturated zone and the development of the resistance to vapour flow. The resistance towards the interior is enhanced through a saturated zone; the resistance towards the exposed face grows with the depth of the dry layer. In our opinion, the creation of the saturated zone is overstated in the original paper and even more in the citing literature. In fact, the resistance towards the interior is already much higher than towards the exposed face, even without moisture accumulation.

In any case, the main argument for a pressure build-up is related to the vapour source. However, the high rate of vaporization claimed in the theory is based on the wrong assumption that the total heat flow entering the concrete is used for vaporization. In reality, only a fraction of the energy is used.

The spalling criterion proposed in the second paper by Harmathy seems questionable. It is difficult to understand, how a movement of the saturated zone could relax the pressure. It would be more plausible to base a criterion on the gas permeability in the dry zone rather than on the liquid permeability in the saturated zone.

Following the ideas of Harmathy, a revised model has been established. It describes the process at the drying front with some simple relations, which have been confirmed by simulations with a more sophisticated finite element model. The results show that the propagation speed of the front is a key factor for the pressure peak. This speed can be calculated from the vapour permeability and the saturation. A low permeability and a high saturation lead to a slow speed of the front. In this case, the front remains close to the hot face



and the high temperature at the front leads to a high pressure. In this context, a moisture accumulation, as described in the moisture clog theory, can increase the pressure to a certain extent.

## REFERENCES

1. Shorter, G. W., and Harmathy, T. Z., "Discussion on the Fire-Resistance of Prestressed Concrete Beams.," *Proc. Inst. Civ. Eng.* **20** (1961) 305–320.
2. Harmathy, T. Z., "Effect of moisture on the fire endurance of Building elements," *Spec. Tech. Publ. No. 385, ASTM Int.* (1965) 74–95.
3. Connolly, R. J., *The spalling of concrete in fires*, PhD thesis, Aston University, 1995.
4. Consolazio, G. R., McVay, M. C., and Ill, J. W. R., "Measurement and prediction of pore pressure in cement mortar subjected to elevated temperature," in *Int. Work. Fire Perform. High-Strength Concr. Gaithersburg, MD*, 1997, 125–148.
5. Powierza, B., Stelzner, L., Oesch, T., Gollwitzer, C., Weise, F., and Bruno, G., "Water Migration in One-Side Heated Concrete: 4D In-Situ CT Monitoring of the Moisture-Clog-Effect," *J. Nondestruct. Eval.* **38** (2019) 1–11.
6. Moreira, M. H., Dal Pont, S., Tengattini, A., Luz, A. P., and Pandolfelli, V. C., "Experimental proof of moisture clog through neutron tomography in a porous medium under truly one-directional drying," *J. Am. Ceram. Soc.* **105** (2022) 3534–3543.
7. Jansson, R., *Fire Spalling of Concrete: Theoretical and Experimental Studies*, PhD thesis, KTH Royal Institute of Technology, Stockholm, 2013.
8. Toropovs, N., Lo Monte, F., Wyrzykowski, M., Weber, B., Sahmenko, G., Vontobel, P., et al., "Real-time measurements of temperature, pressure and moisture profiles in High-Performance Concrete exposed to high temperatures during neutron radiography imaging," *Cem. Concr. Res.* **68** (2015) 166–173.
9. Kalifa, P., Menneteau, F.-D., and Quenard, D., "Spalling and pore pressure in HPC at high temperatures," *Cem. Concr. Res.* **30** (2000) 1915–1927.
10. Weber, B., "Open issues in modelling concrete at high temperature," in *6th Int. Work. Concr. Spalling Due to Fire Expo.*, eds. Huang, S.-S., and Burgess, I., Sheffield, 2019, 214–225.
11. Weber, B., "Alternative Implementation of a Porous Media Model for Simulating Drying of Heated Concrete," in *COMSOL Conf. 2018, Lausanne*, 2018, .
12. Tengattini, A., Dal Pont, S., Cheikh Sleiman, H., Kisuka, F., and Briffaut, M., "Quantification of evolving moisture profiles in concrete samples subjected to temperature gradient by means of rapid neutron tomography: Influence of boundary conditions, hygro-thermal loading history and spalling mitigation additives," *Strain* **56** (2020) 1–14.
13. Stelzner, L., Powierza, B., Oesch, T., Dlugosch, R., and Weise, F., "Thermally-induced moisture transport in high-performance concrete studied by X-ray-CT and 1H-NMR," *Constr. Build. Mater.* **224** (2019) 600–609.

# The role of moisture on crack instability of spalling concrete

Ramin Yarmohammadian<sup>1,\*</sup>, Roberto Felicetti<sup>1</sup>,

Fabienne Robert<sup>2</sup>, Laurent Izoret<sup>3</sup>

<sup>1</sup> Politecnico di Milano, Milano, Italy

<sup>2</sup> CERIB Fire Testing Centre, Epernon, France

<sup>3</sup> SFIC, France

\* Corresponding author (Ramin.yarmohammadian@polimi.it, Milano, Piazza Leonardo Da Vinci, Politecnico Di Milano(edificio 5,DICA) , CAP: 20133 )

## ABSTRACT

Prediction and mitigation of explosive spalling require a deep understanding of its energy source and mechanism. So far, research has been mostly focused on elastic energy due to thermal stress, and the crucial role of thermal energy has been disregarded. However, by comparing the magnitudes of their total quantities in the hot concrete cover, one would find that thermal energy is 4 orders of magnitudes larger. Water vaporization can transform this huge source into the mechanical work required to drive the instability of this event. In order to fully understand the role of moisture content in crack propagation and fragment acceleration, concrete disks (D=100mm, thickness=60mm) were heated on the two opposite faces. In this way, a thermo-hygral transient comparable to the fire-exposed concrete cover could be established while minimizing the contribution of thermal stress. In these tests, moisture loss and temperature were monitored by means of a digital scale and a thermocouple in the mid-plane. In the same section, a crack was initiated by embedding a polymeric insert (PTFE ring). The high thermal expansion of the polymer induces tensile stress across the mid-section of the concrete disks, depending also on the insert thickness. This thickness has been optimized by way of FEM analyses so to govern the temperature at which the crack reaches a critical opening. By measuring the sudden mass drop and the acceleration of two specimen halves, the magnitude of mechanical work performed by vapour expansion has been characterized in different concrete mixes with and without polypropylene fibre. This paper intends to emphasize the dual role of moisture in triggering the fracture process by way of pore pressure, but also in converting the huge thermal energy available into the kinetic energy ensuing from the acceleration of the detached splinters.

**KEYWORD:** Fire-induced spalling, Concrete, Mechanism, Fibre, Moisture content

## INTRODUCTION

Explosive spalling represents a potential threat to the fire resistance of concrete structures. Understanding its underlying mechanisms is a crucial step toward the prediction and mitigation of this event. In literature, spalling is defined as a violent or non-violent detachment of fragments from the heated concrete surface [1]. In addition, two mechanisms are generally indicated to explain this event:

- a) Pore pressure: spalling happens when the tensile stress induced by pore pressure is higher than the tensile strength of concrete. This mechanism is more associated with the thermo-hygral process in heated concrete [2][3][4][5].
- b) Thermal stress: thermal gradients and restrained thermal dilation are accounted for spalling [6][7][8], which is regarded as the buckling of the hot skin in the exposed element.

There is also a third theory based on the combination of the above mechanisms [9][10][11]. Following this latter line of reasoning, two stages can be recognized in the progress of the phenomenon: incipient crack formation and unstable crack propagation. In the first stage, high compressive stress parallel to the heated face, fostered by external loads and combined with orthogonal tension induced by pore pressure, can trigger a fracture. Other promoting factors are mesoscale heterogeneity, discontinuity caused by rebars and stress unbalance due to the local convex shape (e.g. corners). Stable cover delamination is frequently observed in post-fire assessment of concrete elements seemingly not affected by spalling.

Concerning the violent separation of fragments that may follow, searching for the energy source behind this remarkably unstable fracture process is an important step toward understanding the fundamental mechanism and its influencing parameters. Possible sources in hot concrete are elastic energy due to thermal stress and thermal energy due to sensible heat, though most studies have been so far focused on the former component. Using velocity measurements on spalled splinters of known thickness, the range of kinetic energy can be calculated (0.5-2.0 kJ/m<sup>2</sup>, [12]). Moreover, the energy required for repeatedly fracturing the cover is in the order of 0.5 kJ/m<sup>2</sup>, based on the typical size of the splinters [13]. However, the elastic energy stored in a 20 mm layer at 200°C is just about 1 kJ/m<sup>2</sup> [14], whereas the sensible heat accumulated by the same layer is 8000 times larger. This patent disproportion finds its roots in the remarkable net thermal flux entering the exposed cover, which can be as high as 25-50 kW/m<sup>2</sup> in the early stage of a fire (Figure 1). It is then clear that thermal energy is a prominent candidate to drive the unstable dynamic fracture characterizing explosive spalling, on the condition that water vaporization can effectively transform this source into mechanical work. This entails a very fast flow of vapour into the opening crack. Given the low permeability of the surrounding concrete, a short diffusion path is required (the diffusion time goes with the distance squared). As an example, if it is assumed that 3% of moisture from a 0.1 mm layer on both faces of the fracture (14 g/m<sup>2</sup>) is vaporized at 200°C and allowed to expand adiabatically from saturation (1.45 MPa) to ambient pressure, the developed work would be 3.5 kJ/m<sup>2</sup>, that is in line with the energy involved by fracture and acceleration of fragments.

This concept of flash vaporization from a thin layer of rather saturated concrete facing the crack has been validated by way of fast Neutron Radiography scans, showing the sizable drying of a sub-millimetre layer facing an interface already a few hundredths seconds after its depressurization [15]. The requirement of fairly high pore saturation is also consistent with the beneficial effect of polypropylene fibre (which allows concrete drying before the crack is triggered) and with the observation that dry concrete doesn't spall.

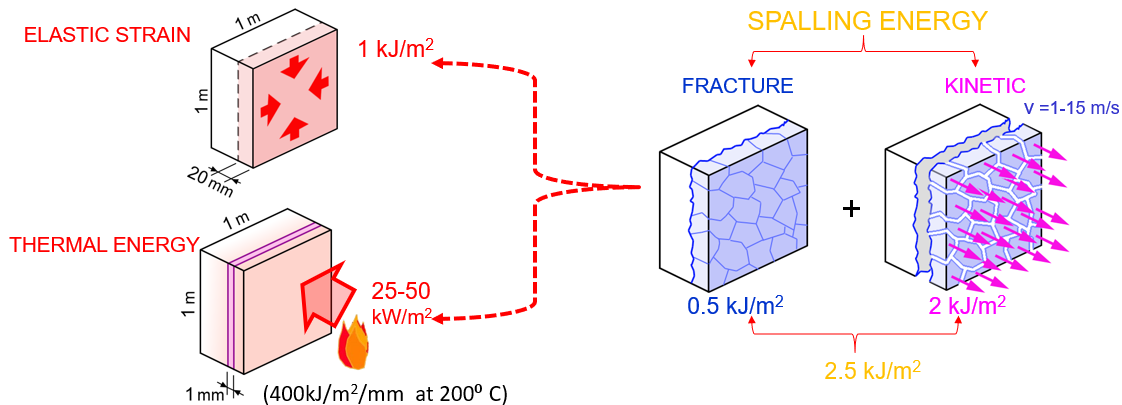


Figure 1 - Comparison of potential energy sources for explosive spalling.

In order to analyse the role of thermal energy and pore saturation in driving the unstable crack propagation in hot concrete, a new setup is here proposed, where a crack is triggered under negligible influence of thermal stress. This is achieved by embedding a polymeric insert in the mid-plane of a concrete disk. The high thermal dilation of polymers, combined with a proper selection of the insert geometry and thickness, allows splitting the heated samples into two halves. The mass loss and the relative acceleration of the two pieces provide indications of the amount of water involved in the process and the effective pressure developed while opening the crack. The path followed during the development of this setup and some early results are presented in the following chapters.

## DESIGN OF THE NEW TEST SET-UP

Spalling takes place in the surface layer of exposed structural elements, where the raise of thermal stress (triggering micro-cracks at the aggregate interface) competes with the progressive drying of pores (stabilizing the incipient cracks). The concept of the proposed test setup is then to reproduce realistic thermal and hygral conditions at the boundaries of the incipient crack whose stability is at issue. This is obtained by ideally mirroring the detaching fragment about the potential fracturing plane, leading to the scheme of symmetrically heating the opposite faces of a concrete disk whose thickness is two times the mean thickness of the detaching splinters. The disk diameter should be large enough to average the inherent material heterogeneity, whilst minimizing the magnitude of thermal stress and its possible contribution to crack instability. The last requirement is to trigger a planar crack across the mid-plane of the disk by way of a properly designed polymeric insert.

The definition of these details was performed through a series of numerical analyses and pilot experimental tests, as summarized in the following.

### Definition of the sample geometry

The size of concrete samples should allow an effective averaging of the inherent material heterogeneity and then it should be scaled on the aggregate size (at least 3.5 times larger according to EN12390-1). Moreover, since a polymeric insert is being embedded in the mid-section, a larger fracturing area is advisable to offset the local disturbance to the material texture. Based on these constraints, concrete disks of 100 mm diameter have been selected as a starting point. Concerning thickness, about 15 mm can be considered as a typical value for the spalled splinters. Then, 40 mm has been selected as the first tentative thickness for the doubly exposed disk. This arrangement allows containing the maximum radial compressive stress within a few MPa. On the other hand, the circumferential tensile stress on the radial

sections gets quite close to the onset of fracture. The risk of radial splitting is further exacerbated by the presence of the expanding polymeric insert. In fact, some first trial samples including a polymer disk confirmed the likely development of radial cracks, which converted to a punching cone in case of too superficial mispositioning of the insert. Following these first results, the disk thickness was increased to 60mm, so to smooth down the circumferential stress and increase the insert cover, enhancing the chance to produce a flat through-crack across the midsection. However, a thicker cover entails longer times for heating and drying, since the time scale of diffusive phenomena goes with the path length squared. For this reason, the heating curve imposed by the radiant heaters has been slowed down by 4 times compared to the standard fire, further relaxing the induced thermal stress. Taking advantage of axisymmetric model in ABAQUS Finite Element software, a sensitivity analysis was performed to understand the effect of each parameter in effectively driving a parallel crack (Figure 2). The ratio between the maximum stress orthogonal to the pursued crack ( $\sigma_{22}$ ) and the maximum radial ( $\sigma_{11}$ ) and circumferential ( $\sigma_{33}$ ) stress can be a good indicator of the chance to split the disk across its mid-plane. This indicator was improved by increasing the disk thickness to 60 mm. This new geometry proved to lead to a more repeatable crack pattern, with some more tolerance to small mispositioning of the insert.

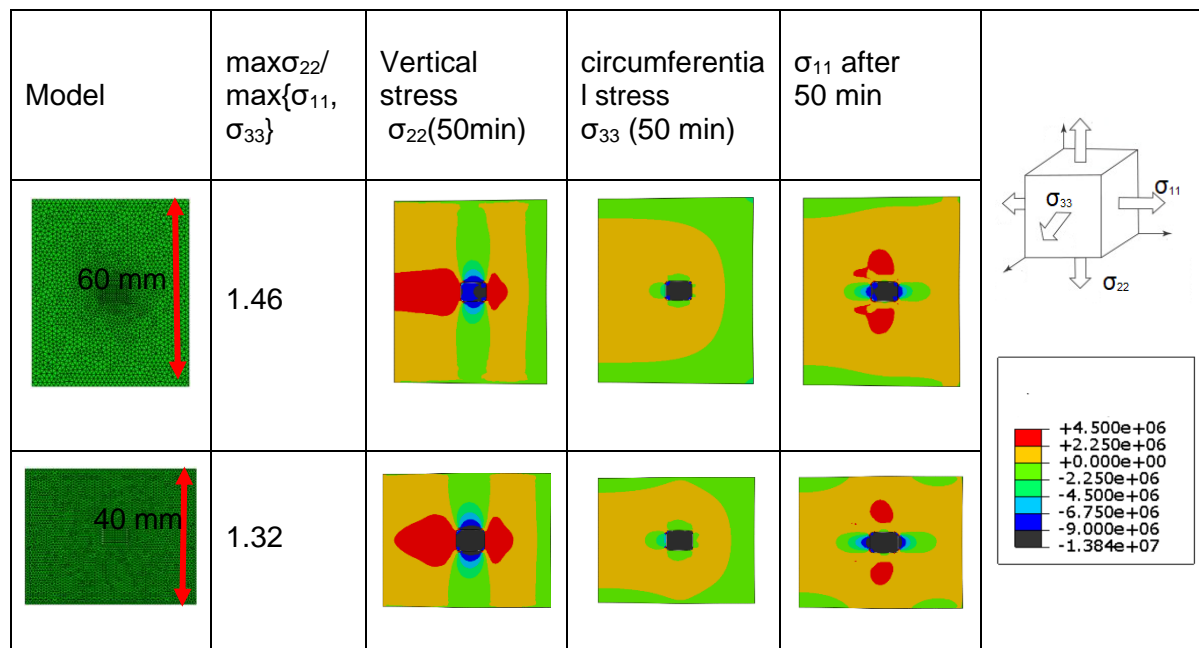


Figure 2 - Stress directions and contours in two selected axisymmetric models.

Concerning thermo-hygral conditions, the original objective of the doubly heated disk was to reproduce the mono-dimensional temperature and moisture transient occurring on the larger flat side of a structural element. For this reason, a lateral sealing system was devised, based on wrapping the disk circumference with an aluminium foil glued with temperature-resistant epoxy resin (3M DP760) or saturating the pores with a low viscosity resin (EPO-TEK 301). Unfortunately, due to the high target temperature and the proximity to the radiant heaters, both solutions proved not very effective (Figure 3), with the further cons of hindering the crack opening and adding extra mass loss and smoke production due to resin decomposition. For these reasons, the original idea was abandoned, and the samples circumference left exposed and unsealed.

The tests have been implemented by way of two opposite radiant heaters (Elstein HTS) fitted with a built-in thermocouple and driven by separate controllers and power regulators. The

sample is positioned on a stand resting on a precision laboratory balance (Kern PBS, 0.01g resolution, real-time digital data transmission also in transient conditions). The balance is screened from radiation by a gypsum fibreboard and the whole setup is enclosed in a laminar flow box, so to draw any smoke produced by the heated polymeric inserts.

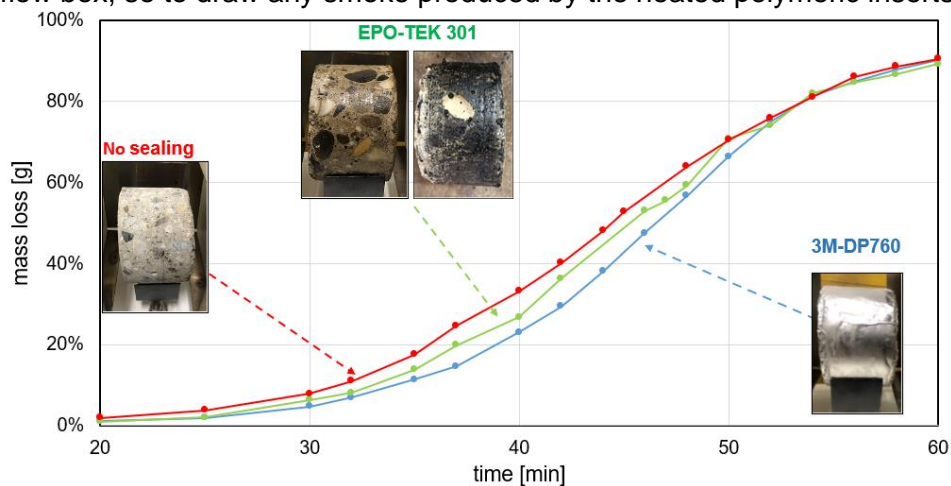


Figure 3 - Sealing test on two different solutions: EPO-TEK301 impregnation and aluminium wrapping with 3M-DP760.

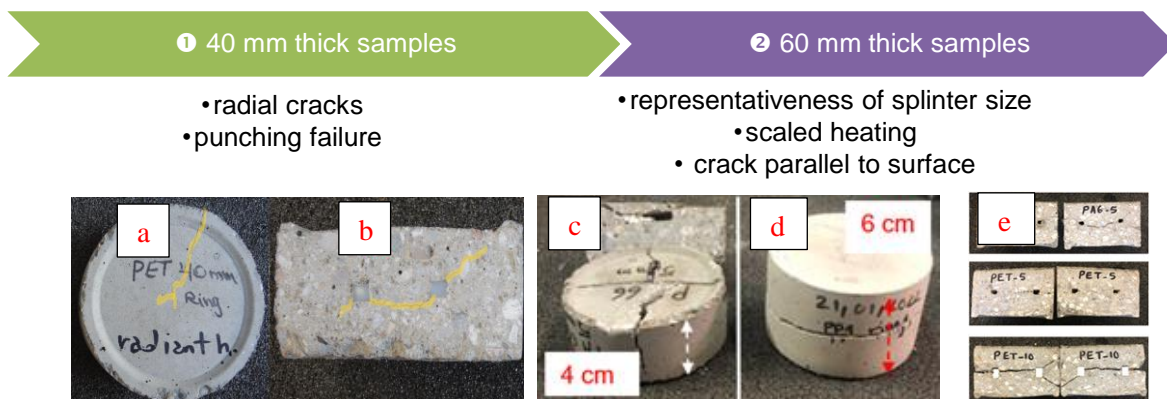


Figure 4 – a: radial cracks in 40mm thickness sample, b: punching cracks, c: punching and radial failure, d: 60 mm thickness sample, e: crack parallel to the surface

### Definition of the polymeric insert to trigger the crack

As mentioned before, to initiate a crack in the mid-plane of the heated disks, a polymer insert was used. As a first tentative, Polyamide 6 (Nylon 6), Polyamide 66 (Nylon 66), and Polyethylene Terephthalate (PET) were used to take advantage of the steep thermal expansion as their respective melting points are approached (220, 260, 250°C), which lie in the typical range of spalling temperature (200-250°C). The problem of this strategy was the penetration of melted polymer through the generated cracks, with possible leaks and loss of pressure. Moreover, the viscous melt tends to promote the inherent tendency of softening materials to minimize energy dissipation by fracturing just on the weakest side, leading to a kind of bending failure. The tentative to keep the melted material separated from concrete, by wrapping the inserts in a thin aluminium foil, proved ineffective because of unintentional air trapped in the shield. To solve the above problems, a higher melting point material was used,



taking advantage of just the thermal dilation, with no phase change. In this new approach, the crack onset is governed primarily by the thickness of the polymeric insert. Polytetrafluoroethylene (PTFE) was selected because of the higher melting point (325°C), market availability and density comparable to concrete, which prevents mispositioning due to floating in the fresh mix. Besides material selection, the shape of the insert is quite an important factor. The disk is an easy shape to produce and position within the concrete sample, but the generated crack pattern was not satisfactory, since punching shear and radial splitting were the most frequent cracking modes. Polymer meshes, can effectively drive a planar crack across the midplane, but moisture and pressure are easily lost because of the early opening of the crack on the perimetral surface. Moreover, a mesh significantly affects the material texture, interfering with the coarse aggregate and taking a significant share of the cross-section area. In the end, the optimal shape turned out to be the ring ( $\varnothing_{\text{ext}} / \varnothing_{\text{int}} = 60 / 46 \text{ mm}$ ), which triggers two fracture fronts (inward and outward), with no early moisture loss nor bending effects. One first series of tests was performed by adopting the following remarkably spalling sensitive concrete mix as such or with the addition of different amounts of polypropylene fibre.

	without fiber	1 kg/m <sup>3</sup> PP fiber	1.5 kg/m <sup>3</sup> PP fiber
Cement CEM III	400	400	400
Filler	280	338	368
Effective water	160	160	160
w/c	0.4	0.4	0.4
Max aggregate size	10	10	10
Plasticizer (%cement weight)	2.2%	3.5%	4.2%
Age at testing	90	90	90

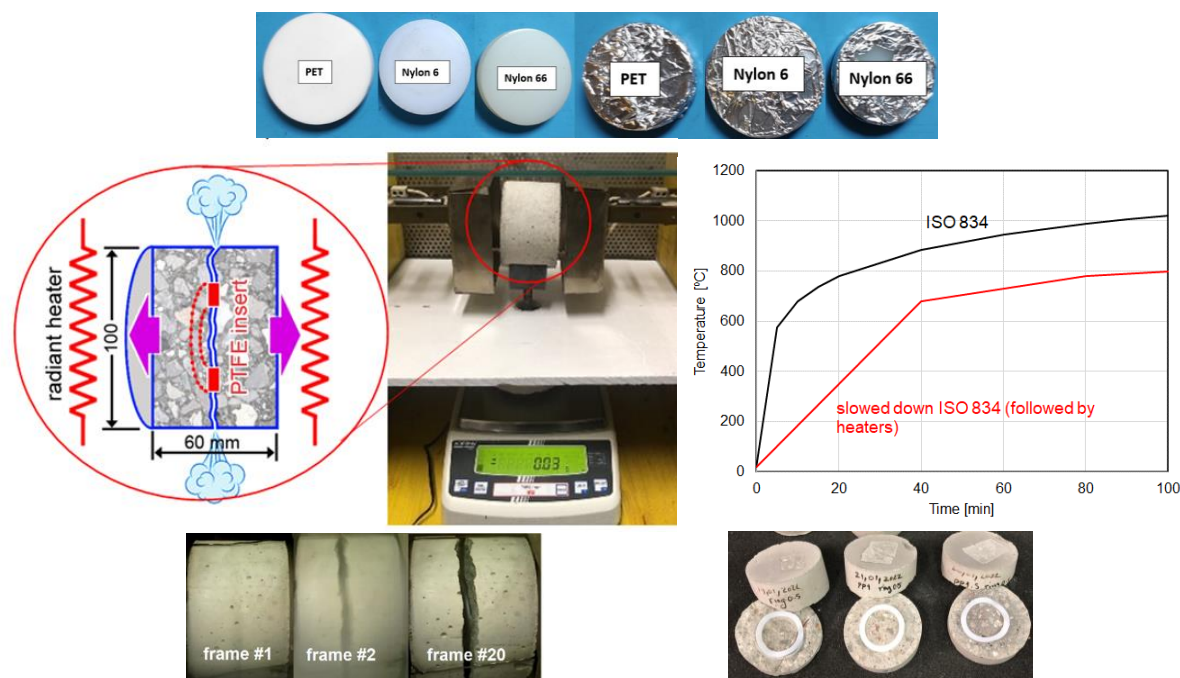


Figure 5 - Polymeric insert materials and shapes, test set up with two opposite radiant heaters, slowed down standard heating curve followed by heaters, frames of a spalling event (taken from a 60 fps video).



### Crack appearance and spalling event

The thickness of the polymer rings governs the magnitude of internal forces and helps determining the range of temperature (or time) at which a crack is triggered. In the following graph (Figure 6), different samples are shown with their explosion times. For each thickness as least 4 different samples were tested. Among the 4 samples with the thickest polymer insert (2 mm), just one of them exploded with a mild even after about 2300 s heating. At that time, the temperature in the cracking region was just 140-150°C, entailing a limited amount of thermal energy for driving water vaporization. In this test, “early crack” is defined as the one generated when concrete temperature is not high enough to build a high pressure to accelerate the broken splinters. On the other hand, “late crack” can be defined correspondingly as the one which is generated at a time when temperature is quite high but concrete is almost dry and no quick vaporization is possible to pressurize the crack. Determining the time/temperature range in which high pressure can develop in the opening crack driving an explosive fracture requires several tests with polymeric inserts of different thickness, the result depending on permeability, initial moisture and tensile strength. Moreover, since in this test the ability of PP fibre to increase permeability is also investigated, the crack onset should take place well beyond fibre melting, to make sure they can effectively release pore pressure and reduce the saturation of the fracturing concrete. The temperature trends presented in following graph are taken from K type thermocouples positioned next to the polymeric insert during sample casting.

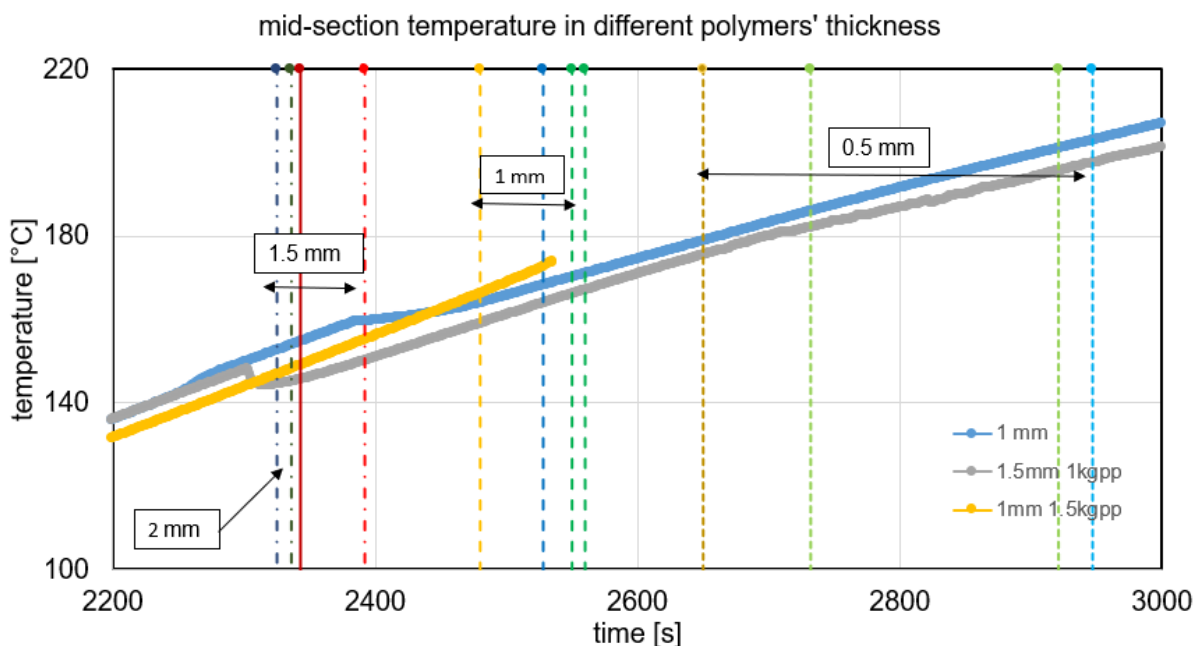


Figure 6 - Temperature trends and spalling time depending on polymer thickness.

### Crack opening monitoring

Some Authors [16] are sceptical about the role of pore pressure in accelerating the cracked particles, because crack opening implies a huge increase of the initial pore volume and, in their perspective, no significant amount of vapour could flow into this gap from the surrounding concrete in the very short time involved by explosive spalling events. Then a sudden pressure drop is expected and just the elastic strain energy due to thermal stress would be converted into fracture and kinetic energy. To further discuss this viewpoint, the relative displacement between the two separating halves of the breaking disk was monitored by means of reflective

photosensors mounted astride the potential fracturing plane. The advantages of photosensors are their fast response (cut-off frequency  $> 2$  kHz), the low cost ( $\approx 1\text{€}$ ) and the very little mass (0.7 g). This latter aspect is important if one considers that 1 MPa pressure in the opening crack would accelerate each half of the disk by  $15000\text{ m/s}^2$ , requiring to minimize all moving masses. The adopted reflective photosensors (Vishay CNY70) comprise an infrared light emitting diode and a detector (phototransistor). The amount of current driven by the detector goes with the amount of IR light reflected by a white target facing the sensor, which in turn depends on their relative distance. The correlation to distance is not linear and shows the highest sensitivity in the near range (about  $1\text{ V/mm}$  with the electrical scheme indicated in Figure 7), which helps monitoring the early stage of crack opening. A small piece of white painted corrugated cardboard was used as a reflective target in this setup. Very flexible 0.1 mm enamelled copper wires were used for connections to the data logger, with no influence on weight monitoring. Due to the high temperature reached by the sample and the radiation ensuing from the heaters, both the sensor and the target should be firmly held at some distance from the specimen (70 mm). Then, two triangular strut-and-tie cantilevers were secured with hose clamps to the two edges of the heated disks. These elements are made of a 2.2/1.7 mm stainless steel capillary pipe, allowing high stiffness and low mass (about 1.5 g each). Compared to aluminium, stainless steel has the advantage of a much lower thermal conductivity (15 times less) for the same stiffness/density ratio. This remarkably reduces the heat flowing along the supports and then the sensor temperature ( $\approx 40^\circ\text{C}$ ).

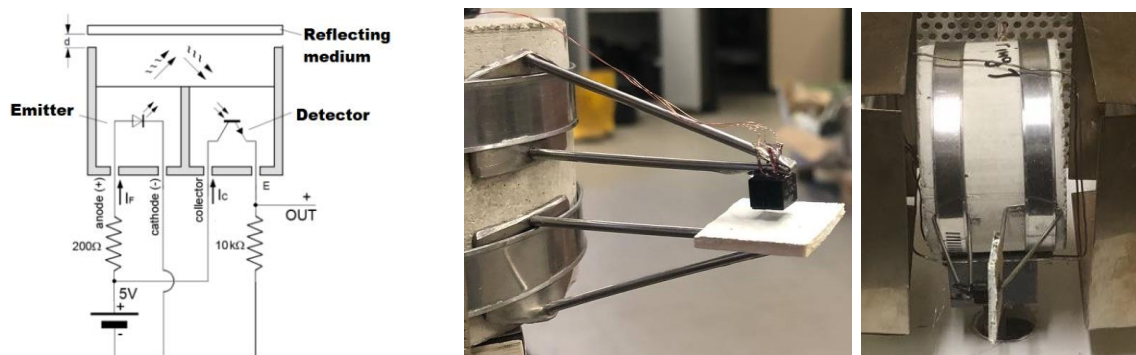


Figure 7 - Photosensor working scheme, lightweight pipe truss structure and target.

The signal produced by the photosensor was captured by a 12-bit USB scope (Picoscope 4424) and then scaled to engineering units. To calculate the relative acceleration experienced by the halves of the disk during a spalling event, the central second derivative finite difference method was used. The internal force separating the two parts can be assessed by way of the second Newton's law of motion under the assumption of splitting into equal masses  $M/2$  (separating force =  $M/2 \times \text{relative acceleration}/2$ ). Since the tested samples accumulate little elastic energy due to thermal stress, it is assumed that the net separation force ensues from the difference between the pressure of vapour filling the crack and the residual cohesive tensile stress borne by the fracturing concrete. To switch from the total force to the mean stress/pressure, the nominal cross-section area is here considered, despite the presence of the ring and the progressively extending fractured area.

As an example, the results obtained in case of a 1 mm PTFE ring triggering a crack after a 2600 s heating are reported in Figure 8 (mid-plane temperature  $175\text{-}185^\circ\text{C}$ , corresponding saturation pressure 12-14 bar). A steeply increasing net pressure is obtained as the cracked area extends and concrete progressively loses its tensile strength. The peak pressure is reached at 0.2 mm crack opening, namely when the material retains just a marginal share of the original strength and the vapour injected in the crack is balanced by the amount leaking at the boundary. The peak of the net pressure is comparable to the saturation pressure,

corroborating the idea that flash vaporization of moisture from the two faces of the crack can effectively pressurize the increasing volume. The whole process takes a very short time ( $\approx 0.3$  ms) during which the remarkable acceleration (up to  $20000 \text{ m/s}^2$ ) gives a relative velocity to the split halves of about  $4 \text{ m/s}$  and then a total kinetic energy of  $0.3 \text{ kJ/m}^2$ .

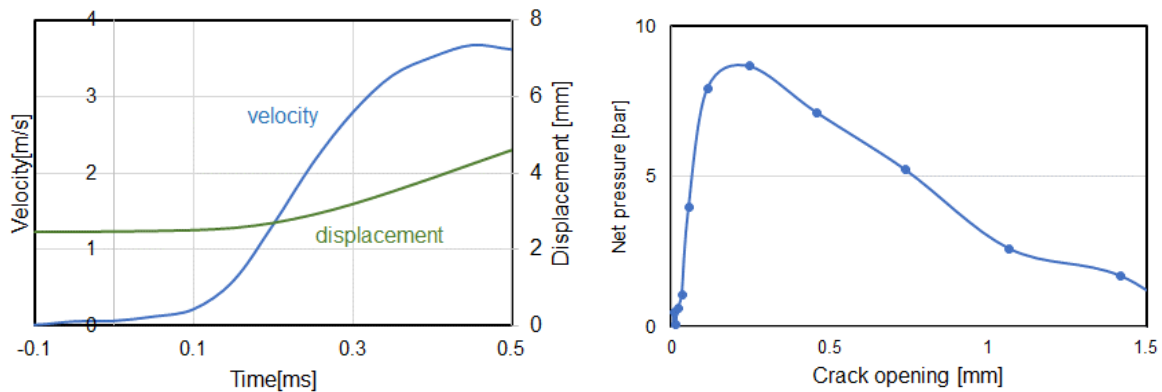


Figure 8 - Relative displacement and corresponding net pressure in the cross section during a spalling event.

### Mass loss during the tests

The continuous monitoring of the sample mass during the heating process provides two types of results: the global drying experienced by the sample at the time of spalling and throughout the heating test, and the sudden mass loss due to the explosive splitting of the disks. All samples underwent a total loss of about  $70 \text{ g}$  ( $-6.3\%$ ) in  $5000 \text{ s}$  (Figure 9). However, the enhanced permeability of mixes including PP fibre translates into a faster drying rate beyond  $2300 \text{ s}$ . It has to be considered that, due to the thermal gradient experienced by the disk, fibre melts somewhat later in the mid-section ( $\approx 2600 \text{ s}$ , see Figure 6). These plots indicate the moisture content at the time of splitting, which in turn is governed by the insert thickness. In the tested samples, this occurred always at rather low temperature ( $<200^\circ\text{C}$ ) and high saturation (Figure 6), leading to quite unstable failures. After the disks are split, the increased specific area translates into a faster drying rate.

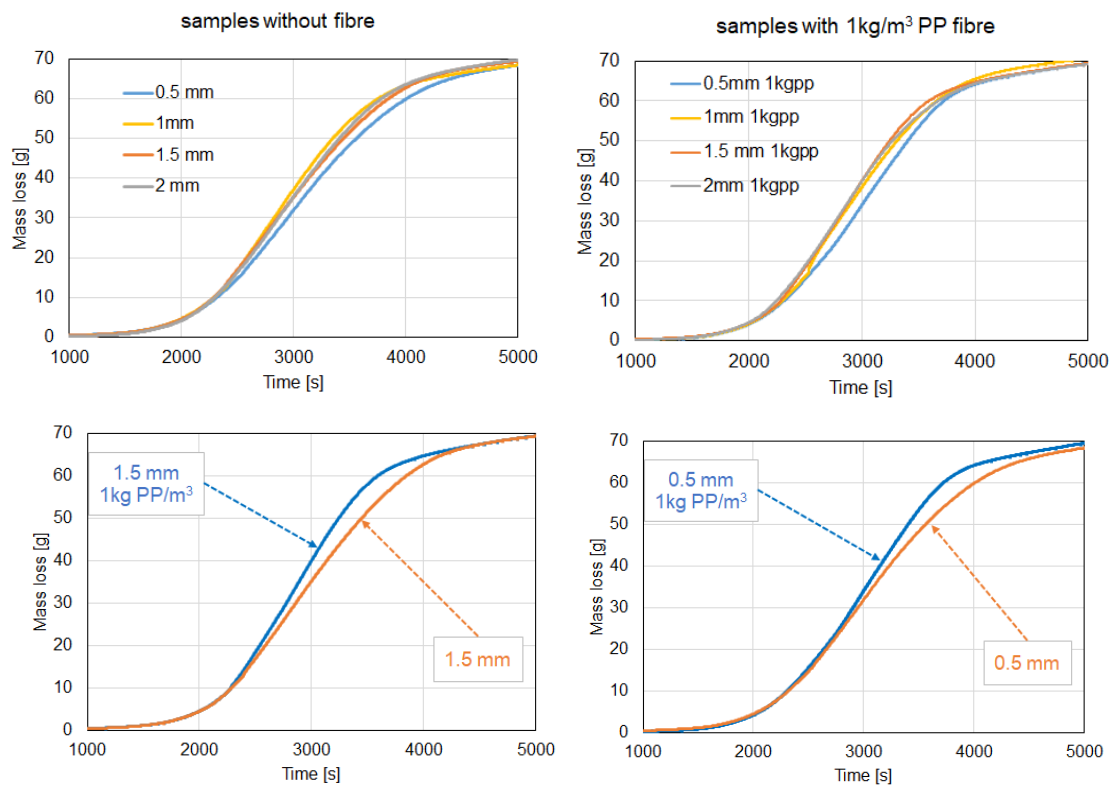


Figure 9 - Drying process of different samples with different fibre content and ring

By enlarging these plots at the spalling time, a hiatus can be noticed (Figure 10), corresponding to the sudden vapour loss which drives the unstable cracking process. The magnitude of this discontinuity (0.2-1.2 g, namely 25-150 g/m<sup>2</sup>) depends on the insert thickness and tends to be larger in the case of violent failures induced by the thinnest rings (Figure 9). Unfortunately, violent failures also entail the loss of small particles or coarser splinters, possibly affecting this measurement (which gives unreasonably high values). Some consistency check will be required in future tests (e.g. 3D survey of any geometric mismatch between the faces of the crack).

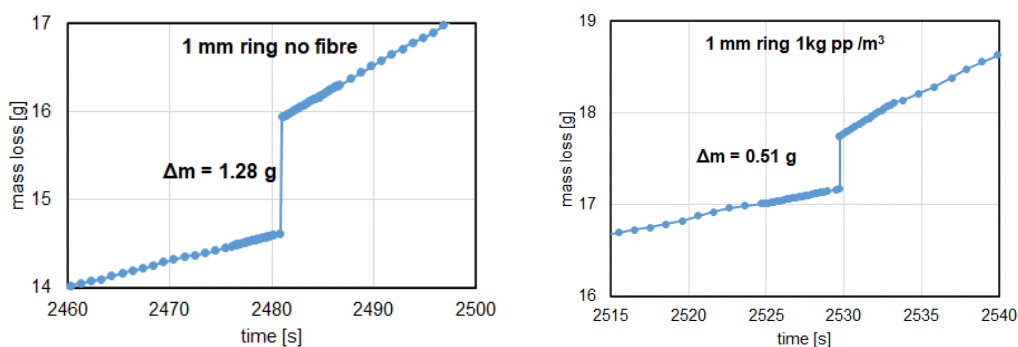


Figure 10 - Sudden mass loss due to explosion in the tests with 1mm rings.

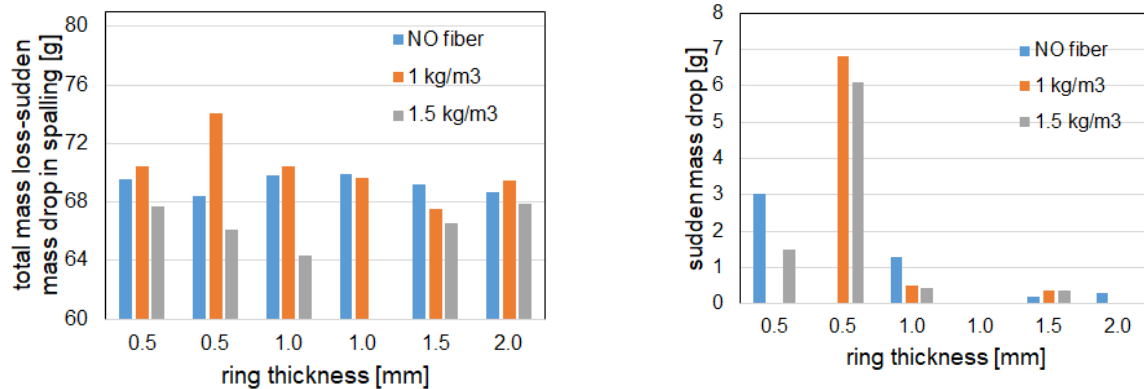


Figure 11 - Total mass loss and sudden mass drop

## CONCLUSIONS:

The objective of this work is to cast new light on the role of thermal energy and fast water vaporization in driving the highly dynamic fracturing of concrete which yields to explosive spalling. To this purpose a new setup was developed, where a planar crack is triggered in a concrete disk by the thermal expansion of a polymeric insert, with negligible accumulation of elastic strain energy. The main findings of this study are summarised as follows:

- Spalling events entail a sudden mass loss (in the order of several tens of  $g/m^2$ ) due to water vaporization. Its magnitude goes with the severity of crack instability.
- The remarkable acceleration undergone by the separating parts and the very short timing are consistent with a significant pressurization of the developing crack, until the vapour leakage prevails due to excessive crack opening.
- The time at which a crack is triggered plays a crucial role. Early and late cracks are more stable because of little thermal energy or pore saturation respectively. Hot concrete retaining a significant moisture in the pores gives the highest spalling severity

The systematic implementation of mass loss and acceleration measurements at different temperature and saturation conditions may provide useful indications about the crack instability domains of fire exposed concrete.

## ACKNOWLEDGEMENT

This work was developed in the framework of the PhD project "Severe spalling in concrete exposed to fire" supported by SFIC (Professional Syndicate of the French Cement Industry).

## BIBLIOGRAPHY

1. Liu, J. C., Tan, K. H., and Yao, Y., "A new perspective on nature of fire-induced spalling in concrete," *Constr. Build. Mater.* **184**, 581–590 2018.
2. Dwaikat, M. B. and Kodur, V. K. R., "Hydrothermal model for predicting fire-induced spalling in concrete structural systems," *Fire Saf. J.* **44**(3), 425–434 2009.
3. Ichikawa, Y. and England, G. L., "Prediction of moisture migration and pore pressure build-up in concrete at high temperatures," *Nucl. Eng. Des.* **228**(1–3), 245–259 2004.
4. Ozawa, M. and Morimoto, H., "Effects of various fibres on high-temperature spalling in high-performance concrete," *Constr. Build. Mater.* **71**, 83–92 2014.

5. Maier, M., Zeiml, M., and Lackner, R., "On the effect of pore-space properties and water saturation on explosive spalling of fire-loaded concrete," *Constr. Build. Mater.* **231**, 2020.
6. Zhao, J., Zheng, J. J., Peng, G. F., and Van Breugel, K., "A meso-level investigation into the explosive spalling mechanism of high-performance concrete under fire exposure," *Cem. Concr. Res.* **65**, 64–75 2014.
7. Zhang, H. L. and Davie, C. T., "A numerical investigation of the influence of pore pressures and thermally induced stresses for spalling of concrete exposed to elevated temperatures," *Fire Saf. J.* **59**, 102–110 2013.
8. Robert, F., Bisby, L., and Centre, F. T., "Fire Spalling of Concrete: Experimental Parametric Study and Numerical Modelling," in *4th International Workshop on Concrete Spalling Due to Fire Exposure* (2015), (October 2015), pp. 1–9.
9. Lo Monte, F., Lombardi, F., Felicetti, R., and Lualdi, M., "Ground-Penetrating Radar monitoring of concrete at high temperature," *Constr. Build. Mater.* **151**, 881–888 2017.
10. Yavus Sertmehmetoglu, "On a mechanism of spalling of concrete under fire conditions," university of London, king's college (1977).
11. Mindeguia, J.-C., Pimienta, P., Carré, H., and Borderie, C. La, "Experimental study on the contribution of pore vapour pressure to the thermal instability risk of concrete," in *1st International Workshop on Concrete Spalling Due To Fire Exposure* (2009), (1), pp. 150–167.
12. Zeiml, M., Lackner, R., and Mang, H. A., "Experimental insight into spalling behavior of concrete tunnel linings under fire loading," *Acta Geotech.* **3**(4), 295–308 2008.
13. Gawin, D., Pesavento, F., and Schrefler, B. A., "Towards prediction of the thermal spalling risk through a multi-phase porous media model of concrete," *Comput. Methods Appl. Mech. Eng.* **195**(41–43), 5707–5729 2006.
14. Gawin, D., Pesavento, F., and Castells, A. G., "On reliable predicting risk and nature of thermal spalling in heated concrete," *Arch. Civ. Mech. Eng.* **18**(4), 1219–1227 2018.
15. Felicetti, R., Yarmohammadian, R., Pont, S. D., and Tengattini, A., "Flash vaporization next to an opening crack: a possible explanation of the explosive nature of concrete spalling," in (6th International Workshop on Concrete Spalling due to Fire Exposure, 2019), pp. 237–247.
16. Bažant, Z. P. and Cusatis, G., "Concrete creep at high temperature and its interaction with fracture: recent progress," in *Concreep 7 Conference: Creep, Shrinkage and Durability of Concrete and Concrete Structures* (2005), pp. 449–460.

# Dehydration model of cement paste for predicting the material properties at elevated temperatures

Simon Peters<sup>1,\*</sup> & Günther Meschke<sup>1</sup>

<sup>1</sup> Ruhr-Universität Bochum, Bochum, Germany

\* Corresponding author (simon.peters@rub.de,  
Ruhr-Universität Bochum, Lehrstuhl für Statik und  
Dynamik, Universitätsstraße 150, 44801 Bochum)

## ABSTRACT

Despite intensive research, the underlining physical process of concrete spalling when subjected to high temperatures is still not fully understood. Since the simultaneously acting multi-physical phenomena render an exact interpretation of experimental data difficult, numerical models can help to gain insights into the individual role of specific hygro-thermo-mechanical processes. One enigmatic nature of concrete spalling is the moisture clog which is caused by the material dehydration and the low permeability of concrete.

In this presentation, a numerical multiscale dehydration model for different hardened cement pastes (CEM I, CEM II and CEM IV) is used to calculate the water release and porosity at elevated temperatures with the heating rate and chemical decomposition taken as input parameters. The dehydration model quantifies the amount of water and CO<sub>2</sub> that can be released at each temperature and takes into account the dehydration kinetics to reach an equilibrium state for different cement pastes without any refitting. This model is used as the basis for a chemical model to predict the porosity.

Various cement pastes with different water to cement ratios ( $w/c = 0.25 - 0.6$ ) are analysed in the context of a sensitivity study and compared in regard to water release and percolation threshold according to the degradation process. It is shown, that high  $w/c$  values lead to an early reach of the percolation threshold, whereas materials with high calcium-carbonate or low  $w/c$  levels reach the percolation threshold only at further elevated temperatures.

Finally, the implementation of the multiscale model in chemo-thermo-hygro-mechanical finite element models is discussed and a potential scheme based on a micromechanical framework is proposed.

**KEYWORDS:** Multiscale Modelling, Dehydration Process, Percolation Threshold

## INTRODUCTION

Concrete spalling is still a research topic due to the simultaneously acting multi-physical phenomena and the role of the moisture clog, which is still not fully understood [1,2,3]. According to the Eurocode 2, the addition of 2 kg/m<sup>3</sup> of polypropylene (PP) fibers prevents concrete spalling. However, recent experimental investigations [4] point out, that modern furnace blast slag and pozzolanic cement compositions are more sensitive to concrete spalling because of the high water loss before the PP-fibers melts. The increased usage of this composites due to the lower CO<sub>2</sub> impact [5] raises again the question about the explosive concrete spalling mechanisms.

Numerical simulations can help gaining insights into the interaction of binder specific dehydration mechanisms of the hardened cement paste and the pore network that forms. Moreover, pore network changes during the heating process can be captured to complement



evidence obtained from laboratory investigations. The first step towards such insights is a mathematical description of the binder specific dehydration behaviour, which is the focus of the paper.

To describe the dehydration process, many researchers [6, 7, 8, 9, 10] used a temperature dependent function neglecting the heating rate, which was improved by [11, 12], who included the dehydration kinetics using an Arrhenius equation. Experiments by Hassen [13] showed that the dehydration process has a maximum water release at each temperature. Thereupon, Feraille-Fresnet [14] extended the proposed model by [11, 12] with an equilibrium of dehydration term to consider this maximum water release at each temperature. As a drawback, however, this model cannot be adapted to different cement pastes without any refitting. This aspect was taken up in [15], where a model is proposed, with the dehydration behaviour of each cement paste constituent being considered by an intrinsic kinetic and equilibrium dehydration term.

In this paper a dehydration model based on [15] is proposed for CEM I, CEM II and CEM IV to calculate the thermal degradation of hardened cement paste at elevated temperatures. The dehydration model quantifies the amount of water and CO<sub>2</sub> that can be released at each temperature and takes into account the dehydration kinetics to reach an equilibrium state for different cement pastes without any refitting.

The paper is organized as follows. The dehydration model is briefly presented in Section 2 along with the considered chemical formulas. A sensitivity study and discussion is contained in Section 3. In Section 4, an outlook regarding the incorporation of the proposed model in a macroscopic Chemo-Thermo-Hydro-Mechanical finite element model is given.

## THEORY AND MODEL CHARACTERIZATION

In Figure 1 the workflow of the algorithm is illustrated. The input parameters of the model are the cement composition (chemical characteristics) and the heating rate. The cement composition is used as input for a hydration model [16] to obtain the initial volume fractions  $f_{CSH}$ ,  $f_{CH}$ ,  $f_{AFm}$  etc. which serve as input for the dehydration model, using Eqs. 1, 2, 3 and 4.

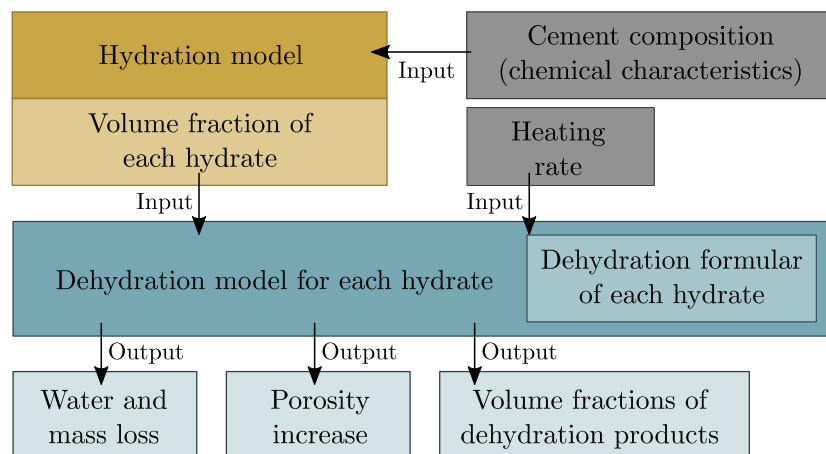


Figure 1 Schematic illustration of the workflow in the proposed model

### Dehydration kinetics

The multi-component dehydration model [15] predicts the equilibrium dehydration for each individual hydrate  $j$  of the hardened cement paste and the mass loss of water from kinetics as

$$\dot{w}_{dehydr} = - \sum_j Q_j^w \cdot \dot{\xi}^j, \quad (1)$$

where  $\dot{\xi}^j$  is the time derivative of the dehydration degree for hydrate  $j$ ,  $Q_j^w$  denotes the chemically bound water contained in the hydrate  $j$  before the dehydration. The rate form of the dehydration degree for each hydrate is given as

$$\dot{\xi}^j = H(T - T_o^j) \cdot \left( \xi_{eq}^j(T) - \xi^j \right) \frac{1}{\tau^j} \exp \left( \frac{E_a^j}{R} \left( \frac{1}{T} - \frac{1}{T_o^j} \right) \right), \quad (2)$$

where

- $\xi_{eq}^j(T)$  is the final dehydration degree at a given temperature  $T$ ,
- $H(T - T_o^j)$  is the Heaviside function,
- $T_o^j$  is the temperature from which the hydrate  $j$  begins to dehydrate (onset temperature),
- $\tau^j$  is the characteristic time associated with hydrate  $j$ , and
- $E_a^j$  is the activation energy associated with hydrate  $j$ .

### Porosity and dehydration model:

According to [10, 12, 17, 18], based on stoichiometric formulas and the volume change of every hydrate of the hardened cement paste, the porosity is calculated with the following formula:

$$f_i^{por} = f_i \cdot \xi_i \cdot N_i^w \frac{\frac{\rho_i}{M_i}}{\frac{\rho^w}{M^w}} \text{ with } i \in \{hydrates\} \quad (3)$$

$f_i$  is the initial volume fraction of a constituent and  $\xi^i$  captures the dehydration kinetics from hydrate  $i$ .  $N_i^w = n_w/n_i$  with  $n_w$  as the number of moles of water decomposed from  $n_i=1$  mol of phase  $i$ , which is provided by the stoichiometric formula.  $\rho$  and  $M$  are the density and molar mass, respectively. In analogy, the volume fraction of the water loss due to dehydration is calculated as

$$f_i^w = f_i \cdot \xi_i \cdot N_i^w \frac{M_i}{M^w} \text{ with } i \in \{hydrates\} \quad (4)$$

### Chemical reactions:

In this subsection the considered chemical reactions involved in the dehydration process of hardened cement paste are discussed, namely C-S-H ( $x\text{CaO} \cdot y\text{SiO}_2 \cdot z\text{H}_2\text{O}$ ), dC-S-H ( $x\text{CaO} \cdot y\text{SiO}_2$ ), portlandite (CH,  $\text{Ca}(\text{OH})_2$ ), ettringite (AFt,  $\text{Ca}_6[\text{Al}(\text{OH})_6]_2(\text{SO}_4)_3 \cdot 26\text{H}_2\text{O}$ ), monosulfoaluminates (AFm,  $\text{Ca}_4\text{Al}_2\text{O}_6(\text{SO}_4) \cdot 12\text{H}_2\text{O}$ ), basanite ( $\text{CaSO}_4 \cdot 0.5\text{H}_2\text{O}$ ), anhydrite ( $\text{CaSO}_4$ ), iron(III)-oxidehydroxide ( $\text{FeO}(\text{OH})$ ), iron(III)oxide ( $\text{Fe}_2\text{O}_3$ ), hydrogarnet (TCA,  $\text{Ca}_3\text{Al}_2\text{OH}$ ), lime ( $\text{CaO}$ ), calcium carbonate ( $\text{CaCO}_3$ ), mayenite ( $\text{Ca}_{12}\text{Al}_{14}\text{O}_{33}$ ). Figure 2 shows the dehydration degree of all considered phases at a heating rate of 5°C/min. The kinetic parameters are summarised in Table 1.

Portlandite dehydrates to lime according to [15]:



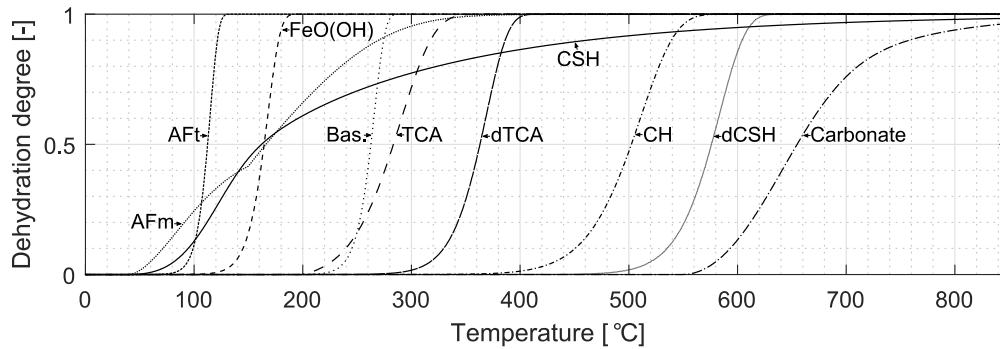
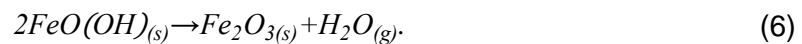


Figure 2 Visualisation of all kinetic parameters until 850°C from Table 1 with a heating rate of 5C/min

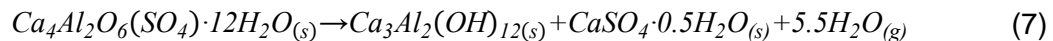
The onset temperature is 375°C [15] and due to the crystalline molecular structure of the CH molecule, the dehydration process takes place in a small temperature range [19]. The subscript in brackets gives information about the physical state with s for solid and g for gas. The melting point of lime is above 2000°C [20], and no further chemical change due to temperature is expected below 850°C.

Iron(III)-oxide-hydroxide dehydrates to iron oxide according to [21]:



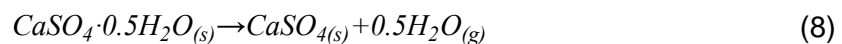
The onset temperature is set to 100°C [21], and due to the crystalline molecular structure of the iron(III)-oxide-hydroxide molecule, the dehydration process takes place in a small temperature range [21].

Monosulfoaluminates dehydrates to basanite and hydrogarnet according to [22]:

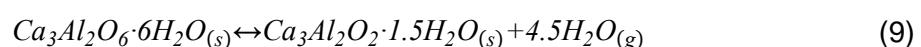


The thermally induced water loss in monosulfoaluminate is based on two different mechanisms. One is the water loss between the layers and the other is the chemically bound water loss [23] also denoted as crystalline water. Interlayer water loss at 40-600°C is induced by the thermally activated change in microstructure at the nanoscale [24], similar to C-S-H. Interlayer water loss leads to shrinkage of the cement paste, whereas the chemically bound water or crystalline water loss leads to new porosity.

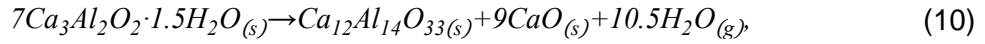
Basanite dehydrates to insoluble  $\beta$ -anhydrite according to [25]:



The onset temperature is set to 230°C [25] and due to the crystalline molecular structure of the basanite molecule the dehydration process takes place in a small temperature range [25]. Hydrogarnet dehydrates to mayenite and lime. In contrast to the before mentioned reaction formulas, the dehydration process of hydrogarnet is a two step dehydration process [26]. Firstly, the crystalline atomic lattice of the hydrogarnet molecule shrinks by releasing water molecules

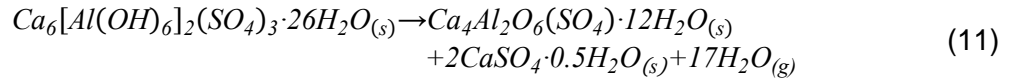


This reaction takes place in a temperature range of 200°C-300°C, with the left side strongly favoured in terms of chemical equilibrium. The first term of the r.h.s. reacts in the temperature range 300-600°C to mayenite and lime [26]



which both are melting at temperatures above 2000°C. Therefore, no more further chemical reaction takes place within the investigated temperature range.

Etringite dehydrates to monosulfoaluminates and basanite according to [27] with the following reaction formula

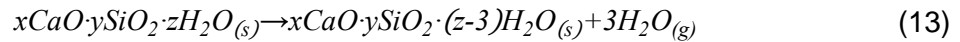


The onset temperature is 70°C [27] and due to the crystalline molecular structure of the ettringite molecule the dehydration process takes place in a small temperature range [27]. Calcium carbonate dehydrates to lime according to [28]:

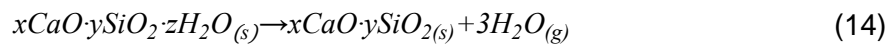


The onset temperature is 650°C [28] and the dehydration process takes place in a temperature range of 650°C to 850°C [28]. The initial porosity of limestone (mostly  $CaCO_3$ ) varies between 5 to 25% [29] due to dissolution processes via groundwater and weathering of the quarry.

The thermal degradation of the C-S-H is a two step process similar to the dehydration process of monosulfoaluminates [30]. The following chemical reaction is assumed for the interlayer loss



This shrinkage inducing reaction happens in a wide temperature range from 40-850 °C, but most of the water release happens in before 200°C, see Figure 2. As pointed out by [30], more high density C-S-H is formed due to the shrinkage process which converts gel into capillary porosity. This conversion is considered by 8% of the gel porosity. The second reaction induces porosity and is given by [30]



The onset temperature of this reaction is 520°C and the dehydration process takes place in a small temperature range of 520°C to 620°C (see Figure 2).

Table 1 Dehydration parameters, molar masses and density for each cement constituent

	$T_o^j$ [C]	$\tau^j$ [h]	$E_a^j$ [kJ/mol]	$N_w g^j$ [-]	$M^j$ [g/mol]	$\rho^j$ [g/cm <sup>3</sup> ]
CSH(layer) [15]	40	1	34	3	365 [56]	1.75 [10]
CH [15]	375	17.4	158.53	1	74.09	2.241 [10]
TCA [15]	200	3.3	85.4	4.5	378.28	2.529 [31]
AFm(layer) [15]	40	0.2	10	5.5	622.52	2.015 [31]
AFm(cryst.) [15]	150	0.5	20	5.5	622.52	2.015 [31]
AFt [27]	70	18.2	162	16	1255.11	1.775 [31]
Basanite [25]	210	16.7	241	0.5	145.14	2.71 [31]
FeO(OH) [21]	100	40	120	0.5	88.86	4.25 [31]
dTCA [26]	340	0.3	340	1.5	74.09	2.529 [31]
dCSH(cryst) [29]	520	10	250	3	311	1.75
Carbonate [28]	480	0.5	92	1	100.09	2.71 [31]
Water [10]	-	-	-	-	18	1.00 [10]

## VALIDATION AND SENSITIVITY STUDY

### Validation

To validate the model two data sets are used to compare the mass loss and porosity increase due to dehydration. Further validations are presented in the next paper. The first data set is obtained from [32], based on an ordinary cement paste specimen CEM I 42.5 with the chemical composition is given in Table 2. The model prediction and experimental data are shown in Figure 3, left. A very good agreement is observed. The model is calibrated at 105°C because the chemical water release is predicted. Therefore, no adsorbed or free water is considered, since this is evaporated at 105°C.

The next data set is given by [33] and the chemical composition is summarized in Table 2. Figure 3, right shows again a good agreement of the experimental data and the model prediction for the porosity.

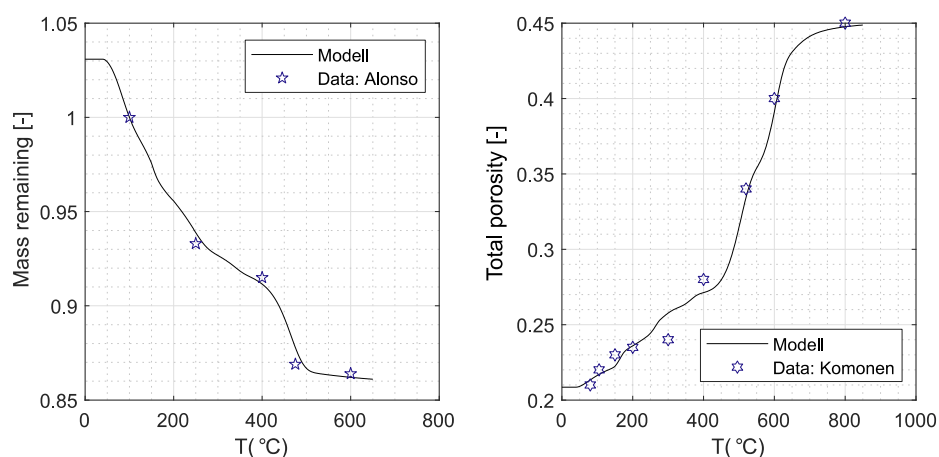


Figure 3 Validation study of the measured and simulated water loss (left) and porosity increase (right)

Table 2 Chemical characteristics (oxide analysis o.a., % by mass) of the cement paste specimens of [32], [33] and sensitivity analysis (s.a)

o.a. %	CaO	SiO <sub>2</sub>	Al <sub>2</sub> O <sub>3</sub>	Fe <sub>2</sub> O <sub>3</sub>	SO <sub>3</sub>	MgO	CaO(f)	L.O.I.
[32]	62.61	19.60	4.43	4.27	3.29	0.95	1.92	3.59
[33]	61.7	19.72	5.15	2.39	3.02	3.05	0.1	3.02
s.a.	64.7	19.1	3.2	2.2	2.7	1.6	0.2	[-]

### Sensitivity analysis:

To reduce CO<sub>2</sub> emissions associated with the concrete production, cement paste often is replaced by e.g. limestone (CEM II), blast furnace (CEM III) or silica fume (CEM IV). By utilizing the dehydration model proposed above, the dehydration behaviour of different binders, namely CEM I, CEM II and CEM IV, regarding the porosity increase and remaining mass at elevated temperatures are investigated.

The dehydration behaviour of CEM I is determined for different w/c values. As input serves the chemical composition in Table 2 and the heating rates is set to 5°C/min. The results are shown in Figure 4. A lower w/c ratio leads to a higher remaining mass due to the amount of

unreacted clinker, which additionally leads to a lower overall porosity, as less C-S-H phases and capillary pores are formed during the hydration process.

Similar investigations are made for CEM II with the same chemical composition, heating rate and  $w/c = 0.45$ . The results are shown in Figure 5. A high amount of calcium carbonate induces a large change in water release and porosity increase when the calcium carbonate decomposes. It should be noted, that the calcium carbonate porosity is set to 20% for limestone, which leads to high early capillary pore space. On the other hand, a low calcium carbonate porosity leads to a low initial capillary porosity which can be critical for high calcium carbonate volume fractions. Therefore, more investigations should be made regarding cements with high calcium carbonate volume fractions under elevated temperatures.

The third investigation is made with CEM IV. Again, the chemical composition as contained in Table 2 and a heating rate of 5 C/min is used. A mix design with a water to binder ratio equal to 0.3, where 0%, 6% and 12% Portland cement is replaced, is investigated. Due to the pozzolanic reaction, less portlandite and more pozzolanic C-S-H is available in the hardened cement, which leads to an earlier water release, see Figure 6, left. The induced porosity at high temperatures is lower because the porosity induced by portlandite is higher than that of C-S-H, Figure 6, right.

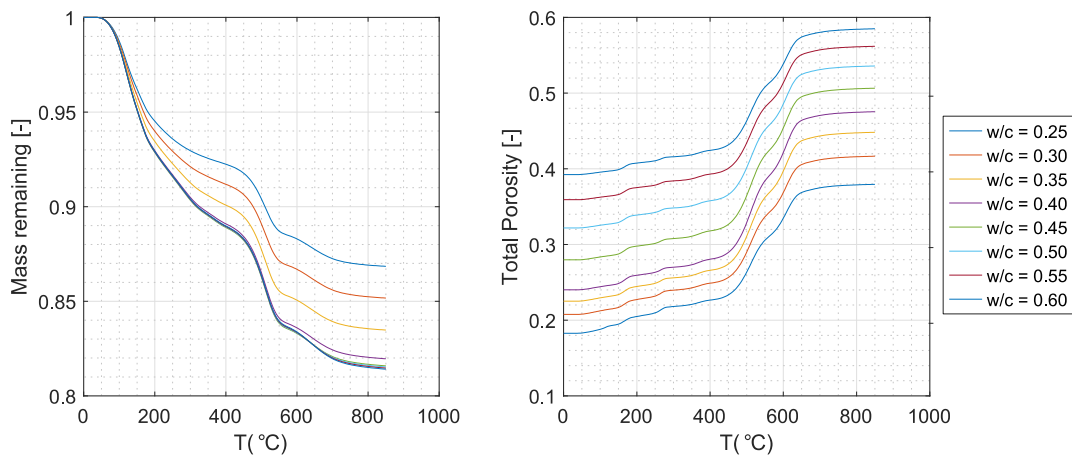


Figure 4 Sensitivity study: Remaining mass of CEM I with different  $w/c$  values (left) and induced total porosity (right) at elevated temperatures

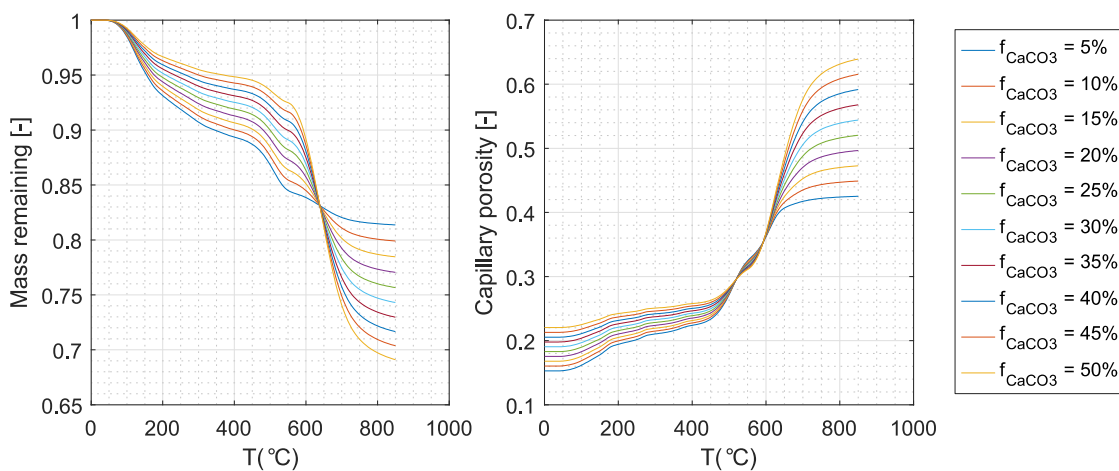


Figure 5 Sensitivity study: Remaining mass for CEM II with  $\text{CaCO}_3$  values at elevated temperatures (left) and induced total porosity (right) with  $w/c = 0.45$ .

The analysis shows, that the addition of silica fume in combination of low w/c values as typically used in high performance concretes have two drawbacks regarding the emergence of a moisture clog. Firstly, more water is released before 180°C (melting point of PP-fibers) and secondly, the percolation threshold of 18% [34], i.e. critical volume fraction of porosity characterised by an interconnected pore structure that causes a rapid increase in the materials permeability, is not reached at these temperatures, leading to an increase of pore pressure in the concrete specimen as the pore water vapour cannot escape from the high temperature regions. This is in perfect agreement with experimental investigations done by [4]. One possibility to generate a percolation network in the concrete could be the addition of high porous calcium carbonate.

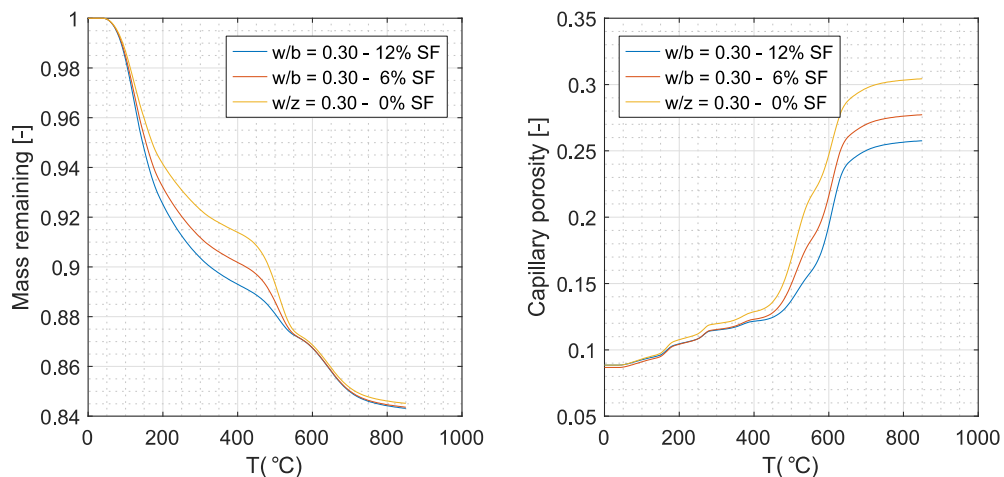


Figure 6 Sensitivity study: Remaining mass for CEM VI with different silica fume volume fractions at elevated temperatures (left) and induced total porosity (right) with w/c = 0.45.

## OUTLOOK

In future analyses, the proposed model will be extended by micromechanical models to determine the Young's modulus, thermal conduction and thermal capacity. A virtual lab for analyses on the structural level will be established by coupling the material model at the integration point level with a sophisticated chemo-thermo-hygro-mechanical finite element model [35]. However, mesoscale analyses on the mortar and concrete specimen scale also is helpful to investigate the interaction of the thermo-mechanical and thermo-chemical degradation of mortar and concrete. Particular attention should be paid to the crack development due to the thermal mismatch of the cement paste and aggregates. A detailed analysis of the thermo-chemo and thermo-mechanical interaction will be addressed in the future.

## CONCLUSION

A dehydration model for CEM I, CEM II and CEM IV at elevated temperatures was presented. The model predictions were compared with experimental measurements, showing an acceptable accuracy. The model provides a quantitative insight into the water release and induced porosity at elevated temperatures. This leads to the following conclusions:

- For CEM I, w/c ratios higher than 0.35 have an almost similar dehydration behaviour corresponding to the percentage mass loss.
- High CaCO<sub>3</sub> volume fractions lead to a delayed mass loss and porosity increase.



- Low porosities and high volume fractions of CaCO<sub>3</sub> prevent an initial pore network.
- Blended cement pastes enriched with silica fume show an earlier water release due to the increased amount of C-S-H.
- Low w/c ratios for CEM IV lead to a very late reach of the percolation threshold which may induce high pore pressures during fire accidents.
- More research needs to be performed for blended cement pastes at elevated temperatures.

## ACKNOWLEDGMENTS

This work has been carried out within the framework of the German Research Foundation (DFG) project “Thermohydraulic spalling mechanisms in concretes with different binders with and without PP-fibers under fire exposure: An experimental and numerical analysis.” This support is gratefully acknowledged.

## REFERENCES

1. McNamee, R., “Fire spalling of concrete: Theoretical and experimental studies”, Ph.D. thesis, KTH Architecture and Built Environment, 2013.
2. McNamee, R., “Fire spalling of concrete - a historical overview”, *MATEC Web of Conferences*, **6**, 01001, 2013.
3. Mróz, K., Hager, I., “Assessment of concrete susceptibility to fire spalling: A report on the state-of-the-art in testing procedures”, *Procedia Engineering*, **108**, 285–292, 2015.
4. Reiners, J., and Müller, C., “Einfluss der Zusammensetzung von Zementstein auf das Abplatzverhalten von Beton im Brandfall, Einfluss der Zusammensetzung von Zementstein auf das Abplatzverhalten von Beton im Brandfall”, *Bautechnik*, **95**, 547–558, 2018.
5. Scrivener, K., John, V., and Gartner, E., “Eco-efficient cements: Potential economically viable solutions for a low-CO<sub>2</sub> cement-based materials”, *Cement and Concrete Research*, **114**, 2018.
6. Khoury, G.A., Majorana, C.E., Pesavento, F., and Schrefler, B.A., “Modelling of heated concrete”, *Magazine of Concrete Research*, **54**, 77-101, 2002.
7. Schrefler, B., Majorana, C., Khoury, G., and Gawin, D., “Thermo-hydro-mechanical modelling of high performance concrete at high temperatures”, *Engineering Computations*, **19**(7), 787–819, 2002.
8. Gawin, D., Pesavento, F., and Schrefler B., “Modelling of hygro-thermal behaviour of concrete at high temperature with thermo-chemical and mechanical material degradation”, *Computer Methods in Applied Mechanics and Engineering*, **192**, 1731–1771, 2003.
9. Tenchev, R., and Purnell, P., “An application of a damage constitutive model to concrete at high temperature and prediction of spalling”, *International Journal of Solids and Structures*, **42**(26), 6550 – 6565, 2005.
10. Lee, L., Xi, Y., Willam, K., and Jung, Y., “A multiscale model for modulus of elasticity of concrete at high temperatures”, *Cement and Concrete Research*, **39**(9), 754–762, 2009.
11. Zhang, Q., and Ye, G., “Dehydration kinetics of portland cement paste at high temperature”, *Journal of Thermal Analysis and Calorimetry*, **110**, 2012.
12. Zhao, J., Zheng, J., Peng, G., and Breugel, K., “Prediction of thermal decomposition of hardened cement paste”, *Journal of Materials in Civil Engineering*, **24**, 592–598, 2012.
13. Hassen, S., “On the modeling of the dehydration induced transient creep during a heating-cooling cycle of concrete”, *Materials and Structures*, **44**(9), 1609–1627, 2011.
14. Feraille-Fresnet, A.F., “Le rôle de l’eau dans le comportement à haute température des bétons.”, Ph.D. thesis, ENPC, 2000.
15. Wang, J., Lacarriere, L., and Sellier, A., “Multicomponent modelling of cement paste dehydration under different heating rates”, *Materials and Structures*, **52**(1), 2019.

16. Lavergne, F., Ben Fraj, A., Bayane, I., and Barthelemy, J., "Estimating the mechanical properties of hydrating blended cementitious materials: An investigation based on micromechanics", *Cement and Concrete Research*, **104**, 37–60, 2018.
17. Zhao, J., Zheng, J., and Peng, G., "A numerical method for predicting young's modulus of heated cement paste", *Construction and Building Materials*, **54**, 197–201, 2014.
18. Zhang, Y., Ju, J.-W. W., and Zhu, H., "A novel multi-scale model for predicting the thermal damage of hybrid fiber-reinforced concrete", *International Journal of Damage Mechanics*, **29**(3), 1–26, 2019.
19. Zelic, J., Ugrina, L., and Jozic, D., "Application of thermal methods in the chemistry of cement: Kinetic analysis of portlandite from non-isothermal thermogravimetric data", in: First International Proficiency Testing Conference. Sinaia, Romania, 2007.
20. Rumble, J., In *CRC handbook of chemistry and physics: A ready-reference book of chemical and physical data*, CRC Press Taylor and Francis Group, 2018.
21. Balek, V., and J. Subrt, "Thermal behaviour of iron(III) oxide hydroxides", *Pure and Applied Chemistry*, **11**, 1839–1842, 1995.
22. Meller, N., Kyritsis, K., and Hall, C., "The hydrothermal decomposition of calcium monosulfoaluminate 14-hydrate to katoite hydrogarnet and  $\beta$ -anhydrite: An in-situ synchrotron X-ray diffraction study", *Journal of Solid State Chemistry*, **182**, 2743–2747, 2009.
23. Dilnesa, B., Lothenbach, B., Renaudin, G., Wichser, A., and Wieland, E., "Stability of monosulfate in the presence of iron", *Journal of the American Ceramic Society*, **10**, 3305–3316, 2012.
24. Leisinger, S., Lothenbach, B., Saout, G. L., and Johnson, C., "Thermodynamic modeling of solid solutions between monosulfate and monochromate  $3\text{CaO}\cdot\text{Al}_2\text{O}_3\cdot\text{Ca}[(\text{CrO}_4)_x(\text{SO}_4)_{1-x}]\cdot n\text{H}_2\text{O}$ ", *Cement and Concrete Research*, **42**, 158–165, 2012.
25. Mirwald, P., "Experimental study of the dehydration reactions gypsum-bassanite and bassanite-anhydrite at high pressure: indication of anomalous behavior of  $\text{H}_2\text{O}$  at high pressure in the temperature range of 50-300", *The Journal of chemical physics*, **128**:7, 074502, 2008.
26. Schneider, W., and Thorvaldson, T., "Dehydration of tricalcium aluminate hexahydrate", *Canadian Journal of Research*, **19B**, 123–128, 2011.
27. Hall, C., Barnes, P., Billimore, A., Jupe, A., and Turrillas, X., "Thermal decomposition of ettringite  $\text{Ca}_6[\text{Al}(\text{OH})_6]_2(\text{SO}_4)_{32}6\text{H}_2\text{O}$ ", *Journal of The Chemical Society*, **92**, 2125-2129, 1996.
28. Tracz, T., and Zdeb, T., "Effect of hydration and carbonation progress on the porosity and permeability of cement pastes", *Materials*, **12**, 192, 2019.
29. Polster, H., Buwert, C., and Herrmann, P.: „Sanierungsgrundlagen Plattenbau. Prüfverfahren.“, IRB-Verlag, 1995
30. Zhang, Q., and Ye, G., "Microstructure analysis of heated portland cement paste", *Procedia Engineering*, **14**, 830–836, 2011.
31. Balonis, M., and Glasser, F., "The density of cement phases", *Cement and Concrete Research*, **39**, 733–739, 2009.
32. Alonso, C., and Fernandez, L., "Dehydration and rehydration processes of cement paste exposed to high temperature environments", *Journal of Materials Science*, **39**, 3015–3024, 2004.
33. Komonen, J., and Penttala, V., "Effects of high temperature on the pore structure and strength of plain and polypropylene fiber reinforced cement pastes", *Fire Technology*, **39**, 23–34, 2003.
34. Bentz, D. P., and Garboczi, E. J., "Percolation of phases in a three-dimensional cement paste microstructural model", *Cement and Concrete Research*, **21**, 325–344, 1991.
35. Schrefler, B., Majorana, C., Houry, G., and Gawin, D., "Thermo-hydro-mechanical modelling of high performance concrete at high temperatures", *Engineering Computations*, **19**(7), 787–819, 2002.

# Underlying Factors Controlling Experimental Test Outputs for Concrete Samples Subjected to Elevated Temperatures

Abbas M. Abubaker<sup>1,\*</sup>, Colin T. Davie<sup>1</sup>

<sup>1</sup>Newcastle University, Newcastle Upon Tyne, UK

\*Corresponding author (A.M.Abubaker2@newcastle.ac.uk, Drummond Building, Newcastle upon Tyne, NE1 7RU)

## ABSTRACT

Spalling of concrete subjected to elevated temperatures remains a controversial research area despite the pursuance of experimental investigation for more than a century. To date, experimental investigations have mostly been aimed at identifying spalling types, factors affecting spalling and methods to reduce spalling risk. However, numerous questions remain due to varied and sometimes contradictory results. To address these inconsistencies, this work investigates how the test methodologies themselves may influence the results and spalling behaviour. To do this, a numerical model was developed in ABAQUS and employed to simulate a consistent set of experiments conducted with different test configurations. The study was extended to investigate factors such as sample size, restraints (including mechanical, self-restraint via the so called 'cold rim' effect and applied load) and load intensity. Fundamentally, it was found that the test boundary conditions may significantly influence spalling behaviour due to their effect on the stress state in the samples. While mechanically restraining a sample may mitigate spalling by limiting stresses, samples with the entire thickness restrained were found to develop less favourable stress states than those with only part of the thickness restrained. However, samples restrained through applied loading tended to develop less favourable stress states than samples restrained mechanically. Increasing load intensity was found to worsen conditions for spalling while the position and eccentricity of loading can significantly vary the compressive regime in a sample. The influence of an unheated 'cold rim' around the sample was found to vary considerably with test configuration and in some cases had little influence on stresses. Sample thickness was found to be more significant, with thicker samples developing less favourable stress states than more flexible thinner samples. In conclusion, reflecting real conditions relating to size, loading and restraints in the test set up is strongly recommended to ensure representative results.

**KEYWORDS:** Concrete and Fire, Concrete Spalling, Cold Rim, Boundary conditions, Sample Size, Load Effects

## INTRODUCTION

Thermal spalling is a failure mode of concrete following exposure to a severe, often unintentional, thermal load such as fire, that is characterised by disintegration of concrete pieces from the structural elements violently or non-violently [1, 2]. Traditionally, several different types of concrete thermal spalling are identified in the literature. These are aggregate spalling, corner

spalling (such as in beams and columns) and surface spalling (such as in slabs) (e.g. Zeiml et al [3]). Spalling has also been characterised in relation to the driving mechanisms as pore pressure spalling, thermal stress spalling and thermal cracking spalling [4].

For the purpose of understanding concrete behaviour and its spalling phenomenon at elevated temperatures, extensive experimental investigations have been performed on different size samples considering different boundary conditions, load types, restraints, and test setups. The nature of undertaken investigations to date have been generally aimed at identifying spalling types, highlighting factors affecting spalling and methods to reduce spalling risk. The implications behind adopting various test methodologies, which have led to different and even contradictory results, have not been well considered. Furthermore, real member boundary conditions are rarely considered as spalling experiments are complex and test setups tend to follow what is available and practical to implement. As a result, findings through these investigations remain open to interpretation and insufficient to produce a standardized test method for spalling.

One of the most important question which will be investigated throughout this paper is whether parameters relating to test setups like sample size, restraints (including mechanical, self-restraint via the so called 'cold rim' effect and applied load), and load intensity may control test outcomes and may have been a reason for contradictory results seen in the literature. Even though these parameters have been investigated individually, the findings are not conclusive because they are based on different sample geometries with various test methodologies. For example, in sample size investigations according to [5] the risk of explosive spalling of concrete increases with the sample size, however it was found in [6] that ductility and stiffness of beam samples increase with increasing beam cross sections under effects of heating. Additionally, it was found in [7] that thinner unloaded, unrestrained samples spall sooner in a more destructive way compared to thicker samples, and it was advised to pursue investigations for larger scale samples considering load and restraints. Regarding investigations of restraint, while it is widely reported in the literature that restraint improves concrete fire resistance [8, 9] these findings tend to be based on comparison of results of restrained and unrestrained samples with the same test configuration and do not compare across test methodologies. Furthermore, comparisons that consider degree of restraint and the mechanical characteristics of the restraint are not so well reported. Finally, in investigating load effects (e.g. [8, 10, 11, 12]) different methodologies relating to the type of load, its intensity, its location with respect to the heating (eccentricity), the detail of application (uniaxial or biaxial) and the friction and fixity of the loading platens have been adopted, which led to different outputs. While it was found that lower load intensity leads to higher fire resistance [8], it was also observed that external loading can cause spalling, which otherwise would not have happened [10]. However, in these cases details about the load intensity, its type and configuration are not well discussed and so it is difficult to draw general conclusions.

Through the following sections, the effects of adopting different test methodologies relating to sample size, restraint and load have been investigated through numerical simulation of experimental tests. Different scenarios have been considered and the stress and displacement results are compared. To do this, the most common aforementioned test set ups have been chosen and simulated with a sophisticated and validated thermo-mechanical model developed in ABAQUS [13].

## **NUMERICAL INVESTIGATIONS**

A validated thermo-mechanical model developed in ABAQUS (v.6.14) has been employed. It is based on a Concrete Damage Plasticity (CDP) model adjusted to capture the coupled thermo-mechanical behaviour of concrete under the simultaneous actions of heating and

loading (both applied loads and/or passive restraints). This is through incorporating temperature dependent material properties in to the model, including conductivity for both siliceous and carbonate aggregate, density, specific heat, thermal expansion and stress-strain relationships in both compression and tension. Importantly, transient thermal strain effects have been considered through a novel approach designed to account for the effects of both applied load and restraint induced stresses [13].

Investigation of the literature and preliminary analyses showed that three key areas were of particular interest and importance in this study. Namely, these are sample thickness, restraint (including mechanical restraint, restraint through applied load and self-restraint via the 'cold rim' effect) and load eccentricity.

Throughout the following sections, each of these key parameters has been investigated considering samples adopted from the literature with different geometries and boundary conditions. The adopted samples were cast from two concrete mixes; 42 MPa and 70 MPa. For the material properties, information given in [12] was followed where available. Moisture content is inherent within the conductivity and other material laws. Maximum aggregate size is 16 mm but type was not indicated. Silicious aggregate assumed for which, and all other properties, provisions given in [13] were followed. The same temperature dependant material properties were used for the 42 MPa and 70 MPa concrete. This is based on the versatility of the adopted model, which was proven to be valid within wide range of concrete compressive strengths. However, the temperature boundary conditions, namely emissivity, was different for each mix. These have been reached based on parametric studies to capture the given temperature profiles of the samples in the test report.

### **Influence of sample thickness**

To investigate the effects of sample thickness an experimental test from [12], labelled here as sample (A), was reproduced. The sample is an unrestrained, unloaded rectangular slab with a compressive strength of 42 MPa and dimensions 600 mm length, 500 mm width and 400 mm thickness. The sample rests over a furnace as shown in **Figure 1-a** with the exposed central section of the bottom face subjected to the ISO834 fire curve. For the analysis, sitting areas are restrained vertically representing through black arrows in **Figure 1-a**. To avoid rigid body motion during analysis, nodes at an outer most edge represented through line 1-1 in **Figure 1-c** were restrained in the other two directions. Two hypothetical cases were also developed with thicknesses 200 mm and 100 mm and all other factors the same.

According to the reported test results the sample spalled three times within a very short period after 660, 720 & 780 seconds of heating to a depth of around 40 mm. **Figure 1-b,c,d** shows the temperature profile (with a predicted maximum temperature of 331°C) along with cut-away views of the minimum and maximum principal stresses at first spalling incidence for the original sample set up with thickness 400 mm. **Figure 2** shows minimum and maximum principal stress profiles through the thickness of the samples at their centre line, for all three sample thicknesses at different times.

As is clear from **Figure 1-c & d**, a compressive zone around 40 mm deep develops central to the exposed surface with stress values exceeding the compression yielding limit of the concrete (shown as black). This transitions quickly to a tensile zone deeper in the sample that surpasses the concrete tensile yielding limit (shown in grey). The compression and tension yielding limits for the unrestrained sample are respectively 10% and 9% of the concrete compressive strength [13]. The high stress values and very steep gradients across this transition correspond very well in time and location to the observed spalling.

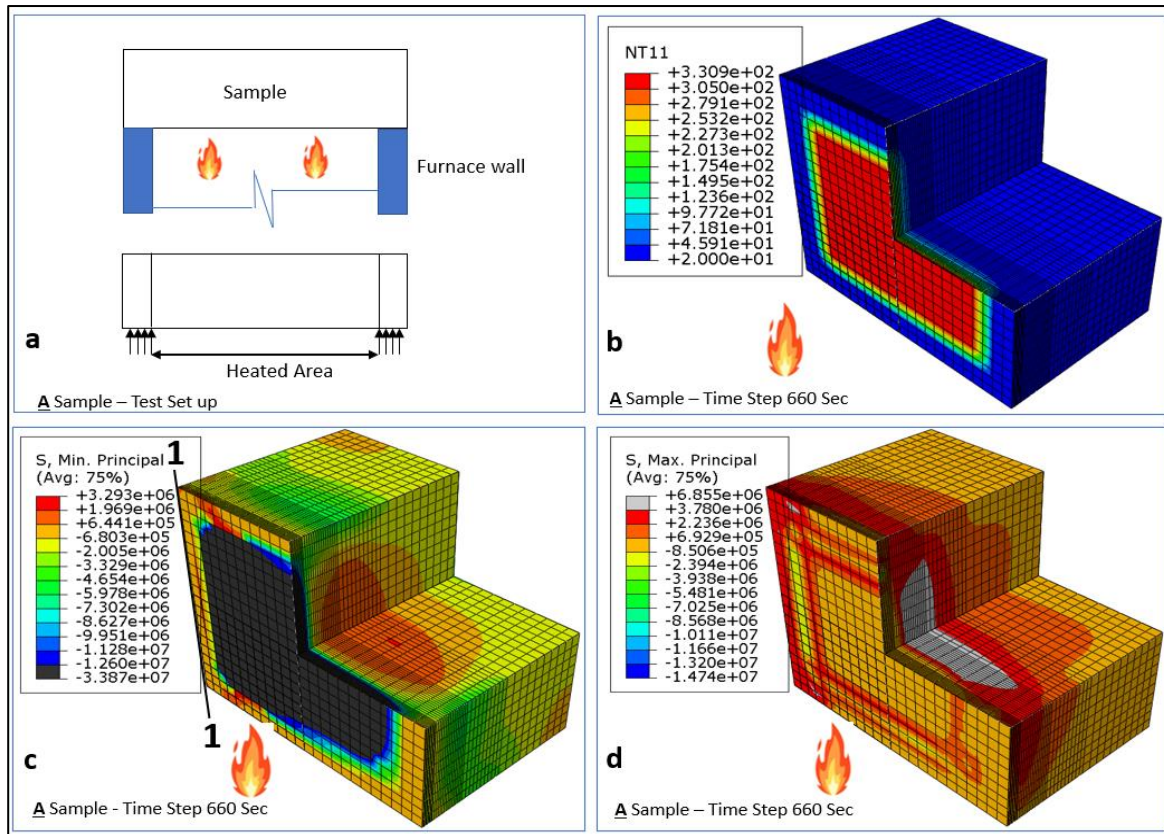


Figure 1: **a** Original Test Set up of Sample (A) with 400 mm Thickness, **b** Temperature Profile of Sample (A) at 660 seconds, **c** Minimum Principal Stress Profile after 660 Seconds, and **d** Maximum Principal Stress Profile after 660 Seconds

Considering **Figure 2**, similar transitions from compression to tension are present in each of the samples and these are seen to develop in time. Early on, the compressive stresses in all three samples are very similar. However, at later heating times the stresses in the thicker samples are larger than in thinner ones. A second compression zone can also be seen in all of the samples near the cold face, furthest from the furnace. In contrast, the magnitude of stresses in this zone are higher in thinner samples than in thicker ones. This appears to be a result of bending of the samples where the thinner samples deform towards the fire, relaxing the stresses at the hot face, while the stiffer, thicker samples resist this effect, developing higher stresses in the hot region.

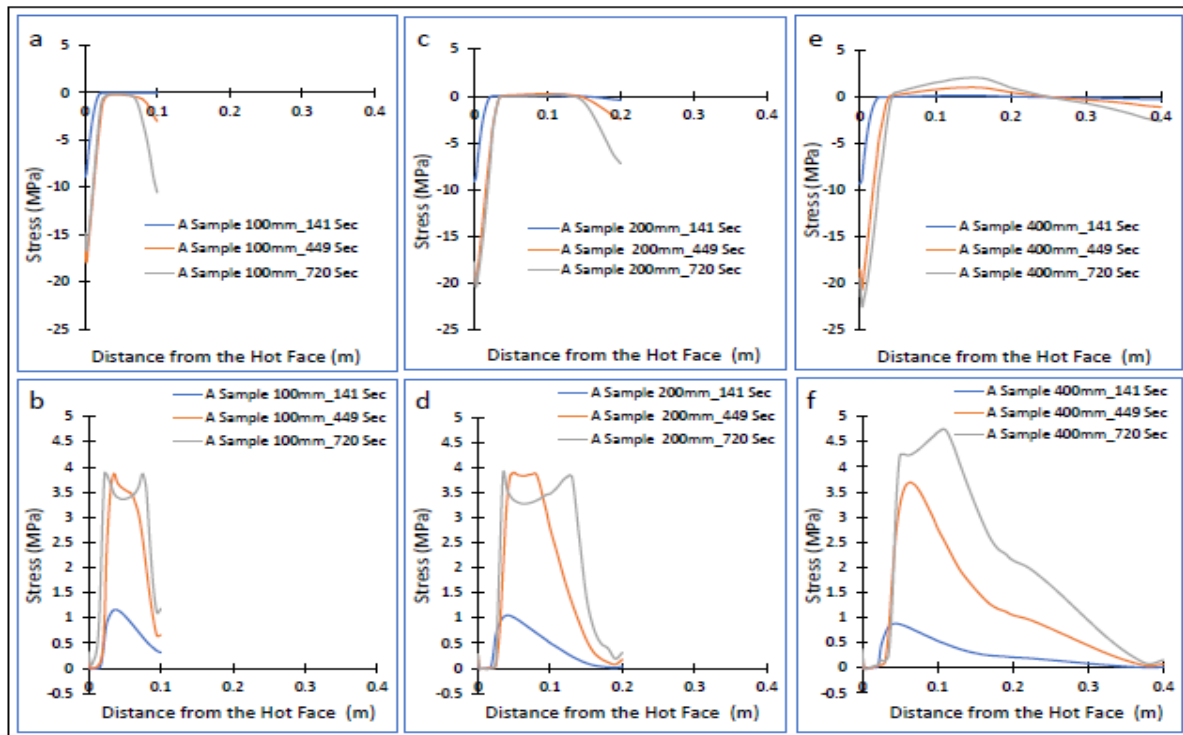


Figure 2: **a,c,e** Minimum and **b,d,f** Maximum Principal Stress Profiles through the Thickness of the Samples at their Centre Line, for all Three Sample Thicknesses at Different Times

The tensile zones in all three samples also develop in time. While in contrast to the compressive stresses, their magnitudes are similar irrespective of sample thickness, the width of the tensile zones is, in some respect proportional to the sample thickness, with more of the concrete susceptible to yielding. Perhaps also significant, it may be noticed that in the thickest sample, the stress state becomes fully tensile in the central portion, with both minimum and maximum principal stresses tensile. This is again likely an effect of the resistance of the thickest sample to bending.

### Influence of restraints

To investigate the effects of restraint, three samples were considered as shown in **Figure 3**; sample (A), as above; sample (B), the same as sample (A) but with the addition of a 50 mm high X 200mm thick steel frame providing restraint around its base (also from [12]); sample (C), a hypothetical extension of sample (B) with the restraining frame over its full height.

Similar to sample (A), the surface temperature at the centre of the fire exposed area of sample (B) (time of spalling 600 seconds) was predicted to be 304°C and the depth of first spalling was reported to be 60 mm [12]. Cut-away views showing the minimum and maximum principal stresses close to the time of first spalling for samples (A), (B) & (C) are presented in Figure 3.



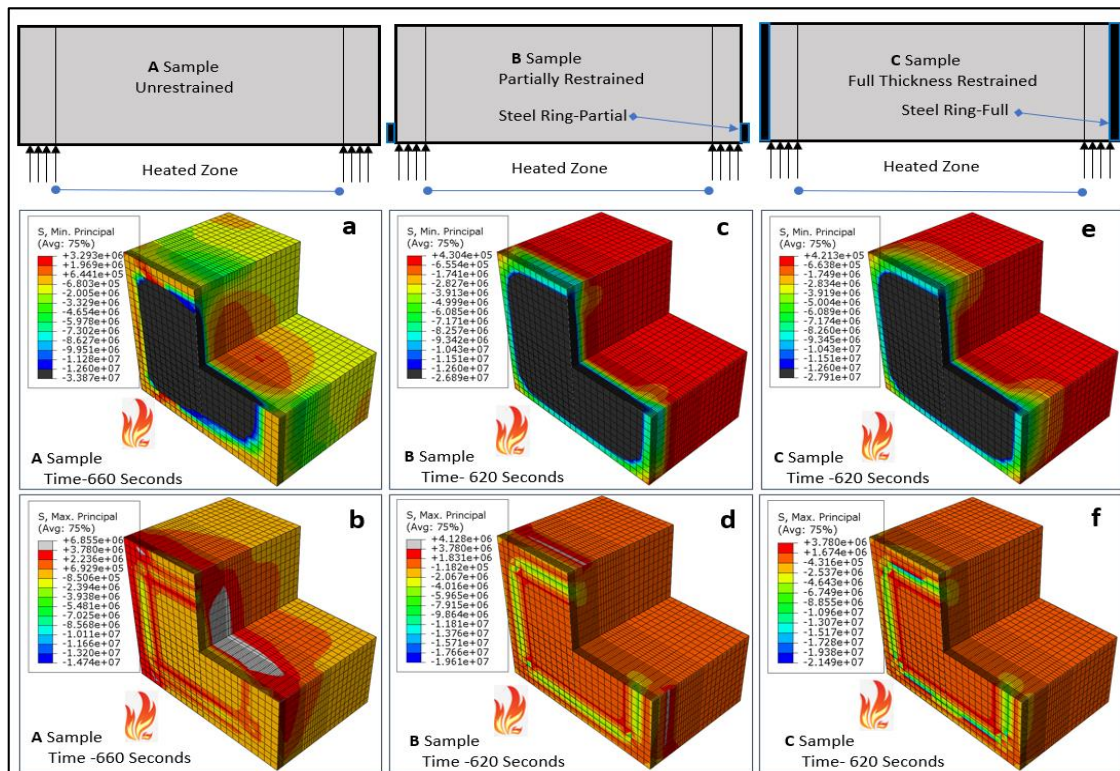


Figure 3: Minimum and maximum principal stress of **a,b** Sample (A), **c,d** Sample (B) & **e,f** Sample (C) at time of spalling

As can be seen from Figure 3-a,c,e, all three samples show zones of compressive stresses near the fire exposed faces that exceed the compressive yielding limit (shown as black). For restrained sample, compression yielding limit is 30% of the concrete compressive strength [13]. The magnitude of the stress in the unrestrained sample (A) is much higher than in the two restrained samples (B) & (C), although the area of the yielded zone in sample (A) is smaller than those in (B) & (C). This can be attributed to the effects of the restraints increasing the stiffness of samples (B) & (C) against the lateral displacement that tends to occur due to thermal expansion and hence concentrating stress in circumferential areas and even into the cold rim beyond the fire exposed areas. Conversely, the unrestrained sample has more freedom to expand laterally resulting in higher deformations in the central heated area and higher stresses.

Although all three samples show the transition to tensile zones further from the heated face **Figure 3-b,d,f**, the intensity of the transition is less in the restrained samples and only in the unrestrained sample (A) does the stress exceed the tensile yielding limit (9% of concrete compressive strength [13]) (shown as grey). This reduction in the stress gradients in the restrained samples likely reduces the risk of spalling.

In contrast, a strip around the outside of the partially restrained sample (B), just above the restraint frame, shows tensile yielding, while the fully restrained sample (C) shows none at all. The reasons behind these different behaviours are again related to the restraints in controlling the way that the samples deform. The restraints stiffen samples (B) & (C), limiting lateral displacement and hence the development of stresses at depth in the colder regions of the sample. For the partially restrained sample (B), the region just beyond the 50 mm thick restraint frame is free to displace laterally and thus a tensile stress concentration develops at this point. Other than this difference between samples (B) & (C), the stress regime under fully or partially

restrained conditions are very similar and restraining a sample against expansion close to the heating source seems to be sufficient to limit stresses and hence potentially, spalling behaviour.

In addition to mechanical restraint, the effects of potential self-restraint due to the so called 'cold rim' effect are of interest. This phenomenon occurs when unheated areas surround a fire exposed area. In real cases, cold rims might appear where structural elements are partially heated during a fire, however, in laboratory testing cold rims often result from practical considerations of test set up, where the sample necessarily rests on the walls of a furnace and the periphery is consequently unheated.

The effect of these cold rims has often been considered to act as self-restraint that may impose stresses in the heated concrete and has been shown to affect the behaviour of concrete under heating (e.g. [14]). To investigate cold rim effects, two hypothetical scenarios extended from the unrestrained sample (A) and the fully restrained sample (C) have been developed, labelled as samples (D) & (E) (**Figure 4**), in which their entire surfaces were subjected to heating. Minimum and maximum principal stress profiles through the thickness of the samples at their centre line are shown in **Figure 4**.

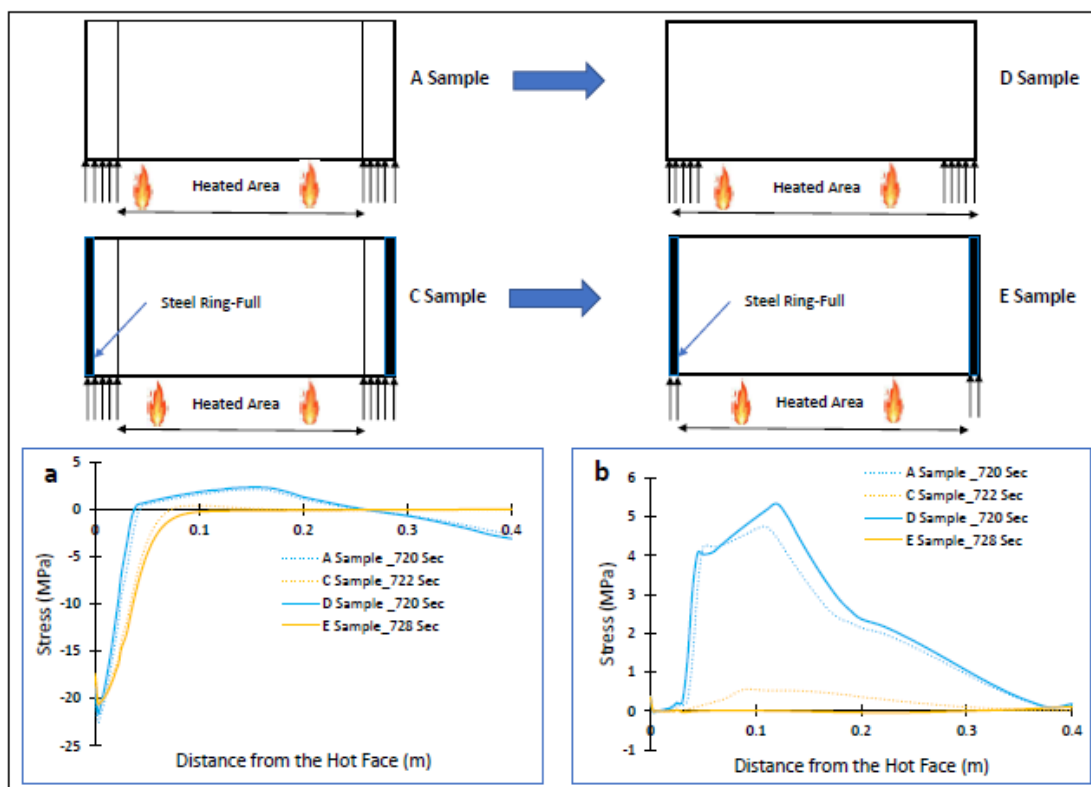


*Figure 4: a Minimum and b Maximum Principal Stress Profiles through the Thickness of the samples (A), (C), (D), & (E) at their Centre Line, Close to Time of First Spalling*

In the compressive zone, very little difference can be seen between the samples with and without a cold rim whether the sample is restrained externally or not.

In terms of the tensile zone, again only a small difference can be noticed between the samples with and without a cold rim (Figure 4-b) although the effects seem to be opposite for the samples with and without external restraint. For the unrestrained samples (A) & (D), the peak

tensile stress is increased by around 0.5 MPa whereas in the restrained samples (C) & (E) it is reduced by about the same amount and almost to zero. Arguably, in the unrestrained samples this would slightly increase the gradient of the transition from compression to tension, thereby potentially worsening the conditions in respect of spalling, while in the restrained samples the transition gradient is reduced, thereby potentially improving the conditions away from spalling. However, in neither case is the cold rim effect sufficient to change the overall stress state significantly.

### Influence of load eccentricity

Similar to cold rims, another factor that may occur both in real structures and as an artifact of experimental test set up is the presence of eccentricity in the applied restraint or load.

To investigate the effects of load eccentricity an experimental test from [12], labelled here as sample (F), was reproduced. The sample is a uniaxially but eccentrically loaded rectangular slab with a compressive strength of 70 MPa and dimensions 3500 mm length, 1200 mm width and 300 mm thickness. As shown in **Figure 5**, the sample is placed in front of a vertical furnace and subjected to the ISO834 fire curve. An additional hypothetical case (sample G) was developed with the eccentric load applied to the rear rather than front of the end of the slab. Minimum and maximum principal stress profiles through the thickness of the samples at their centre line, at different times, are also shown here. **Figure 5-a,b**. As with previous examples, both samples show a strong compressive zone near to the fire with a rapid transition to tension deeper in the colder regions of the concrete.

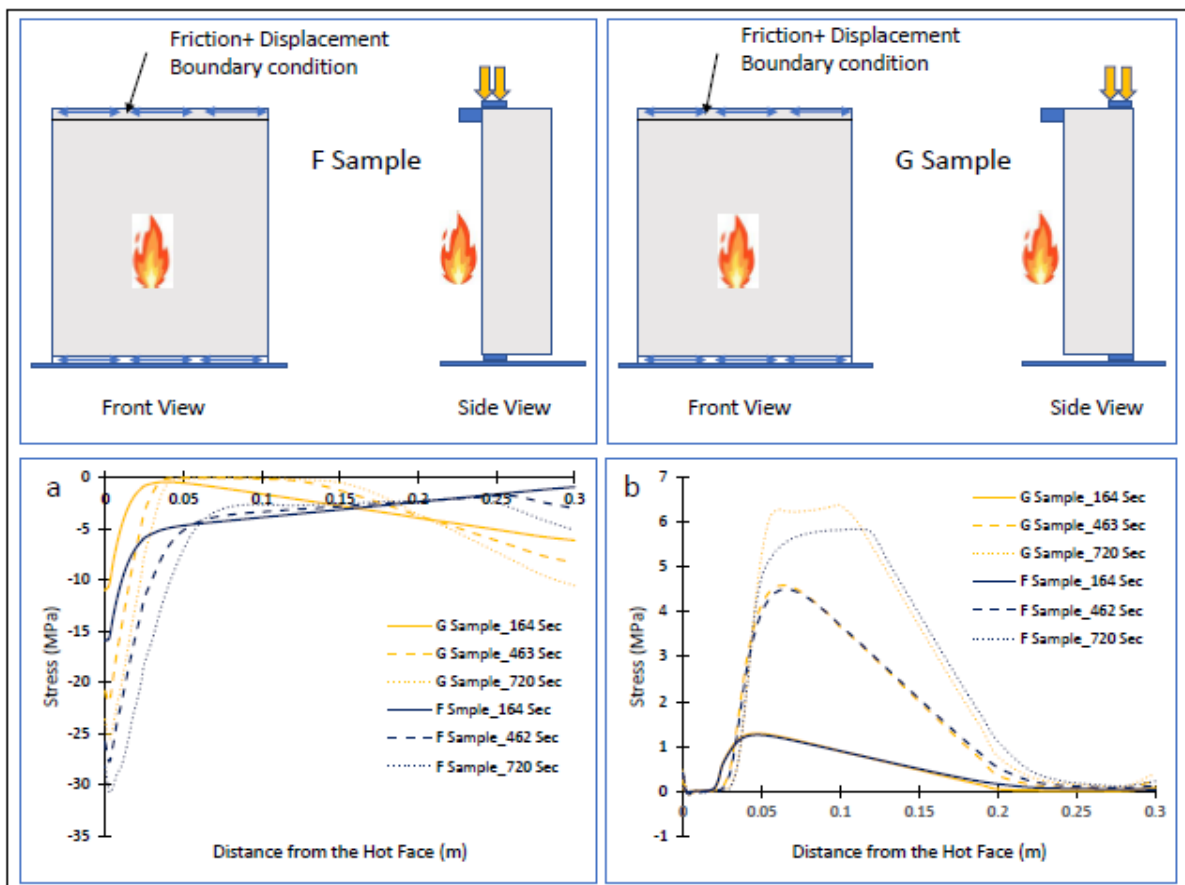


Figure 5: **a** Minimum and **b** Maximum Principal Stress Profiles through the Thickness of Samples (F) & (G) at their Centre Line, at Different Times

Interestingly, the central tensile zone is largely unaffected by the position of the applied load although the peak tensile stress is slightly higher in sample (G), probably because the peak is farther from the position of the applied load than it is in sample (F).

However, the magnitude of the compressive stress is clearly affected by the eccentricity of the load with the peak stress in sample (F) around 5 MPa higher than in sample (G). This is a result of the summative effect of the applied load and the compression derived from thermal behaviour, whereas sample (G) develops a second strong compression zone near the cold face of the sample as a result of the applied load. In fact, the magnitude of this second compression zone exceeds the stress from the applied load due to the effects of deformation.

As can be seen in **Figure 6** and as might be expected, the samples initially displace by the same amount due to the bending caused by the eccentrically applied loads, with sample (F) displacing away from the fire and sample (G) displacing towards it.

As heating increases, again as is to be expected, sample (F) starts to displace towards the fire. However, after a very small magnitude of displacement it then seems to stop and remains with a curvature concave to the fire. Conversely, upon heating, sample (G), displaces continuously towards the fire with a much greater magnitude as it is encouraged by the position of the load to deform convexly to the fire.

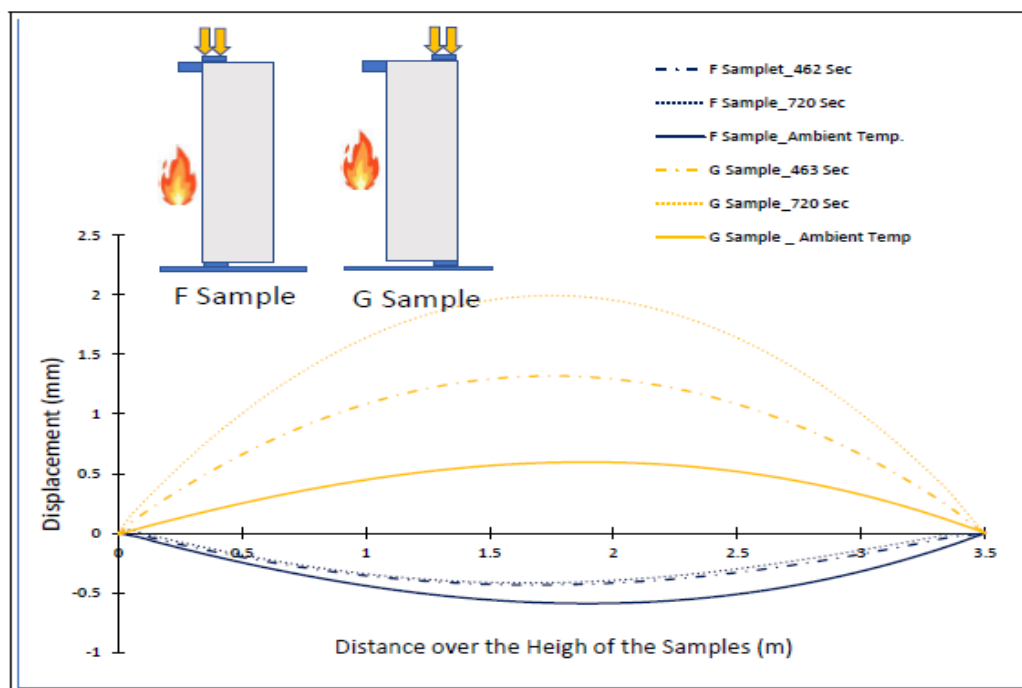


Figure 6: Displacement of the Fire Exposed Surface along a Central Axis over the Height of Samples (F) & (G) at Different Times (with positive displacement towards the fire)

Physically, this means that sample (F) behaves in a stiffer manner than sample (G), which shows a softer response purely as a result of differences in the testing set up. In addition to this stiffer response, it can be inferred that the more severe transition between compressive and tensile stresses seen in sample (F) might increase its vulnerability to spall over that of sample (G). Thus, a shift in the eccentricity of an applied load could significantly change the test outcomes.

## CONCLUSIONS

This work focused on an investigation of how test methodologies themselves may influence observed results concerning spalling behaviour. Samples from experimental studies in the literature were reproduced numerically using a thermo-mechanical model for concrete developed in ABAQUS to understand the stress states and deformations of the samples under heating. Underlying physical parameters relating to test set up and sample geometry such as size, restraint, and load eccentricity have been investigated in this work to determine how they could control concrete behaviour and its spalling while subjected to high temperature.

In all samples and test configurations the stress states inside the samples followed a generally consistent pattern. A zone of high compression developed close to the fire exposed surface that then transitioned quickly to a zone of tensile stresses in the cooler parts of the concrete. The location and timing of spalling observed in the experimental work seems to correlate very well with the region of high stress gradients in this transition zone. However, the magnitude of the stresses, particularly the tensile stresses, and hence the severity of the stress gradients was seen to be affected by the test configuration and sample geometry.

Thickness of the sample was found to have a crucial effect on the stress state under heating. Thinner samples were able to relax some of the stress build up through bending while thicker, stiffer samples resisted this effect making them more susceptible to high stress gradients and potentially spalling. Therefore, consistency between a real case and the test sample is highly recommended in order to derive more representative test outcomes.

The application of mechanical restraint was found to have a significant role in reducing tensile stress and thereby reducing stress gradients in the samples. This appears to correlate with the findings from literature that show restraint to reduce the potential for spalling.

In contrast, the potential self-restraint that may be perceived to develop due to the 'cold rim' effect, where an unheated zone exists surrounding a fire exposed face, was found to have only a very small effect on stress states. Ultimately, this would imply a negligible effect on the potential for spalling. This generally contradicts findings in the literature and so more work should be conducted in this area.

The eccentricity of a restraining load was found to have significant effects in altering the response of a sample to heating, changing both the magnitude and direction of the deflection of the slab and fundamentally altering the stress state. Most importantly, relying on a particular eccentricity scenario related to test set up could lead to underestimating the stresses and therefore potential for spalling in a real, structural situation.

Based on observations from this work, it is strongly recommended to reflect the expected real behaviours of concrete members in test configurations aimed at predicting potential for spalling.

## REFERENCES

1. D. Gawin, F. Pesavento, and A. G. Castells, "On reliable predicting risk and nature of thermal spalling in heated concrete," *Archives of Civil and Mechanical Engineering*, vol. 18, no. 4, pp. 1219–1227, 2018.
2. K. Hertz, "Limits of spalling of fire-exposed concrete," *Fire Safety Journal*, vol. 38, no. 2, pp. 103–116, 2003.

3. M. Zeiml, R. Lackner, and H. A. Mang, "Experimental insight into spalling behavior of concrete tunnel linings under fire loading," *Acta Geotechnica*, vol. 3, no. 4, pp. 295–308, 2008. [Online]. Available: <https://doi.org/10.1007/s11440-008-0069-9>
4. Y. Fu and L. Li, "Study on mechanism of thermal spalling in concrete exposed to elevated temperatures," *Materials and Structures*, vol. 44, no. 1, pp. 361–376, 2011.
5. V. K. R. Kodur and L. Phan, "Critical factors governing the fire performance of high strength concrete systems," *Fire Safety Journal*, vol. 42, no. 6, pp. 482–488, 2007.
6. E. Ryu, Y. Shin, and H. Kim, "Effect of loading and beam sizes on the structural behaviors of reinforced concrete beams under and after fire," *International Journal of Concrete Structures and Materials*, vol. 12, no. 1, pp. 1–10, 2018.
7. T. Hulin, C. Maluk, L. Bisby, K. Hodicky, J. Schmidt, and H. Stang, "Experimental studies on the fire behaviour of high performance concrete thin plates," *Fire Technology*, vol. 52, no. 3, pp. 683–705, 2016.
8. M. Dwaikat and V. Kodur, "Response of restrained concrete beams under design fire exposure," *Journal of structural engineering*, vol. 135, no. 11, pp. 1408–1417, 2009.
9. G. L. Albuquerque, A. B. Silva, J. P. C. Rodrigues, and V. P. Silva, "Behavior of thermally restrained rc beams in case of fire," *Engineering Structures*, vol. 174, pp. 407–417, 2018.
10. I. Rickard, N. Gerasimov, L. Bisby, and S. Deeny, "Predictive testing for heat induced spalling of concrete tunnel linings—the potential influence of sustained mechanical loading," in *5th International Workshop on Concrete Spalling due to Fire Exposure, 12-13 October 2017, Bors, Sweden, 2017*, pp. 337–344.
11. Y. Anderberg and S. Thelandersson, *Stress and deformation characteristics of concrete at high temperatures: experimental investigation and material behaviour model*. Bulletin of Division of Structural Mechanics and Concrete Construction, Bulletin 54; Vol. Bulletin 54. Lund Institute of Technology Lund, Sweden, 1976.
12. L. Boström, R. McNamee, J. Albrektsson, and P. Johansson, "Screening test methods for determination of fire spalling of concrete," RISE Research Institute of Sweden AB, RISE Report no. 2018:05, 2018.
13. A. M. Abubaker and C. T. Davie, "A generalised model for direct prediction of stresses in concrete at high temperatures," *Magazine of Concrete Research*, pp. 1–34, 2022, DOI: 10.1680/jmacr-2021-294
14. K. Mróz, I. Hager, and M. Tekieli, "Effect of cold rim on extent and type of concrete fire spalling,". Proceedings from the 5th International Workshop on Concrete Spalling At: Borås, Sweden, 12-13 October 2017.



# Systematic mapping studies on the impact of spalling on punching shear strength of RC slabs exposed to fire

Andreia Romero Fanton<sup>1</sup>, Luiz Carlos de Almeida<sup>2</sup>, Leandro Mouta Trautwein<sup>2</sup>

<sup>1</sup> PhD Student, University of Campinas, Campinas, Brazil

<sup>2</sup> PhD Professor, University of Campinas, Campinas, Brazil

\* Corresponding author( a145318@dac.unicamp.br, Rua Hermantino Coelho, 1127, Campinas, SP, Brazil)

## ABSTRACT

Flat slabs are widely used in underground structure, such as parking garages, due to their large surface area, static efficiency, and large span-depth ratios. There are two different mechanisms for the failure of flat slabs: flexural and punching shear. The first one is a ductile failure and gives visual tensile cracks in the member. The second one is a brittle failure and do not give visible crack warning signs. Possible explosive concrete spalling during fire influences the reduction of strength and stiffness of the constituent concrete and steel materials. Concrete spalling reduces the concrete section, and it is associated with the thermal restraint provided to the slabs. The spalling occurs because of the redistribution of internal forces due to the difference in temperature between the internal structure and the surrounding structure. There are very limited studies on the cover spalling impact on punching shear strength. This paper presents a systematic mapping study (SMS) to quantify the impact of spalling on the reduction of punching shear strength of reinforced concrete slabs exposed to fire and to map experimental and numerical studies. Parameters of the study were the fire direction, load levels, spalling depth, compressive strength of concrete and flexural reinforcement ratio.

**KEYWORD:** fire, punching shear, spalling, reinforced concrete slabs.

## INTRODUCTION

Traditionally, fire has represented a real threat to the safety of buildings and civil structures. The effects of high temperature on structures are two-fold. The first is that the mechanical properties of building materials (strength and stiffness) are negatively affected by temperature. The second is that thermal expansion and the deformations and displacements bring in supplementary “indirect actions” that can significantly increase internal forces (Bamonte et al., 2011 [1]). The structural system called flat slabs consists of reinforced or prestressed concrete slabs that are supported directly on columns. This system has a complex structural behaviour, especially in slab-column connections, where punching failure can occur due to shear stress (Díaz, 2018 [2]). Flat slabs have become extensively used due to the simplicity of construction and the higher structural efficiency, with respect to other structural systems. The serviceability limit state (possible large deflections) and the ultimate limit state (punching shear) are the crucial factors limiting the slenderness and determining the thickness of a flat slab (Bamonte et al., 2009 [3]). In a fire situation, many properties of concrete undergo significant changes:



physical, chemical, or mechanical. According to Reddy and Ramaswamy (2017) [4], the mechanical properties are lost because the high temperature in cement paste removes the chemically bound water and weakens the cement mortar, and due to complex physical and chemical changes within this heterogenic material. In many cases, fire-exposed concrete elements may have their layers fragmented due to an explosion of the material, a phenomenon known as spalling. In the last decades, associated with experimental research, numerical analyses were also developed using Finite Elements Method (FEM). For the study of punching shear, this analysis is very useful, given that carrying out experimental tests on slabs is expensive and difficult to perform. Although there are several studies related to punching in flat slabs, the number of studies that refer to simulations of fire performance of slabs subjected to this type of failure are scarce. This is due to the difficulty of correctly representing the effects of spalling in the numerical model, as well as the limitations of some commercial programs. So, it is necessary to review the different alternatives for the numerical modelling to study the spalling impact on punching shear in slabs exposed to fire. The impact of spalling on punching resistance has been the subject of only few experimental and theoretical research. In general, the studies conclude that explosive concrete spalling during fire reduces the load bearing capacity of the structure, once the concrete section is locally reduced. Spalling on the bottom concrete cover contributes to a large deal to the loss of punching shear resistance during fire (Annerel and Taerwe, 2015 [5]). The objective of this paper is elaborating a systematic mapping study (SMS) to understand the spalling effects on punching shear strength of reinforced concrete slabs exposed to a fire scenario.

## **RESEARCH SIGNIFICANCE**

Nowadays, punching shear of slabs is a well-understood phenomenon once it has been extensively investigated in the past (both experimentally and theoretically) (Bamonte et al., 2009 [3]). When talking about punching shear analysis on slabs in a fire scenario, there are just a few references, both experimental and numerical research. The first part of this paper is devoted to the systematic mapping study, a process to provide an overview of the scope of the area and to discover research gaps. The second part is the literature review itself.

## **SYSTEMATIC MAPPING STUDIES**

Systematic mapping study (SMS) is a process to identify, categorize and analyse literatures that are related to a certain research area. There are different characteristics of the process of systematic literature reviews and SMS with respect to the research questions, search process, search strategy requirements, quality evaluation, and results. The aim of a SMS is to develop an overview of papers on the topic area, mapped to a classification. Hence, SMS provides an overview of the scope of the area and allows to discover research gaps and trends. The outcome of a SMS is a classified portfolio of publications on the research area (Kitchenham et al., 2009 [6]). To survey the state of the art of research on the impact of spalling on punching shear strength of reinforced concrete slabs exposed to fire, a systematic mapping of the literature was carried out. The steps are presented below.

- Step 1: the questions that guided the mapping are: What are the most used research methods for punching shear analysis of RC slabs exposed to fire? How many of these studies have analysed the impact of spalling?
- Step 2: from step1, the following expression was defined for the search: (("reinforced concrete slabs" OR "RC slabs" OR "concrete slabs" OR "concrete slab\*") AND ("fire" OR "high temperature") AND ("spalling") AND ("punching shear"))

- Step 3: two databases were considered for the search: Scopus and Web of Science. The criteria for selecting articles were: search expression present in the title, abstract or keywords; only journal papers; only English papers.

Comparing the articles obtained in the two databases, the repeated articles and those related to areas other than Engineering were excluded. Thus, of the 7 articles obtained (4 in the Scopus database and 3 in the Web of Science), 4 documents resulted. After reading the titles and, later, the abstracts, the papers that did not adhere to the theme of the work were excluded, which were captured through the search expression on account of synonyms used in different areas. With this, 4 papers were selected for the elaboration of the review about the impact of spalling on punching shear strength of reinforced concrete slabs in fire.

To understand the behaviour of reinforced concrete slabs exposed to fire, focused on punching shear, a second expression was defined for the search: (*"reinforced concrete slabs" OR "RC slabs" OR "concrete slabs" OR "concrete slab"*) AND (*"fire" OR "high temperature"*) AND (*"punching shear"*)

Comparing the articles obtained in the two databases, the repeated articles and those related to areas other than Engineering were excluded. Thus, of the 36 articles obtained (19 in the Scopus database and 17 in the Web of Science), 20 documents resulted. After reading the titles and, later, the abstracts, the papers that did not adhere to the theme of the work were excluded, which were captured through the search expression on account of synonyms used in different areas. With this, 19 papers were selected for the elaboration of the review about the punching shear strength of reinforced concrete slabs exposed to fire. Also, through the "snowball" sampling from the selected documents on both expressions, 10 papers were included, resulting in 29 papers from journals. The articles collected in the international databases were classified according to the categories presented in Table 1.

*Table 1 Classification of selected documents according to the research question.*

Category	Papers covering...
FEM	... Finite Element analysis of punching shear strength of slabs exposed to fire
EA	... Experimental analysis of punching shear strength of slabs exposed to fire
Theory	... literature review about punching shear strength of RC slabs exposed to fire

The articles were also classified according to the year of publication and the country of the first author's institution. United Kingdom and Iraq concentrate most of the selected documents, about 23% and 13%, respectively, as shown in Figure 1.

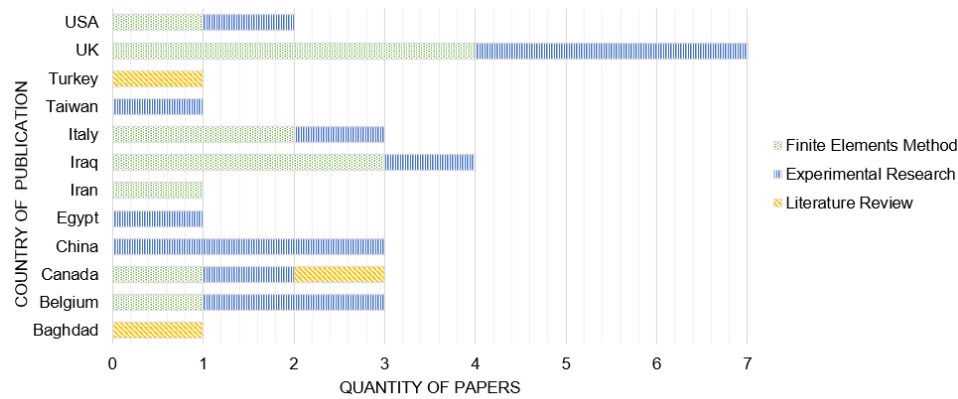


Figure 1 Distribution of selected papers according to the countries of the first author's institution and the research question.

The first studies surveyed were published between 2009 and 2012 and focused essentially on highlighting the difference between standard fire and natural fire exposure (Bamonte et al., 2009 [3]), modelling transient thermal creep and stress relaxation (Gales et al., 2009 [7]), nonlinear FEM model to understand a whole-building structural behaviour (Bailey and Ellobody, 2009 [8]), to identify the high risk of punching failure at slab-column connections (George and Tian, 2012 [9]), a development of a mechanical model for calculating fire effect on punching capacity (Salem et al., 2012 [10]), adapting the well-known Critical Shear Crack Theory to include the effects of high temperature and fire (Bamonte et al., 2012 [1]). These themes continue to be addressed in works published in the following years. Figure 2 presents a chronological distribution of selected papers.

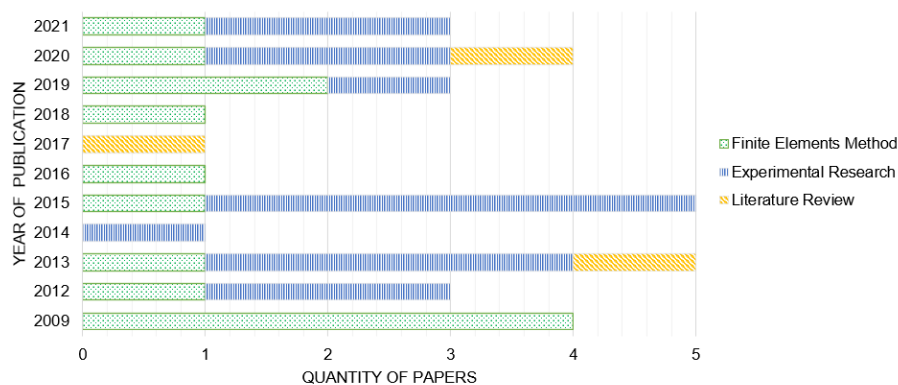


Figure 2 Chronological distribution of selected papers according to research question.

## CONCRETE SLABS IN FIRE

In a building, slabs have the highest levels of accidental loading among the elements ( $\xi = 0.5$ ).  $\xi$  is given by the relationship between the characteristic values of the variable action and the permanent actions. It is dimensionless and represents the level of accidental loading (Fantoni, 2019 [11]). As the main variable action on the structure grows relative to the permanent action, the design value of the total action on the structure in a fire situation decreases. The calculation value of shares in an exceptional situation is lower than the value in a normal situation; the probability that all actions occur simultaneously during an event is greatly reduced, which justifies the value of the reduction factor ( $\eta_{fi}$ ) being less than 0.9. In a building, the slabs are the elements of the structure that are less loaded and are the ones with the greatest ductility, that is, they have a great capacity for deformation. In a fire situation, the slabs remain stable

after the Ultimate Limit State is exceeded (Costa, 2008 [12]). However, the slabs must guarantee the physical integrity of the structure in terms of subdivision. If extreme deformations occur, insulation and tightness can be affected. If it collapses, the fire will spread between the floors, the structural damage will be higher.

## **CONCRETE SPALLING**

In a fire situation, many properties of concrete undergo significant changes, whether physical, chemical, or mechanical. According to Reddy and Ramaswamy (2017) [4], the mechanical properties are lost with the removal of existing water in the cement paste – which was chemically bound – due to high temperatures, thus causing its weakening. The capacity of reinforced concrete structures can be reduced properties when explosive spalling happens, and this high temperature is a load that must be considered in the design of buildings classified as strategic, as presented by Lo Monte et al. (2017) [13]. When heating a concrete element on only one side, two moving fronts appear: a heat front and a humidity front. Both move away from the heated face and walk to the unheated side. Ali et al. (2011) [14] show that the speed of such fronts is a function of several factors, one of which is the heating rate in the region where the two fronts meet within the concrete.

The spalling of concrete subjected to high temperatures is one of the factors that reduce its fire resistance. Lo Monte and Felicetti (2017) [15] show that spalling varies depending on several parameters of the constituent materials of concrete (moisture content, porosity, permeability, tensile strength, and compressive strength) and structural factors (heating rate and actions at which the building is subject). Such aspects contribute to the evolution of the main factors that cause spalling: the stress that arises due to gradient-type thermal loads and external loads; and the pore pressure that develops due to the vaporization of water. According to Bazant and Kaplan (1996) [16], the spalling phenomenon has two main reasons. The first refers to the hypothesis that the increase in temperature leads to high water vapor pressures in the pores of the concrete. As a result, internal stresses increase, and spalling occurs. The second reason is related to the hypothesis that heating rapidly leads to thermal expansion, and this is controlled by the surrounding concrete. In this way, a compressive stress arises that can result in the spalling of the concrete, causing damage to its surface layer. Lo Monte et al. [17] carried out an experimental campaign on high-performance concrete. The concrete spalling started in all the cases with a violent event on heated area. According to the authors, spalling is not strictly related to local mechanisms regarding aggregate-to-cement paste interaction and that a more general explanation can be given based on temperature, pressure, and stress fields.

There are two phenomena of spalling: progressive spalling and explosive spalling. From a regulatory point of view, only the explosive spalling term is used. The second one is characterized by violent burst-out of concrete pieces characterized by a sudden release of energy. This phenomenon may occur during the first 30 minutes of fire. It is characterized by large or small pieces of concrete being violently expelled from the surface, accompanied by a loud noise. Explosive spalling of concrete exposed to fire consists in the violent expulsion of shards from the hot surface due to the interaction between cracking and pore pressure build-up. The pore pressure alone cannot cause explosive spalling. If the pore pressure is involved, the role may be only as a trigger, i.e., the pressure leads to a slight deformation that initiates the process of thermal stress promoted brittle fracture.

## PUNCHING SHEAR STRENGTH

Flexural-punching and punching shear are the two main modes of punching failure, and the first one is the most desirable as it is a ductile failure mode, and it is controlled by the amount of reinforcing steel in a slab. Punching mode is governed by shear. Shear failures are sudden and brittle, hence it should be avoided (Ghoreishi et al., 2013 [18]). Flexural and shearing stresses cause an inclined crack that creates shear failure in a slab. Concrete is the only material that carries shear force before cracking. After that, it is carried by shear force developed in the concrete compression zone ( $V_c$ ), the vertical component of aggregate interlock ( $V_a$ ), and the dowel shear force developed by reinforcing bars crossing the crack ( $V_d$ ). Equation 1 shows the shear resistance of a slab ( $V_r$ ) without shear reinforcement [17].

$$V_r = V_c + V_a + V_d \quad (1)$$

where 25% to 50% of the total force on concrete elements are from  $V_c$ , 33% to 50% from  $V_a$  and 15% to 25% from  $V_d$  [18]. Increasing the crack width, the dowel shear mechanism causes splitting crack. Hence, shear force is carried by the concrete compression zone above the crack. Finally, as loading increase, splitting cracks appear on the tension side and spalling of concrete happens followed by punching failure. Unconservative design of slab-column connections, slab overloading, and deterioration of strength of concrete and reinforcement can lead to punching failure (Salem et al., 2012 [10]).

## PUNCHING SHEAR STRENGTH OF RC SLABS EXPOSED TO FIRE

Current codes do not define guidance on determining the punching shear capacity of slabs exposed to fire, and it is not clear if empirical and mechanical models can be adopted (Ghoreishi et al., 2013 [18]). In fire, punching shear in slabs is much more expressive because are to be expected significant increases of the internal forces, as in Figure 3.

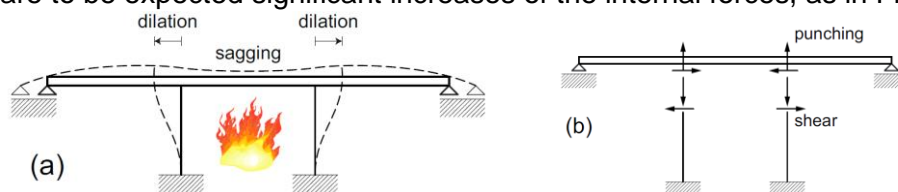


Figure 3 Flat slabs in fire: a) temperature-induced displacements; b) indirect actions [1].

Bamonte et al. [1] present an extension of CSCT (Critical Shear Crack Theory) to the case of high temperature or fire. CSCT is a semi-empirical approach, aimed at the evaluation of the punching resistance of flat slabs. The displacement profile is given by Eq. (2):

$$w_{tot} = w_{load} + w_{th} \quad (2)$$

where  $w_{tot}$  is the total displacement,  $w_{load}$  is the load-induced displacement and  $w_{th}$  is the thermal displacement. In this case, 2 assumptions are done: the load rotation ( $\Psi$ ) is constant and  $w_{load}$  is a linear function of the radial ( $r$ ); and  $w_{th}$  is a 2nd-order parabola.

Ghoreishi et al. [18] present an extensive review of the critical parameters affecting the punching shear capacity, are they: critical section perimeter, concrete compressive strength, flexural reinforcement (reinforcement ratio, yield strength, concrete cover, effective depth, and reinforcement arrangement), column aspect ratio, critical section perimeter to thickness ratio and size effect. Punching shear capacity of concrete flat slabs reduces at elevated

temperature. Depending on the reinforcement ratio, the punching shear capacity may reduce by 20-30% when a slab is exposed to elevated temperature reaching close to 300°C for an hour or more. Thermal problem is complex because heat transfer through the members occurs in three dimensions. It can be simplified observing that heat transfer inside the column is two-dimensional (corner effects). For a slab, heat transfer is mainly one-dimensional. Eurocode 2 (1992) [19] suggests that the shear strength of a reinforced concrete beam or column can be evaluated using conventional approach based on the reduced cross-section under 500°C. The analysis carried out by George and Tian, 2012 [9] indicates that, if the depth of concrete underneath the inclined shear crack is less than 70% of the total slab depth, punching failure may have occurred at 60 min of heating. Even though 90% of the slab section is assumed as effective in resisting shear, the shear demand will be much higher than the shear capacity after 90 min of fire loading.

Arna'ot et al. [20] explain that a real fire exposure (full-scale fire tests) caused a less severe thermal field than ISO 834 standard fire, which means less deterioration in the material properties. However, redistribution of internal forces was more severe in the real fire. Annerel et al. [21] investigated how much the overload coming from an increase of the axial load due to thermal restraint is allowed to be before failure occurs. They tested 6 real scale slab specimens for punching failure, from which 2 at ambient and 4 at high temperatures (120 min ISO 834 fire curve). Following the ISO 834 fire curve, spalling occurred at the bottom of the flat slabs and corners of the column stub. Spalling depths of up to 100 mm were found. From the fire tests carried out by Annerel et al. [5], it was clear that concrete cover spalling contributes to a large deal to the loss up to 10-15% of punching shear resistance during fire. Spalling damage was observed for all slabs testes for fire. Annerel et al. [22] carried out a thermo-mechanical model of an underground car park structure using ABAQUS. The highest increase of the axial load was found when the modulus of elasticity is kept constant to its initial value. Spalling was not considered in the model, since a fully-coupled hygro-thermo-mechanical analysis would be necessary to simulate.

Liao et al. [23] tested twelve specimens, half for fire resistance. Punching shear failure occurred in all specimens within 3-5h following exposure to fire. High-strength concrete specimen showed spalling on 90% of the heated surface, but the damaged depth of the concrete was very small. No spalling occurred on specimens exposed to elevated temperature on the tension side due to cracking and low constraint conditions. Because cracks that formed on the heated surface increased the thermal energy penetrating the slab, the deflections of the slabs with fire loading on the tension side were far greater than those of the specimens with fire loading on the compression side. The experimental program carried out by Ghoreishi et al. [24] consisted of six specimens. Spalling was not observed. It has shown that the code provisions for estimating the punching shear strength cannot effectively predict the bearing capacity under fire exposure. Smith et al. [25, 26, 27] tested a series of fifteen slab-column specimens in punching shear at both ambient and elevated temperature. A comparison was made to the results to Muttoni's critical shear crack theory, which is modified for high temperatures by degrading material properties.

Hamd et al. [28, 29] carried out an experimental setup simulated using ABAQUS. The results clearly show that LITS (load-induced thermal strains) accounts for the apparently anomalous experimental deflection results seen in punching shear experiments in the fire. If LITS is not included in analyses, this will not only result in incorrect deflection predictions but may also lead to nonconservative estimates of fire resistance times. A numerical investigation on punching shear of slabs exposed to fire was performed by Sadaghian and Farzam [30], using ATENA. Parameters of the study were the fire direction, flexural reinforcement ratio, load

levels, shear reinforcement and compressive strength of concrete. It was concluded that increasing the flexural reinforcement ratio changes the failure mode from flexural punching to brittle punching in most cases. ISO834 fire curve was used. Application of the fire from the top face causes the slab to deflect upwards and in an opposite direction to the gravity-load induced deflections up to the 70% of pure gravity failure load. Zhang et al. [31] tested slabs for punching and post-punching strengths of slab-column connections. The residual punching strength of slab-column connections after cooling from a high temperature up to 800°C applied on the compression face of slab was 1.9–7.5% lower than the slab-column connections without experiencing high temperatures. A finite element simulation was performed using ABAQUS. It was concluded that the numerical simulation predicted a premature punching failure and thus underestimated the residual punching strength of slab-column connections with previously applied high temperatures by 8.8–11%. Gharbi and Mahmoud [32, 33] performed a nonlinear finite element transient thermal-structural analysis at fire conditions using ANSYS. Increasing the ratio of length to thickness by 33% increased the deflection of the slabs by 108% and 123% in ambient temperature and fire conditions.

Naji et al. [34] did a review on numerical analysis of flat slabs exposed to fire. They concluded that fire exposure times increase the slab rotation affecting the shear strength of the slab column connection since it increases the inclined cracks. Three full-sized flat slabs were tested at ambient and high temperatures by Wang et al. [35]. The slabs were submitted to the ISO 834 fire curve for 180 minutes. A rigid-plastic model based on unified strength theory was used to calculate the effect of fire on the punching capacity of the flat slab. The calculated results were compared with the test data. The loss of punching bearing capacity after fire was about 32%. Spalling was not measured. According to Salem et al. [10], the punching capacities of flat slabs subjected to fire would be worse when this affects the tension side rather than the compression one, due to the formation of cracks and possible reduction of strength of main reinforcement. The experimental program carried out consisted of fourteen specimens, with two concrete covers (25 and 10mm), three hours of fire exposure. They observed extensive cover spalling in the tension side of slab close to failure. The decrease in punching strength due to sudden cooling is explained by the sudden shrinkage of concrete which cause new cracks resulting in considerable strength reduction and spalling of concrete cover. They proposed a model to obtain punching capacity from equilibrium of external forces and internal stresses. The load carried by column is assumed equally distributed along the four supporting edges of the slab, each side carries one-fourth of the total load as in Figure 4, where  $C_u$  is the concrete ultimate compressive force in concrete in compression zone;  $d$  is the effective depth of slab;  $a$  is the height of the equivalent stress block; and  $L$  is the cantilever length.

Wang et al. [36] presented an experimental study on the post-fire residual behaviour of concrete slabs. The ultimate load and failure mode of each span were dependent on its maximum temperatures, its residual material properties, effective thickness, and spalling, and thus the interaction or boundary restraint between various heated or unheated spans can be neglected at the ultimate state. According to the authors, the current punching shear theories should be modified when considering the effect of the serious spalling.



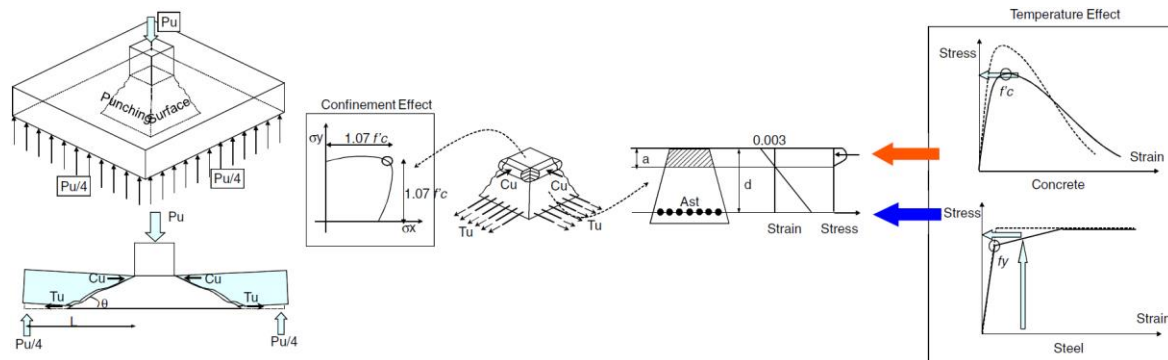


Figure 4 Proposed model for estimating punching strength of slabs under fire [10].

The experimental investigation carried out by Wang et al. [37] showed that, compared to the fire spread direction and time delay, the reinforcement ratio, reinforcement arrangement and slab's thickness have more important effects on the residual ultimate loads of the fire-damaged continuous slabs. Dalaf and Mohammed [38] tested nine half-scale flat slabs, 1,5% fibre volume fraction. Fiber reinforced slabs failed gradually in a more ductile mode. The failure was sudden with brittle mode in slabs that contained no fibers. In the fiber reinforced specimens, the spalling in the concrete cover was more controlled. Mohmmad et al. [39] tested geopolymer concrete slabs reinforced by FRP bars after fire. Compared to the residual compressive strength, the residual tensile strength was much lower, which indicates that the subjection to increased temperature has a more severe impact on the tensile strength compared to the compressive strength. Geopolymer concrete exhibited greater resistance to spalling and cracking under high temperatures than ordinary concrete.

## CONCLUSIONS

It was concluded, from the available data, that concentric flat plate-column joints from structures exposed to fire are affected by temperature in two main ways. The first one is related to the material properties, that is a directly effect. Mechanical and thermal properties decay dramatically, and this property degradation might reach 100% at 1000°C. The second way is an indirect effect and is related to the unbalanced heating due to the different lengths of the adjacent spans, and could add a 50%-higher axial load than in ambient conditions. The most effective parameters for punching shear behaviour of structures exposed to high temperatures are the time-temperature exposure, support conditions, exposure surface, nominal strength of concrete, reinforcement, fire scenario, and preloading and stress history. The increase of the axial load due to thermal restraint can be an important factor regarding the structural safety of flat slabs exposed to fire.

From the literature involving experimental research, it was concluded that the residual strength of specimens with high concrete strength and a high reinforcement ratio that were exposed to fire on their compression surface, was more deteriorated by fire than those with a low compressive strength and low reinforcement ratio. The effect of shear reinforcement on the residual strength of a slab-column assembly after high temperature exposure was minimal. Sudden cooling after exposure to high temperatures led to more strength deterioration than gradual cooling. Experimental studies on punching shear of reinforced concrete slabs are rare and more numerical and experimental studies are required to enhance the understanding of punching shear in a fire scenario. Although the concrete spalling is a factor that reduces fire resistance and could even modify the current punching shear theories, only a few experimental studies have investigated its effect. This lack of studies is mainly due to the difficulties and high cost associated with test setup and experimental facilities in high temperature. Further

experimental and numerical research works are suggested to increase the knowledge about the influence of fire-exposure and spalling on punching shear strength.

## REFERENCES

1. Bamonte, P., Felicetti, R. and Gambarova, P.G., "Punching shear strength of R/C slabs subjected to fire", Proceedings of the 7th International Conference on Structures in Fire – SiF 2012, 689-698, 2012.
2. Díaz, R.A.S., "Análise numérica da resistência à punção de lajes lisas protendidas com cabos não aderentes", Thesis, University of Campinas, 2018.
3. Bamonte, P., Felicetti, R. and Gambarova, P.G., "Punching shear in fire-damaged reinforced concrete slabs", *ACI Spec. Publ.*, **265**, 345-366, 2009.
4. Reddy, D. H. and Ramaswamy, A., "Influence of mineral admixtures and aggregates on properties of different concretes under high temperature conditions I: Experimental study", *Journal of Building Engineering*, **14**, 103–114, 2017.
5. Annerel, E. and Taerwe, L., "Design considerations for shear failure of flat concrete slabs exposed to fire", Proceedings of the Concrete – Innovation and Design – *fib* Symposium, Copenhagen, Denmark, 18-20, May, 2015.
6. Kitchenham, B. et al., "Systematic literature reviews in software engineering – A systematic literature review", *Information and Software Tech.*, **51**, 7–15, 2009.
7. Gales, J., Bisby, L.A., MacDougall, C. and MacLean, K., "Transient high-temperature stress relaxation of prestressing tendons in unbonded construction", *Fire Safety Journal*, **44**, 570-579, 2009.
8. Bailey, C.G. and Ellobody, E., "Whole-building behaviour of bonded post-tensioned concrete floor plates exposed to fire", *Engineering Structures*, **31**, 1800-1810, 2009.
9. George, S.J. and Tian, Y., "Structural Performance of Reinforced Concrete Flat Plate Buildings Subjected to Fire", *International Journal of Concrete Structures and Materials*, **6**, 111-121, 2012.
10. Salem, H., Issa, H., Gheith, H. and Farahat, A., "Punching shear strength of reinforced concrete flat slabs subjected to fire on their tension sides", *HBRC Journal*, **8**, 36-46, 2012.
11. Fanton, A.R., "Análise numérica do comportamento termomecânico de lajes de concreto armado expostas ao fogo", Thesis, University of Campinas, 2019.
12. Costa, C.N., "Dimensionamento de elementos de concreto armado em situação de incêndio", PhD Thesis, University of São Paulo, 2008.
13. Lo Monte, F., Lombardi, F., Felicetti, R. and Lualdi, M., "Ground-Penetrating Radar monitoring of concrete at high temperature", *Construction and Building Materials*, **151**, 881–888, 2017.
14. Ali, F., Nadjai, A. and Abu-Tair, A., "Explosive spalling of normal strength concrete slabs subjected to severe fire", *Materials and Structures*, **44**, 943–956, 2011.
15. Lo Monte, F. and Felicetti, R., "Heated slabs under biaxial compressive loading: a test set-up for the assessment of concrete sensitivity to spalling", *Materials and Structures/Materiaux et Constructions*, **50**, 1–12, 2017.
16. Bazant, Z. P. and Kaplan, M. F., "Concrete at High Temperatures: Material Properties and Mathematical Models", *Concrete Design and Construction*, 1996.
17. Lo Monte, F., Felicetti, R. & Rossino, C., "Fire spalling sensitivity of high-performance concrete in heated slabs under biaxial compressive loading", *Materials and Structures*, **52**, 1-11, 2019.

18. Ghoreishi, M., Bagchi, A. and Sultan, M.A., "Review of the Punching Shear Behavior of Concrete Flat Slabs in Ambient and Elevated Temperature", *Journal of Structural Fire Engineering*, **4**, 259-278, 2013.
19. Eurocode 2, "Design of concrete structures. Part 1-2: General rules—structural fire design (ENV1992)", Brussels: European Committee for Standardization, 1995.
20. Arna'ot, F.H., Abid, S.R., Ozakça, M. and Taysi, N., "Review of concrete flat plate-column assemblies under fire conditions", *Fire Safety Journal*, **93**, 39-52, 2017.
21. Annerel, E., Lu, L. and Taerwe, L., "Punching shear tests on flat concrete slabs exposed to fire", *Fire Safety Journal*, **57**, 83-95, 2013.
22. Annerel, E., Taerwe, L., Merci, B., Jansen, D., Bamonte, P. and Felicetti, R., "Thermo-mechanical analysis of an underground car park structure exposed to fire", *Fire Safety Journal*, **57**, 96-106, 2013.
23. Liao, J.S., Cheng, F.P. and Chen, C.C., "Fire Resistance of Concrete Slabs in Punching Shear", *Journal of Structural Engineering*, **140**, 1-9, 2014.
24. Ghoreishi, M., Bagchi, A. and Sultan, M.A., "Punching Shear Behavior of Concrete Flat Slabs in Elevated Temperature and Fire", *Advances in Structural Engineering*, **18**, 659-574, 2015.
25. Smith, H.K.M., Stratford, T.J. and Bisby, L.A., "Deflection response of reinforced concrete slabs tested in punching shear in fire", Proceedings of the Applications of Structural Fire Engineering, Dubrovnik, Croatia, 15-16, October, 2015.
26. Smith, H.K.M., Stratford, T.J. and Bisby, L.A., "The Punching Shear Mechanism in Reinforced-Concrete Slabs under Fire Conditions", Proceedings of the PROTECT 2015 - Fifth International Workshop on Performance, Protection & Strengthening of Structures under Extreme Loading, 704-711, 2015.
27. Smith, H.K.M., Stratford, T.J. and Bisby, L.A., "Punching Shear of Reinforced Concrete Slabs under Fire Conditions: Experiment vs. Design", Proceedings of the First International Conference on Structural Safety under Fire & Blast, 1-10, 2015.
28. Hamd, R.A., Gillie, M., Torelli, G., Warren, H., Stratford, T.J. and Wang, Y., "The Effect of LITS on Punching Shear in Fire", Proceedings of the 9th International Conference on Structures in Fire (SiF), 1-9, 2016.
29. Hamd, R.A., Gillie, M., Torelli, G., Warren, H., Stratford, T.J. and Wang, Y., "The effect of load-induced thermal strain on flat slab behaviour at elevated temperatures", *Fire Safety Journal*, **97**, 12-18, 2018.
30. Sadaghian, H. and Farzam, M., "Numerical investigation on punching shear of RC slabs exposed to fire", *Computers and concrete*, **23**, 217-233, 2019.
31. Zhang, C., Ma, W., Liu, X., Tian, Y. and Orton, S.L., "Effects of high temperature on residual punching strength of slab-column connections after cooling and enhanced post-punching load resistance", *Engineering Structures*, **199**, 1-12, 2019.
32. Gharbi, A.H. and Mahmoud, A.S., "Punching shear behavior of reinforced concrete slabs under fire using finite elements", *Journal of Engineering*, **26**, 106-127, 2020.
33. Gharbi, A.H. and Mahmoud, A.S., "Finite element modelling of punching shear in reinforced concrete slabs at ambient temperature and fire conditions", *AUS Revista*, **26**, 344-358, 2021.
34. Naji, H.F., Khalid, N.N. and Medhloom, M.K., "A review on numerical analysis of RC flat slabs exposed to fire", *Tikrit Journal of Engineering Sciences*, **27**, 1-5, 2020.
35. Wang, D., Dong, Y., Zhang, D., Wang, W. and Lu, X., "Punching shear performance of concrete slabs under fire", *Engineering Structures*, **225**, 1-14, 2020.
36. Wang, T., Chen, Z., Jiang, Y., Huang, Z., Zhang, Y., Huang, Y., Li, L., Wu, J. and Guo, W., "Residual properties of three-span continuous reinforced concrete slabs subjected to different compartment fires", *Engineering Structures*, **208**, 1-19, 2020.

37. Wang, T., Jiang, Y., Huang, Z., Li, L., Huang, Y., Zhang, Y., Zhang, G., Zhang, X. and Duan, Y., "Post-fire behaviour of continuous reinforced concrete slabs under different fire conditions", *Engineering Structures*, **226**, 1-16, 2021.
38. Dalaf, A.N. and Mohammed, S.D., "The impact of hybrid fibers on punching shear strength of concrete flat plates exposed to fire", *Engineering, Technology & Applied Science Research*, **11**, 7452-7457, 2021.
39. Mohmmad, S.H., Gulsan, M.E. and Çevik, A., "Behaviour of Geopolymer Concrete Two-Way Slabs Reinforced by FRP Bars After Exposure to Elevated Temperatures", *Arabian Journal for Science and Engineering*, 1-23, 2021.

# Numerical studies on the effect of spalling on the concrete cone capacity of single headed stud during fire

Hitesh Lakhani<sup>1,\*</sup> & Jan Hofmann<sup>1</sup>

<sup>1</sup> Institute of Construction Materials, University of Stuttgart, Germany

\* Corresponding author (hitesh\_lakhani06@rediffmail.com,  
Pfaffenwaldring 4, 70567 Stuttgart, Germany)

## ABSTRACT

A fastener intended to be used for structural application should at least have a fire resistance equal to the structural elements being connected or the element in which the fastener is installed. A metal fastener loaded in tension can exhibit four possible failure modes viz., steel failure, Concrete Cone (CC) failure, splitting failure and pull-out failure. Mostly steel failure is found to be the decisive failure mode during fire for most of the unprotected fasteners made of carbon steel. Moreover, in practice CC failure can be avoided by increasing the embedment depth of the fastener i.e., setting a fastener deeper into the concrete. Thus, increasing the CC breakout capacity. But the above approach may work only under the assumption that spalling does not occur during fire.

The paper presents the first set of results from a numerical study conducted to investigate the effect of spalling on CC breakout capacity of a headed stud with embedment depth ( $h_{ef}$ ) of 50 mm installed away from the edge. A validated 3D sequentially coupled thermo-mechanical Finite Element (FE) model developed in Ansys ® Mechanical is used for conducting the investigation. The temperature dependent thermal and mechanical properties of concrete are taken as per Eurocode 2. The parameters investigated includes depth of spalling ( $0.2 \cdot h_{ef}$  &  $0.4 \cdot h_{ef}$ ) and diameter of the area ( $1 \cdot h_{ef}$  &  $2 \cdot h_{ef}$ ) around the headed stud which is affected by spalling.

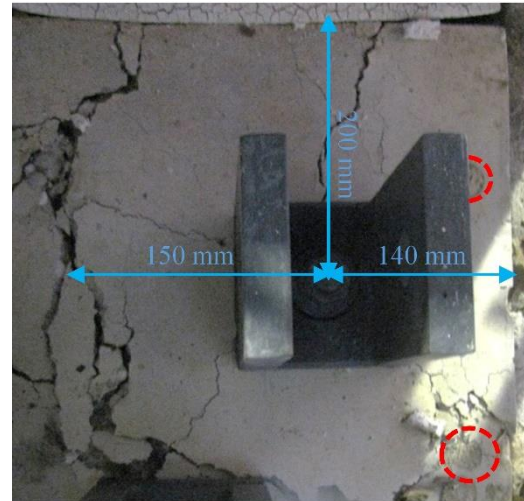
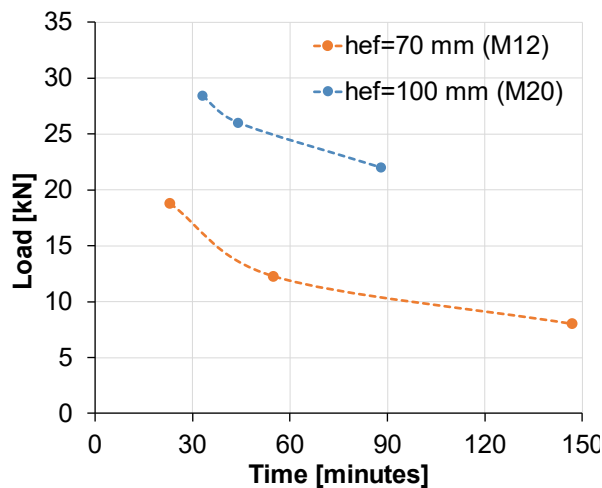
**KEYWORD:** Fasteners, Concrete Cone Capacity, Spalling, Headed Stud, Fire Resistance

## INTRODUCTION

The use of fasteners in concrete construction has increased significantly, both for structural application and installing safety related systems or other equipment. Hence, a failure of fasteners poses threat to human life during the escape and firefighting phase. Therefore, the fasteners are designed to have a fire resistance at least equal to that of the structural element in which the fastener is installed. As per the current design guidelines [1], the fire resistance of fasteners should be checked for all failure modes as for ambient conditions. The failure modes which are required to be verified at ambient conditions for metal anchors under tension loads are namely, steel failure, concrete cone failure, pull-out failure, and concrete splitting failure.

Generally, steel failure is found to be the decisive failure mode in most cases of unprotected fasteners loaded in tension. But due to the negative effects of fire on concrete namely, the increase in temperature of concrete; development of steep thermal gradients;

degradation in material strength & stiffness; thermal cracking etc., the load capacities for concrete related failure modes (e.g., concrete cone failure, concrete blow-out failure etc.) are also reduced drastically. Therefore, for fasteners made of stainless steel which performs better during fire and/or larger (bolt) sizes, concrete cone failure may become the decisive failure mode for small anchorage depths. Results of recent experiments performed by Lakhani and Hofmann (2021) [2] on torque-controlled expansion anchors made of stainless steel, shown in Figure 1, supports the above statement. The concrete cone failure was found to be the governing failure mode for sizes M12 & M20, with embedment depth of 70 mm & 100 mm, i.e., concrete cone failure occurred before steel failure under standard fire exposure.



(a) Experimental results for concrete cone failure under fire

(b) CC failure for size M20 ( $h_{ef} = 100$  mm)

Figure 1 Experimental results for torque-controlled expansion anchors tested by Lakhani and Hofmann (2021) [2]

As per EN1992-4 [1] the reduction factor for concrete cone capacity is a linear function of embedment depth ( $h_{ef}$ ). For fire exposure up to 90 minutes the reduction factor is given by  $h_{ef}/200$ , which is further reduced to  $0.8 \cdot h_{ef}/200$  for fire exposure between 90 to 120 minutes. This implies that the CC capacity of fasteners with  $h_{ef} = 200$  mm, not influenced by edge, is unaffected up to 90 minutes of standard fire exposure. But this may not be the case if spalling occurs during fire.

In recent years, effect of spalling on the fire resistance of structural members has gained attention of researchers [3–6]. But the effect of spalling on fire resistance of fasteners has still not been investigated. The paper presents the first set of results from a numerical study conducted to investigate the effect of spalling on CC breakout capacity of a headed stud.

## MODELLING PROCEDURE

A sequentially coupled 3D thermomechanical FE model is developed in Ansys ® Mechanical [7] for performing the numerical investigation presented in this paper. The geometric details of the headed stud and the concrete slab are shown in Figure 2. To optimise the computation time only one-fourth of the geometry is modelled using symmetry boundary conditions. The dimensions for the concrete are same as those used by Periskic (2009) [8]. Since simulation results from Periskic (2009) [8] are used for validating the model at ambient conditions. The dimensions of the headed stud are based on those used

in practice since no such information was found in Periskic (2009) [8]. The diameter of the shaft ( $D_s$ ), diameter of the head ( $D_h$ ) and the thickness of the head ( $T_h$ ) for the headed stud are taken as 10 mm, 19 mm, and 7.1 mm respectively.

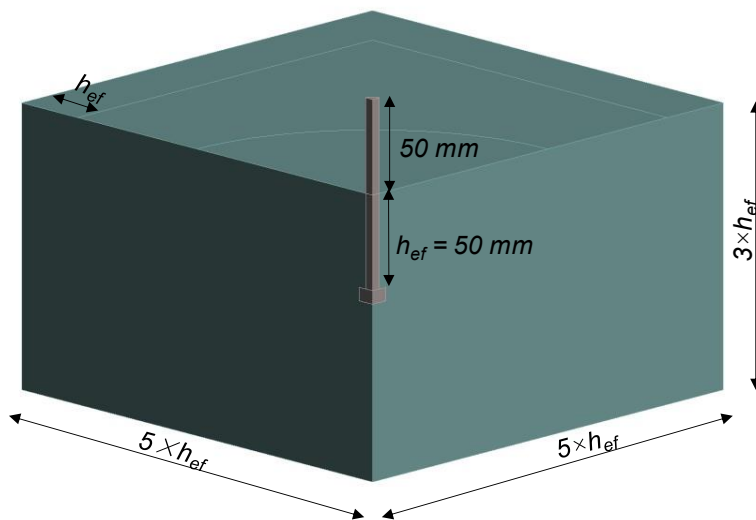


Figure 2 Geometric details of the headed stud and the concrete slab (one-fourth)

Before proceeding with the parametric study to investigate the effect of spalling on the CC breakout capacity of headed study under fire. The model is validated first at ambient conditions and then under standard fire exposure. The validation is presented in the next sections.

### Validation: CC capacity at ambient condition

The boundary conditions applied during the static structural / mechanical analysis are shown in Figure 3. The contact between the headed stud and concrete is modelled using frictionless contact based on Pure Penalty formulation. The geometry is discretised using quadratic (higher order) 3-D 10-node tetra-hedral elements (CPT 217) and 20-noded hexahedral elements (CPT 216) for concrete & steel, respectively. The steel is assumed to be linear elastic with modulus of elasticity = 200000 MPa and Poisson's ratio = 0.33. This assumption is justified since in the presented study only concrete cone failure is investigated.

- A → symmetry along Z-axis
- B → symmetry along X-axis
- C → Compression only support  
(Displacement restrained only along +ve Y-axis)
- D → Incremental displacement

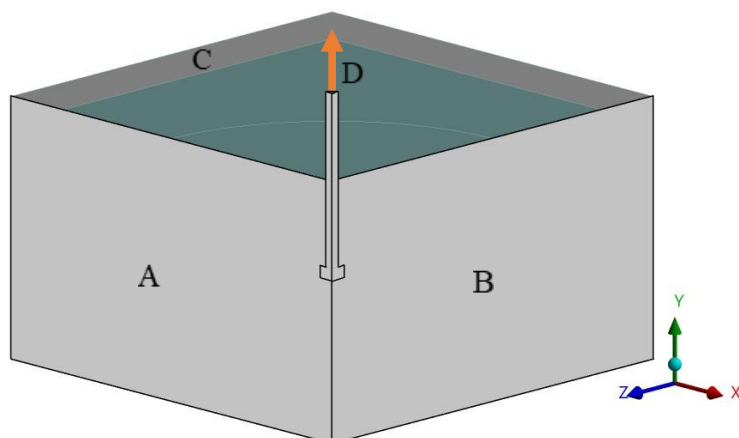


Figure 3 Applied boundary conditions for static structural analysis



The mechanical properties of concrete at ambient conditions are given in Table 1. The nonlinear behaviour of concrete is modelled using Drucker-Prager yield surface in compression combined with Rankine tension yield surface.

Figure 4 (a) compares the predicted load-displacement response with the simulation results available in literature [8]. The cracking at 80% of the peak load is shown in Figure 4 (b), which clearly shows a CC breakout failure. Based on the validation results presented it can be concluded that the model can correctly capture the response of headed stud loaded in tension at ambient temperature.

Table 1 Mechanical properties of concrete at ambient temperature

Cylindrical compressive strength ( $f_c$ )	21.25 MPa
Tensile strength ( $f_t$ )	2.00 MPa
Poisson's ratio ( $\nu$ )	0.18
Modulus of elasticity ( $E$ )	28000 MPa
Biaxial compressive strength ( $f_{cb}$ )	24.44 MPa
Tensile fracture energy ( $G_f$ )	0.1265 N/mm

### Validation: CC capacity under ISO834-1 fire

After having validated the model for ambient temperature. The next step is to validate the model for its ability to capture the CC breakout failure during fire. For this step a sequentially coupled thermomechanical analysis is performed. The concrete slab and the headed stud are exposed to ISO834-1 [9] standard fire only from the side on which the anchor is set. The headed stud is allowed to expand freely during the targeted exposure duration (30 / 50 / 90 / 120 minutes) and thereafter it is loaded by applying incremental displacement on the top face of the anchor.

The heat transfer from the surrounding hot gases to the exposed surface is modelled using radiation and convection boundary conditions. The effective emissivity for radiation heat transfer is taken as 0.8 and the convective heat transfer coefficient is taken as 25 W/m<sup>2</sup> K as recommended by Eurocode 1 [10]. The temperature dependent density, specific heat and conductivity of concrete are taken from Eurocode 2 [11]. Specific heat for dry concrete and lower limit conductivity is used for the simulations. The choice of thermal properties for concrete is based on the validation performed by Lakhani et al. (2013) [12]. The temperature dependent thermal properties of steel are taken according to Eurocode 3 [13]. The contact between headed stud surfaces and concrete surfaces is taken as bonded for the thermal analysis. The geometries are discretised using higher-order elements (Solid291 for concrete and Solid279 for steel/headed stud), which have a single degree of freedom i.e., temperature at each node.

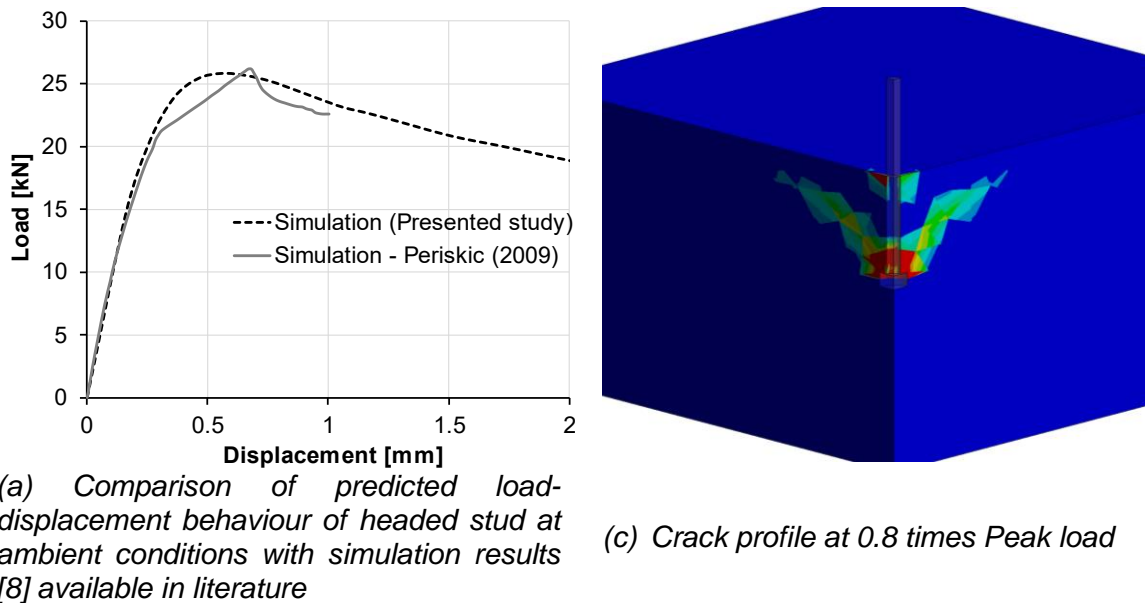


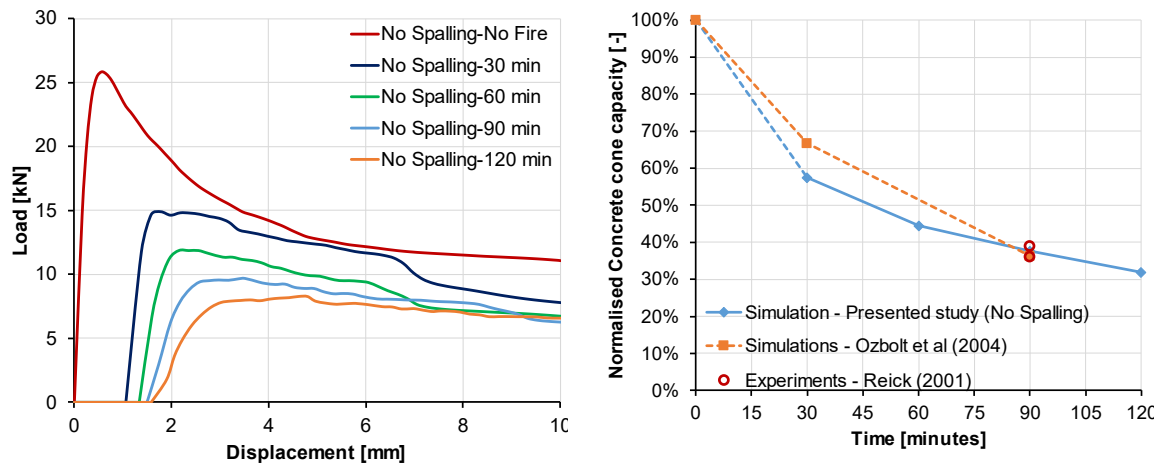
Figure 4 Simulation results for CC capacity at ambient temperature

The concrete is assumed to be made of calcareous aggregates, hence, the corresponding compressive strength degradation and thermal strain from Eurocode 2 [11] are used. The compressive strength degradation above 1100 °C is assumed to be same as for 1100 °C. Furthermore, the tensile strength at and above 600°C is kept constant at a value corresponding to 10% of ambient value. The above-mentioned deviations from Eurocode 2 [11] are made to avoid convergence difficulties which may arise due to zero material strength.

The Drucker-Prager model used for the simulations at ambient temperature is extended with temperature dependent material properties. The temperature dependent constitutive stress-strain relationship under compression as recommended by Eurocode 2 [11] with linear softening is used with the modification that the stress level at & beyond ultimate strain remains at 20% of the corresponding compressive strength at that temperature. Since the Drucker-Prager yield surface under compression is combined with Rankine's tension yield surface, there is no requirement for defining any material model parameters like dilatation factor etc. Other important material parameters and assumptions are listed below:

1. The concrete (under compression) is assumed to be linear up to 30% of the peak stress at each temperature.
2. The tension fracture energy is assumed to be independent of temperature.
3. The residual tensile stress level under at each temperature, beyond critical crack opening is assumed to be 10% of corresponding tensile strength.
4. To suppress steel failure, the steel for headed stud is assumed to be linear elastic with no reduction in strength at higher temperature. But the thermal strain for steel is considered according to Eurocode 3 [13].

Figure 5 (a) shows the predicted load-displacement behaviour of headed stud at 30, 60, 90 & 120 minutes of standard fire exposure. Furthermore, a comparison between the normalised CC capacity obtained in the current study, experimental results from Reick, (2001) [14] (for  $h_{ef} = 50$  mm) and the numerical results from Ozbolt et al. (2004) [15] (for  $h_{ef} = 50$  mm) is shown in Figure 5 (b). A very good comparison is found between numerical & experimental results available in literature and the results predicted in the present study. Thus, validating the numerical model.



(a) Predicted load-displacement behaviour of headed stud at different exposure duration  
 (b) Comparison of predicted reduction in CC capacity with simulation [15] and experiments [14] available in literature

Figure 5 Simulation results for CC breakout failure under standard fire exposure

The crack pattern at 80% of the peak load in the post peak region at 30 minutes and 90 minutes are shown in Figure 6 (a) and (b), respectively. At both exposure duration a clear CC breakout failure can be seen. The principal strain contour indicated by red colour in Figure 6, corresponds to a crack width greater than 0.3 mm.

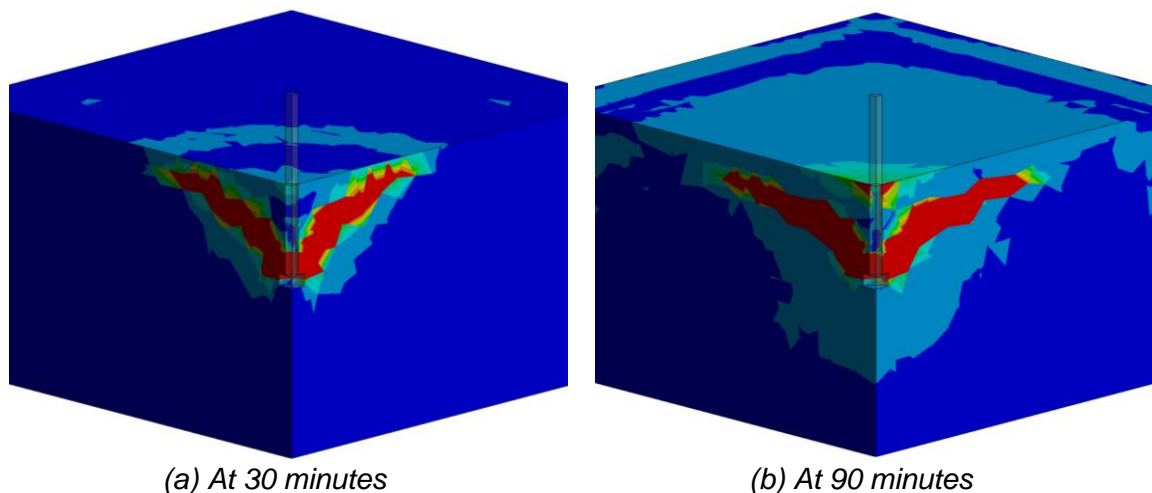


Figure 6 Crack profile at 0.8 times Peak load at different exposure duration (No spalling case)

## NUMERICAL INVESTIGATION

To investigate the effect of spalling on the CC breakout capacity of headed stud under fire, the following parameters are selected:

1. Radius of the area around the headed stud which is affected by spalling. For this parameter two values as  $1 \cdot h_{ef}$  (50 mm) and  $2 \cdot h_{ef}$  (100 mm) are selected. These values are referred as R1 $h_{ef}$  and R2 $h_{ef}$  in the discussion.
2. Uniform depth of spalling in the area affected by spalling. For this parameter two values as  $0.2 \cdot h_{ef}$  (10 mm) and  $0.4 \cdot h_{ef}$ , (20 mm) referred to as D0.2 $h_{ef}$  and D0.4 $h_{ef}$  for discussion, are selected.

The above-mentioned parameters lead to a total of four combinations viz., R1 $h_{ef}$ -D0.2 $h_{ef}$ ,

R1hef-D0.4hef, R2hef-D0.2hef and R1hef-D0.4hef, as shown in Figure 7. It should also be noted that for the present study the spalling is assumed to happen from the start of the fire duration.

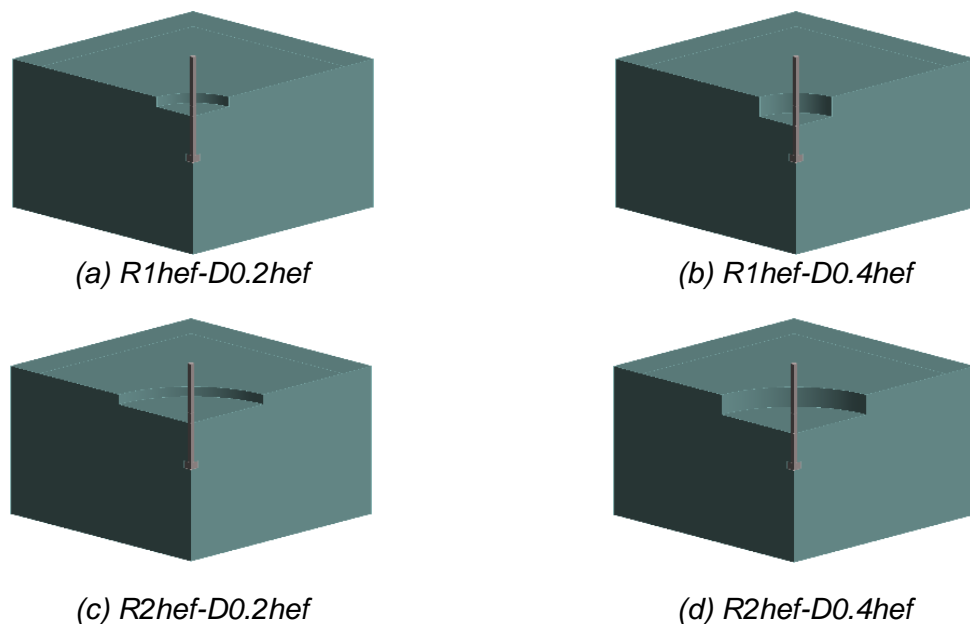


Figure 7 Investigated spalling configurations

The calculated temperature gradients along the headed stud and the thickness of the concrete slab away from the headed stud, are shown in Figure 8 (a) & (b) at 30 & 90 minutes of standard fire exposure. The results in Figure 8 shows that the temperature is higher near the headed stud due to higher thermal conductivity of steel. The high conductivity of steel is also the reason why the radius of the area around the headed stud affected by spalling does appear to affect the thermal gradient near headed stud significantly.

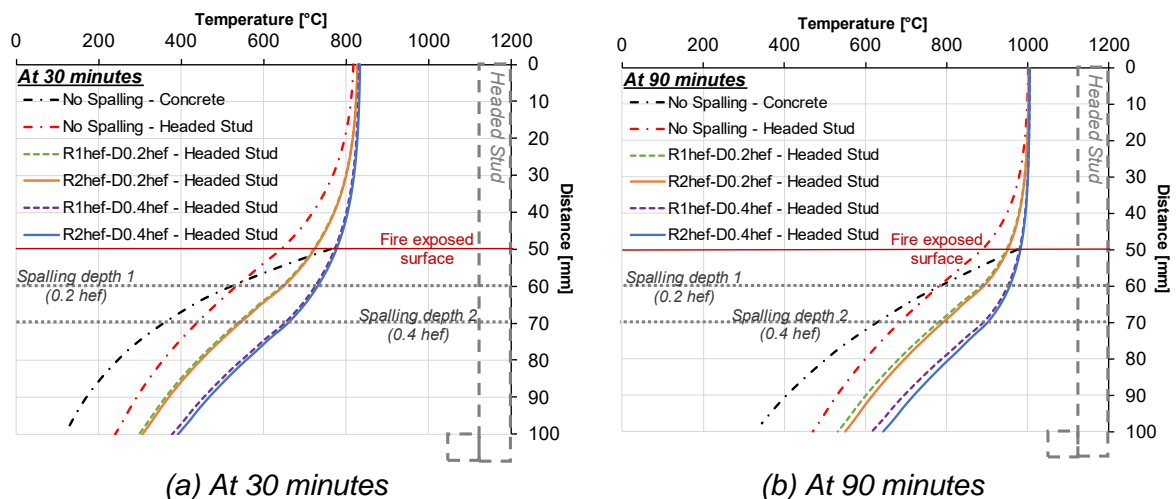


Figure 8 Temperature gradients along headed stud and concrete thickness

In addition to computing the CC breakout capacity for each of the four spalling configurations at 30, 60, 90 and 120 minutes of standard fire exposure. The CC breakout capacities for the spalling configurations are also assessed without fire. These simulations

are performed with an object to estimate the effect of changes in geometry due to removal of concrete (assumed to have spalled) on the CC capacity at ambient temperature. Results of all the simulations in terms of CC breakout capacities normalised with reference to the no-spalling & no fire case are shown in Figure 9.

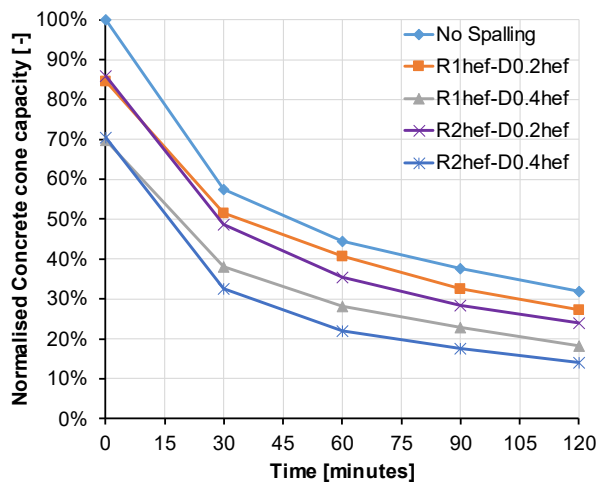


Figure 9 Normalised CC breakout capacity for all the simulated configurations (with and without spalling)

At ambient temperature (i.e., time  $t=0$  minutes) the CC breakout capacity for same spalling depth but different radius of spalled area is (almost) identical. This implies that the reduction obtained in the capacity is only because of the reduction in the embedment depth due to spalling of concrete. This observation can be explained based on the size of the CC breakout which reduces with reduction in embedment depth. Hence, if the radius of the spalled area is equal or greater than the expected CC breakout it would not have an influence on the capacity at ambient temperature. Figure 10 (a) and (b) shows the CC breakout for cases R1hef-0.4hef & R2hef-D0.4hef, and it can be observed that the sizes of the CC breakout are similar.

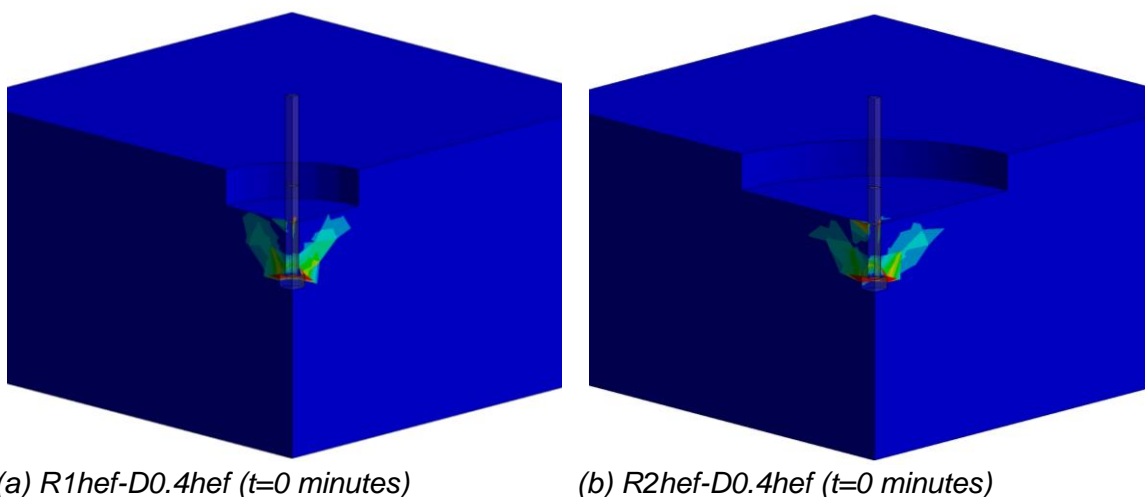


Figure 10 Crack profile at 0.8 times Peak load (without fire)

Whereas, during fire, a wider spalled area for the same depth of spalling has a higher negative effect on the capacity. This is because of the difference in the temperature ingress (distribution) into the concrete slab especially in the zone through which the conical cracks of CC breakout are formed. Moreover, during fire a larger concrete cone is

expected to breakout of the concrete slab in comparison to ambient temperature as can be observed from the crack profiles shown in Figure 4 (ambient temperature) and Figure (during fire). Furthermore, as seen from the crack profiles in Figure 11 (a) and (b), for a smaller radius of spalled zone the CC breakout under fire may extend beyond this radius. Thus, reducing the negative effect of spalling. Another factor that may have contribute is the compressive stresses in the top layer of concrete. These stresses are the result of restrained thermal expansion of top layer by the relatively colder next layer just below it.

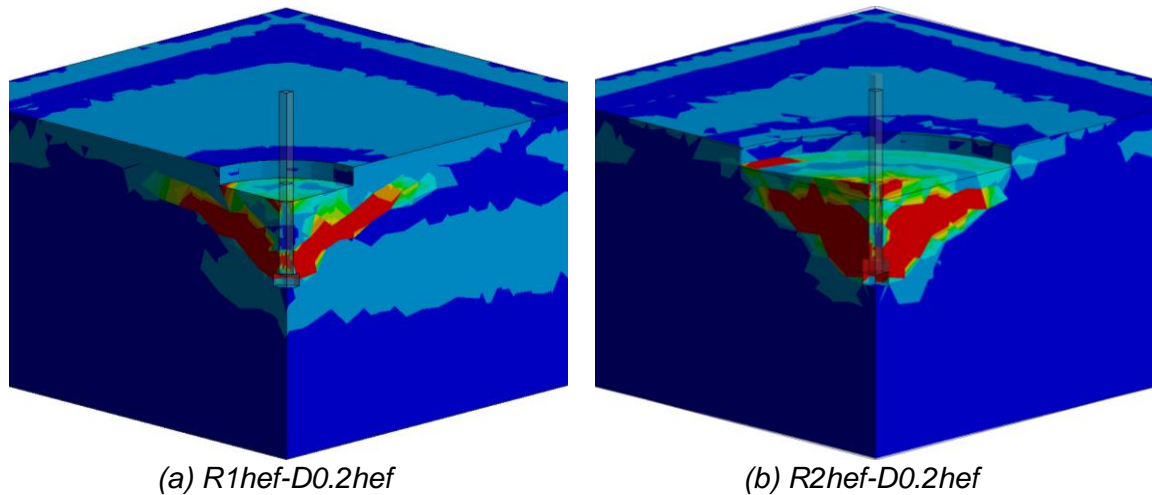


Figure 11 Crack profile at 0.8 times Peak load at 90 minutes

## CONCLUDING REMARK

Spalling affects the concrete cone breakout capacity of a fastener in two ways:

1. It reduces the embedment depth of the fastener, and
2. It increases the temperature ingress (deeper) into the concrete slab.

Both the effects mentioned above negatively affect the CC breakout capacity, but the adversity of these effects would depend on spalling depths and the area affected by spalling around the fastener. The paper presented the results of the first set of numerical investigations conducted to investigate the effect of spalling on the concrete cone breakout capacity of headed stud under standard fire. The headed stud investigated had an embedment depth of 50 mm. The investigated parameters included spalling depth and radius of the spalled area around the headed stud. A comparison of the predicted variation of CC breakout capacity with standard fire exposure duration for different spalling configurations and the current design guidelines (EN1992-4:2018 [1]) is shown in Figure 12.



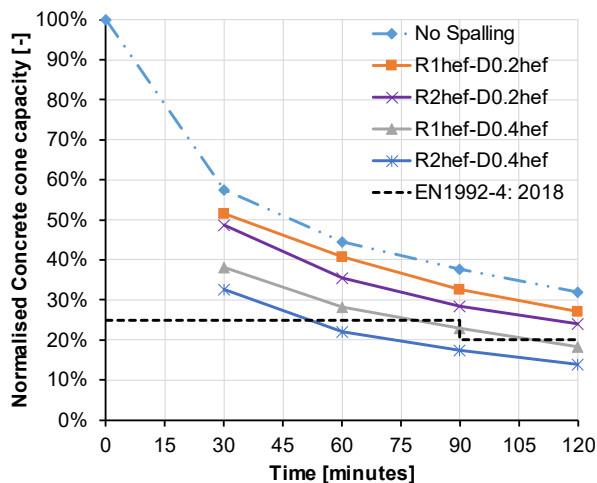


Figure 12 Comparison of predicted degradation of CC capacity under fire for different spalling configurations and EN1992-4

For the investigated embedment depth of 50 mm, it was found that for spalling depth up to 40% of the embedment depth the headed stud may still be able to satisfy the fire resistance requirement of 30 minutes for CC failure. This is because of the high safety margins in the current design guidelines for lower fire resistance durations. This also implies that it is possible to back calculate the spalling depth which may be allowed for different fire resistance durations requirements without the current design approach. But to generalise this approach further investigations are needed for different embedment depths.

## REFERENCES

1. EN1992-4:2018. Eurocode 2 - Design of concrete structures - Part 4: Design of fastenings for use in concrete. Brussels: European Committee for standardization; 2018.
2. Lakhani, H., and Hofmann, J., "Concrete cone failure of post installed fasteners during fire", Proceedings of 9th International Conference on Composite Construction in Steel and Concrete, Stromberg, Germany: 2021.
3. Kodur, V.K.R., and Dwaikat, M.B., "Effect of Fire Induced Spalling on the Response of Reinforced Concrete Beams", *International Journal of Concrete Structures and Materials*, **2**, 71–81, 2008. <https://doi.org/10.4334/IJCSM.2008.2.2.071>.
4. Lakhani, H., and Hofmann, J., "Effect of loss of concrete cover on the fire resistance of Reinforced Concrete (RC) beams: Numerical study using fiber beam-column element", Proceedings of the 6th International Workshop on Concrete Spalling due to Fire Exposure, Sheffield, UK: 2019.
5. Lakhani, H., and Hofmann, J., "Effect of spalling on predicted temperature gradients and flexural capacity: numerical model", *Journal of Structural Fire Engineering*, **11**, 151 – 65, 2020. <https://doi.org/10.1108/JSFE-01-2019-0010>.
6. Lakhani, H., Pham, D.T., Msaad, Y., Pimienta, P., and Jansson, R., "Effect of loss of concrete cover due to spalling on response of simply supported RC beam during fire", Proceedings of the fib Symposium 2020, 872-881, Online, Shanghai, China: 2020.
7. Ansys® 2021R2. Ansys® Academic Research Mechanical, Release 2021 R2. 2021.
8. Periškić, G., Entwicklung eines 3D thermo-hygro-mechanischen Modells für Beton unter Brandbeanspruchung und Anwendung auf Befestigungen unter Zuglasten, PhD Thesis, University of Stuttgart, 2009. [In German]
9. ISO 834-1:1999. Fire-resistance tests - Elements of building construction - Part 1: General requirements. International Organization for Standardization; 1999.



10. EN1991-1-2:2002. Eurocode 1: Actions on structures: Part 1.2 General actions: Actions on structures exposed to fire. Brussels: European Committee for standardization; 2002.
11. EN1992-1-2:2004. Eurocode 2: Design of concrete structures - Part 1-2: General rules - Structural fire design. Brussels: European Committee for standardization; 2004.
12. Lakhani, H., Kamath, P., Bhargava, P., Sharma, U.K., and Reddy, G.R., "Thermal analysis of reinforced concrete structural elements", *Journal of Structural Fire Engineering*, **4**, 227–244, 2013. <https://doi.org/10.1260/2040-2317.4.4.227>.
13. EN1993-1-2:2005. Eurocode 3: Design of steel structures - Part 1-2: General rules — Structural fire design. Brussels: European Committee for standardization; 2005.
14. Reick, M., Brandverhalten von Befestigungen mit großem Randabstand in Beton bei zentrischer Zugbeanspruchung, PhD Thesis, University of Stuttgart, 2001.
15. Ozbolt, J., Kozar, I., Eligehausen, R., and Periškić, G., "Transient thermal 3D FE analysis of headed stud anchors exposed to fire", Proceedings of European Congress on Computational Methods in Applied Sciences and Engineering ECCOMAS 2004, Jyväskylä: 2004.

# The influence of the physical and chemical properties of hardened cement paste on the fire-induced spalling of concrete

Jochen Reiners<sup>1\*</sup>, Christoph Müller<sup>1</sup>, Jochen Zehfuß<sup>2</sup>, Frank Dehn<sup>3</sup>

<sup>1</sup> VDZ Technology gGmbH, Düsseldorf, Germany

<sup>2</sup> Institut für Baustoffe, Massivbau und Brandschutz, TU Braunschweig, Germany

<sup>3</sup>Karlsruher Institut für Technologie (KIT)

Institut für Massivbau und Baustofftechnologie

Baustoffe und Betonbau, Germany

\*Corresponding author

(jochen.reiners@vdz-online.de,

Toulouser Allee 71, 40476 Düsseldorf)

## ABSTRACT

This paper summarises the results of a research project carried out at the VDZ in Düsseldorf. The experimental programme and first experiments were already presented at the "6<sup>th</sup> international workshop on concrete spalling due to fire exposure" in Sheffield [1]. The objective of the project was to examine the influence of the cement type as well as the physical and chemical properties of the hardened cement paste on the fire-induced explosive spalling of concrete. A particular focus was set on studying the way in which the concrete's moisture content contributes to the spalling phenomenon.

The findings obtained for the different concretes examined in the dedicated experimental programme were evaluated to better explain the mechanisms causing the fire-induced explosive spalling of concrete.

**KEYWORD:** Cement type, pore size distribution, moisture content

## TESTS PREVIOUSLY CARRIED OUT

In a research project carried out at the VDZ between 2015 and 2017 [2], modified "PTM tests" [3] had been used to examine the behaviour of concretes with different cement types during heating and the potential occurrence of explosive spalling.

In the tests, explosive spalling had occurred for

- high performance concretes containing silica fume  
as well as for

- concretes without silica fume with blast furnace cement (CEM III/A) and Portland fly ash cement (CEM II/B-V).

It had never occurred for

- concretes without silica fume with Portland cement (CEM I) or Portland limestone cement (CEM II/A-LL).

If explosive spalling had occurred, very small pore pressures (less than 0.1 MPa) had been measured. No correlation had been found between the measured pore pressures and the occurrence of explosive spalling. It had therefore been concluded that high pore pressures are not the primary factor causing the occurrence of explosive spalling of concrete. This confirms the conclusions of other authors (e.g. [4]).

## SCOPE OF THE PRESENT RESEARCH PROJECT

In [2], three hypotheses had been presented on the processes contributing to the explosive spalling observed in concretes containing silica fume as well as the concretes without silica fume with CEM III/A or CEM II/B-V cements. The hypotheses are summarised in Table 1.

Table 1 Overview of three hypotheses on the mechanisms behind the explosive spalling of concrete

Common characteristics of the concretes susceptible to spalling	Corresponding hypothesis
Compared to the concretes that did not spall, the concretes susceptible to spalling have a lower proportion of capillary pores and a higher proportion of gel pores.	<b>Hypothesis 1 („moisture weakening“):</b> Due to their pore size distribution, the concretes susceptible to spalling have a comparatively high moisture content at typical ambient relative humidities. A higher moisture content has a negative effect on the mechanical properties of concrete during heating. The associated lower resistance of the concrete to heat-induced impacts and external loads is responsible for or contributes to the occurrence of explosive spalling.
The hardened cement paste of the concretes susceptible to spalling contains a comparatively high ratio of CSH versus Ca(OH) <sub>2</sub> .	<b>Hypothesis 2 („dehydration-induced internal thermal stresses“):</b> In the temperature range, in which explosive spalling occurs (< 300 °C), the higher proportion of calcium silicate hydrates (CSH) in the hardened cement paste causes an increased dehydration of the heated paste. This in turn results in a more pronounced shrinkage of the paste. The internal stresses resulting from the restraint of the increased thermal strains are responsible for or contribute to the occurrence of explosive spalling.
In the concretes susceptible to spalling, the interfacial transition zone (ITZ) between aggregates and hardened cement paste is comparatively weakly defined	<b>Hypothesis 3 („incompatibility of thermal strains“):</b> In concretes with a weakly defined interfacial transition zone (ITZ), the incompatibility between the thermal strain of the expanding aggregates and the shrinking hardened cement paste creates significant tensile stresses in the paste of heated concrete. These tensile stresses are responsible for or contribute to the occurrence of explosive spalling.

In the present study, the three hypotheses were verified in a dedicated experimental programme. Moreover, in order to verify if the results of the PTM tests are transferable to specimens with larger dimensions, concrete slabs with a base area of 800 mm x 700 mm and a thickness of 240 mm were subjected to a standard fire according to ISO 834-1 [5] on an oil-fired furnace. Concretes with four different cement types were examined. An overview of all concrete compositions examined is given in [1].

## GENERAL CONSIDERATIONS

- The hydration rate and the strength development of pozzolanic binders (like fly ash and silica fume) and latent hydraulic binders (like blast furnace slag) is initially moderate while they show a continuous subsequent hardening over many months. To obtain a high degree of hydration and comparable test results, the concrete specimens used in the experimental study were stored for longer than twelve months under water or in a climate chamber a 20 °C/100 % relative humidity (RH). Only after this period, the specimens were positioned in air-conditioned rooms or desiccators with lower relative humidities. The moisture content was defined as a key parameter of the experimental study. It was

therefore varied in most tests carried out in order to examine its influence on the test results.

- It is known that a high heating rate is a parameter which has a decisive influence on the occurrence of concrete spalling. For this reason, in the present study, high heating rates (up to 10 K/min) and consequently high thermal gradients were deliberately chosen for some material tests in order to account for the resulting effects (e.g. on the thermal expansion and the evaporation of moisture from the specimens). Radial temperature differences across test specimens in these tests were therefore significantly greater than recommended by RILEM for testing the mechanical properties of concrete at high temperatures (e.g. [6]).

## VALIDATION OF THE RESULTS OF THE PTM TESTS THROUGH TESTS ON LARGER SLABS

According to Juknat et al. [7] and Klimek [8], the spalling behaviour observed when testing small-sized concrete specimens does not always correspond to the spalling characteristics of large concrete elements. It was therefore considered important to validate the observations from the PTM tests through tests on larger specimens. For this purpose, 14 concrete slabs with a base area of 800 mm x 700 mm and a thickness of 240 mm were produced. After a storage time of one year under water, the specimens were placed in a climate chamber at 20 °C/65 % RH. 18 months after production, the slabs were transported to the Institute of Building Materials, Concrete Construction and Fire Safety (iBMB) at the TU Braunschweig (Germany), where the specimens were subjected to an ISO 834-1 [5] fire on an oil-fired furnace in order to examine their susceptibility to explosive spalling.

The slabs were placed horizontally onto the furnace, which had an open base area of 1500 mm x 1000 mm. As two specimens were tested simultaneously, seven tests were carried out in total. An area of 700 mm x 700 mm of each concrete slab was exposed to the furnace chamber. For 10 out of the 14 slabs tested, the thermal expansion was restrained in one direction. To generate the restraint, U 240 steel channels on two opposite sides of each slab were pulled together with six galvanized steel threaded rods size M 30 equipped with bolts (Figure 1). Each bolt was tightened with a torque wrench to a torque of 200 Nm during installation and retightened again immediately before the start of the test.

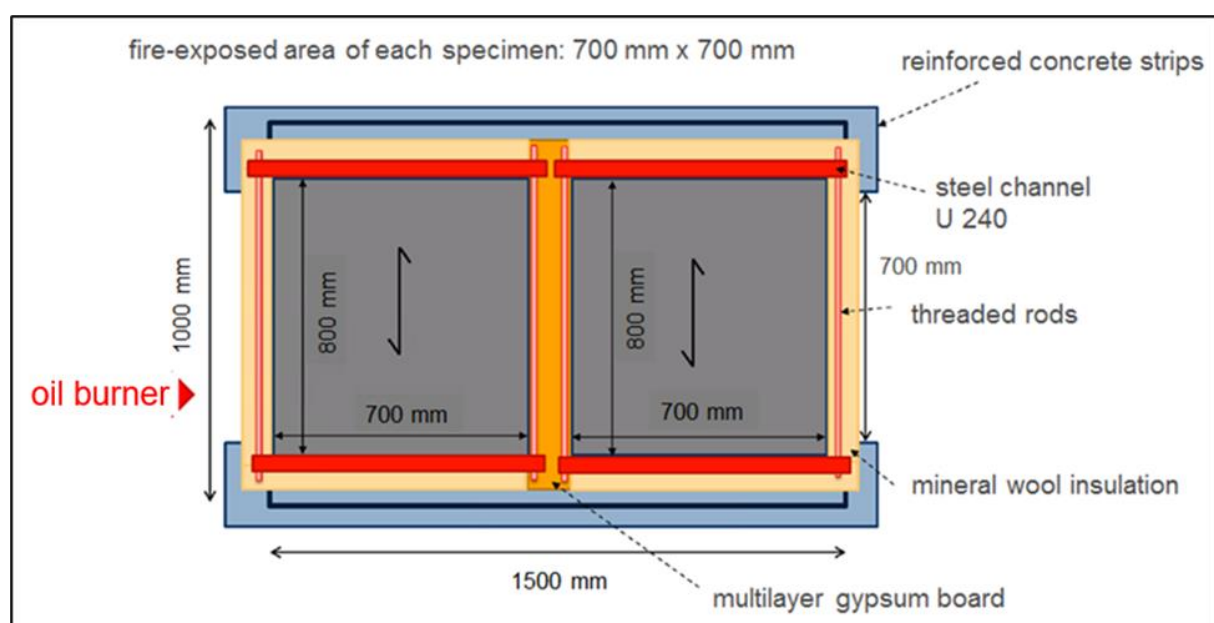


Figure 1: Test setup for the fire tests (illustration: J.Lyzwa, iBMB)

Table 2 shows the concrete compositions tested and the explosive spalling observed in the tests. Explosive spalling affecting the entire specimen surface occurred for the concretes in the shaded cells, while the concretes in the unshaded cells showed no or only minor, local spalling. If large-scale spalling was observed, it started 4 to 6 minutes after the beginning of heat exposure and came to an end within the first half hour of the test. As an example, Figure 2 shows the surfaces of concrete B13 and B15, both tested without lateral restraint.

*Table 2 Result of the spalling tests: shaded cells: large-scale spalling; not shaded: no spalling or locally confined spalling; the maximum spalling depth is indicated in brackets*

Reference concrete composition: cement content 350 kg/m <sup>3</sup> ; w/c=0.55; Rhine gravel/sand grading curve B16				
Cement type->	CEM I Portland cement 42.5 R	CEM II/A-LL Portland limestone cement 42.5 N	CEM II/B-V Portland fly ash cement 42.5 R	CEM III/A Blast furnace cement 42.5 N
Reference concrete composition	B1 46.4 MPa with lateral restraint <b>(1 mm)</b>			B4 42.4 MPa with lateral restraint <b>(32 mm)</b>
as reference, but w/c=0.50	B13 58.2 MPa with <b>(1 mm)</b> and without lateral restraint <b>(0 mm)</b>	B30 47.2 MPa with <b>(1 mm)</b> and without lateral restraint <b>(0 mm)</b>	B14 56.8 MPa with <b>(20 mm)</b> and without lateral restraint <b>(15 mm)</b>	B15 56.1 MPa with <b>(30 mm)</b> and without lateral restraint <b>(25 mm)</b>
as reference, but w/c=0.50; addition of PP fibres (2 kg/m <sup>3</sup> ); superplasticiser 0.22 % by weight of cement				B18 56.9 MPa with lateral restraint <b>(4 mm)</b>
450 kg/m <sup>3</sup> cement; 50 kg/m <sup>3</sup> silica fume;; 175 l/m <sup>3</sup> water; Rhine gravel/sand B16; superplasticiser 0.22 % by weight of cement	B23 94.7 MPa with lateral restraint <b>(35 mm)</b>		B25 96.8 MPa with lateral restraint <b>(65 mm)</b>	
450 kg/m <sup>3</sup> cement; 50 kg/m <sup>3</sup> silica fume; 175 l/m <sup>3</sup> water; Rhine gravel/sand B16; addition of PP fibres (2 kg/m <sup>3</sup> ); superplasticiser 0.30 % by weight of cement			B28 92.5 MPa with lateral restraint <b>(0 mm)</b>	

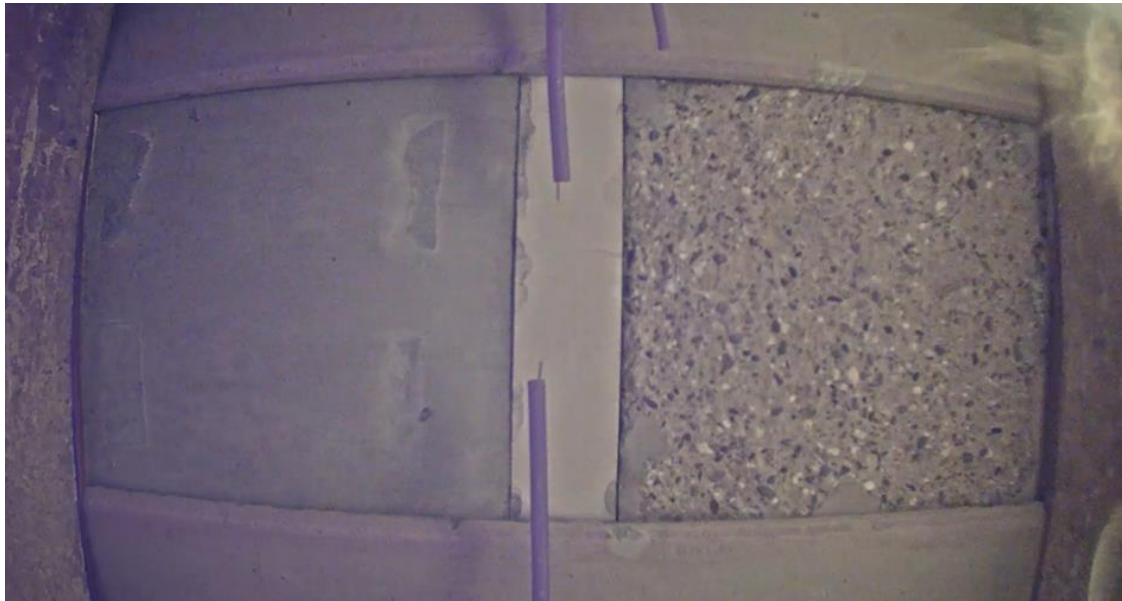


Figure 2: Concrete specimens B13 (CEM I;  $w/c=0.50$ ; left) and B15 (CEM III/A;  $w/c=0.50$ ; right), both tested without lateral restraint, at the end of the fire test

The tests results coincide very well with the findings from the PTM tests:

- Large scale spalling was observed for concretes with CEM III/A and CEM II/B-V without silica fume as well as for concretes containing silica fume.
- For concretes with CEM I and CEM II/A-LL without the addition of silica fume, no or only locally confined spalling was observed.

The addition of PP fibres reliably prevented notable explosive spalling.

#### **VERIFICATION OF HYPOTHESIS 1 (“MOISTURE WEAKENING”)**

The following experiments were carried out to verify hypothesis 1:

- determination of desorption isotherms of concretes in the experimental programme in order to confirm that the concretes with a higher volume of gel pores and a lower capillary pore volume have higher equilibrium moisture contents across the range of typical ambient relative humidities
- comparison of the compressive and flexural strength of specimens with different moisture contents to verify the assumption that a higher moisture content of concrete results in a greater strength loss.

Sorption isotherms were determined according to the desiccator method described in ISO 12571 [9] by placing test specimens in desiccators in which defined relative humidities had been established. When the mass of the specimens had become constant, the absolute moisture content (in % by mass) corresponding to each of the chosen target relative humidities was determined by oven-drying at 105 °C. In the present study, desorption isotherms were determined, i.e. initially water-saturated specimens were stored at various target relative humidities lower than 100 %.

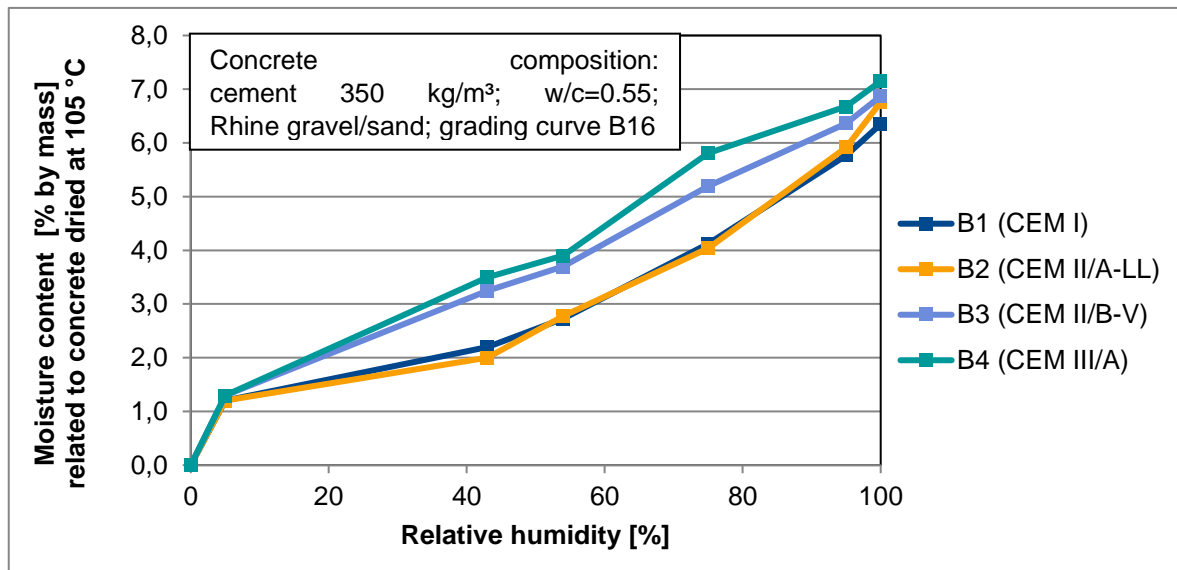


Figure 3: Desorption isotherms of concretes B1 to B4 (cement 350 kg/m<sup>3</sup>; w/c=0.55)

Exemplarily, in Figure 3 the desorption isotherms of concretes B1 to B4 are compared. The concrete with blast furnace cement (B4) and the concrete with Portland fly ash cement (B3) (i.e. those concretes that were found to be susceptible to spalling [2]) show significantly higher equilibrium moisture contents than the concretes with Portland cement (B1) and Portland limestone cement (B2), i.e. those concretes that did not exhibit any spalling [2]. The assumption expressed in hypothesis 1 that due to their pore size distribution the concretes susceptible to spalling have a comparatively high equilibrium moisture content at typical ambient relative humidities (e.g. in the range between approximately 30 % to 70 % in indoor living and working areas) is therefore supported. Apart from the concrete's sorption isotherm, the moisture content of a concrete specimen at the time of a fire tests is influenced by the rate by which a water-saturated specimen dries after it has been exposed to a dryer climate. In the present study, concretes with silica fume or with blast furnace cement or Portland fly ash cement dried slower (i.e. they lost less moisture over time) than the concretes which were demonstrated to be not susceptible to spalling.

The first assumption expressed in hypothesis 1 is therefore supported. Consequently, even though the storage conditions were identical for all specimens tested in the large-scale fire tests described above, the concretes susceptible to spalling had a comparatively high moisture content at the time of the test.

In order to examine the influence of the moisture content on the strength of heated concrete, the compressive and flexural strength of prismatic specimens 160 mm x 40 mm x 40 mm with three different degrees of water saturation (mass equilibrium at 95 % RH, 75 % RH and 54 % RH) were tested. The specimens' "nominal size" (40 mm according to [10]) was hence smaller than three and a half times the maximum aggregate size (3.5 x 16 mm = 56 mm). This represented a deviation from the corresponding requirement in EN 12390-1 [10]. In order to be able to obtain a uniform moisture distribution in the specimens within the duration of the research project, it was however not feasible to choose specimens with a larger cross section. In spite of the small specimen size, the reproducibility of the test results was found to be adequate when several specimens of the same composition were tested.



The tests were carried out with

- unsealed specimens, heated “fast” (approximately 7 K/min) to maximum temperatures of 150 °C and 300 °C, tested after cooldown.
- sealed specimens, heated slowly (approximately 0.5 K/min) to maximum temperatures of 150 °C and 190 °C, tested at elevated temperatures (“hot state”). The sealing method is described in [1].

In all tests, the relative loss of the compressive strength due to heating was in the order of magnitude described in the literature. For specimens heated to 150 °C, the loss of strength was more pronounced than for specimens heated to 300 °C. This confirms the “strength dip” which is often described in this temperature range (e.g. [11]).

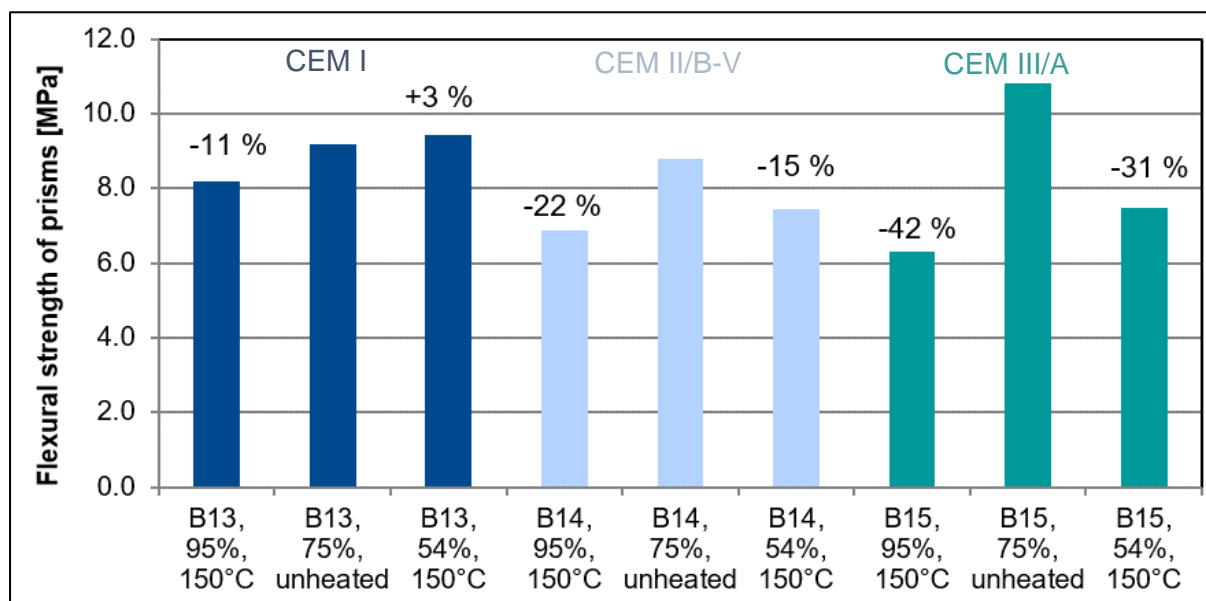


Figure 4 Residual flexural strength of prismatic specimens with different degrees of saturation (concrete composition: 350 kg/m<sup>3</sup> cement; w/c=0.50; Rhine gravel/sand B16), heated to a maximum temperature of 150 °C. The percentages above the bars indicate the strength loss or gain relative to the strength of the unheated specimens.

The loss of flexural strength in tests with maximum temperatures of 150 °C or 190 °C, for both

- unsealed specimens heated with a "high" heating rate and tested after cooldown (example: Figure 4) and
- sealed specimens heated slowly and tested in the hot state,

reached an order of magnitude of up to 50 % (or in a few cases even greater) relative to the strength at ambient temperatures. This order of magnitude substantially exceeds the range of test results for the reduction of tensile strength at these temperatures in the literature which were determined with unsealed specimens heated more slowly (e.g. [12]). This suggests that the large reduction of the flexural strength is attributable to the chosen test conditions.

Under both test conditions

- unsealed, high heating rate
- sealed, low heating rate,

water which would have escaped from slowly heated, unsealed specimens was still present inside the specimens at the time when the maximum temperature was reached.

At the same time, the temperature-induced strength loss of

- slowly heated, sealed specimens tested after cooldown  
and of

- pre-dried (105 °C) specimens which were sealed, slowly heated and tested in a hot state was found to be considerably less distinct.

Together with the additional observation that for maximum heating temperatures of 150 °C or 190 °C, a higher degree of saturation resulted in a higher strength loss, this clearly confirms the significant impact of the concrete's moisture content on the reduction of the flexural strength at these temperatures.

For concretes which had an increased susceptibility to spalling in the PTM tests and the large-scale tests carried out, a greater relative loss of flexural strength was observed.

In summary, the tests carried out support hypothesis 1:

Under the chosen test conditions, a higher moisture content has a negative effect on the mechanical properties of concrete. The tests showed that the moisture particularly affects the concrete's tensile strength in the temperature range between 150 °C and 190 °C. This corresponds to the range of temperatures at the spalling plane when spalling occurred in the PTM tests and the large-scale fire tests carried out.

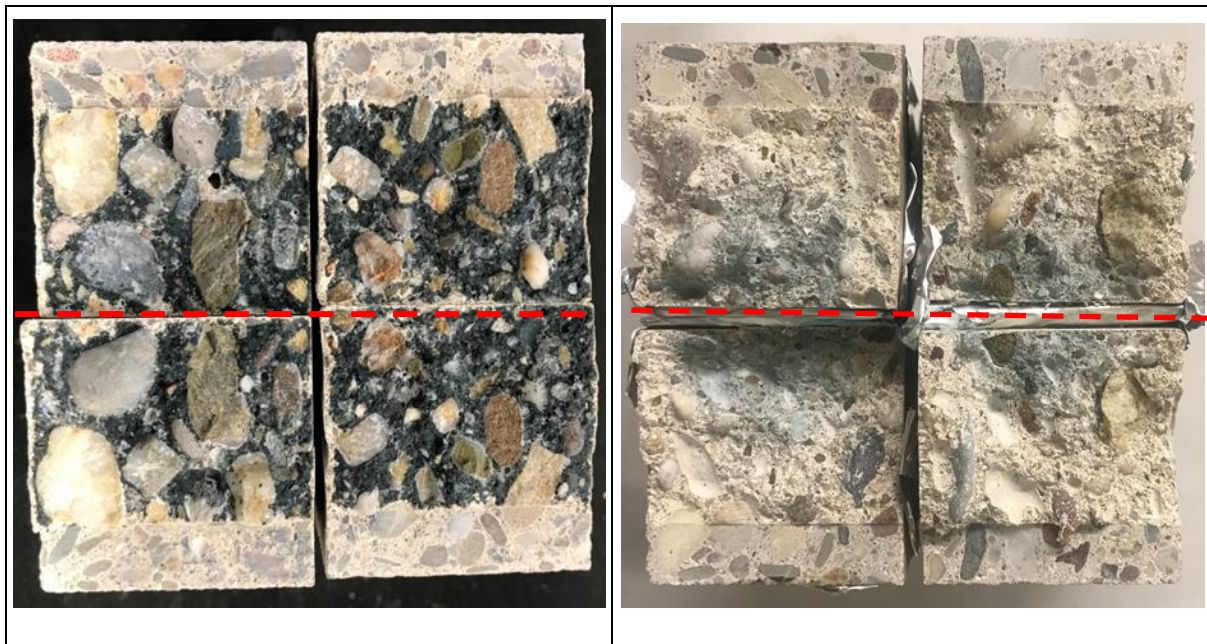


Figure 5 B4 (CEM III/A;  $w/c=0.55$ ): fracture surfaces of notched prismatic concrete specimens after test: unheated (left) and heated to 190 °C (right); dashed line = mirror axis

A visual observation of specimens' fracture surfaces after the flexural strength tests showed that concretes with a weakly defined ITZ, which tend to have transgranular fracture surfaces when unheated (i.e. the fracture mainly runs through the aggregates), showed predominantly intergranular fracture surfaces after heating (i.e. the fracture proceeded predominantly along the interfaces between aggregates and hardened cement paste). An example is displayed in Figure 5. This observation shows that under the chosen test conditions the paste-aggregate bond was weakened and supports hypothesis 3 (see below). For concretes with a pronounced ITZ (concretes with CEM I and CEM II/A-LL cements), the fracture surfaces were predominantly intergranular in the unheated state as well as after heating.

## VERIFICATION OF HYPOTHESIS 2 ("DEHYDRATION-INDUCED INTERNAL THERMAL STRESSES")

Hypothesis 2 was verified by measuring the thermal strain of tubular concrete specimen. The tubular form was selected because due to the relatively small wall thickness of only 14 mm, a uniform moisture distribution could be reached in a practicable time. At the same time, relevant compressive loads could be applied in the specimens' longitudinal direction without a premature buckling failure (which would have had to be expected for thin solid specimens).

The tubular specimens were stored for one year in a climate chamber at 20 °C/100 % RH and then in three different relative humidities (95 % RH, 75 % RH or 54 % RH) until mass equilibrium had been reached. The specimens were placed in a tube furnace (Figure 6) which was heated to temperatures of up to 500 °C. The objective of the tests was to verify if the thermal strain of concrete containing silica fume, blast furnace slag or fly ash differs from the thermal strain of concrete without these additions/main constituents.

Test were carried out with and without a compressive axial load. The furnace was heated with a heating rate of 10 K/min. The temperatures and the thermal strain during the tests were measured over a 50 mm high section at mid-height of the tubular specimens (Figure 7).

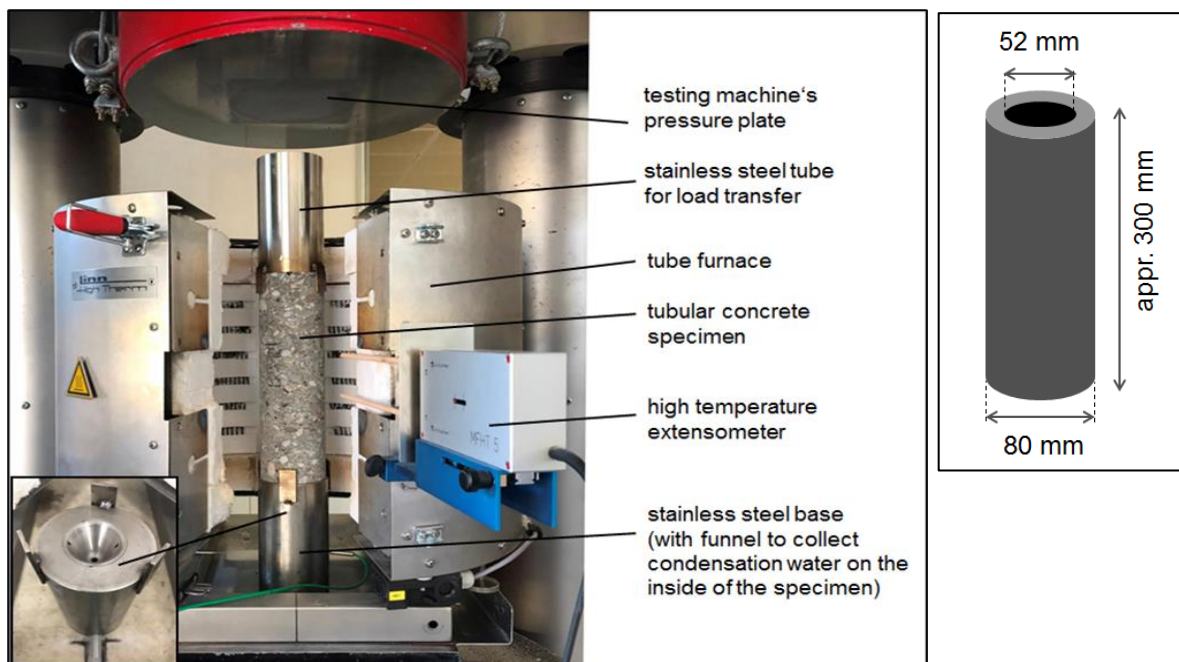


Figure 6 Setup to measure the thermal expansion of tubular concrete specimens

In tests with unloaded and loaded tubular concrete specimens, no marked influence of the ratio of the hydration products calcium silicate hydrates (CSH) and calcium hydroxide  $\text{Ca}(\text{OH})_2$  in the hardened cement paste on the concrete's thermal strain could be identified in the spalling temperature range and above (up to 450 °C). Hypothesis 2 was therefore not supported by the test results.

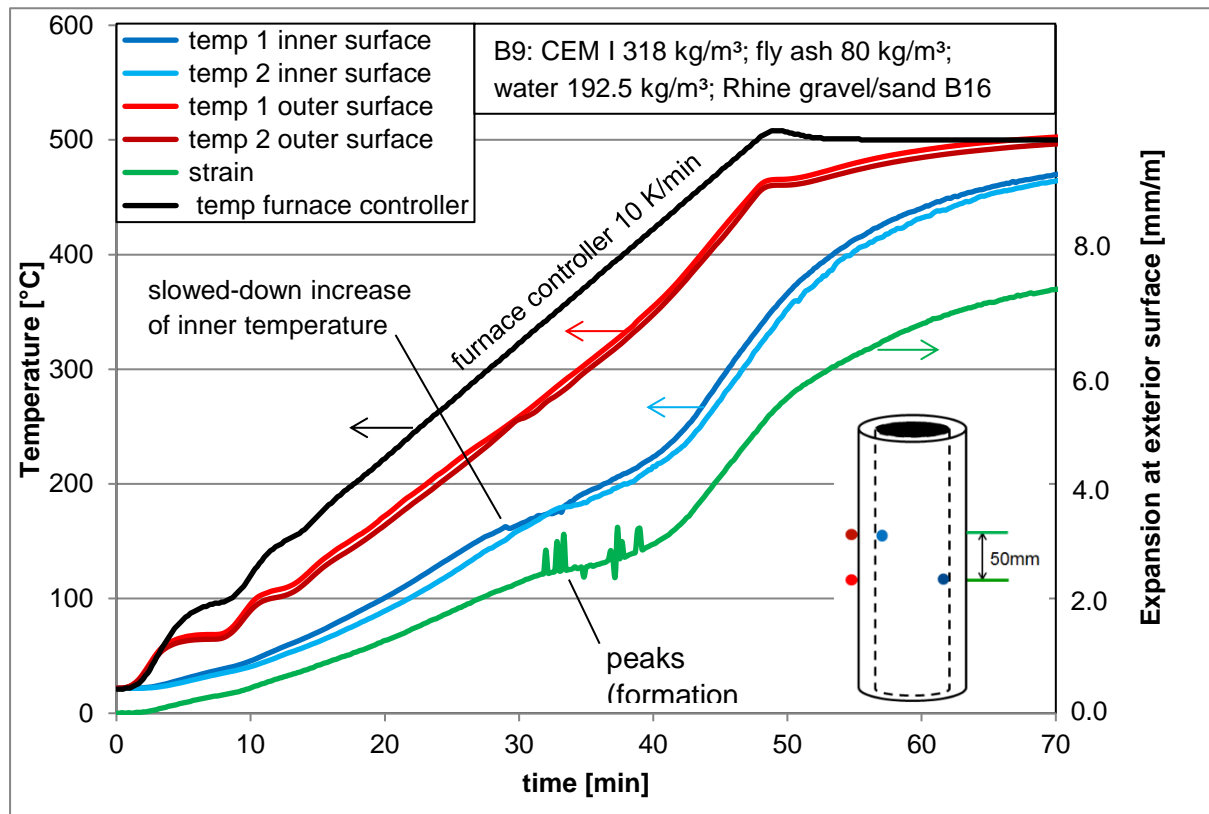


Figure 7 Example of temperature and strain development, concrete B9 (unloaded)

Figure 7 shows the development of the temperatures and the expansion in a typical unloaded test. The following observations can be made:

- From an inner temperature of around 150 °C to 160 °C, a delay in the increase of the inner temperature can be observed. This delay has previously been described by other authors (e.g. [13]) and is attributed to the energy required for the vaporisation of water. According to the saturation vapour pressure curve for water, a temperature of 150 °C to 160 °C indicates that the water vaporises under a pressure of 0.4 MPa – 0.5 MPa above atmospheric pressure.
- The expansion at the exterior surface correlates more closely with the interior temperature than with the exterior temperature, which indicates that the expansion at the outer surface "waits" for the temperature rise of the inner surface. As a consequence, compressive stresses will develop at the heated surface, where the temperature continues to rise without slowdown.
- Also from an interior temperature of about 150 °C, peaks are visible in the strain curve. Apparently microcracks which allow an intermittent escape of water vapour are formed in the outer/heated surface. The microcracks close again when the water vapour has locally left the specimen. The observation of such microcracks was more frequent for specimens with a higher degree of saturation.

In summary, it can be concluded that the composition of hardened cement paste does have a marked impact on the stress distribution in a heated concrete element. However, contrary to the assumption expressed in hypothesis 2, the influence does not stem from the ratio between calcium silicate hydrates and calcium hydroxide but rather from the pore size distribution: As described above, concretes with blast furnace cement, Portland fly ash cement or the addition of silica fume tend to have comparatively high (equilibrium) moisture contents. Since energy is consumed for the vaporisation of water, a high moisture content causes pronounced thermal



gradients in a heated concrete element, particularly for high heating rates. These thermal gradients entail

- internal stresses between layers at different distances from the heated surface and
- compressive stresses at the heated surface.

Moreover, for concretes with a higher moisture content, the formation of microcracks perpendicular to the heated surface (Figure 7) was observed more frequently. While pore pressure was relieved through these microcracks, presumably at the same time the concrete was weakened and its tensile strength reduced.

### VERIFICATION OF HYPOTHESIS 3 (“INCOMPATIBILITY OF THERMAL STRAINS”)

To verify hypothesis 3, cubes with a side length of 100 mm were produced from selected concretes and stored for one year in a climate chamber at 20 °C/100 % RH. From the cubes, prismatic slices with an area of 60 mm x 40 mm and a thickness of 10 mm were cut with a diamond saw (Figure 8). The slices were stored at 20 °C in three different relative humidities (95 % RH, 75 % RH or 54 % RH) until mass equilibrium had been reached.

The concrete slices were heated to a maximum temperature of 300 °C in an electric circulating air oven with the maximum heating rate permitted by the oven (approximately 7 K/min). After the oven had reached 300 °C, the temperature was held constant for 20 minutes to establish a uniform temperature distribution throughout the specimens. The oven was then switched off and the concrete specimens were allowed to cool down to ambient temperature inside the closed oven. Subsequently, the slices were impregnated under vacuum with a casting resin which fluoresces under UV light and then polished to a layer thickness of 30 µm. The thin sections were inspected under a reflected light microscope (Zeiss Axioplan) to examine the crack pattern in the hardened cement paste.

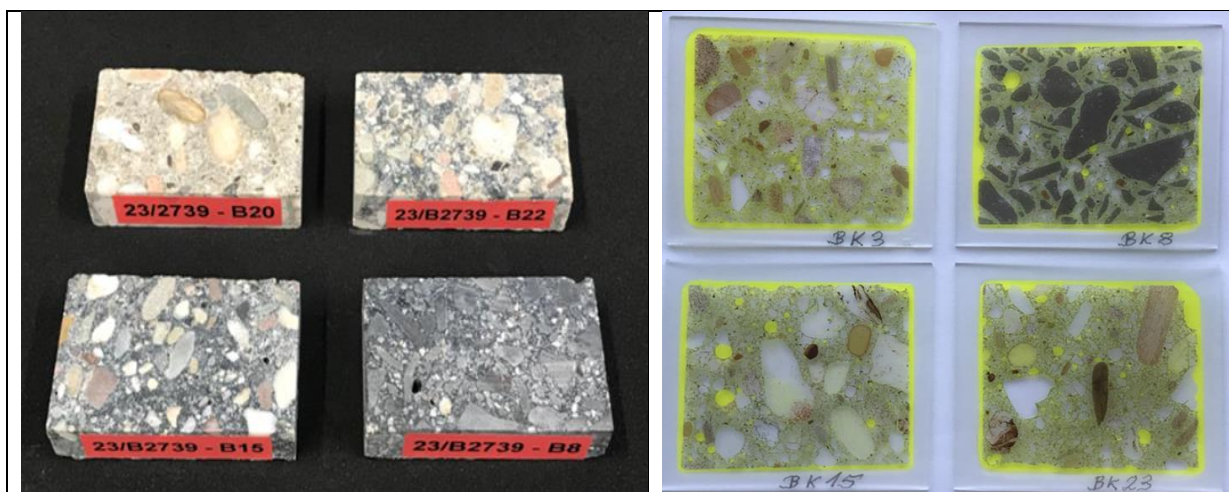


Figure 8 Concrete slices (left) and thin polished sections (right)

Concretes with CEM I and CEM II/A-LL cements which have a pronounced interfacial transition zone (ITZ) between the aggregates and the hardened cement paste showed no or very few microcracks when they were rapidly heated to temperatures of 300 °C (example: Figure 9, left). In contrast, concretes with a weakly defined ITZ, namely

- high performance concretes with the addition of silica fume
- concretes without silica fume with CEM II/B-V or CEM III/A cements

showed a distinct formation of microcracks in the paste (example: Figure 9, right). A close relation therefore exists between the formation of microcracks and the susceptibility of the

concretes to explosive spalling observed in the PTM tests or the large-scale fire tests carried out. These findings support hypothesis 3.

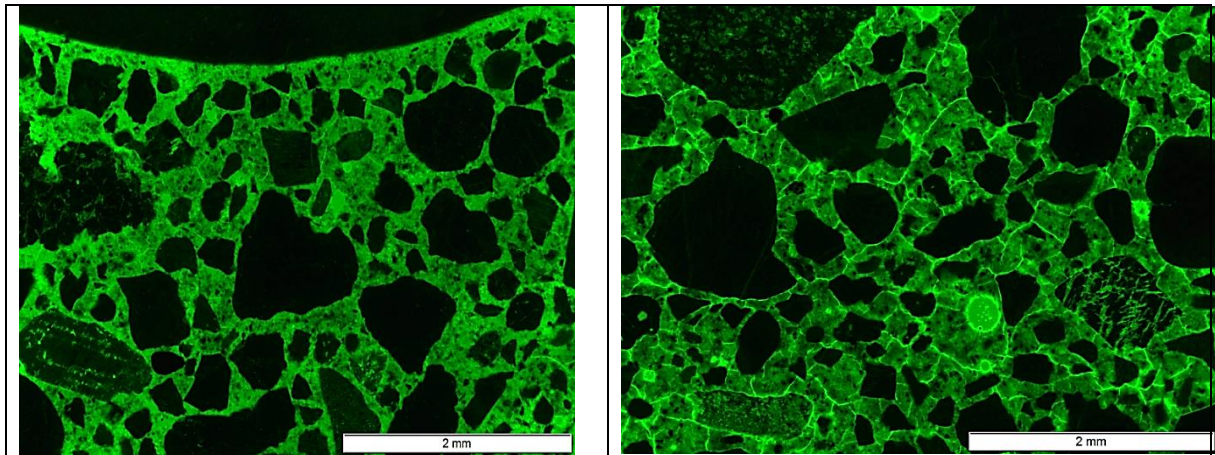


Figure 9 Reflected-light microscopy of thin polished sections (degree of saturation 95 %). Left: concrete B1 (CEM I;  $w/c=0.55$ ), right: concrete B4 (CEM III/A;  $w/c=0.55$ ),

When concrete specimens of the same composition were compared, a correlation between the degree of saturation and the quantity of microcracks could be observed. This suggests that in the case of weakly defined ITZs, „trapped“ water vapour creates additional stresses at the contact zones between the aggregates and the hardened cement paste. In the concretes with well-defined ITZs, even for high degrees of saturation, no or very few microcracks were observed.

## SUMMARY

Table 2 shows the evaluation of the three hypotheses.

A close link can be established between hypothesis 1 and hypothesis 3: apart from the incompatibility between the thermal strain of the aggregates and the hardened cement paste, trapped moisture vapour which cannot escape freely from the heated specimens creates stresses in the contact zones between aggregates and paste. This is an explanation for the influence of the moisture content on the reduction of flexural strength at high temperatures (as observed in the experimental programme for hypothesis 1).

In summary, the results of the experimental programme show that explosive spalling may be caused by the following processes in heated concrete:

- In concretes with a comparatively high moisture content and a low permeability, a zone with a high degree of water saturation (“moisture clog”) forms.
- The slowed-down temperature increase in the water-saturated zone (“temperature plateau”) due to the energy required for the vaporisation of water results in pronounced thermal gradients perpendicular to the heated surface.
- The thermal gradients result in inner stresses as well as in compressive stresses in the near-surface concrete layer.
- A fracture plane forms parallel to the heated surface due to the inner stresses and the incompatibility between the thermal strain of the expanding aggregates and the shrinking hardened cement paste.
- The detached near-surface concrete, which is under compression, buckles outward.

Moisture in concrete

- on the one hand enhances the temperature gradients in heated concrete elements and
- on the other hand contributes to local stresses at the contact zones between aggregates and the hardened cement paste and hence to the formation of a fracture plane.

Table 2 Evaluation of the three hypotheses

Hypothesis	Evaluation of the results of the experimental programme
<p><b>Hypothesis 1 („moisture weakening“):</b></p> <p>Due to their pore size distribution, the concretes susceptible to spalling have a comparatively high moisture content at typical ambient relative humidities.</p> <p>A higher moisture content has a negative effect on the mechanical properties of concrete during heating.</p> <p>The associated lower resistance of the concrete to heat-induced impacts and external loads is responsible for or contributes to the occurrence of explosive spalling.</p>	<p>By determining desorption isotherms, it was demonstrated that the concretes susceptible to spalling have comparatively high equilibrium moisture contents at typical ambient relative humidities. As the drying rate was also found to be lower for these concretes, the specimens had a higher moisture content at the time when the fire tests were carried out.</p> <p>Under the chosen test conditions, by which the escape of moisture from the specimens during heating was impeded, a higher loss of flexural strength was observed than described in literature for the corresponding temperature range. Furthermore, a correlation between a higher moisture content of the tested specimens and a higher loss of flexural strength in the spalling temperature range was observed.</p> <p><b>Hypothesis 1 is therefore supported by the results of the tests carried out in this study.</b></p> <p>The visual observation of the fracture surfaces showed that the influence of moisture on the flexural strength particularly comes into effect at the interfaces between aggregates and hardened cement paste (-&gt; link to hypothesis 3)</p>
<p><b>Hypothesis 2 („dehydration-induced internal thermal stresses“):</b></p> <p>In the temperature range, in which explosive spalling occurs (&lt; 300 °C), the higher proportion of calcium silicate hydrates (CSH) in the hardened cement paste causes an increased dehydration of the heated paste. This in turn results in a more pronounced shrinkage of the paste. The internal stresses resulting from the restraint of the increased thermal strains are responsible for or contribute to the occurrence of explosive spalling.</p>	<p>In the tests carried out in this study, the chemical composition of the hardened cement paste was not found to have a systematic influence on the thermal strain of loaded or unloaded concrete specimens.</p> <p><b>Hypothesis 2 is therefore not supported by the experimental study.</b></p> <p>Observations made in the experiments carried out to verify hypothesis 2 were:</p> <ul style="list-style-type: none"> <li>- Since energy was consumed for the evaporation of water, the moisture present in the concrete pores caused an increase of the thermal gradients in a heated concrete specimen. As a consequence, the inner stresses and the compressive stresses in the near-surface zone must also have increased.</li> <li>- Microcracks perpendicular to the heated surface allowed the relief of pore pressures in the hardened cement paste.</li> </ul>



<p><b>Hypothesis 3 („incompatibility of thermal strains“):</b></p> <p>In concretes with a weakly defined interfacial transition zone (ITZ), the incompatibility between the thermal strain of the expanding aggregates and the shrinking hardened cement paste creates significant tensile stresses in the paste of heated concrete. These tensile stresses are responsible for or contribute to the occurrence of explosive spalling.</p>	<p>When concretes with a weakly defined interfacial transition zone were heated, the formation of a high quantity of microcracks in the hardened cement paste was noticed. Moreover, specimens with a higher degree of saturation showed a denser crack pattern. For concretes with a pronounced ITZ, the heated specimens remained largely free of microcracks.</p> <p>For the concretes with a weakly defined interfacial transition zone, the bond between the hardened cement paste and the aggregates was impaired under the influence of heat. A transition from</p> <ul style="list-style-type: none"> <li>- a predominantly transgranular failure type at ambient temperatures</li> <li>to</li> <li>- a predominantly intergranular failure type after the exposure to high temperatures</li> </ul> <p>could be observed.</p> <p><b>Hypothesis 3 is therefore supported by the results of the tests carried out in this study.</b></p>
--	--

## REFERENCES

1. Reiners, J.; Müller, C. – Influence of the chemical and physical properties of hardened cement paste on the fire-induced spalling of concrete Proceedings of the 6th International Workshop on Concrete Spalling due to Fire Exposure, Sheffield, United Kingdom, 19–20 September 2019
2. Reiners, J.; Müller, C. – Influence of the chemical and physical properties of hardened cement paste on the fire-induced spalling of concrete Proceedings of the 5th International Workshop on Concrete Spalling due to Fire Exposure, Borås, Sweden, 12–13 October 2017
3. Kalifa, P. et al. – Spalling and pore pressure in HPC at high temperatures. Cement and Concrete Research 2000, 30, pp 1915-1927
4. Bažant, Z.P. – Analysis of Pore Pressure, Thermal Stress and Fracture in Rapidly Heated Concrete, International Workshop on Fire Performance of High-Strength Concrete, NIST, Gaithersburg, MD, February 13-14, 1997
5. ISO 834-1:1999-09 - Fire-resistance tests - Elements of building construction, Part 1: General requirements
6. RILEM, Ed. RILEM TC 129-MHT – Test methods for mechanical properties of concrete at high temperatures: Recommendations Part 6 - Thermal strains. Materials and Structures. 1997, 30(196), pp 17-21
7. Juknat, M.; Dehn, F. – Brand- und Abplatzverhalten von Tunnelbetonen: Einfluss der Probekörperabmessungen und einer äußeren mechanischen Beanspruchung. Beton- und Stahlbetonbau 2018, 113(3), pp 184-193
8. Klimek, A.; Hothan, S.; Rogge, A. – Investigation of Size Effects in Concrete Spalling. Proceedings of the 6th International Workshop on Concrete Spalling due to Fire Exposure, Sheffield, United Kingdom, 19–20 September 2019
9. ISO 12571:2013 - Hygrothermal performance of building materials and products - Determination of hygroscopic sorption properties
10. EN 12390-1:2021 - Testing hardened concrete – Part 1: Shape, dimensions and other requirements for specimens and moulds
11. Phan, L.T.; Carino, N.J. Mechanical Properties of High-Strength Concrete at Elevated Temperatures. NIST Interagency/Internal Report (NISTIR), National Institute of Standards and Technology, Gaithersburg, MD 2001

12. Behnood, A.; Ghandehari, M. – Comparison of compressive and splitting tensile strength of high-strength concrete with and without polypropylene fibers heated to high temperatures. *Fire Safety Journal*. 2009, 44(8), pp 1015-1022
13. Klingsch, E.W. – Explosive spalling of concrete in fire. Zürich, ETH, 2014

# An Experimental Study into the Behaviour of Self-Prestressing, Self-Compacting Concrete at Elevated Temperatures

Hussein Mohammed<sup>1\*</sup>, Fariza Sultangaliyeva<sup>2</sup>, Mateusz Wyrzykowski<sup>3</sup>, Giovanni Pietro Terrasi<sup>3</sup>, Luke Bisby<sup>1</sup>

<sup>1</sup>School of Engineering, The University of Edinburgh, UK

<sup>2</sup>Université de Pau et des Pays de l'Adour, E2S UPPA, SIAME, Anglet, France.

<sup>3</sup>Empa, Swiss Federal Laboratories for Materials Science and Technology, Switzerland.

\* Corresponding author (Hussein.Mohammed@ed.ac.uk)

## ABSTRACT

A novel concrete mix has been developed at Empa that can achieve high levels of self-prestressing through controlled chemical expansion of the concrete (while hardening) with embedded high modulus carbon fibre reinforced polymer bars. This controlled expansion has been shown to not adversely affect the mechanical properties and durability of the mix at ambient temperature. Until now, the behaviour of self-prestressed concrete elements at elevated temperatures has not been extensively studied. These novel structural elements consist of high performance self-compacting concrete with a compressive strength of more than 50 MPa; scoping experiments have shown that it is susceptible to heat induced explosive spalling when subjected to steep thermal gradients. To investigate this behaviour, three self-prestressed, self-compacting concrete (SPSCC) samples were prepared and cast into moulds with dimensions 500 mm × 200 mm × 45 mm; and one 600 mm × 200 mm × 45mm. Each sample (or plank) was reinforced with two ultra-high-modulus (UHM) carbon fibre reinforced polymer (CFRP) tendons ( $E_{11} = 502$  GPa). Five high-strength self-compacting concrete (HSSCC) samples (600 mm × 200 mm × 45 mm) were also cast and mechanically prestressed. A further three non-prestressed HSSCC samples were also cast. The samples were subjected to severe heating on one surface at an age of more than three months. Thermal exposure was accomplished using a mobile gas-fired radiant panel array (RPA) at the University of Edinburgh. The effects of the type of concrete mix and the method of prestressing (i.e., mechanical versus self-prestressing) on the samples' behaviour under exposure to one-sided heating was studied. This paper also investigates the effects of mechanical prestressing (i.e., pre-compressive concrete stress), the effects of super absorbent polymers (SAP) within the concrete mix, and the samples' moisture content on the heat-induced spalling behaviour of the planks.

**KEYWORD:** Spalling, Pre-stressing, CFRP, simulated ISO 834, Moisture Content, Self-compacting Concrete

## INTRODUCTION

Prestressing of concrete (particularly with CFRP) enables a reduction in the amount of dead load in concrete structures, and reduces their carbon footprints by utilising sections of the concrete that would otherwise be disregarded (i.e., concrete in the tensile zones) [1].

Prestressing is typically accomplished by pre- or post-tensioning tendon(s) cast within the concrete and/or by anchoring the tendons at the extremities of the prestressed elements. A novel, expanding, self-compacting concrete (SPSCC) mix has recently been developed by researchers at Empa that can deliver comparable prestress levels through the controlled expansion of the concrete (with embedded UHM CFRP tendons) after casting [2], [3]. This method of prestressing (sometimes referred to as chemical prestressing) allows simplification of prestressing work and reduces health and safety risks associated with normal tendon tensioning procedures (i.e., failure of prestressing tendons or anchorages during tensioning). Comparatively little research has been carried out to date using SPSCC. The developers of the mix have performed experiments to determine the mechanical properties of the mix at ambient temperature [2], [3]. Their work shows that the mix can provide chemical prestressing whilst remaining stable in the longer term. However, no research has yet been presented regarding the behaviour of this mix at elevated temperatures or in fire. This paper presents studies on the behaviour of SPSCC planks (prestressed with UHM CFRP) when subjected to steep thermal gradients similar to those that would be expected when subjected to an ISO 834 standard fire exposure. The behaviour of SPSCC samples is compared to that of mechanically prestressed HSSCC samples subjected to similar thermal loading.

## METHODOLOGY

### Concrete mixes, sample production, and curing

Using the mix proportions reported in [3], three SPSCC planks (A,B,C) were produced (500 mm × 200 mm × 45 mm) in June 2015. A single sample (D) of dimensions (600 mm × 200 mm × 45 mm) was also produced using the mix proportions provided in Table 1 (in November 2021). A further set of 8 samples of HSSCC (A-H), with dimensions 600 mm × 200 mm × 45 mm, was also cast in 2021. Five of the HSSCC samples were mechanically prestressed using 5.4 mm diameter, sand coated UHM CFRP prestressing wires ( $E_{11}=502$  GPa). The thickness of the samples was chosen based on the reported applications of CFRP prestressed concrete elements in the construction industry, where the concrete cover could be reduced by using corrosion-free CFRP tendons [4].

Table 1 Mix composition of concrete

Composition	SPSCC (Samples A, B, C) (kg/m <sup>3</sup> ) (2015)	SPSCC (Sample D) (kg/m <sup>3</sup> ) (2021)	HSSCC (A-H) (kg/m <sup>3</sup> ) (2021)
Cement CEM I 52.5R	520	491	443
Aggregates (0-8 mm)	1462	1486	1594
Silica fume	-	-	20
Limestone powder	26	24.6	-
Shrinkage reducing agent	15.7	14.9	-
Superplasticiser	2%	1.3%	0.79 %
Water	220	223	204
Super Absorbent Polymer (SAP)	1.85	2.70	-
Calcium-sulfoaluminate cement or CSA cement	83	78.6	-
Fly Ash	-	-	120
Spread (mm); BS EN 206 [5]	550	745	520

The details of the UHM CFRP tendons are reported in [6]. The levels of prestress in the samples at the time of testing are given in Table 2. A thermocouple (TC) tree was installed during casting of the HSSCC samples and SPSCC D to record in-depth temperatures during the heating tests using a radiant panel array (RPA) [7], [8]. Figures 1 and 2 show the cross section of the samples (with TC tree) and the locations of the CFRP tendons, as well as the front view of the samples with the heat-exposed area for all the samples except SPSCC samples A, B, and C; the heat exposed area for SPSCC (A-C) was 400 mm by 200 mm.

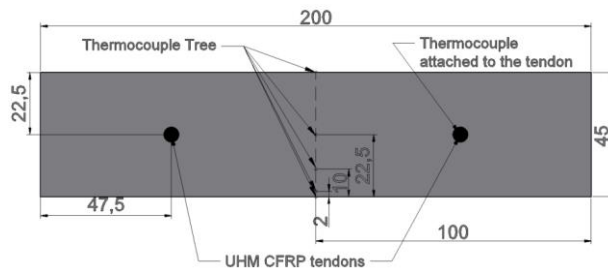


Figure 1 cross section of the concrete planks

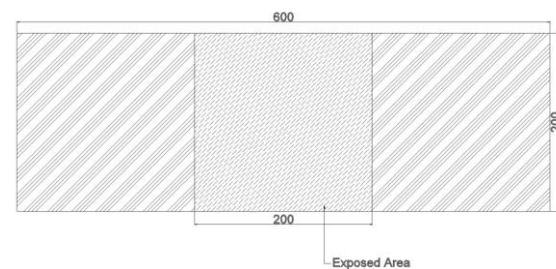


Figure 2 front view of the samples and the exposure area

Mixing was done in accordance with the procedure reported in [3]. In total, five prestressed HSSCC samples (A-E), three non-stressed (i.e., only passively reinforced with CFRP bars) HSSCC samples (F-H), three SPSCC samples (A-C) and one other SPSCC sample (D) were produced at Empa in Switzerland (see Table 2). HSSCC samples were demoulded after 36 hours from casting and were kept in a climate-controlled chamber at 57% relative humidity (RH) and 20 °C. HSSCC samples remained in this chamber for 163 days. Samples were then shipped to the University of Edinburgh and were kept in an uncontrolled laboratory climate (temperature range of 5-15 °C and 60-70% relative humidity) until they were tested.

SPSCC samples were demoulded 24 hours after casting and then placed in a water bath (20 °C) for 28 days. Samples (A-C) were cured in a climate chamber at 70% RH (20 °C), while sample (D) was transferred to the same room where HSSCC samples were kept. The evolution of compressive stress in SPSCC samples (induced by the presence of the UHM CFRP tendons and the expansion of the concrete) is shown in Figures 3 and 4. Prestress levels were measured by gluing foil strain gauges directly onto the CFRP tendons. The mechanically induced compressive stress in the section for HSSCC planks (A-E) is shown in Figure 5. The maximum average value of compressive stress in the cross section was measured as 4.93, and 3.63 MPa for SPSCC samples (A-C) and (D), respectively. Prestress for HSSCC (A-E) planks was 4.94 MPa.

The final prestress value for HSSCC (A-E) planks was calculated to be 3.13 MPa after considering prestress losses due to shrinkage, creep, and elastic shortening [9]. The calculation of the level of prestress loss was based on a model proposed in [10]. The levels of prestress in SPSCC samples need not be corrected for prestress losses, since prestress development was directly monitored by strain gauges bonded to the middle of the CFRP tendons. Refer to Table 2 for details.

The authors note that there was a gap of 5.25 years between the casting of SPSCC samples (A-C) and SPSCC (D). This time gap is the main reason for the difference seen in the mix proportions, mechanical properties, and the exposure area during testing (see Table 2 and 3). The varying parameters are the result of the SPSCC being a novel mix that has been the subject of a continuous optimization process during these five years.

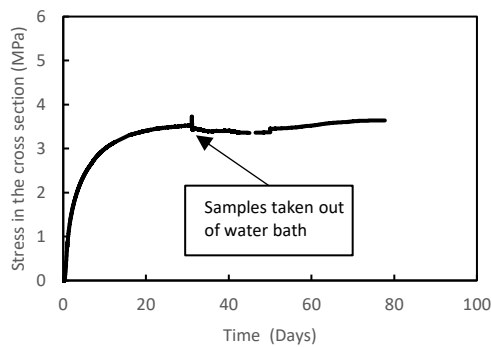


Figure 3 Evolution of precompression in SPSCC (D)

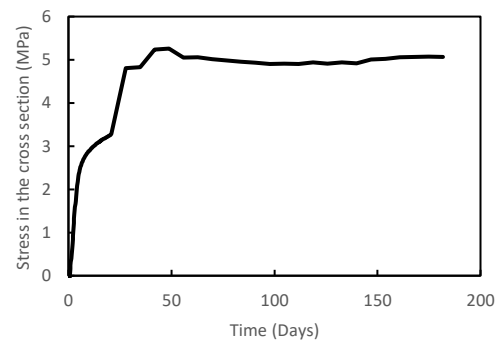


Figure 4 Evolution of precompression in SPSCC A-C

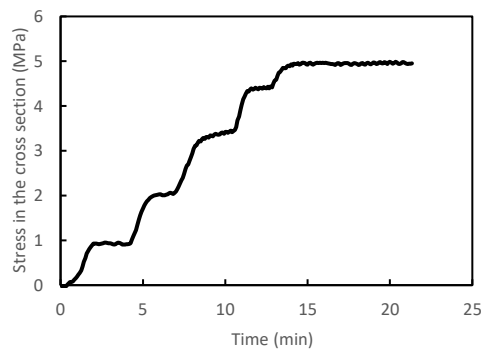


Figure 5 Mechanical prestressing of HSSCC(A-E)

## Testing

Spalling experiments were carried out using a gas-fired RPA at the University of Edinburgh. The details and benefits of this testing approach are outlined in [8], [11], [12]. The RPA can achieve high heat fluxes that enables its users to simulate a variety of in-depth heating regimes, including simulation of the in-depth heating that would occur during an ISO 834 standard fire test in a fire testing furnace. Validations of this approach (widely termed an ‘H-TRIS’ approach) have been reported in [7] and were used for the experiments presented in this paper. Figures 6 and 7 show the comparison of in-depth temperatures for samples exposed to the simulated ISO 834 [13] and the simulated modified hydrocarbon fire (HCM) [14] curves, respectively. The in-depth temperatures used in this comparison were obtained from experiments reported in [9], [12]. It is noteworthy that only the first 7 minutes of the HCM fire curve could be accurately replicated using the RPA, due to the very severe heat fluxes involved and practical limitations on the power of the RPA. For this reason, after the 7<sup>th</sup> minute, the incident heat flux was maintained constant.

Figures 6 and 7 therefore confirm the capability of the H-TRIS approach to replicate both ISO 834 and HCM fire curves. The maximum difference between in-depth temperature (at 10 mm from the exposed surface) of samples tested using H-TRIS and samples tested in a furnace (with ISO 834 fire curve) is about 40 °C (for HSSCC A). Fig 7 shows similar agreement for the HCM curve up to the 7<sup>th</sup> minute into the experiment, after which point, the curves start to deviate, as explained.

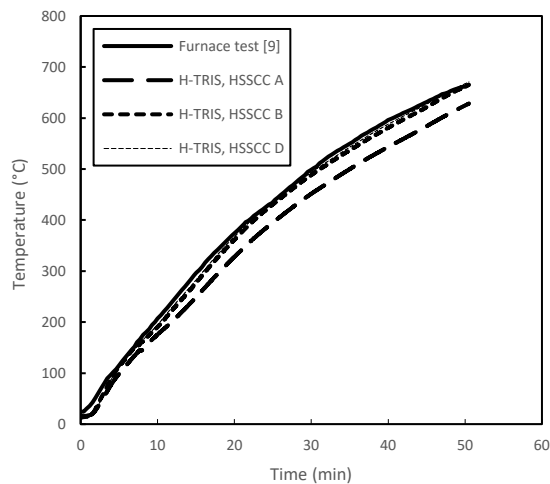


Figure 6 In-depth temperature (@10 mm) comparison between H-TRIS and ISO 834 furnace tests [9]

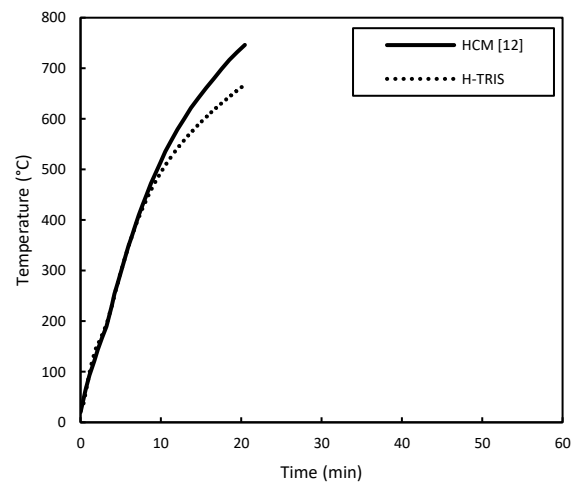


Figure 7 In-depth temperature (@10 mm) comparison between H-TRIS and HCM furnace tests [12]

A summary of the samples and the testing matrix is provided in Table 2. It should be noted that only two samples (out of three) from (A-C) were instrumented with strain gauges for monitoring the evolution of self-prestressing (see Figure 4), and the value of prestress in the remaining sample was assumed based on these gauges.

Table 2 Description of the samples

Reference	Length (mm)	Prestress (MPa)	Heating regime (simulated)	Exposure area (mm <sup>2</sup> )	Age (days)
SPSCC A	500	4.9	ISO 834	400 × 200	90
SPSCC B	500	4.9	ISO 834	400 × 200	90
SPSCC C	500	4.9	ISO 834	400 × 200	90
SPSCC D	600	3.63	ISO 834	200 × 200	150
HSSCC A	600	3.13	ISO 834	200 × 200	205
HSSCC B	600	3.13	ISO 834	200 × 200	205
HSSCC C*	600	3.13	--		203
HSSCC D	600	3.13	ISO 834	200 × 200	206
HSSCC E	600	3.13	HCM	200 × 200	216
HSSCC F	600	Non prestressed	ISO 834	200 × 200	210
HSSCC G*	600	Non prestressed	--		212
HSSCC H	600	Non prestressed	Slow heating**	200 × 200	218

\*Experiments were stopped/disregarded due to technical difficulties.

\*\* Slow heating comprised a 1.2 kW/m<sup>2</sup> increase per minute up to a maximum incident heat flux value of 60 kW/m<sup>2</sup>.

Figure 8 shows the development of temperature (as a function of time) for Sample HSSCC H and Sample HSSCC A, which were exposed to a semi-arbitrary slow heating regime and a simulated ISO 834 fire curve, respectively.



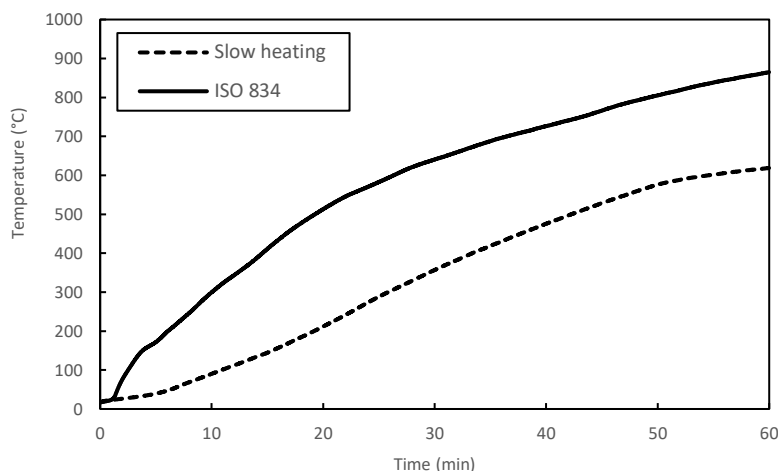


Figure 8 Comparison between in-depth temperature (at 2 mm) for samples subjected to a simulated ISO 834 fire curve, and a semi-arbitrary slow heating regime

All samples were tested in an externally unrestrained condition (i.e., free to expand on heating). Six linear potentiometers (LPs) were used (3 at each end) to measure the expansion of concrete and the potential draw-in (or end slippage) of the two CFRP tendons due to loss of bond (see Figure 15). Another three LPs were positioned at the centre and both edges of the cold side of the sample to measure thermal bowing of the samples during one-sided heating.

### Mechanical properties of the tested samples

The mechanical properties of the tested samples (at ambient temperature) are shown in Table 3. HSSCC mixes were fire tested at a later age than SPSCC samples (refer to Table 2), therefore some of the values that are shown for HSSCC samples cannot not be given be for SPSCC samples.

The compressive strength and modulus of elasticity for SPSCC (A-C) was higher than SPSCC (D), this was due to the higher cement content in the samples A-C (see Table 1).

Table 3 Mechanical properties of the tested samples

Reference	Compressive strength (28d) (SD)	Emod (GPa)(28d) (SD)	Compressive strength (MPa)(180d) (SD)	Emod (GPa)(180d) (SD)	Moisture content (at the time of testing) %	Age at the time of testing (days)
SPSCC (A-C)	73.3 (3.0)	28 (1.0)	-	-	7.3	90
SPSCC D	52.1 (3.75)	20.5 (0.1)	-	-	6.3	150
HSSCC (A-H)	79.6 (0.5)	30.2 (0.3)	91.2 (2.0)	30.8 (0.8)	3.4	210

Moisture content for each mix was determined by drying three small circular samples (50 mm × 50 mm) in an electric oven at 105 °C for the first 24 hours, then at 200 °C (such a high temperature was used due to the high density of the samples, as it was feared that a lower temperature would not lead to the evacuation of moisture from the centre of the samples due to their very low porosity). Drying continued until the difference between two consecutive measurements, taken 24 hours apart, was less than 0.1 by mass%.

The higher levels of moisture content in the SPSCC samples are considered likely due to the presence of SAP in the mix. SAP is added to reduce the autogenous shrinkage that limits the

level of prestressing in the expanding planks if unmitigated [3], [15]. These compounds absorb moisture during mixing [16] without becoming solvent. This moisture is gradually released back into the cement paste which reduces the magnitude of self-desiccation and autogenous shrinkage. It is possible that not all the absorbed moisture is released from the SAP by the time the experiment was carried out, and hence the higher moisture contents (see Table 3). Moisture content in the SPSCC samples is also likely to be higher because they were tested at a slightly younger age (see Table 2) than the HSSCC samples.

## Results and discussion

### General

All SPSCC samples spalled explosively in less than 11 minutes of heating. HSSCC samples, however, did not experience any spalling. The details of spalling events are outlined in Table 4. Simulated ISO 834 tests were performed for 60 minutes unless spalling occurred, in which case the experiment was halted to avoid damaging the equipment. The sample that was subjected to slow heating was tested for 70 minutes. The HCM test was terminated after 20 minutes.

*Table 4 Main summary of the experimental results*

Reference	Exposure (simulated)	Spalling	Time to spall (min ' sec'')	Remarks
SPSCC A	ISO 834	Yes	9'08''	Explosive
SPSCC B	ISO 834	Yes	10'17''	Explosive
SPSCC C	ISO 834	Yes	9'59''	Explosive
SPSCC D	ISO 834	Yes	9'00''	Explosive
HSSCC (A-H)	ISO 834 HCM Slow heating	No	-	Longitudinal cracks along the tendons

The occurrence of spalling was sudden and violent, without any warning. The depth of first spalling was in the range of 4-20 mm. Figures 9 and 10 show the spalled samples. SPSCC samples A, B, and C had a heat-exposed area of 400 × 200 mm, while only the middle 200 mm of SPSCC D was subjected to direct heating, as shown in Figure 2. This variation in exposure resulted in a similar variation of the spalling pattern; sample SPSCC D spalled only in the heat-exposed area (see Figure 10) whereas SPSCC (A-C) samples experienced spalling over almost their entire exposed surfaces (see Figure 9).

HSSCC samples did not experience any spalling at all. These samples were observed to develop a fine network of cracks at their exposed surfaces, which may have helped to release internal stresses.



*Figure 9 SPSCC A-C samples*



*Figure 10 SPSCC D*

It was not possible to determine at which stage this fine network of cracks (shown in Figure 11) was formed due to the severity of the testing environment. The HSSCC samples also (for every thermal exposure regime) developed two cracks, along the tendons, on their unexposed faces (Figure 12). The cracks are thought to be the result of the differences in transverse coefficient of thermal expansion (CTE) between the CFRP tendons and the concrete matrix. These cracks formed at different stages, depending on the applied heating regime. When samples were exposed to ISO 834 and HCM curves, the first visible cracks were observed between 5 minutes 59 seconds (5'59'') and 9'32''. However, this was delayed to 19'42'' when a slow heating curve was used.



*Figure 11 the exposed face of the sample after exposure to simulated ISO 834 fire curve*



*Figure 12 Longitudinal cracks developing at the unexposed face when exposed to simulated HCM fire curve*

### **Moisture transport**

The formation of longitudinal cracks along the CFRP prestressing tendons appears to have created pathways for moisture to escape the samples on their unexposed faces. This can be clearly seen in Figure 12. The rate of moisture escape from the unexposed face appeared to be related to the severity of heating (i.e., more severe the heating led to more obvious and rapid moisture escape). It is worth noting, however, that the first instance of moisture escape was often observed to be through the exit point of the TC wires, rather than through the longitudinal cracks. This could be because of the direct path that the TCs provide as opposed to the dense concrete matrix. TCs can also perturb material around them creating a transition zone and air bubbles during casting which facilitates moisture transfer. The longitudinal cracks became the main path for moisture escape once they formed. Longitudinal cracks along the tendons were not observed in the SPSCC samples, except for SPSCC C which had the deepest spalling depth, and in this case the tendons were also exposed (see Figure 9). For SPSCC C, the heating source was kept in place after the first spalling instance (at 9'59'') up to the 14<sup>th</sup> minute into the experiment. During this time, 14 occasions of spalling were observed.

The formation of the longitudinal cracks is thought to be due to thermal incompatibility between the CFRP tendons and the surrounding concrete. CFRP tendons have a transverse coefficient of thermal expansion that is three times larger than concrete [9], [17]. When heated, this incompatibility likely generates tensile (bursting) stresses in the surrounding concrete, leading to the formation of such cracks. Figures 13 and 14 (please note that these 2 figures have different horizontal axes) show the in-depth temperature for samples SPSCC D (which spalled

after 9'00"), and HSSCC D (which did not spall). It is observed that the tendon temperature at the time of spalling (9<sup>th</sup> minute) was 105 °C. The tendon temperature in HSSCC D was 100 °C at the same time. Longitudinal cracks were observed to form at 7'33" in HSSCC D, when the tendon temperature was 74°C. Lack of spalling in HSSCC samples, therefore, could be influenced by the formation of these cracks that allowed the moisture vapour to escape, thus reducing internal pressure.

The reason why longitudinal cracks along the CFRP tendons occurred in HSSCC samples, but not in the SPSCC samples, is not yet known and is currently being investigated by the authors.

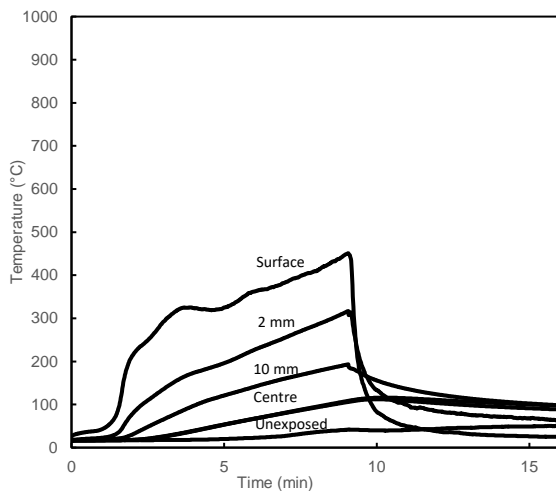


Figure 13 In-depth temperature for SPSCC D subjected to simulated ISO 834 curve

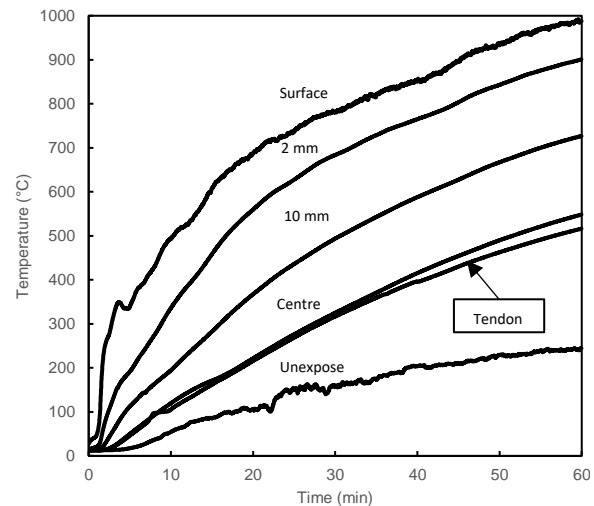


Figure 14 In-depth temperature for HSSCC D subjected to a simulated ISO 834 curve

Moisture movement and escape thus appears to play a significant role in spalling prevention for these samples. In all the samples where moisture escape was clearly observed, no spalling occurred. Furthermore, the samples which spalled all had a higher moisture content (see Table 3) than those where no spalling occurred. This effect has been reported widely in literature [18] with some researchers [19] reporting that concrete samples avoided spalling altogether when pre-dried at 80 °C to drive the free moisture out. Other researchers [20] have indirectly highlighted the significance of moisture content through the application of combined curing.

### Release of thermal stresses

Figure 14 shows the in-depth temperature for sample HSSCC D, subjected to a simulated ISO 834 fire curve. A temperature difference of 440 °C was recorded, which would lead to the generation of thermal stresses that could contribute to spalling. However, these thermal stresses could have been released by the elongation and the bowing of the sample since it was tested in an unrestrained condition and was quite flexible out of plane. Thermal bowing was measured to be 3.64 mm at the middle of the sample (at 60 minutes). The overall thermal elongation was 1.2 mm.

Due to the unrestrained nature of the experiments, a firm conclusion could not be formed with regards to the effects of thermal stresses in spalling. Nonetheless, SPSCC samples, which all had high moisture contents, spalled explosively despite being tested in a set up identical to the HSSCC samples. This suggests the effect of moisture content as a governing factor in spalling, regardless of whether differential thermal stresses are present or not (i.e., released through thermal bowing).

### The effect of the presence of SAP

As mentioned earlier, SPSCC samples included SAP, but HSSCC samples did not. The presence of SAP has been shown to reduce the compressive and the flexural strength of concrete, especially when the concrete is young [15]. This is likely due to the more porous nature of the concrete mix when SAP is added, which reduces strength [21]. High temperature mechanical properties of SPSCC mixes have not been quantified to date but it is possible that they may deteriorate at more rapidly than HSSCC mixes, making the SPSCC mixes more prone to spalling. SAPs will also oxidise at temperatures between 241-397 °C [22]. The oxidation of the SAP particles yields a more porous matrix (compared to a sample that does not contain any SAP). Furthermore, samples with SAP contain a higher amount of free moisture (see Table 3). Given the roles moisture plays in spalling [23], samples with SAP would be expected to be more susceptible to explosive spalling. However, research has shown that SAP, albeit when used with polypropylene (PP) fibres, may reduce spalling [21] by helping to create a connected pore network once the SAP particles become dehydrated. It is therefore possible that the addition of SAP alone is the key risk factor for heat-induced spalling; these hypotheses require further work to be interrogated.

### The effect of prestressing and tendon slippage

The effect of prestress (or pre-compressive stress in the concrete) on spalling was inconclusive from these experiments. Even though prestressed and non-prestressed HSSCC samples were produced, none of these samples spalled. The behaviour of the prestressed samples (HSSCC A-E) was generally similar to the non-prestressed samples (HSSCC F-H). All samples cracked on their unexposed faces, and moisture escaped through these cracks. However, it was observed that moisture also escaped through the ends of the non-prestressed samples, at the tendon positions (as well as through the cracks opening on their unexposed faces), as shown in Figure 15. This could be the result of the smaller area filled up by the prestressed CFRP tendons compared with the size filled up by the non-prestressed tendons (due to Poisson's effect); so that there would be a greater capacity for moisture to move along the tendons within the anchorage zones.

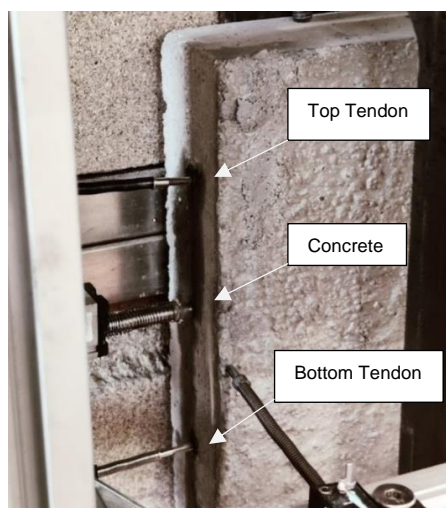


Figure 15 Moisture escaping through the ends from the tendons. The picture shows the LPs used to measure the draw-in of the tendons and the expansion of the samples (HSSCC F)

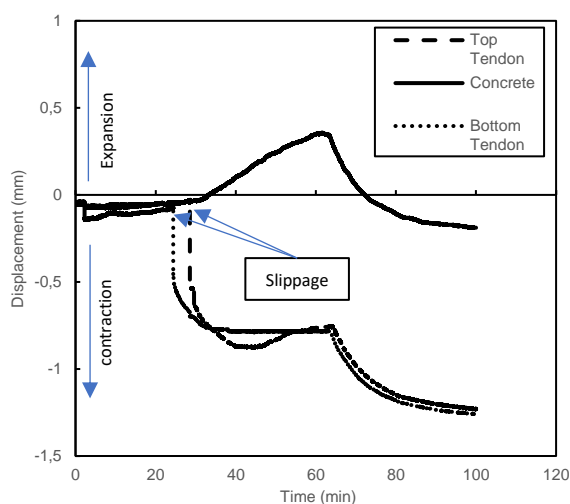


Figure 16 The slippage of the tendons and the elongation of the concrete (HSSCC B)



The samples which spalled were all prestressed, corroborating prior research showing that the presence of compressive stress exacerbates spalling in fire [18]. However, some researchers have argued that compressive stress indirectly affects the spalling behaviour of concrete through effects on permeability [24]; compressive stress reduces the gas permeability of concrete (when applied in such a way that it causes cracks to close), and permeability is known to affect the susceptibility of HPC for spalling [25].

The elongation of the samples was accompanied by elongation of the embedded tendons (see the “Concrete” trace in Figure 16). This overall elongation was eventually followed by the slippage of the tendons when the cracks formed at the unexposed surface, and propagated to the ends of the sample (see the “Tendon” traces in Figure 16). For samples where the longitudinal cracks did not propagate to the ends of the specimen, no slippage was recorded (even though the tendons are almost certain to have de-bonded in the heated region). Table 5 shows the details of the tendon slippage during testing, including the time-to-slip and the temperature at of the surface of the tendons at the time of slippage. Since no SPSCC samples showed any tendon slippage, these are not included.

*Table 5 Details of the slippage of tendons during testing*

Reference	Slippage	Slippage time (min' sec'')	Tendon temperature (°C)	experiment duration (min)
HSSCC A	Yes	25'09''	247	60
HSSCC B	Yes	28'31''	255	60
HSSCC D	Yes	21'23''	231	60
HSSCC E	No	-	-	20
HSSCC F	Yes	26'41''	240	60
HSSCC H	No	-	-	70

The slippage recorded for the non-prestressed sample (HSSCC F) is counterintuitive, since there was no prestress force in them. However, the tendons in this sample (and indeed all other samples) experienced some elongation due to the expansion of the concrete specimen they were embedded in (due to them being bonded to the surrounding concrete which was expanding). Table 5 shows that the temperature at which tendon slippage occurred ranged between 230-250 °C. Interestingly, the elongation of the concrete can be seen (refer to Figure 12) to accelerate once the tendons have slipped (i.e., the tendons restrained the concrete until they slipped, due to their high modulus in tension).

The slippage of the tendons also affected the thermal bowing of the samples, as is shown in Figure 16. The accelerated expansion of concrete meant that more thermal stresses were released, making spalling less likely.

## Conclusions

The spalling of high-performance concrete at elevated temperatures has previously been widely reported. Various theories exist regarding the causes and the mechanism through which spalling occurs [26]. For prestressed concrete, spalling is arguably more important given its exacerbation by precompressive stresses in the concrete. This paper investigated a novel concrete mix that uses controlled (chemical) expansion of the concrete to induce prestressing (i.e., by self prestressing), as opposed to traditional mechanical prestressing (i.e., mechanical pretensioning) using UHM CFRP tendons. It was found that:

- Self-prestressed samples (SPSCC) were highly susceptible to explosive spalling when subjected to a simulated ISO 834 heating regime. Every SPSCC sample

spalled in less than 11 minutes from the start of the experiments. This is considered likely to be due to the higher level of moisture content in the SPSCC samples.

- Mechanically prestressed samples comprising UHM CFRP tendon did not spall under any heating regime. Samples developed longitudinal cracks along the CFRP tendons (on the unexposed surface) where moisture escape was visibly evident. Moisture escape through the cracks (both on the exposed and the unexposed surfaces) could explain why the HSSCC samples did not spall. Further experiments are planned to interrogate this.
- SPSCC samples had a much higher percentage of moisture content (between 6.2% and 7.3% by mass) than HSSCC samples (3.2%). The higher water content in the SPSCC was deliberate via the addition of SAP, and was aimed at providing internal curing and enhancing controlled expansion.
- No longitudinal cracks (along the CFRP tendons) were observed in SPSCC samples, except for one case, as all SPSCC samples spalled in under 11 minutes. Such cracks were observed for all the samples without SAP, and moisture escape was recorded from these cracks. This further corroborates the theory that moisture content and moisture migration are key factors influencing heat-induced explosive spalling of concrete.
- Slippage of tendons was observed to occur in samples once the temperature of the immediate surrounding of the CFRP tendons in the centre of the heated region reached 230-250 °C. Tendon slippage caused further relaxation of the samples as they were able to expand freely.

### Outlook and future work

The authors are currently investigating ways to confirm some of the hypotheses that have been put forward in this paper, as well as to find ways to mitigate or minimise explosive spalling of SPSCC prestressed with UHM CFRP tendons. This includes the addition of polymer fibres to the mix, as well as characterisation of the mix on a smaller scale. Besides this, further work is planned to investigate the effects of the CFRP tendons on spalling.

### Acknowledgement

This work was possible thanks to a fantastic team of technicians at both EMPA and The University of Edinburgh. Therefore, we would like to acknowledge the efforts of Mr Daniel Volke, Sebastiano Valvo, Janis Justs, Christian Rohrer, Angelo Scioscia, Mark Partington, And Michal Krajcovic.

### References

1. P. Bhatt, *Prestressed Concrete Design to Eurocodes*. Routledge, 2012.
2. M. Wyrzykowski, G. Terrasi, and P. Lura, "Expansive high-performance concrete for chemical-prestress applications," *Cem. Concr. Res.*, vol. 107, no. February, pp. 275–283, 2018, doi: 10.1016/j.cemconres.2018.02.018.
3. M. Wyrzykowski, G. Terrasi, and P. Lura, "Chemical prestressing of high-performance concrete reinforced with CFRP tendons," *Compos. Struct.*, vol. 239, no. December 2019, p. 112031, 2020, doi: 10.1016/j.compstruct.2020.112031.
4. G. Pietro Terrasi, "Prefabricated Thin-walled Structural Elements Made from High Performance Concrete Prestressed with CFRP Wires," *J. Mater. Sci. Res.*, vol. 2, no. 1, pp. 1–14, 2012, doi: 10.5539/jmsr.v2n1p1.



5. British Standards Institution, "BS EN 206:2013+A1:2016, Concrete — Specification , performance , production and conformity," UK, 2016.
6. G. Terrasi, E. R. E. McIntyre, L. A. Bisby, T. D. Lämmlein, and P. Lura, "Transient thermal tensile behaviour of novel pitch-based ultra-high modulus CFRP tendons," *Polymers (Basel)*, vol. 8, no. 12, pp. 10–20, 2016, doi: 10.3390/polym8120446.
7. C. Maluk, L. Bisby, M. Krajcovic, and J. L. Torero, "A Heat-Transfer Rate Inducing System (H-TRIS) Test Method," *Fire Saf. J.*, vol. 105, pp. 307–319, 2019, doi: 10.1016/j.firesaf.2016.05.001.
8. H. Mohammed, D. Morrisset, A. Law, and L. Bisby, "Quantification of the thermal environment surrounding radiant panel arrays used in fire experiments," in *12th Asia-Oceania Symposium on Fire Science and Technology (AOSFST 2021)*, 2021, no. December, pp. 7–9, doi: 10.14264/6efaa82.
9. C. Maluk, G. Pietro Terrasi, L. Bisby, A. Stutz, and E. Hugi, "Fire resistance tests on thin CFRP prestressed concrete slabs," *Constr. Build. Mater.*, vol. 101, no. Part 1, pp. 558–571, 2015, doi: 10.1016/j.conbuildmat.2015.10.031.
10. T. D. Lämmlein, F. Messina, M. Wyrzykowski, G. Terrasi, and P. Lura, "Low clinker high performance concretes and their potential in CFRP-prestressed structural elements," *Cem. Concr. Compos.*, vol. 100, no. February, pp. 130–138, 2019, doi: 10.1016/j.cemconcomp.2019.02.014.
11. C. Maluk, J. Tignard, A. Ridout, T. Clarke, and R. Winterberg, "Experimental study on the fire behaviour of fibre reinforced concrete used in tunnel applications," *Fire Saf. J.*, vol. 120, no. August 2020, p. 103173, 2020, doi: 10.1016/j.firesaf.2020.103173.
12. I. Rickard, "Explosive Spalling of Concrete in Fire: Novel Experiments under Controlled Thermal and Mechanical Conditions," The University of Edinburgh, 2020.
13. International Organization for Standardization, "Fire resistance tests -- Elements of building construction -- Part 11: Specific requirements for the assessment of fire protection to structural steel elements," 1975.
14. AFNOR, "NF EN 1992-1-2 / NA Eurocode 2 : Calcul des structures en béton — Partie 1-2 : Règles générales — Calcul du comportement au feu - Annexe Nationale a la NF EN 1992-1-2:2005 - Calcul du comportement au feu," vol. 2, no. Octobre 2007, p. 30, 2007.
15. J. Justs, M. Wyrzykowski, D. Bajare, and P. Lura, "Internal curing by superabsorbent polymers in ultra-high performance concrete," *Cem. Concr. Res.*, vol. 76, pp. 82–90, 2015, doi: 10.1016/j.cemconres.2015.05.005.
16. J. Justs, M. Wyrzykowski, F. Winnefeld, D. Bajare, and P. Lura, "Influence of superabsorbent polymers on hydration of cement pastes with low water-to-binder ratio: A calorimetry study," *J. Therm. Anal. Calorim.*, vol. 115, no. 1, pp. 425–432, 2014, doi: 10.1007/s10973-013-3359-x.
17. M. A. Aiello, "CONCRETE COVER FAILURE IN FRP REINFORCED BEAMS UNDER THERMAL LOADING," *J. Compos. Constr.*, vol. 3, no. 1, 1999, doi: [https://doi.org/10.1061/\(ASCE\)1090-0268\(1999\)3:1\(46\)](https://doi.org/10.1061/(ASCE)1090-0268(1999)3:1(46)).
18. H. Mohammed, H. Ahmed, R. Kurda, R. Alyousef, and A. F. Deifalla, "Heat-Induced Spalling of Concrete: A Review of the Influencing Factors and Their Importance to the Phenomenon," *Materials (Basel)*, vol. 15, no. 5, 2022, doi: 10.3390/ma15051693.
19. J. C. Mindeguia, P. Pimienta, H. Carré, and C. La Borderie, "Experimental analysis of concrete spalling due to fire exposure," *Eur. J. Environ. Civ. Eng.*, vol. 17, no. 6, pp. 453–466, 2013, doi: 10.1080/19648189.2013.786245.
20. G. F. Peng, X. J. Niu, Y. J. Shang, D. P. Zhang, X. W. Chen, and H. Ding, "Combined curing as a novel approach to improve resistance of ultra-high performance concrete to explosive spalling under high temperature and its mechanical properties," *Cem.*

- Concr. Res.*, vol. 109, no. March, pp. 147–158, 2018, doi: 10.1016/j.cemconres.2018.04.011.
21. P. Lura and G. Pietro Terrasi, “Reduction of fire spalling in high-performance concrete by means of superabsorbent polymers and polypropylene fibers: Small scale fire tests of carbon fiber reinforced plastic-prestressed self-compacting concrete,” *Cem. Concr. Compos.*, vol. 49, pp. 36–42, 2014, doi: 10.1016/j.cemconcomp.2014.02.001.
  22. M. Zhang, S. Zhang, Z. Chen, M. Wang, J. Cao, and R. Wang, “Preparation and characterization of superabsorbent polymers based on sawdust,” *Polymers (Basel)*., vol. 11, no. 11, 2019, doi: 10.3390/polym11111891.
  23. G. Choe, G. Kim, M. Yoon, E. Hwang, J. Nam, and N. Guncunski, “Effect of moisture migration and water vapor pressure build-up with the heating rate on concrete spalling type,” *Cem. Concr. Res.*, vol. 116, no. August 2017, pp. 1–10, 2019, doi: 10.1016/j.cemconres.2018.10.021.
  24. M. J. Miah, H. Kallel, H. Carré, P. Pimienta, and C. La Borderie, “The effect of compressive loading on the residual gas permeability of concrete,” *Constr. Build. Mater.*, vol. 217, pp. 12–19, 2019, doi: 10.1016/j.conbuildmat.2019.05.057.
  25. P. Kalifa, F. D. Menneteau, and D. Quenard, “Spalling and pore pressure in HPC at high temperatures,” *Cem. Concr. Res.*, vol. 30, no. 12, pp. 1915–1927, 2000, doi: 10.1016/S0008-8846(00)00384-7.
  26. C. G. Bailey and G. A. Houry, *Performance of Concrete Structures in Fire*. MPA – The Concrete Centre, 2011.

# Investigation of the Thermo-Hydral Behaviour of Concrete with Recycled Fibres via Neutron and X-Ray Tomographies

Yifan Li<sup>1\*</sup>, Stefano Dal Pont<sup>2</sup>, Alessandro Tengattini<sup>2</sup>, Shan-Shan Huang<sup>1</sup>

<sup>1</sup>The University of Sheffield, Sheffield, the United Kingdom

<sup>2</sup>Université Grenoble Alpes, Grenoble, France

\* Corresponding author (yli101@sheffield.ac.uk, D120, Department of Civil and Structural Engineering, the University of Sheffield, Sheffield, UK, S1 4BT)

## ABSTRACT

High-performance concrete has a high propensity to explosive spalling under fire exposure. It can cause structural failure, which has an enormous economic impact, and can potentially lead to loss of life. Current effective measures to mitigate the fire-induced spalling include the addition of polypropylene (PP) fibres into concrete. To improve the sustainability of this mitigation method, this study contributes to an exploration of the use of a novel substitution of manufactured PP fibres with Recycled Tyre Polymer Fibres (RTPF). The coupled thermo-hydral mechanisms by which PP fibres mitigate the fire-induced spalling remain not fully understood, not mention that of RTPF. In this paper, for the first time, in-situ neutron and X-Ray tomographies are acquired simultaneously while heating RTPF concrete. The neutron tomographies reveal the evolving moisture profile, confirming the presence of the heat-induced “moisture clog”. The change of dry volume after heating is quantified, where the initial decrease of dry volume is firstly explained. The X-ray results show the change in the porous structure of concrete before and after heating. The role of RTPF in accelerating the drying rate of concrete was confirmed.

**KEYWORD:** Recycled Tyre Polymer Fibre, Neutron Tomography, X-Ray, Fire Spalling

## INTRODUCTION

When concrete structures are exposed to fire, layers of concrete can break off explosively from the heated surface, so called explosive fire-induced spalling. This reduces the sectional area of concrete, exposing the steel reinforcement to high temperature, hence reducing the overall load-bearing capacity of the whole structure. Compared to normal strength concrete, concrete with higher compressive strength is more prone to explosive spalling under heat exposure [2-4], due to its dense microstructure.

Four prevention methods are proposed in Eurocode 2 to tackle this problem for high strength concrete [5]. Adding polypropylene (PP) fibres is one of the spalling mitigation methods that have been richly investigated and proven to be effective [6, 7]. PP fibres melt at around 160 °C, which creates connected channels inside concrete [8]. The increase in concrete permeability can facilitate vapour migration toward the outside and inside of the concrete, hence relieving the increased vapour pressure due to heating [9]. With the inspiration of virgin manufactured produced PP fibres, more sustainable recycled tyre polymer fibres (RTPF) are

investigated for their ability to mitigate the fire spalling. Previous studies have indicated that RTPF is as effective as manufactured PP fibres [10, 11], with its extra potential to bring great environmental benefits. However, the actual role of RTPF is still unspecified as the mechanism of fire spalling was not fully understood.

The cause of explosive fire spalling comprises of two main mechanisms. One is the mechanical stress gradient induced by the thermal gradient. This mechanism can be modelled at the macroscale, by applying solid mechanics knowing the concrete thermal properties in isotherms [5, 12]. The other mechanism is the thermal-induced pore pressure build-up in the porous structure of concrete. This is a less known mechanism due to the lack of effective tools to measure vapour pressure and moisture distribution inside the heated concrete. Recent research has introduced new approaches to measure the gas pressure of concrete (with or without fibres) during heating. Because of the heterogeneity of concrete, different heating conditions and the intrusion nature of the measurement tool, a wide range of results were found in the literature [13-16]. The lack of consistency in experimental results creates complexity for modelling and the understanding of underlying physics. Extra information such as moisture migration, pore structure and aggregate geometry of heated concrete could be pivotal for future modelling and study of the mechanism of fire spalling.

To provide detailed information on the moisture transport and macropore structure of concrete at elevated temperatures, neutron and X-ray tomographies was conducted at the Institut Laue-Langevin (ILL), France. The principles of neutron tomography is similar to X-ray tomography: the target object is placed in between the radiation source and the detector to measure the attenuations of different matters inside the object. X-ray interacts with the outer electron shell of the atom, making the X-ray attenuation sensitive to the electron number of atoms, hence to the density of a matter. The sensitivity to density makes X-ray tomography an ideal tool to investigate the pore structure of concrete. Unlike X-ray, neutrons interact with the nucleus of atoms. For the cold neutron used in this research, the high attenuation of hydrogen atoms in water and low attenuation of quartz aggregates makes it effective for detecting moisture. These two tomography techniques were adopted in this study for their complementarity.

Neutron and X-ray tomographies are proven effective for monitoring the full-field information of mortar and concrete-like materials. The first 3D analysis of moisture distribution was completed by Dauti et al. followed by mesoscale numerical modelling [1, 17]. The test setup was then upgraded to create a uniaxial heating condition to investigate the moisture clog theory [18]. Another research also completed the ambient temperature microstructural analysis using both neutron and X-ray [19]. In this paper, simultaneous in-situ neutron and X-ray scanning of heated concrete with RTPF fibre was conducted for the first time.

The goal of this study is to investigate the influence of RTPF on high-performance concrete (HPC) at elevated temperatures, in particular, the underlying physics. The macropore structure, moisture distribution and their coupling effect were studied using both neutron and X-ray tomographies. Image processing techniques were used for quantitative data analysis.

## SPECIMEN PREPARATION AND TEST SETUP

### Concrete specimen

The concrete mixture for the tomography tests is based on the sample from Dauti's experiment [1] to facilitate comparison, as shown in Table 1. A little variation in aggregate size was adopted due to material availability. 2 % superplasticizer (based on cement mass) was added because RTPF can severely reduce the workability of concrete. Specimens were cast in 34 mm \* 60 mm cylinders moulds, which were made by split water pipes with thermocouples connecting through the notches at 3 mm, 10 mm and 20 mm.

Table 1 Concrete mixture table for plain concrete and RTPF concrete.

Material	Dosage (kg/m <sup>3</sup> )
Cement I	488.00
Silica Fume	122.00
Aggregate 0-1.18 mm	632.00
Aggregate 1.18-4.75 mm	949.00
Superplasticizer SIKA 30HE (2.0%)	9.76
Water	189.10
RTPF (for fibre added concrete only)	2.00
w/b ratio	0.31

Specimens with 2 kg/m<sup>3</sup> RTPF and control specimens without fibres were cast to quantify the influence of RTPF. The waste tyre fluff is contaminated with rubber particles and dusts and it is entangled. Devices, which clean the waste tyre fluff, open it up and disperse it uniformly into concrete, were developed. Figure 1 (a) shows the cleaned and untangled RTPF. The typical lengths of RTPF ranges from 0.8 mm to 16 mm. Their diameters range from 7.5  $\mu$ m to 60  $\mu$ m. The bulk density is around 400 – 600 kg/m<sup>3</sup>, depending on source of the waste tyres. The melting point of RTPF is also slightly higher than polypropylene fibre, at around 170 °C. The specimens have been cured for 28 days at 90 % relative humidity and 20 °C. A picture of the concrete specimen is shown in Figure 1 (b). The details of the test samples are shown in Table 2.



Figure 1 (a) Cleaned and untangled RTPF (b) Concrete specimen in aluminium foil.

Table 2 Specimens parameters.

Name	RTPF (kg/m <sup>3</sup> )	Age (days)	Strength (MPa)	Temp (°C)	Quantity
Plain Concrete	0	28	125	500	1
RTPF	2	28	143	500	1

### Heating and scanning equipment

The specimens were put into a heating chamber during the test. The side surface of the specimen was wrapped with aluminium foil to prevent moisture leak through the side boundary. The outer shell of chamber is also made of aluminium, since it is transparent to neutrons. An alumina insulation blanket was placed between the specimen and the chamber shell. A ceramic infrared radiator was placed very close to the top surface of the sample, leaving a small gap for the extraction of water steam and possible dust in case spalling occurs. The HPC used in this research has a very high probability of spalling at high temperatures. To prevent spalling and its subsequent influence on the moisture transport in pore structure, the radiator temperature was limited to 500 °C while the concrete surface temperature is around 300 °C during heating. The assembled test setup is shown in Figure 2 (a). The scanning was conducted in the Neutron and X-ray Tomograph system (NeXT) in the ILL [20]. This system allows neutron and X-ray tomography scanning simultaneously. A drawing of the NeXT system is shown in Figure 2 (b).

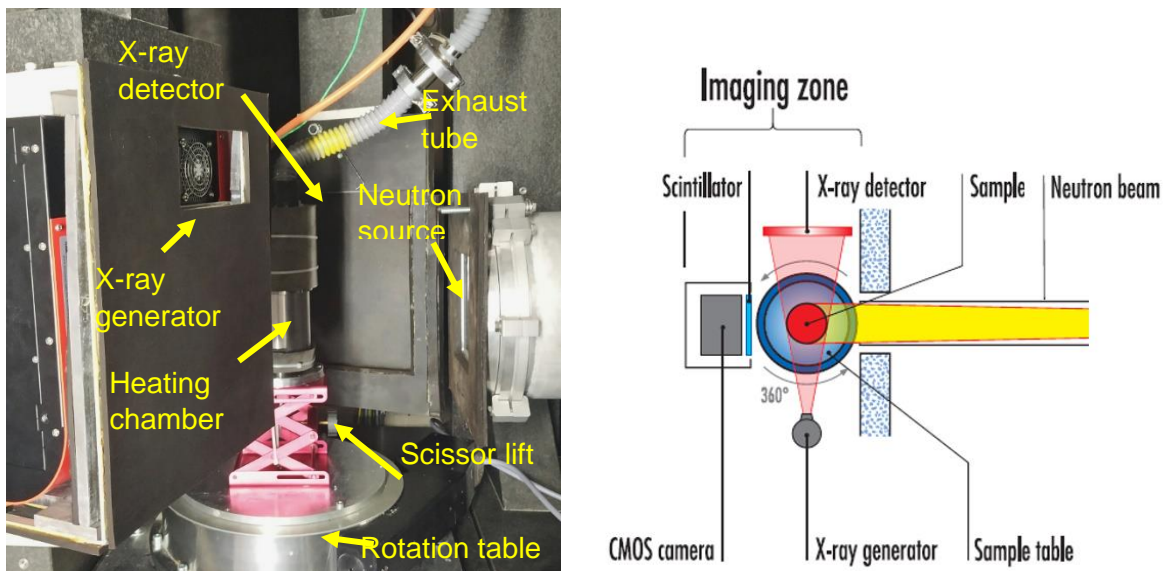


Figure 2 (a) Specimen with heating chamber placed in NeXT (b) Layout of NeXT, ILL.

## DATA ANALYSIS AND RESULT

### Temperature data and TC calibration

The location of the thermocouple can be seen from the X-ray tomography as the metal wire has a distinctive density compared to concrete, Figure 3 (a) shows the thermocouples in the X-ray image of the RTPF specimen. The depth of the thermocouple head can be measured directly from the image. The calibrated depth of thermocouples in RTPF and plain concrete specimens are 1.6 mm, 9.5 mm, 17.8 mm and 2.5 mm, 9.3 mm, 17.7 mm,

respectively. During the tests, the radiator reaches 500 °C in three minutes and then stays constant.

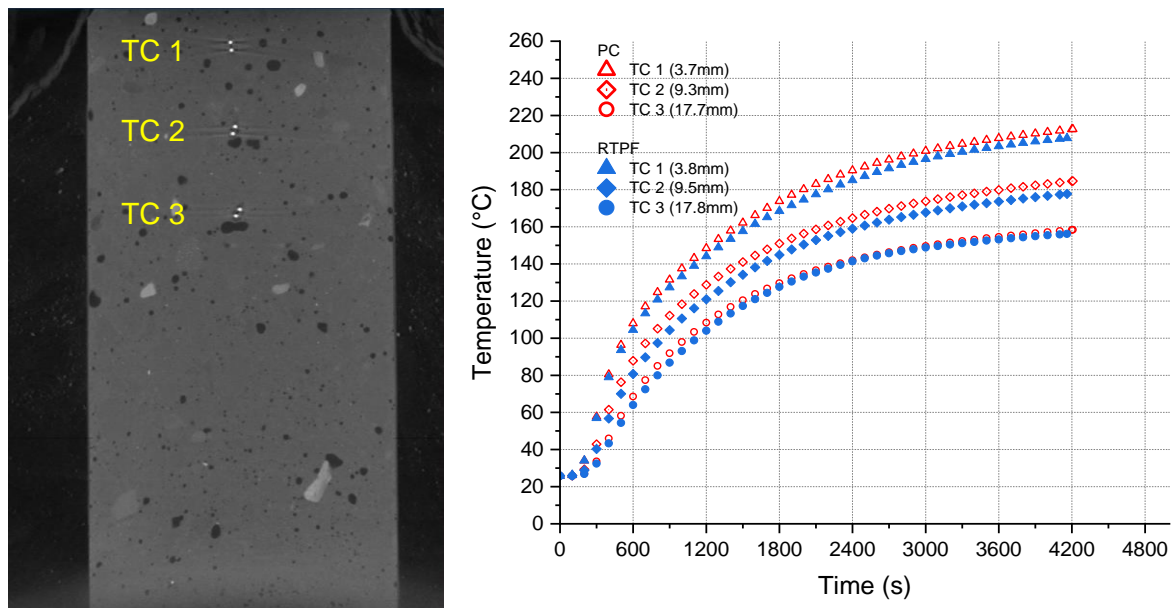


Figure 3 (a) Location of thermocouples in X-ray tomography (b) Temperatures at different depths of plain concrete and RTPF specimens.

As shown in Figure 3 (b), the temperature of plain concrete is slightly higher than that of the RTPF specimen. The maximum temperature difference between two specimens is 8 °C at TC2, at 1300 s. This modest temperature difference re-confirms that the addition of fibres has little influence on the temperature distribution of heated concrete [6, 21].

### Neutron image processing

After heating, the moisture drying near the side surface of the specimen is inevitable, even though aluminium wrapping and alumina heat insulation were adopted. To analyse the uniaxial drying of concrete, the boundary effect was removed by disregarding the part of the specimen close to the perimeter during the scanning image processing. With pixel size about 200  $\mu\text{m}$ , the overall radius of the specimen is approximately 85 pixels and a core of 60-pixels radius was chosen for the image processing, as shown in Figure 4 (a).

To differentiate the dry and wet volumes within an image, image segmentation was adopted. This is a process of separating images into multiple groups, where the pixels in each group share the same characteristics. The segmentation method used in this project is histogram-based segmentation. The grey values of pixels are collected and transferred to a histogram, where the darker pixels (dry) have lower grey values and brighter pixels (wet) have higher grey values, as shown in Figure 4 (b). The threshold is determined where the two peaks of the histogram intersect (the valley). After heating, dark pixel intensity increases on the left of the histogram, indicating the increase in drying volume. On the right, bright pixel intensity decreases, demonstrating the decrease of wet volume.



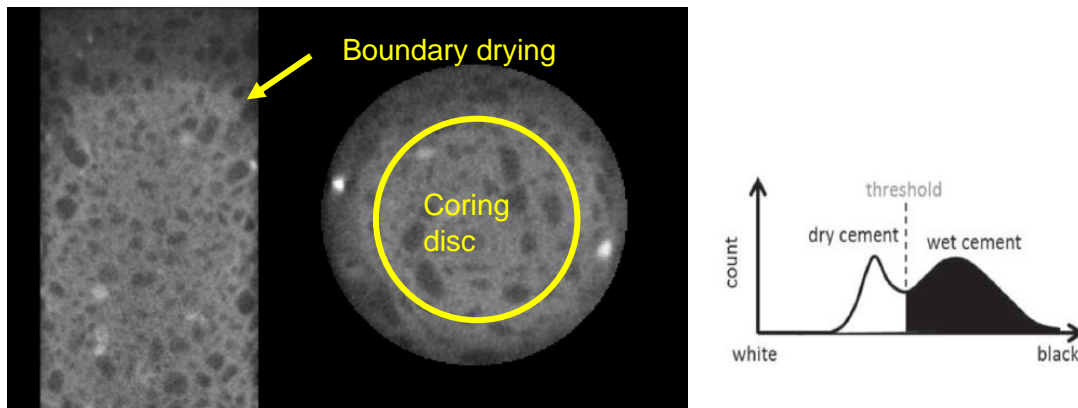


Figure 4 (a) Boundary drying of specimen and the coring range (b) Thresholding method based on the pixel histogram [1].

The cored images assigned with colourmap are shown in Figure 5. The red-orange colour represents dry area, including heat-induced dry area and dry aggregates. Most aggregates are dry and impermeable which makes them distinct from the wet mortar. An additional dried area in the centre of the plain concrete specimen is induced due to cracking. The X-ray image in Figure 8 (b) clearly shows the geometry of the crack, which might be caused by the air bubbles formed during the mixing stage. After 15 min of heating, clear drying fronts occur and they move towards the inner part of the specimen as heating progresses. As the drying migrates further from 45 min, an accelerated drying region can be seen at the left side of both plain concrete and RTPF specimens. This is due to the air bubbles and cavities formation near the thermocouples. It should be noted that the change of concrete microstructure from intrusive sensors is inevitable, despite the small size of the sensors [22].

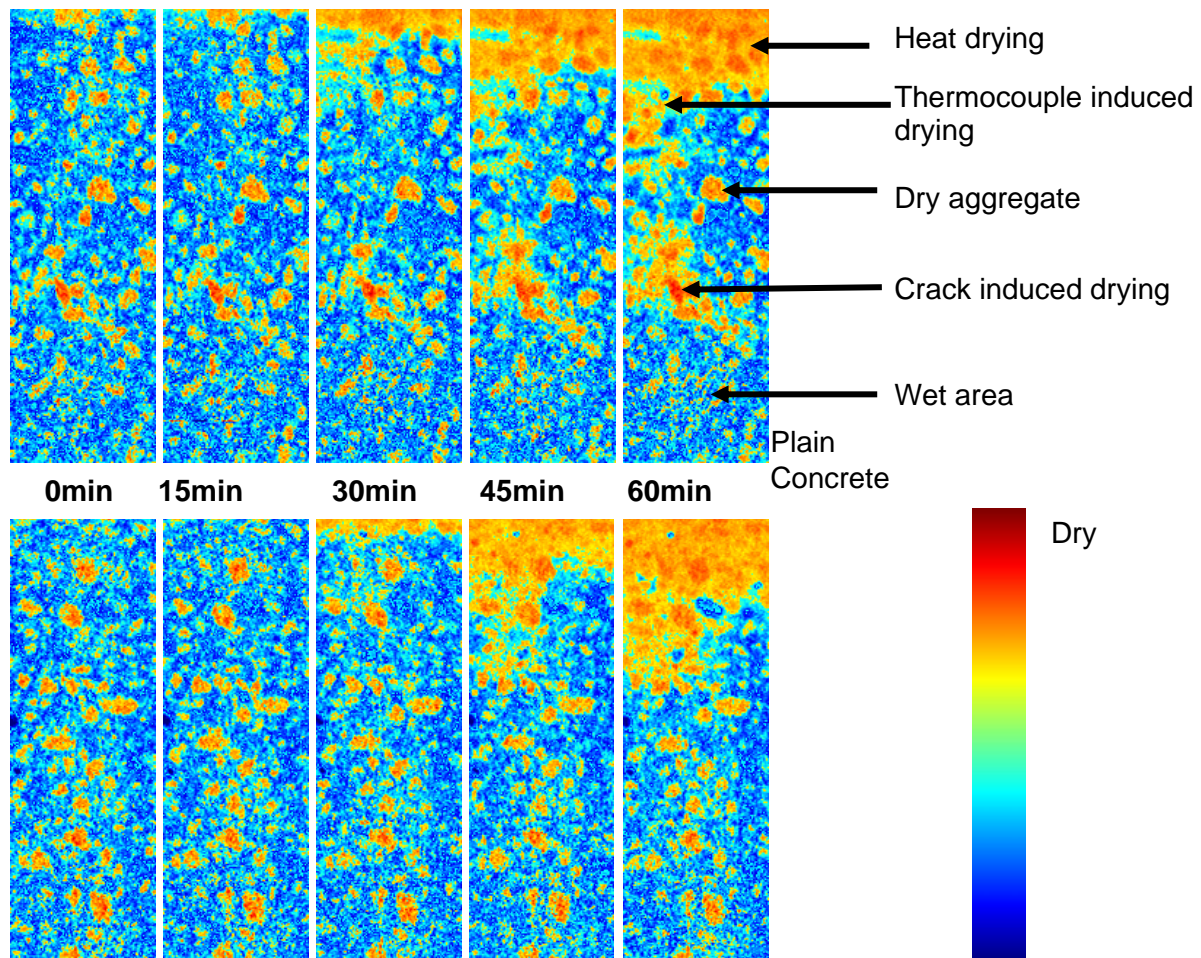


Figure 5 Drying of specimens at multiple, equivalent stages of the test.

To quantify the influence of RTPF on the drying speed, the actual drying rate of both specimens is presented in Figure 6 (a). Based on the pre-defined threshold, the drying volume of each specimen is determined as the ratio of the number of dry pixels to the total number of pixels. Since cracks can largely increase the drying speed and the large crack in the plain concrete exists before heating, the cracked section of the plain concrete and the corresponding section of the RPFT specimen are excluded from the image processing. The initial dry aggregates are also excluded from the processing. Figure 6 (b) shows the results.

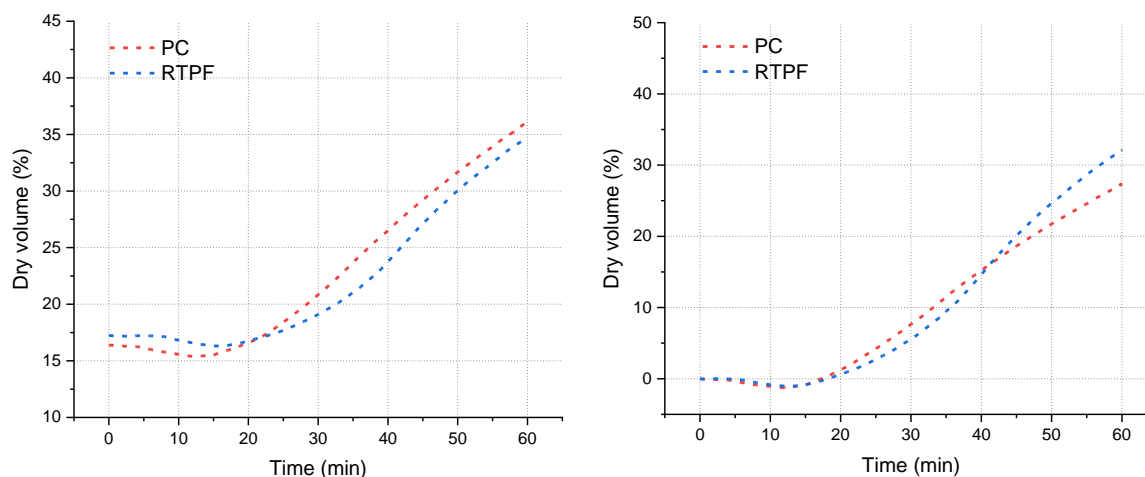


Figure 6 Drying volume ratios (a) with aggregate and pre-heating crack (b) without.

Figure 6 indicates that the dry volume decreases during the initial heating stage and reaches the bottom at 13 min for both specimens. Even the decreased amount stays marginal at 1.25 %, it draws the authors' attention as similar phenomena were observed in past work [18]. The following explanation is proposed to describe this dry volume decrease.

A considerable part (~10 mm) of the specimens reaches 100 °C after 13 min of heating, as shown in Figure 7. Previous studies have observed noticeable increase in pore pressure when concrete reaches 100 °C [9, 14]. This rise in pore pressure drives the water in saturated pores to dry pores. In this research, the imaging threshold will allocate “wet pixels” to the newly formed wet pores to consider this phenomenon. Although there is moisture loss due to heating, it is still very little at this stage. The above mentioned moisture redistribution from saturated pores to dry pores dominates, which explains the decline of dry volume during initial heating. Further analysis will be performed to verify this speculation by looking at the local porous structures.

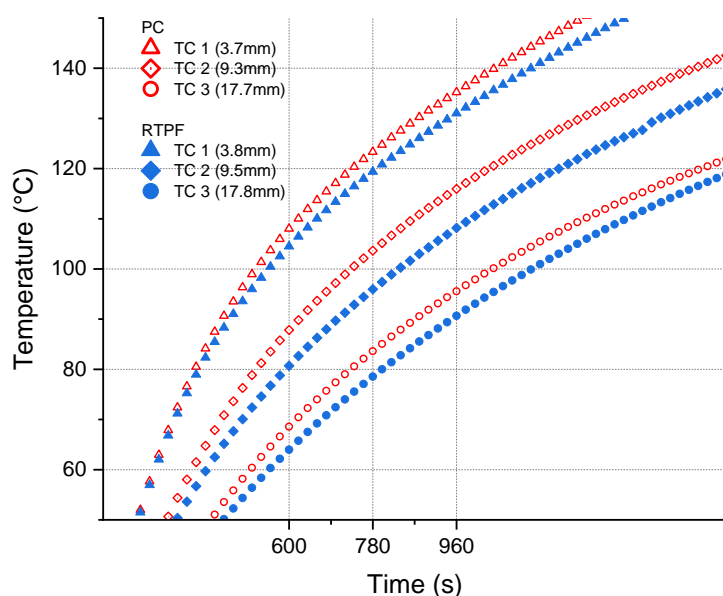


Figure 7 Temperature distribution around 13 min (780s).

To track the moisture accumulation within the concrete, the average grey value of the core of specimens at a given height was computed. Figure 8 (a) shows its evolution against time, with

higher attenuation indicating higher moisture content, highlighted with a colormap. The water accumulation is determined by the difference between the average grey value at a time and the initial value, as shown in Figure 8 (b).

The interface between the high attenuation (blue) and low attenuation (red) zones is defined as the “drying front”. The inclination angle of the drying front indicates the drying rate of the specimen. In Figure 8 (a), the drying rate of RTPF is larger than that of the plain concrete specimen, indicating RTPF might help the moisture migrate towards the inner part of concrete. However, due to the limitation of the specimen quantity, and the cracking of the plain concrete specimen, further research is needed to confirm this. As time progresses, moisture moves deeper into concrete, creating a section that has higher neutron attenuation levels than the original. The highest value of accumulation lies just below the drying front, showing as the brightest area in the water accumulation map, indicating the formation of the “moisture clog”, as shown in Figure 8 (b). The “sawtooth” shape of the map is caused by the air voids around the thermocouples, which shows the correlation between moisture distribution and the pore structure of heated concrete.

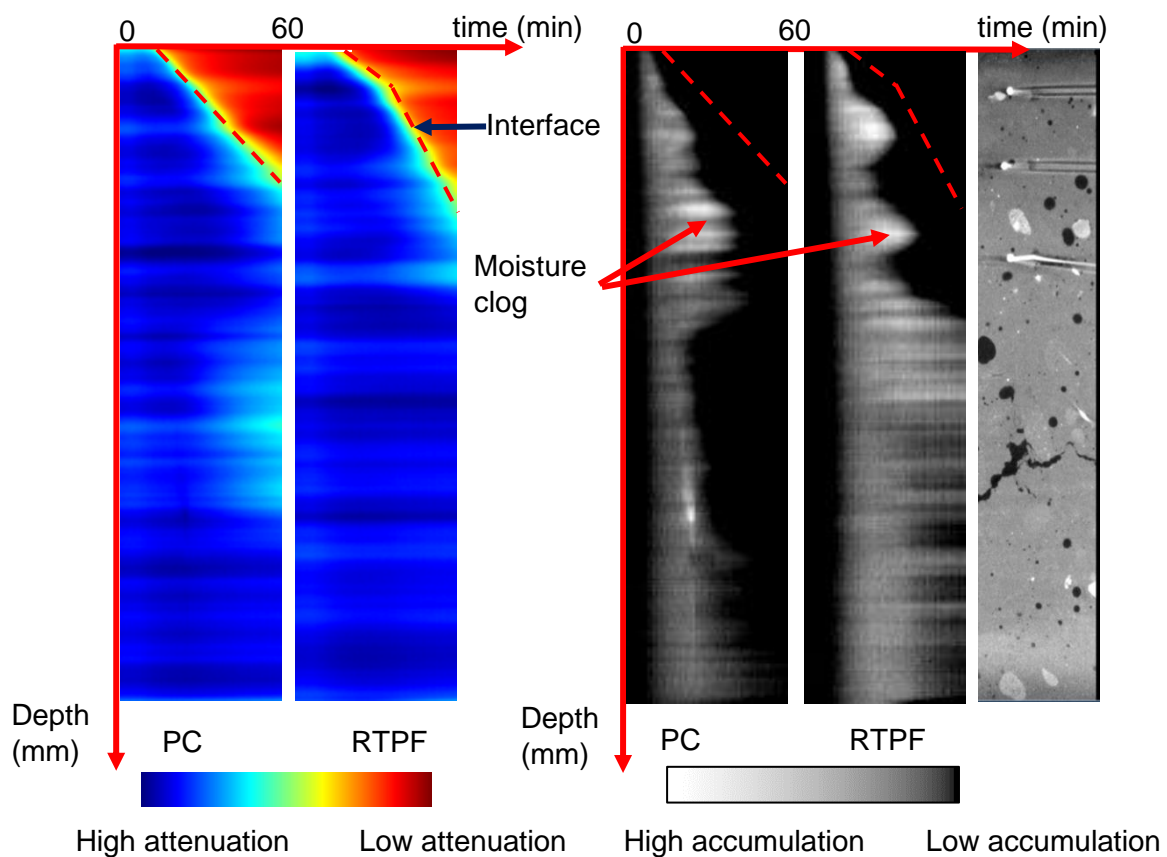


Figure 8 (a) Average grey value map

(b) Water accumulation map.

### X-ray image processing

The X-ray tomography was carried out to investigate the macroporous structure of concrete before and after heating. The image processing method of X-ray tomography is different from neutron because of the difference in image properties. As the density of the aggregates used is of high variability, some aggregates are shown in bright pixels, as highlighted in Figure 9 (a). To correctly identify the pores, the bright aggregates were firstly removed using Otsu's threshold. Then the images were segmented by Otsu's method again to create a binary image, only the pores remained. After applying a median blur, the results are shown in Figure 9 (c). To quantify the influence of RTPF, the sections influenced by cracking and thermocouples were removed. The macropore (pore size above 45  $\mu\text{m}$ ) volume ratios in both specimens before and after heating were summarised in Table 3.

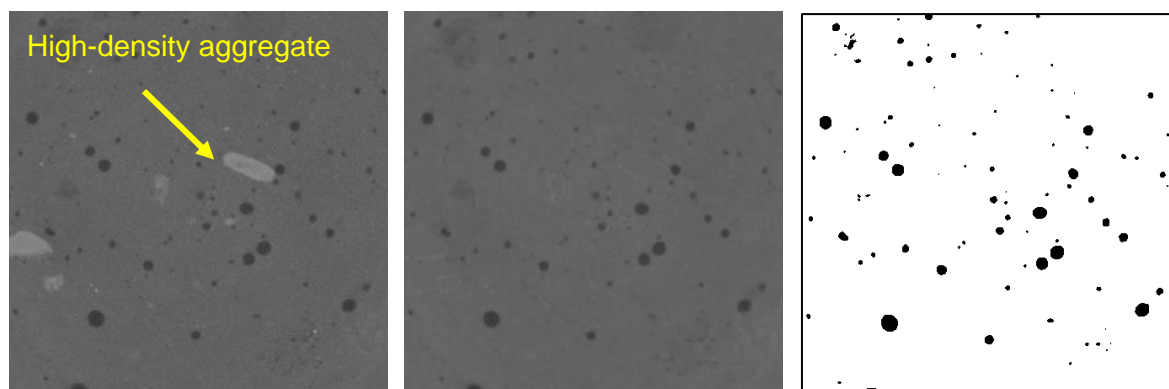


Figure 9 (a) Initial image (b) High-density aggregate moved (c) Binary image of pores.

Table 3 Pore volume ratio of concrete before and after heating

Condition	Initial	Post heating	Initial	Post heating
Sample	Plain concrete	Plain concrete	RTPF	RTPF
Pore ratio (%)	1.95	2.08	3.03	3.19
Change in pore ratio (%)	0.13		0.16	
Change of ratio in percentage (%)	6.7		5.3	

The pore volume ratios of the plain concrete and RTPF specimens both increased after heating, where the initial pore volume ratio of RTPF is higher than that of the plain concrete. The increase of the pore ratio of RTPF after heating is 0.16 %, which is higher than that of the plain concrete (0.13 %). To compare with the initial pore volume, the increase of pore volume ratio in percentage of plain concrete is higher than that of the RTPF specimen, indicating that the addition of RTPF has no major contribution to the increase of macro pores during heating. In the future, higher-resolution X-ray tomography can be conducted to investigate finer pores created by RTPF, with pixel sizes below the average diameter of RTPF, around 15  $\mu\text{m}$ .

## CONCLUSION

This paper presents an investigation of the thermo-hydral behaviour of concrete with recycled fibre, using simultaneous neutron and X-ray tomography scanning. The results reveal a glimpse of the mechanism of RTPF in full-field of heated concrete, demonstrating the substantial power of this novel investigation technique. The following conclusions are drawn based on the findings:

1. The drying rate of the heated RTPF specimen is faster than the plain concrete, indicating the role of RTPF in facilitating the moisture migration process. The effectiveness of RTPF in fire spalling is confirmed again further to previous spalling tests.
2. At the beginning of heating, a decrease in the dry volume is observed, which is speculated to be due to the redistribution of moisture triggered by the rise of pore pressure when the temperature exceeds 100 °C.
3. Water accumulation and the moisture clog theory are confirmed in RTPF fibre added concrete. Preheating cracks (due to poor vibration) and the air voids induced by thermocouples can influence the water accumulation inside the concrete.
4. There is no major influence of RTPF on the macropores (above 45  $\mu\text{m}$ ) of concrete after heating, possibly due to the small diameter of RTPF.
5. Further scanning with higher resolution tomography with more specimens is recommended to future understand the working mechanism of RTPF in fire spalling mitigation.

## ACKNOWLEDGEMENTS

This work has been supported by Institut Laue-Langevin at test instrument D50 T. Data collection is available for ILL user club members at <https://dx.doi.org/10.5291/ILL-DATA.UGA-104>. The test setup is developed by SDP and AT, specimens are prepared by YL and SSH. All authors have participated in planning and testing.

## REFERENCES

1. Dauti, D., et al., Analysis of moisture migration in concrete at high temperature through in-situ neutron tomography. *Cement and Concrete Research*, 2018. **111**: p. 41-55.
2. Jansson, R. and L. Boström, *Factors influencing fire spalling of self compacting concrete*. *Materials and structures*, 2013. **46**(10): p. 1683-1694.
3. Morita, T., et al., An Experimental Study On Spalling Of High Strength Concrete Elements Under Fire Attack. *Fire Safety Science*, 2000. **6**: p. 855-866.
4. Kodur, V.K.R., Spalling in High Strength Concrete Exposed to Fire: Concerns, Causes, Critical Parameters and Cures, in *Advanced Technology in Structural Engineering*. 2000. p. 1-9.
5. BSI, Eurocode 2: Design of concrete structures, in Part 1-2: General rules - Structural fire design. 2004, British Standards Institution: London.
6. Kalifa, P., G. Chene, and C. Galle, *High-temperature behaviour of HPC with polypropylene fibres: From spalling to microstructure*. *Cement and concrete research*, 2001. **31**(10): p. 1487-1499.
7. Bilodeau, A., V.K.R. Kodur, and G.C. Hoff, Optimization of the type and amount of polypropylene fibres for preventing the spalling of lightweight concrete subjected to hydrocarbon fire. *Cement and Concrete Composites*, 2004. **26**(2): p. 163-174.



8. Li, Y., K.H. Tan, and E.-H. Yang, Influence of aggregate size and inclusion of polypropylene and steel fibers on the hot permeability of ultra-high performance concrete (UHPC) at elevated temperature. *Construction and Building Materials*, 2018. **169**: p. 629-637.
9. Bangi, M.R. and T. Horiguchi, Effect of fibre type and geometry on maximum pore pressures in fibre-reinforced high strength concrete at elevated temperatures. *Cement and Concrete Research*, 2012. **42**(2): p. 459-466.
10. Li, Y., et al. Mitigation of Fire-Induced Spalling of Concrete using Recycled Tyre Polymer Fibre. in *Fire Spalling 2019*. 2019. the University of Sheffield.
11. Huang, S.-S., et al., *Reused tyre polymer fibre for fire-spalling mitigation*. Applications of Structural Fire Engineering, 2015.
12. Millard, A. and P. Pimienta, *Modelling of Concrete Behaviour at High Temperature*. 2019: Springer.
13. Kalifa, P., F.-D. Menneteau, and D. Quenard, *Spalling and pore pressure in HPC at high temperatures*. *Cement and concrete research*, 2000. **30**(12): p. 1915-1927.
14. Phan, L.T., *Pore pressure and explosive spalling in concrete*. *Materials and structures*, 2008. **41**(10): p. 1623-1632.
15. Bangi, M.R. and T. Horiguchi, Pore pressure development in hybrid fibre-reinforced high strength concrete at elevated temperatures. *Cement and Concrete Research*, 2011. **41**(11): p. 1150-1156.
16. Choe, G., et al., Effect of moisture migration and water vapor pressure build-up with the heating rate on concrete spalling type. *Cement and Concrete Research*, 2019. **116**: p. 1-10.
17. Dauti, D., et al., Modeling of 3D moisture distribution in heated concrete: From continuum towards mesoscopic approach. *International Journal of Heat and Mass Transfer*, 2019. **134**: p. 1137-1152.
18. Moreira, M.H., et al., Experimental proof of moisture clog through neutron tomography in a porous medium under truly one-directional drying. *Journal of the American Ceramic Society*, 2021. **n/a**(n/a).
19. Kim, H.-T., et al., Reconstruction of concrete microstructure using complementarity of X-ray and neutron tomography. *Cement and Concrete Research*, 2021. **148**: p. 106540.
20. Tengattini, A., et al., *NeXT-Grenoble, the Neutron and X-ray tomograph in Grenoble*. *Nuclear Instruments and Methods in Physics Research Section A: Accelerators, Spectrometers, Detectors and Associated Equipment*, 2020. **968**: p. 163939.
21. Ozawa, M., et al., Preventive effects of polypropylene and jute fibers on spalling of UHPC at high temperatures in combination with waste porous ceramic fine aggregate as an internal curing material. *Construction and Building Materials*, 2019. **206**: p. 219-225.
22. Dauti, D., et al., Some Observations on Testing Conditions of High-Temperature Experiments on Concrete: An Insight from Neutron Tomography. *Transport in Porous Media*, 2020. **132**(2): p. 299-310.



# Performance of metakaolin-based alkali activated concrete at elevated temperatures

Jitong Zhao<sup>1</sup>, Alena Bartsch<sup>1</sup>, Marco Liebscher<sup>1\*</sup>, Thomas Köberle, Viktor Mechtcherine<sup>1</sup>

<sup>1</sup> Technische Universität Dresden, Institute of Construction Materials, 01062 Dresden, Germany

\* Corresponding author (marco.liebscher@tu-dresden.de)

## ABSTRACT

The use of alkaline activated materials (AAM) or geopolymers (GP) as binder materials in concrete attracts in recent years an increasing interest since they can offer comparable mechanical properties to Portland cement-based concrete by enhanced sustainability, lower density, superior thermal properties, and fire resistance. In the present study heat-resistant cement-less concrete matrices for large-scale structural application of fiber-reinforced concrete are investigated. Metakaolin (MK), blast furnace slag, fine and coarse sand aggregates as well as potassium alkali activator have been used to prepare various concrete mixtures. Hot-tested mechanical properties (bending and compression tests) have been investigated for pure metakaolin-made as well as blended metakaolin and slag made alkali activated concrete (AAC) after exposure to elevated temperatures, 100 °C and 200 °C. The incorporation of 30% of slag showed inherently superior flexural and compressive strength of the concrete both at room temperature and elevated temperatures as well as better workability in the fresh status than the pure metakaolin-made concrete, which lie in the same range of ordinary Portland cement (OPC) concrete. Porosity measurements and microscopic observations indicated a denser microstructure without visible cracks and better thermal resistance when using a moderate proportion of the slag presence. In summary, MK–slag based alkali activated concrete system offer a feasible alternative in practical thermal applications for the structure elements.

**KEYWORD:** Geopolymer, Metakaolin, Alkali activated concrete, Elevated temperature, Mechanical properties.

## INTRODUCTION

Due to an increasing demand of infrastructures, ordinary Portland cement (OPC) production is associated with the considerable emission of greenhouse gases [1]. To this end, geopolymers (GP) or alkali-activated materials (AAM) utilising industrial by-products have gained worldwide interest in recent years as a more environmental-friendly alternative binders to reduce the carbon footprint [2]. As precursor materials silicon- (Si) and aluminium-rich (Al) metakaolin (MK) [3] or low calcium fly ash [4,5] as well as high calcium fly ash [6] and blast furnace slag [7] can be used for their production. MK was adopted in current studies as the main alumina-silicate binder on pure paste [8,9], mortar [10] or concrete [11] due to its high rate of dissolution in the reactant solution, its homogenous properties across different

manufacturers and superior bond strength in repairing [12]. However, it requires high water demand to meet favourable workability and cost for manufacturing [11].

GP combine unique properties and structural characteristics of polymers, ceramics, and cements to some extent, which exhibits comparable mechanical strength to OPC, exceptional heat/fire resistance, high durability, low shrinkage, no degradation under UV light, high corrosion-resistance to all organic solvents and acids and good adhesion with fiber substrate [13–17]. They are usually recognized in the existing literature as a special type of alkali-activated materials with low Ca and higher Al and alkali (Na, K) contents and essentially three-dimensional molecule structure [18–21].

The introduction of calcium supplied from latent hydraulic slag into the system results in the formation of calcium silicate hydrate or calcium aluminum silicate hydrate (CASH), while hindering the formation of 3D network structure in GP gel [22]. The binders and their reaction products will evidently influence both early and late age properties of alkali activated concrete including the workability, curing regime, setting time, mechanical properties, pore structure and durability [23]. The AAM synthesized by pure slag or high slag content generally delivers high compressive strength, even over 100 MPa, but at the cost of low workability and high shrinkage [23]. Hence, slag is mostly applied as additives mixed with other raw materials to enhance the ambient temperature curing capacity [24].

For construction safety, such as in the case of fire, it is necessary to gain a deep understanding about the thermal behaviour of AAM concrete. Conventional OPC may suffer to fire attack during their service life, resulting in severe structural damages and property losses [25,26]. AAM systems, independent on the precursors and post-treatment, generally present superior stability when exposed to high temperatures than OPC [27]. Therefore, this research aims to assess the thermal behaviour of concrete based on binder systems made with metakaolin with or without slag exposed to high temperature through microstructural and mechanical property characterizations.

## **EXPERIMENTAL PROGRAM**

### **Materials and production of samples**

High reactive MK powder (trade name METAMAX), supplied by BASF, Ludwigshafen, Germany and ground-granulated blast-furnace slag (GGBS) powder, supplied by Dyckerhoff, Niederorschel, Germany, were used as binder materials in concrete. A pre-dried, light-colored sand (0/2 mm) from Ottendorf, Germany, with a maximum grain size of 2 mm was used as the coarse aggregate. The quartz sand BCS 413 from Strobel, Germany, with a maximum particle size of 0.3 mm was selected as macro-fillers. An industrial potassium silicate solution Geosil® 14517 from Woellner, Ludwigshafen, Germany, with a  $\text{SiO}_2/\text{K}_2\text{O}$  molar ratio of 1.7 and water content of 55% was used as the activating alkali liquid. Note, a better flowability and fewer volumetric deformation at elevated temperatures are usually suggested for the K-based activator in comparison with the Na-based activator [28–31]. The partial replacement of MK with 30% slag yielded in a reduction in water-to-binder ratios (W/B) from 0.65 to 0.55, due to the less water demand of the slag. A moderate proportion of slag in the range of 20% to 30% is recommended in respect of compressive strength, workability, setting time and low shrinkage in past work [32].

To prepare the mixtures, a 5L-planetary mixer HSM20 from Hobart, Leipzig, Germany, was used. Mixing comprised the following processes, (i) dry-mixing of the MK/slag powder for 1 min

at low speed of 198 rpm; (ii) addition of the activator liquid; (iii) mixing for another 5 min; (iv) addition of the activator liquid; (v) mixing for another 3 min followed by high speed mixing (at 365 rpm) for 2 min and again low speed mixing for 1 min. The fresh mixtures were cast into prismatic moulds with dimensions of 40\*40\*160 mm<sup>3</sup> and compacted using a vibrating table. The specimens were demoulded 20 h after casting and stored under polyethylene foils at 20 °C and 65% relative humidity until 28 days. The flowability was determined by means of a Hägermann slump funnel in accordance with DIN EN 1015-3 [33] without strokes. The characteristic values determined with the empirical rheological methods indicated similar flowability for the both concrete mixtures when taking into account the small variation.

Particle size distribution of the solid components was determined using a laser diffraction particle size analyser LS 13320 from Beckmann Coulter, USA; see Table 1. The effective measuring range of the laser particle sizer is limited to less than 2 mm.

Table 1. Grain size transitions  $d_5$ ,  $d_{50}$  and  $d_{95}$  of all solid materials used for the concrete matrices.

Particle finesse	Density [g/cm <sup>3</sup> ]	$d_{10}$	$d_{50}$	$d_{95}$
Metakaolin	2.5	0.65	2.84	9.72
Slag	2.9	0.76	7.87	32.45
Fine sand BCS 413	2.7	94.5	152.1	220.3
Sand Ottendorf 0/2	2.7	213	712	1715

Table 2. Chemical composition of binder materials used of concrete matrices.

Element compositions	SiO <sub>2</sub>	Al <sub>2</sub> O <sub>3</sub>	CaO	Fe <sub>2</sub> O <sub>3</sub>	TiO <sub>2</sub>	K <sub>2</sub> O	Others
Metakaolin	53.0	43.8	0.02	0.4	1.7	0.2	S, Mg, Na
Slag	33.6	8.4	47.5	-	1.4	-	S, Mg

Table 3. Mix designs of the alkali activated concrete matrices used.

Concrete composition	100% MK	70% MK 30% Slag
	[g]	
Metakaolin	519	363
Ground-granulated blast-furnace slag		156
Fine sand BCS 413	264	264
Sand 0/2 (Ottendorf)	759	759
Potassium silicate solution	613	519
<b>Properties</b>		
Mortar slump flow [mm]	182	190

### Characterisation of concrete specimens

Three-point bending tests were performed using a servo-hydraulic universal testing machine (max. load capacity: 200 kN) on mortar prisms with a span of 100 mm in accordance with DIN EN 196-1 [34]. At least 3 specimens for each series were tested under a displacement rate of 1 mm/min of the cross-head. Before testing, heating was conducted in an electric furnace from

Memmert GmbH + Co. KG, Schwabach, Germany. A gradual increase of 3 °C/min upon reaching the target temperatures is followed by 2 h and 4 h of heating at 100 °C and 200 °C, respectively, to ensure complete evaporation of water. The duration required to heat up the entire specimen was determined using a type-K thermocouple embedded in the centre of the prism concrete block in the preliminary test. After the heating process, the specimens were immediately tested, representing a “quasi in-situ” experiment.

The morphological observations on the fracture surfaces were carried out using an environmental scanning electron microscope (ESEM) Quanta 250 FEG from FEI, Eindhoven, the Netherlands. Pore size distributions were measured by mercury intrusion porosity (MIP) measurements through a Porotec Porosimeter PASCAL 140/440 with a mercury surface tension of 0.48 N/m, a contact angle of 140° and testing pressure ranging from 0 to 400.71 MPa. Before the analysis, all specimens were treated with iso-propanol to remove free pore water and were subsequently dried by solvent evaporation.

## RESULTS AND DISCUSSION

The variation of hot-tested mechanical properties and density of the ambient-cured concrete after exposure to (~20 °C), 100 °C and 200 °C are summarized in Table 4. Figure 1 gives a comparison of the curves of the strength retention. The addition of 30% slag resulted in increased flexural and compressive strengths as well as density, which can be traced back to an increase C-A-S-H content by the introduced CaO from the slag, faster dissolution in alkaline environments and accelerated chemical reactions of the aluminosilicate minerals [35]. With increasing testing temperatures, the flexural strength of both concrete matrices decreased gradually arising from the excessive dehydration of alkali-activated materials and the respective thermal shrinkage/expansion. A similar decreasing phenomenon has been observed for the hot-tested compressive strength of the pure MK system. Conversely, the exposure to elevated temperatures led to a slight increase in MK/slag blended system.

*Table 4. The average flexural and compressive strength and density of fine-grained, alkali-activated concrete matrices containing pure MK and 70% MK with 30% slag from 20 °C to 200 °C standard deviations are given in parentheses.*

Exposure temperature [°C]	Flexural strength [MPa]		Compressive strength [MPa]		Density [g/cm <sup>3</sup> ]	
	100% MK	70% MK 30% slag	100% MK	70% MK 30% slag	100% MK	70% MK 30% slag
20	7.44 (0.51)	8.89 (1.13)	62.77 (3.72)	66.81 (5.02)	2.00 (0.03)	2.08 (0.01)
100	5.44 (0.56)	7.32 (0.27)	59.90 (3.85)	71.14 (1.88)	1.89 (0.03)	2.02 (0.01)
200	4.39 (0.27)	4.88 (0.09)	53.29 (2.07)	74.98 (2.95)	1.77 (0.04)	1.90 (0.02)

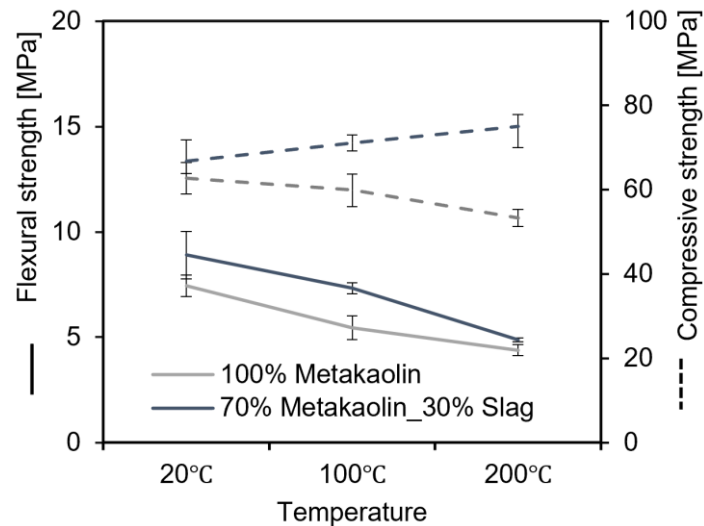


Figure 1 Temperature impact on the mechanical strength of unblended and blended MK/slag concrete.

Figure 2 shows the morphologies of the concrete specimens with 0 and 30 mass% slag at 20 °C and 200 °C, respectively. The pure metakaolin-based structure at ambient temperature show a relatively dense morphology of reaction products with high content of unreacted or partially reacted residual MK particles (Fig. 2e and f). Voids at the nanoscale were formed in the material's microstructure from dissolving MK particles [15]. The relatively high proportion of unreacted particles might enhance the damage evolution through the thermal expansion. In contrast, the concrete with 30 mass% slag presented a denser structure with less unreacted MK and without significant laminar structure, which demonstrates that the addition of slag results in tighter packing of the constituent particles. Hence, slag can accelerated the formation of connected gel-like structure [23]. Note, the sand components were also well compacted by the binder materials used; see Fig. 2a and b.

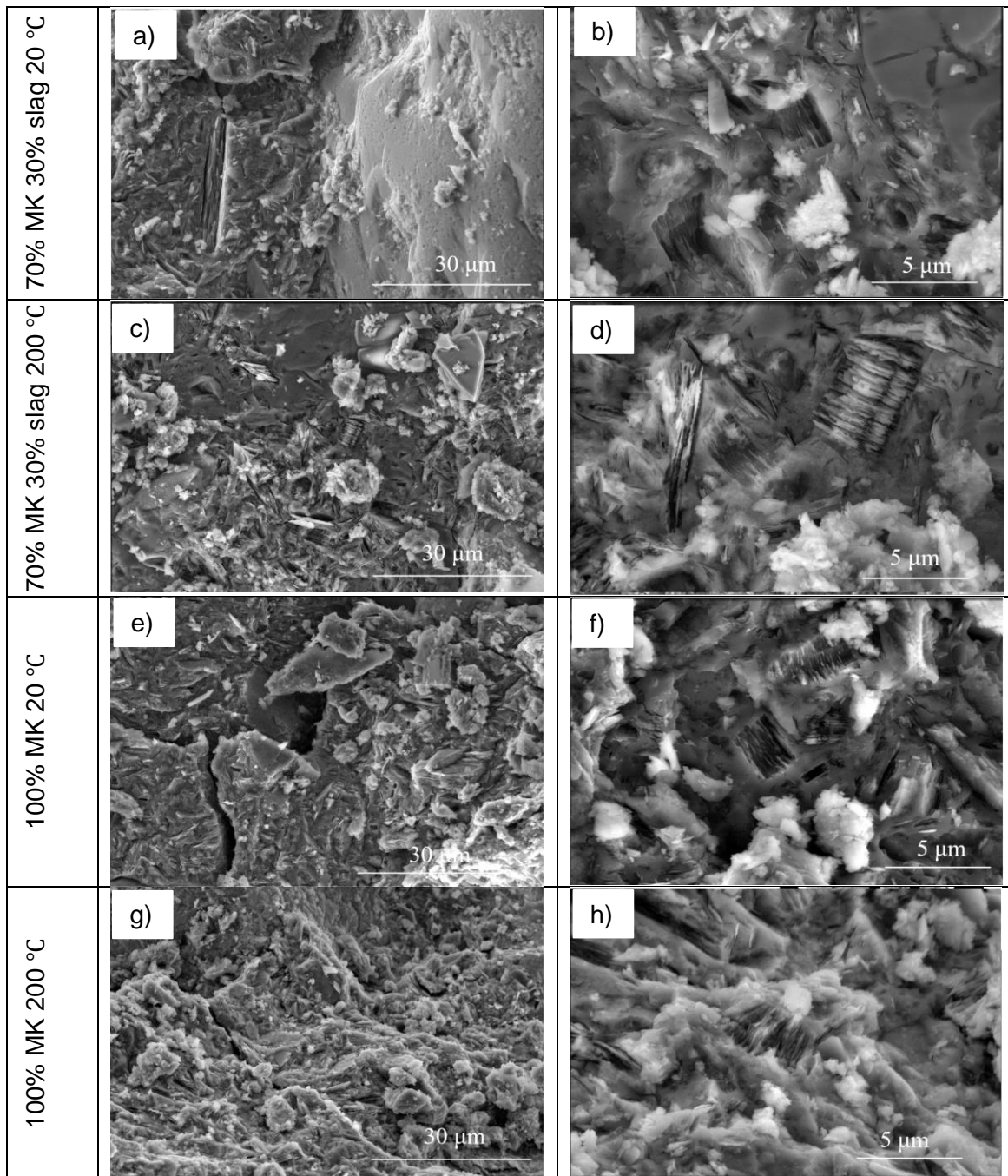


Figure 2 SEM images of ambient cured concrete containing (a-d) 0% and (e-h) 30% slag as partial replacement for MK at 20 °C and 200 °C.

At higher temperatures, the unblended and blended concrete matrices indicated an increasing size of voids, accompanied by increases in the numbers of voids. A smooth, more compact and less damaged gel microstructure can still be seen in the blended MK/slag concrete (Fig. 2c and d), which confirms a high strength after heating. The unblended system revealed a loose and less compacted microstructure, but with a reduced content of unreacted particles (Fig. 2g and h).

To further elaborate the impact of the slag and elevated temperatures on the pore structure of the alkali-activated concretes, the pore size distribution is shown in Fig. 3. Owing to the improvement of the particle packing by combining different particle sizes and the introduction

of calcium-based reaction products, the total pore volume effectively reduced, especially large pores. With increase of the elevated temperatures, both concrete matrices revealed an increasing number and size of pores. Among them, the macropores and the total pore volume of the MK/slag blended system was evidently lower than that of the pure MK system under temperature loading, confirming a densification of the structure and enhancement in strength evident in ESEM analyses.

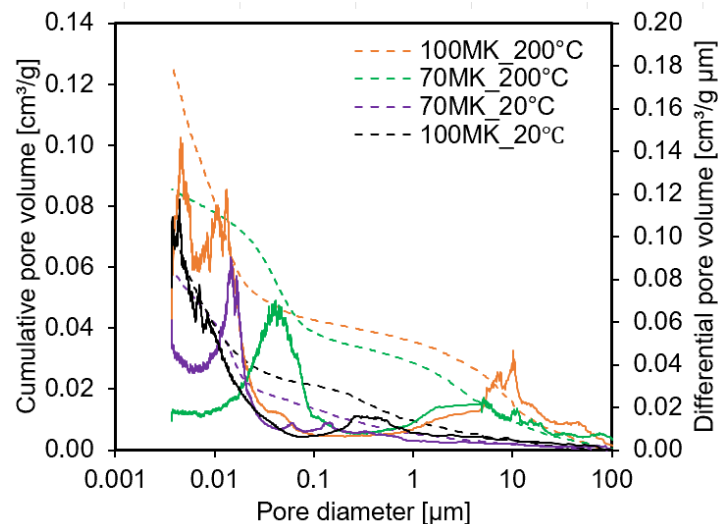


Figure 3 Total pore volume and pore size distribution of the alkali-activated concretes depending on the slag content and heating temperatures.

## CONCLUSION

In this work, the performance of the alkali-activated concrete based on pure MK binder system and combined MK/slag binder system at elevated temperatures was investigated regarding their physical behaviour, mechanical strength and microstructural changes.

Pure MK system presented an intermediate hardening time within the first 24 h while blended MK/slag system yielded in a relatively fast hardening. The blended and unblended systems in this study indicated sufficient flowability required for the continuous or discrete fiber reinforcement with appealing mechanical performances. The morphology and size of the slag particle resulted in enhanced flowability and component packing of concrete. The blended MK/slag precursors, and Ca content contribute to developing higher flexural and compressive strength. MIP and morphological observations demonstrated that the slag addition can reduce the pore size and number effectively, and produced a denser gel structure, a more homogenous surface, a lower content of unreacted material and an increased density. After exposure to elevated temperatures up to 200 °C, both concrete systems showed reductions in flexural strength and significantly more porous microstructures. However, the blended MK/slag concrete increased the compressive strength slightly arising from a denser structure without visible cracks after heating.

The follow-up study should focus on the effects of higher temperatures and dimensional stability as well as the application in fiber-reinforced concrete and macroscale structural elements.



## REFERENCES

1. Abed. Turkey, F., Bt. Beddu, S., Najah Ahmed, A., Al-Hubboubi, S., "A review – Behaviour of geopolymer concrete to high temperature", *Materials Today: Proceedings* 2021.
2. Kumar Sarker P., Kelly S., Yao Z., "Effect of fire exposure on cracking, spalling and residual strength of fly ash geopolymer concrete", *Materials and Design*, **63**, 2014.
3. Davidovits J., "High-Alkali Cements for 21st Century Concretes", *Special Publication*, **144**, 383–398, 1994.
4. Hardjito D., Wallah SE., Sumajouw DMJ., Rangan BV., "On the development of fly ash-based geopolymer concrete", *ACI Materials Journal*, **101**, 467–472, 2004.
5. Fernández-Jiménez AM., Palomo A., López-Hombrados C., "Engineering properties of alkali-activated fly ash concrete", *Materials Journal*, **103**, 106–112, 2006.
6. Chindaprasirt P., Chareerat T., Sirivivatnanon V., "Workability and strength of coarse high calcium fly ash geopolymer", *Cement and Concrete Composites*, **29**, 224–229 2007.
7. Partha SD., Pradip N., Prabir KS., "Strength and permeation properties of slag blended fly ash based geopolymer concrete", *Advanced Materials Research*, **651**, 168–173, 2013.
8. Ozer I., Soyer-Uzun S., "Relations between the structural characteristics and compressive strength in metakaolin based geopolymers with different molar Si/Al ratios", *Ceramics International* **41**, 10192–10198, 2015.
9. Kuenzel C., Vandeperre LJ., Donatello S., Boccaccini AR., Cheeseman C, "Ambient temperature drying shrinkage and cracking in metakaolin-based geopolymers", *Journal of the American Ceramic Society* **95**, 3270–3277, 2012.
10. Pacheco-Torgal F., Moura D., Ding Y., Jalali S, "Composition, strength and workability of alkali-activated metakaolin based mortars", *Construction and Building Materials* **25**, 3732–3745, 2011.
11. Pouhet R., Cyr M., "Formulation and performance of flash metakaolin geopolymer concretes", *Construction and Building Materials* **120**, 150–160, 2016.
12. Alanazi H., Yang M., Zhang D., Gao Z., "Early strength and durability of metakaolin-based geopolymer concrete", *Magazine of Concrete Research* **69**, 46–54, 2016.
13. Zhao J., Wang K., Wang S., Wang Z., Yang Z., Shumuye ED., et al, "Effect of Elevated Temperature on Mechanical Properties of High-Volume Fly Ash-Based Geopolymer Concrete, Mortar and Paste Cured at Room Temperature", *Polymers (Basel)*, **13**, 2021.
14. Zhao J., Liebscher M., Tzounis L., Mechtcherine V., "Role of sizing agent on the microstructure morphology and mechanical properties of mineral-impregnated carbon-fiber (MCF) reinforcement made with geopolymers", *Applied Surface Science* **567**, 150740, 2021.
15. Zhao J., Liebscher M., Michel A., Junger D., Trindade ACC., Silva F de A, et al., "Development and testing of fast cured mineral impregnated carbon fiber (MCF) reinforcements based on geopolymers from metakaolin", *Cement and Concrete Composites* **116**, 103898, 2021.
16. Junger D., Liebscher M., Zhao J., Mechtcherine V., "Joule heating as a smart approach in enhancing early strength development of mineral-impregnated carbon-fibre composites (MCF) made with geopolymer", *Composites Part A: Applied Science and Manufacturing* **153**, 106750, 2022.
17. Zhao, J., Liebscher, M., Schneider, K., Junger, D., Mechtcherine, V., "Influence of Processing Conditions on the Mechanical Behavior of Mineral-Impregnated Carbon-Fiber (MCF) Made with Geopolymer", In: 10th International Conference on FRP

- Composites in Civil Engineering. CICE 2021. Lecture Notes in Civil Engineering, Springer, Cham 198, 2022.
18. Provis JL., "Alkali-activated materials", *Cement and Concrete Research*, **114**, 40–48, 2018.
  19. Lecomte I., Henrist C., Liégeois M., Maseri F., Rulmont A., Cloots R., "(Micro)-structural comparison between geopolymers, alkali-activated slag cement and Portland cement", *J Eur Ceram Soc*, **26**, 3789–3797, 2006.
  20. Duxson P., Provis JL., Lukey GC., Separovic F., van Deventer JSJ., "Si NMR Study of Structural Ordering in Aluminosilicate Geopolymer Gels", 2005.
  21. Rahier H., Simons W., van Mele B., Ans MB., "Low-temperature synthesized aluminosilicate glasses Part III Influence of the composition of the silicate solution on production, structure and properties", *Journal of materials science* **32**, 2237–2247, 1997.
  22. Ferone C., Colangelo F., Cioffi R., Montagnaro F., Santoro L., "Mechanical Performances of Weathered Coal Fly Ash Based Geopolymer Bricks", *Procedia Engineering* **21**, 745–752, 2011.
  23. Puligilla S. and Mondal P., "Role of slag in microstructural development and hardening of fly ash-slag geopolymer", *Cement and Concrete Research* **43**, 70–80, 2013.
  24. Zhang P., Gao Z., Wang J., Guo J., Hu S., Ling Y., "Properties of fresh and hardened fly ash/slag based geopolymer concrete: A review", *Journal of Cleaner Production* **270**, 122389, 2020.
  25. Ma Q., Guo R., Zhao Z., Lin Z., He K., "Mechanical properties of concrete at high temperature—A review", *Construction and Building Materials* **93**, 371–383, 2015.
  26. Bernal SA., Rodríguez ED., Mejía De Gutiérrez R., Gordillo M., Provis JL., "Mechanical and thermal characterisation of geopolymers based on silicate-activated metakaolin/slag blends", *Journal of Materials Science* **46**, 5477–5486, 2011.
  27. Trindade, A. C. C., Liebscher, M., Curosu, I., de Andrade Silva, F., Mechtcherine V., "Influence of elevated temperatures on the residual and quasi in-situ flexural strength of strain-hardening geopolymer composites (SHGC) reinforced with PVA and PE fibers", *Construction and Building Materials* **314**, 125649, 2021.
  28. Lahoti M., Wong KK., Tan KH., Yang EH., "Effect of alkali cation type on strength endurance of fly ash geopolymers subject to high temperature exposure", *Materials and Design* **154**, 8–19, 2018.
  29. Duxson P., Lukey GC., van Deventer JSJ., "Thermal evolution of metakaolin geopolymers: Part 1 – Physical evolution", *Journal of Non-Crystalline Solids* **352**, 5541–5555, 2006.
  30. Kong DLY., Sanjayan JG., Sagoe-Crentsil K., "Factors affecting the performance of metakaolin geopolymers exposed to elevated temperatures", *Journal of Materials Science* **43**, 824–831, 2007.
  31. Fang G., Ho WK., Tu W., Zhang M., "Workability and mechanical properties of alkali-activated fly ash-slag concrete cured at ambient temperature", *Construction and Building Materials* **172**, 476–487, 2018.
  32. Schneider K., Butler M., Mechtcherine V., "Carbon Concrete Composites C3 – Nachhaltige Bindemittel und Betone für die Zukunft", *Beton- und Stahlbetonbau* **112**, 784–794, 2017.
  33. DIN EN 1015-3 : methods of test for mortar for masonry - part 3: determination of consistence of fresh mortar (by flow table), 2007.
  34. DIN EN 196-1 - Methods of testing cement - Part 1: Determination of strength, 2016.

35. Chen L., Wang Z., Wang Y., Feng J., "Preparation and Properties of Alkali Activated Metakaolin-Based Geopolymer", *Materials* **9**, 767, 2016.

## Concrete drying kinetics: development of an accelerated drying protocol for fire testing

T. Sayari<sup>1,2,\*</sup>, T. Honorio<sup>1</sup>, S. Mohaine<sup>2</sup>, F. Robert<sup>2</sup>, J.-L. Adia<sup>3</sup>, M. Lion<sup>4</sup>, P. Gotteland<sup>5</sup>, C. Clergue<sup>6</sup>, L. d'Aloia<sup>7</sup>, F. Benboudjema<sup>1</sup>

<sup>1</sup> Université Paris-Saclay, CentraleSupélec, ENS Paris-Saclay, CNRS, LMPS - Laboratoire de Mécanique Paris-Saclay, Gif-sur-Yvette, France

<sup>2</sup> Centre d'Essais au Feu du CERIB (Centre d'Etude et de Recherche de l'Industrie de Béton), Epernon, France

<sup>3</sup> EDF Lab. Les Renardières, Département MMC, Moret-sur-Loing, France

<sup>4</sup> EDF, Direction Industrielle, Département TEGG, Aix-en-Provence, France

<sup>5</sup> FNTF, Direction Technique Recherche, Paris, France

<sup>6</sup> EIFFAGE – Génie Civil, Département Innovation Représentation Matériaux (D.I.R.M.), Vélizy Villacoublay, France

<sup>7</sup> Centre d'Etudes des Tunnels (CETU), Bron, France

\* Corresponding autor (takwa.sayari@ens-paris-saclay.fr)

### ABSTRACT

The fire behavior of concrete elements is dependent on the moisture content of the material. In fire test standards, the tests are performed on specimens after at least three months of storage in an ambient atmosphere. These tests are costly and time-consuming, and their representativity when it comes to moisture content can be questioned, i.e., the concrete at three months will not have the amount of water it would have after several years of service. Water content could be measured using destructive or non-destructive tools and it could be estimated numerically. This work proposes an accelerated drying protocol that allows reaching a hydric and mechanical state representative of normal service conditions of concrete structural elements. The short-term study of water profile monitoring and spalling susceptibility for the two modes of drying will be presented in this paper, i.e., the standardized 3-month drying and the representative accelerated drying. An experimental campaign on four concrete mixes is carried out, including drying tests (ambient and accelerated) and fire spalling tests at different storage times and types. In parallel, the accelerated drying protocol is proposed based on the drying modeling at moderate temperatures. According to the predictive study, a target moisture content can be achieved under several drying conditions: standardized drying and representative accelerated drying. It is shown that accelerated drying protocols can be defined in an extensive range of temperatures, meaning that ad hoc solutions can be proposed. The temperature chosen for our study is 40°C to reduce any microstructural changes. The accelerated drying protocol has been built based on this temperature. The reproducibility of the protocol is essential to broaden its applicability in both research and industrial laboratories.

**KEYWORD:** Concrete drying, water content, spalling, drying kinetics

## INTRODUCTION

The fire behavior of concrete is a critical aspect of civil engineering since spalling can lead to durability and safety problems. Fire characterization tests are therefore required to study and prevent spalling. The spalling of concrete is a complex phenomenon involving several mechanisms, such as water vapor pressure, liquid water thermal pressurization, thermomechanical stresses, and deformation incompatibility between cement paste and aggregates [1]–[4]. Furthermore, spalling depends on the hydric state and material permeability [5]. The fire resistance test standard NF EN 1363-1 [6] stipulates that at the testing time, the condition of the specimen should be representative of its normal service condition (mechanical strength and water content), considered to be obtained at equilibrium after storage in an ambient atmosphere 23°C and around 50% RH. This storage mode has been estimated initially from the temperature and relative humidity evolution in buildings and is used later for all constructions. A conditioning period of at least three months is preconized. Therefore, drying processes play a crucial role in the characterization of concrete susceptibility to spalling and should be studied carefully. Concrete drying is a complex phenomenon involving several mechanisms, i.e., molecular diffusion, Knudsen diffusion, surface diffusion, pore-blocking and/or cavitation, sorption and sorption-induced deformations, and permeation [7]. The hydric and hygric gradient between the material and its external environment generates the movement of liquid water, water vapor, and dry air. Several research works describe the drying mechanisms [8]–[10] and show that concrete drying occurs in two main stages. The first stage is fast, lasts only a few hours to a few days, and is generally associated with liquid water permeation. The second stage is much slower and evolves as a square root of time. This last phase is even slower in massive structures. Thus, the recommended conditioning period may overestimate the susceptibility to spalling when combined with high water content. This shortcoming is also reported by [11], who observed that a longer standardized conditioning period reduces the susceptibility of concrete to spalling.

Our study aims to optimize the conditioning mode (duration, temperature, and relative humidity) through the definition of a hydric state representative of a structure with a few years of operation. The approach adopted is based on an experimental and numerical study of drying in concrete in addition to a campaign of characterization of spalling in the various modes of conditioning. The drying experimental campaign allows to identify the material parameters (porosity, density, etc.), to characterize the drying kinetics (desorption isotherm test, mass loss monitoring, water content measurement, etc.), and to validate the numerical predictions of the water profiles in concrete structures. The fire tests will enable a comparison of the spalling, first, in the case of a normalized drying in both short and long terms (3 months and two years) to evaluate the representativity of the existing protocol. And second, in the case of a representative, accelerated drying in both short and long terms to conclude about the effectiveness of the proposed protocol.

## MATERIAL AND METHODS

### Materials

Four mix designs covering two categories of concrete were selected for this study: two high-performance concretes (PERFDUB38 [12] and PERFDUB41 [12]), and two ordinary concretes (VERCORS [13] and CETU). Table 1 below shows the main characteristics of each concrete. The average compressive strength  $f_{cm}$  is measured at 28 days on 12 specimens per concrete

mix (cylinder specimens). The porosity is measured at 28 days, also according to the AFPC-AFREM recommendations [14].

Table 1. The main characteristics of the studied concrete formulations.

Concrete formula	Binder/additive	$f_{cm}$ [MPa]	Porosity [%]
PERFDUB38 [12]	CEM I 52.5 N + 8.4 % of silica fume	86 ± 2.3	12.3 ± 0.2
PERFDUB41 [12]	CEM I 52.5 N +25 % of metakaolin	93 ± 3.3	11.7 ± 0.2
VERCORS [13]	CEM I 52.5 N	45 ± 2.0	15.4 ± 0.3
CETU (Centre d'Etudes des Tunnels) (Containing polypropylene fibers 300g/m <sup>3</sup> )	CEM I 52.5 N	44 ± 3.3	21.1 ± 0.9

## Concrete drying simulation

### Drying at an ambient temperature

We briefly recall the nonlinear diffusion equation describing concrete drying. The formulation is based on the assumption of mass conservation. It allows simulating the movement of water in its liquid and vapor forms in cementitious materials using the Darcy and Fick laws [15]. This model does not consider the cement hydration couplings and the wall effects. The liquid phase is assumed to be incompressible, so the density is constant. The gaseous phase decomposes into dry air and water vapor. A constant temperature of 23 °C is considered [16], [17]. The Van Genuchten model is used to simulate the desorption isotherm [18]. The balance equation used in the simulation reads:

$$\rho_l \left[ \Phi \left( 1 - \frac{\rho_v}{\rho_l} \right) \right] \frac{\partial S_l}{\partial t} = \text{div} \left[ \frac{\partial p_c}{\partial S_l} (K_{eq}) \text{grad}(S_l) \right] \quad (1)$$

Where  $\rho_l$  is the liquid density,  $\rho_v$  is the vapor density,  $\Phi$  is the porosity,  $p_c$  is the capillary pressure,  $S_l$  is the liquid water saturation degree,  $\mu_l$  is the dynamic liquid water viscosity,  $K_{eq}$  is the equivalent apparent permeability,  $T$  is the temperature, and  $t$  is the time.

The transport properties are identified on experimental mass loss curves. The parameters of the Van Genuchten model are determined by the least-squares method using experimental desorption isotherm curves. Boundary conditions are Dirichlet-type ones, shown to be sufficient to simulate drying in cementitious materials [10], [19], [20].

### Drying at a moderate temperature

The choice of temperature is limited to moderate temperatures (up to 60 °C) [21] in order to avoid any significant microstructural changes. For this study, the temperature is taken equal to 40 °C ± 2°C. The equivalent transfer coefficient is used in the drying simulation, as shown in equation (1). The temperature effect on the material parameters (porosity, density, intrinsic permeability, etc.) is negligible [6]. We explicitly account for the temperature dependence of

the water viscosity, the saturation vapor pressure [22], and the desorption isotherm [23]. The same method performed at 23°C is used to identify the transfer and desorption isotherm parameters (use of experimental mass loss and isotherm curves at 40°C).

### **Experimental program**

The reference geometry corresponds to the specimens of the fire test, *i.e.*, slabs of dimensions 1.7 x 1 x 0.3 m<sup>3</sup>. Given the difficulty of directly monitoring the drying in the slabs, the numerical study and the characterization of moisture content profile evolution are carried out on cylinders Ø 15x30 cm, which dry unidirectionally along with the height of the specimen. This drying mode is representative to the one occurring on the middle of the slab.

#### *Drying kinetics characterization*

The experimental characterization of the drying process consisted firstly of measurements, at both 23°C and 40°C, of mass loss, porosity, and desorption isotherms for the numerical identification of the concrete transfer parameters. Secondly, water content measures were carried out at different conditioning durations to validate the numerical prediction. The water content profile is measured on slices of 2.5 cm thickness cut from a cylinder Ø 15x30 cm after 1D drying. The cuts are conducted with a low velocity to limit microstructural damage, *i.e.*, microcracks. The variability on this measurement has been evaluated and it shows a good reliability and repeatability. The maximum variation coefficient is around 10%. The drying characterization tests were launched in these two conditioning modes:

- 23 °C, 50 % RH, which corresponds to the normalized conditioning (specimens are directly exposed to drying after the formwork remove), and
- 40 °C, 65 % RH, which corresponds to the accelerated drying (determined numerically for each concrete) after 7-day conservation in sealed condition.

#### *Effect of the accelerated drying on microstructure: investigation of carbonation and micro-cracking*

The evaluation of carbonation consists of spraying phenolphthalein on the Ø 11x10 cm cylinders, having dried for 13 months unidirectionally. Microcracking is observed with a confocal optical microscope (Keyence) on Ø 11x10 cm cylinders dried at 40 °C, 65 % RH, and cylinders of the same geometry and size dried at 23 °C, 50 % RH. In both conditioning modes, the drying lasted 13 months and occurred in all directions.

#### *Fire testing*

Table 2 summarizes all the fire tests: those of the short-term evaluation, already been carried out. In this article, only the short-term study results will be presented.



Table 2. Summary of the fire testing experimental program

	Standardized drying	Tested concretes	Status	Representative accelerated drying	Tested concretes	Status
Short-term evaluation	90 days	All concretes	completed	15 days	PERF38 et PERFDUB41	completed
Long-term evaluation	730 days	All concretes	ongoing	90 days	All concretes	ongoing

Table 3 provides the different parameters of the tests already conducted on PERFDUB concretes as a short-term evaluation. As fire tests are costly, for a first evaluation of the accelerated drying effect on spalling susceptibility, tests were carried out on PERFDUB concretes only, logically the most sensitive to fire due to their high compressive strength and very low permeability. The main objective of that test is to have an initial assessment of the representativeness of accelerated drying in the short term and to be able to optimize it before carrying out a test in the long term. Fire tests were carried out at three months of standardized conditioning that corresponds to the usual test on concrete elements. An examination under the ISO 834 fire curve is conducted on PERFDUB concrete slabs subjected to the representative accelerated drying protocol. This accelerated drying is representative of a 3-month drying period under standard conditions according to the first approach of the numerical study. The accelerated drying protocol was tested only on PERFDUB concretes. Indeed, the study's main objective is to set up an accelerated drying protocol representative of drying for a few years in ambient conditions.

Table 3. Assessment of the fire tests carried out to date on the PERFDUB concrete mixes.

Concrete	Fire curves	Specimens	Conditioning period	Conditioning mode
PERFDUB38 and PERFDUB41	ISO 834	Two slabs (1,7 x 1 x 0,3 m3)	90 days	Normalized conditioning
	ISO 834	Two slabs (1,7 x 1 x 0,3 m3)	15 days	Representative accelerated drying

## RESULTS AND DISCUSSION

### Prediction of concrete drying under normalized conditioning

As the characterization of the drying process lasts several months, the experimental campaign has been launched, and the first phase of drying simulation has been carried out on VERCORS concrete because it is the concrete for which the drying data (desorption isotherm and mass loss curves) are available and provided by the EDF lab. The following figure illustrates the numerical results after identifying material parameters for VERCORS concrete compared to the experimental results.

Figure 1 shows the theoretical/experimental results of the average water content per 2.5 cm slice in VERCORS concrete. For the first slice (0 – 2.5 cm), which corresponds to the skin area, the drying is underestimated, which may suggest the impact of wall effects (i.e., the effect of the formwork, microcracking, hydration evolution, etc.). In the two following slices, the theoretical and experimental results are very close, considering the standard deviation on the experimental measurement. In the last slice (7.5 – 10 cm), the drying is again underestimated.

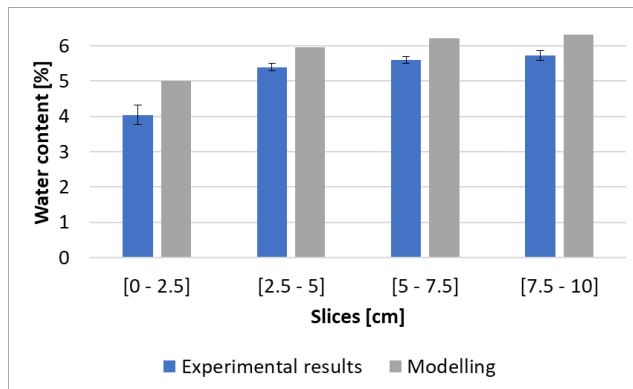
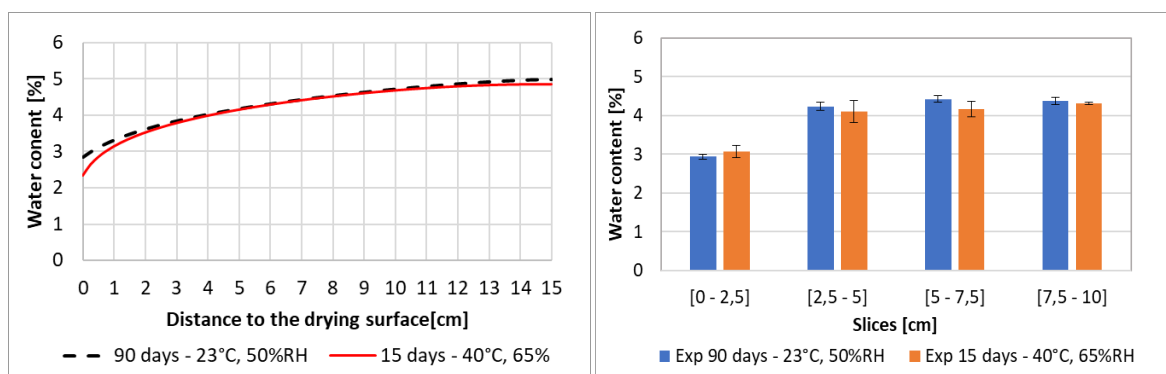


Figure 1. Water content per 2.5 cm slice (cut from a  $\varnothing$  15x30 cm cylinder) after uni-directionally drying for 90 days (VERCORS concrete).

## Development of an accelerated drying protocol

### Numerical prediction and validation

According to the numerical results, to reach a similar water profile as a 23 °C, 50 % RH curing condition after 90 days, it is sufficient to cure for 15 days concrete specimens at 40 °C, 65 % RH after a 7-day conservation in sealed condition. This period is necessary to allow the hydration to progress. The allowed deviation is equal to  $\pm 0.4$  % in absolute value for the water content. It is set to be similar to the maximum uncertainty value in the experimental measurements after a literature review [24], [25]. Of course, it would not be germane to put a permissible deviation more restrictive than uncertainty. The accelerated drying protocol is tested on PERFDUB concrete. Figure 2 shows the comparison between the moisture profile measured after 90 days of normalized drying and 15 days of accelerated drying. This first comparison shows that it is possible to achieve a given moisture profile target by modifying the drying conditions and duration. The difference between the two profiles remains very small compared to the precision of experimental measurement of water content, i.e.,  $\pm 0,5\%$ . There is no information so far, in literature, on the impact of that value on the spalling behavior. The experimental results show good consistency between the moisture content predicted in the two drying modes. The deviation is low and remains below the permissible deviation. The proposed numerical approach needs to be further validated by comparing the water profiles after normalized drying to after accelerated drying and by comparing the spalling behavior. (cf. Figure 2).



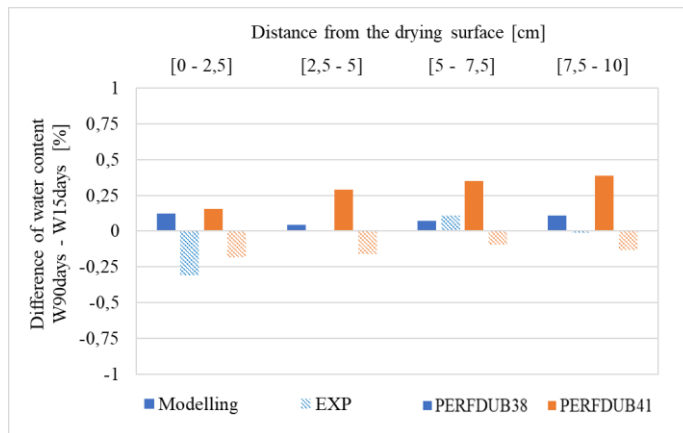


Figure 2. On the left side, the predicted water profile of a uni-directionally drying (PERFDUB38 concrete) after 90 days of normalized drying compared to the profile after 15 days of accelerated drying. On the right, the average water content per 2,5 cm from the drying surface to the core of Ø 15x30 cm cylinder. On the underside, a comparison of the water content difference, obtained numerically and experimentally.

### Effect of accelerated drying on microstructure

Carbonation and microcracking are the two main possible microstructural changes that may occur because of the drying acceleration at moderate temperature. Indeed, at ambient temperature, carbonation risk is maximum for a RH range of [40%-70%] and thermal gradient could enhance microcracking rate by shrinkage. This study aims at developing an accelerated representative drying protocol. So, it is important to limit the possible microstructural changes. Drouet and *al.* [26] have recently shown, through accelerated carbonation tests temperature in concretes formulated with CEM I at temperatures ranging from 20 °C to 80°C, that the increase in the carbonation depth is not significant. Therefore, the effect of the accelerated drying protocol (40 °C, 65 % RH) on the increase of the carbonation risk remains low. The evaluation of carbonation at 23 °C, 50 % RH, and 40 °C, 65 % RH confirms this hypothesis. At 23 °C, 50 % RH, the observed carbonate thickness ranges from 0 to 1 mm in PERFDUB concretes, from 0 to 3 mm in VERCORS concrete, and from 2 to 5 mm in CETU concrete. At 40 °C, 65 % RH, the carbonate thickness observed in PERFDUB concretes varies from 0 to 2 mm. It goes the same way in VERCORS concrete and from 2 to 3 mm in CETU concrete (cf. Figure 3).

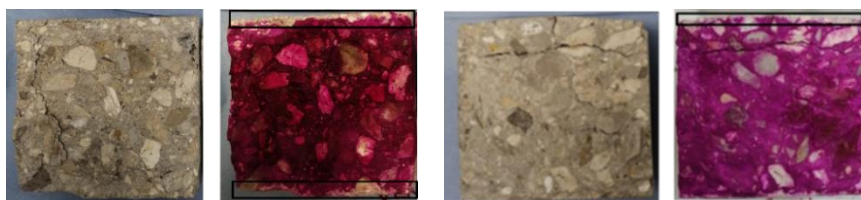


Figure 3. Evaluation of carbonation by coloured indicator (Phenolphthalein) in specimens of CETU concrete after unidirectional drying for 13 months at 23°C, 50% RH (left), and at 40 °C, 65 % RH (right).

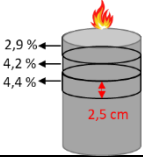
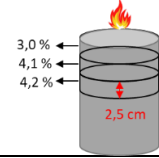


Comparing the cracking rate observed for the two drying modes in each concrete, the microcracking is almost identical (insignificant) for PERFDUB concretes and more critical in the case of drying at 23 °C for both VERCORS and CETU concretes. In this case, the effect of the deformations due to the thermal gradients passing from 23 °C to 40 °C might be negligible. The impact of the water gradient will be investigated for a better understanding. So far, the

result obtained is encouraging because the microcracking rate is not higher in the case of accelerated drying.

### Spalling sensitivity: effect of the concrete conditioning

The effect of the storage conditions on fire spalling has been tested on both PERFDUB mixes. Table 4 compares spalling sensitivity, water content, and compressive strength between the normalized conditioning and the accelerated drying in the PERFDUB38 mix. Results show good representativity of the accelerated protocol compared to the normalized conditioning of 3 months. In the case of a drying time of 3 months, only the first centimeters of the specimen have dried, and the core remains almost saturated. Therefore, for a water state representative of a short duration standardized drying ( $\leq 3$  months), the 40 °C, 65 % RH accelerated drying protocol is validated. Furthermore, this accelerated drying protocol is also validated for a representative skin water state regardless of the drying duration. The same findings are observed in the PERDUB41 mix.

Table 4. The impact of the storage conditions on the spalling susceptibility of the PERFDUB38 mix.

Storage		90 days under 23 °C, 50 % RH	15 days under 40 °C, 65 % RH
$f_{cm}$ [MPa]		91	88
Water content			
Spalling	Begins at	8 minutes	10 minutes
	Max depth [mm]	21	25
	Mean depth [mm]	12	12
	Topography		
Spalled surface [%]		45	55

### CONCLUSION AND PERSPECTIVES

The experimental study allowed us to identify the concrete drying parameters and validate the theoretical predictions in this work. The drying prediction allowed us to evaluate the hydric profile evolution in the reference structure in the short and long term and define the target

profile and then the optimal drying conditions to reach it in a few months only. The main conclusions are:

- The numerical study shows an interest in determining the drying acceleration factor from ambient to moderate temperature and, second, the conditioning time required to reach the target moisture profile. In addition, it has effectively replaced an additional experimental drying campaign that was both tedious and time-consuming.
- According to the numerical results so far, drying for 15 days at 40°C, 65% RH after preservation in sealed condition for seven days allows to reach the same water profile as drying 90 days at 23 °C, 50% RH: a drying period six times shorter. This result has been validated on high-performance concretes, which are very sensitive to spalling due to their resistance class, and any change in water profile would be seen in the fire behavior.
- The first test of the accelerated drying protocol shows good consistency between theoretical predictions and experimental results of concrete water content.
- The susceptibility to spalling of PERFDUB concretes is very similar between the case of normal drying and the case of representative accelerated drying. Given the dependence of spalling on the water profiles, notably by pore pressure and water moisture clog, the application of accelerated drying shows great interest in optimizing the drying time.
- The current results, combined with the long-term characterization, will allow evaluating the representativeness of the 3-month standardized conditioning mode and the efficiency of the accelerated drying protocol.

The ongoing work of this study includes optimizing the numerical study and refining the accelerated drying protocol. Also, we envision validating the accelerated drying protocol in the long term by assuming a target hydric state in a structure with a few years of operation. Applications of this study are broad and can go beyond fire behavior because of the strong dependence on the water profile of, for instance, delayed behavior and pathologies in concrete.

## REFERENCES

1. K. Hertz, 'Heat-induced explosion of dense concretes,' *Tech. Univ. Den. Inst. Build. Des.*, 1984.
2. F. Robert, H. Colina, and G. Debicki, 'La durabilité des bétons face aux incendies', in *La durabilité des bétons*, Presses des Ponts et Chaussées., 2008.
3. G. Choe, G. Kim, M. Yoon, E. Hwang, J. Nam, and N. Guncunski, 'Effect of moisture migration and water vapor pressure build-up with the heating rate on concrete spalling type,' *Cem. Concr. Res.*, vol. 116, pp. 1–10, Feb. 2019, doi: 10.1016/j.cemconres.2018.10.021.
4. J.-C. Mindeguia, H. Carré, P. Pimienta, and C. L. Borderie, 'Experimental discussion on the mechanisms behind the fire spalling of concrete,' Jun. 2014, Accessed: Nov. 08, 2019. [Online]. Available: <https://hal-cstb.archives-ouvertes.fr/hal-01102429>
5. M. Maier, M. Zeiml, and R. Lackner, 'On the effect of pore-space properties and water saturation on explosive spalling of fire-loaded concrete,' *Constr. Build. Mater.*, vol. 231, p. 117150, Jan. 2020, DOI: 10.1016/j.conbuildmat.2019.117150.
6. CEN, 'Eurocode 2: calcul des structures en béton - Partie 1-2: Règles générales - Calcul du comportement au feu. C. E. d. Normalisation.' 2004.

7. M. J. Abdolhosseini Qomi, L. Brochard, T. Honorio, I. Maruyama, and M. Vandamme, 'Advances in atomistic modeling and understanding of drying shrinkage in cementitious materials,' *Cem. Concr. Res.*, vol. 148, p. 106536, Oct. 2021, doi: 10.1016/j.cemconres.2021.106536.
8. B. Bissonnette, P. Pierre, and M. Pigeon, 'Influence of key parameters on drying shrinkage of cementitious materials,' 1999, DOI: 10.1016/S0008-8846(99)00156-8.
9. V. Baroghel-Bouny, 'Water Vapour Sorption Experiments on Hardened Cementitious Materials: Part I: Essential Tool for Analysis of Hygral Behaviour and its Relation to Pore Structure,' *Cem. Concr. Res.*, vol. 37, pp. 414–437, Mar. 2007, DOI: 10.1016/j.cemconres.2006.11.019.
10. J. Carette *et al.*, 'Identifying the mechanisms of concrete drying: An experimental-numerical approach,' *Constr. Build. Mater.*, vol. 230, p. 117001, Jan. 2020, DOI: 10.1016/j.conbuildmat.2019.117001.
11. C. Lenglet, 'Evolution of spalling with time and age,' *2nd Int. RILEM Workshop Concr. Spalling Due Fire Expo.*, p. 6, 2011.
12. 'Projet National PERFDUB', *PERFDUB*, 2019 2015. <https://www.perfdub.fr/> (accessed Nov. 30, 2020).
13. L. Charpin *et al.*, 'Ageing and air leakage assessment of a nuclear reactor containment mock-up: VERCORS 2nd benchmark', *Nucl. Eng. Des.*, vol. 377, p. 111136, Jun. 2021, DOI: 10.1016/j.nucengdes.2021.111136.
14. J. P. Ollivier, 'Les modes opératoires AFPC-AFREM sur la durabilité des bétons, application au diagnostic du béton', 1998, pp. 51–57. Accessed: May 30, 2022. [Online]. Available: <http://pascal-francis.inist.fr/vibad/index.php?action=getRecordDetail&idt=1818832>
15. M. Mainguy, 'Modèles de diffusion non linéaire en milieux poreux. Applications a la dissolution et au séchage des matériaux cimentaires', Ph.D thesis, Ecole Nationale des Ponts et Chaussées, 1999. Accessed: Apr. 22, 2020. [Online]. Available: <https://tel.archives-ouvertes.fr/tel-00869152>
16. M. Thiery, V. Baroghel-Bouny, N. Bourneton, G. Villain, and C. Stéfani, 'Modélisation du séchage des bétons', *Rev. Eur. Génie Civ.*, vol. 11, no. 5, pp. 541–577, May 2007, doi: 10.1080/17747120.2007.9692945.
17. M. Mainguy, O. Coussy, and V. Baroghel-Bouny, 'Role of Air Pressure in Drying of Weakly Permeable Materials,' *J. Eng. Mech.-Asce - J ENG MECH-ASCE*, vol. 127, Jun. 2001, DOI: 10.1061/(ASCE)0733-9399(2001)127:6(582).
18. M. Th. van Genuchten, 'A Closed-form Equation for Predicting the Hydraulic Conductivity of Unsaturated Soils', *Soil Sci. Soc. Am. J.*, vol. 44, no. 5, pp. 892–898, 1980, DOI: 10.2136/sssaj1980.03615995004400050002x.
19. M. Bakhshi, B. Mobasher, and C. Soranakom, 'Moisture loss characteristics of cement-based materials under early-age drying and shrinkage conditions,' *Constr. Build. Mater.*, vol. 30, pp. 413–425, May 2012, DOI: 10.1016/j.conbuildmat.2011.11.015.
20. Z. Zhang and U. M. Angst, 'Effects of model boundary conditions on simulated drying kinetics and inversely determined liquid water permeability for cement-based materials,' *Dry. Technol.*, vol. 0, no. 0, pp. 1–18, Aug. 2021, DOI: 10.1080/07373937.2021.1961800.
21. J. Jabbour, 'Méthodes d'essais de vieillissement accéléré des bétons à l'échelle des ouvrages', thesis, Université Paris-Saclay (ComUE), 2018. Accessed: Mar. 05, 2020. [Online]. Available: <http://www.theses.fr/2018SACLN038>
22. B. Bary, M. V. G. de Morais, S. Poyet, and S. Durand, 'Simulations of the thermo-hydro-mechanical behaviour of an annular reinforced concrete structure heated up to 200°C', *Eng. Struct.*, vol. 36, pp. 302–315, Mar. 2012, DOI: 10.1016/j.engstruct.2011.12.007.

23. P. Chhun, 'Modélisation du comportement thermo-hydro-chemo-mécanique des enceintes de confinement nucléaire en béton armé-précontraint', Thèse, y, 2017. Accessed: Mar. 10, 2020. [Online]. Available: <http://thesesups.ups-tlse.fr/3612/>
24. Q. Wu, 'Isothermes de désorption de matériaux cimentaires: étude d'un protocole accéléré et estimation du VER', 2014. Accessed: Nov. 21, 2019. [Online]. Available: <http://www.theses.fr/2014LIL10149/document>
25. N. Chan, 'Étude de la variabilité expérimentale et modélisation discrète du comportement des matériaux cimentaires: effet combiné du séchage et d'un chargement mécanique', Ph.D thesis, Université Paris-Saclay, 2021. Accessed: Jan. 11, 2022. [Online]. Available: <https://tel.archives-ouvertes.fr/tel-03366043>
26. E. Drouet, S. Poyet, P. Le Bescop, J.-M. Torrenti, and X. Bourbon, 'Carbonation of hardened cement pastes: Influence of temperature,' *Cem. Concr. Res.*, vol. 115, pp. 445–459, Jan. 2019, doi: 10.1016/j.cemconres.2018.09.019.



# Investigation of the fire behaviour of small-format ceiling-type building components

Peter Harsányi<sup>1,\*</sup>, Martin Schneider<sup>1</sup> & Lukas Treffner<sup>1</sup>

<sup>1</sup> Carinthia University of Applied Sciences, Villach, Austria

\* Corresponding author (harsanyi@cuas.at, Europastraße 3, 9500 Villach)

## ABSTRACT

In the event of a fire in buildings, detachment of concrete layers from multi-layer ceiling systems occur regularly. The causes of this type of component failure in ceiling systems have not been adequately investigated to date and require a more detailed examination of the failure mechanisms in the concrete and the composite joint, especially for targeted rehabilitation planning. For this purpose, a total of 24 small-format single- and two-layer test specimens with the dimensions 30 \* 30 \* 30 cm (l \* w \* h) were manufactured for the conduct of fire tests. In the case of the two-layer test specimens, the base specimens were manufactured with a base height of 15 cm and then provided with topping concrete. The influencing parameters for the tests were the concrete compressive strength and the surface properties of the specimens. To simulate a fire-induced chloride load some test specimens were provided with inserted PVC pipes in addition to conventional reinforcement, which in the event of fire lead to the release of chlorides in the concrete after an internal temperature of 120 C°. For the simulation of a ceiling underside, selected slabs were additionally provided with adhesive primer and thin-set mortar, as well as with gypsum plasterboard, and then tested in a fire test. The fire load was applied in a fire container by means of standard gas burners directly under the specimen. Following the fire test, an extinguishing process was simulated in order to reproduce its effects on the test specimens, if necessary. The tests were followed by non-destructive and destructive material tests to determine the compressive strength of the concrete, tensile strength of the steel, carbonation depth in the concrete, chloride content and tensile adhesion strength. Special attention was also paid to the bond joint between the different concrete layers. The investigations yielded interesting findings for the component behaviour of ceiling systems in the event of a fire.

**KEYWORD:** ceilings, bonded joint, small scale fire testing

## INTRODUCTION

In the event of damage caused by fire, the basic procedure for investigating the structure is largely established. National guidelines such as <sup>1</sup> provide the expert and the designer with a basic procedure for assessing the load-bearing behaviour and condition of load-bearing structures. However, the behaviour of lattice girder slabs in the event of fire has not been scientifically investigated to any great extent to date. Damage events, particularly in residential buildings, repeatedly present planners with the challenge of estimating the extent of the necessary rehabilitation measures. The effects on the composite behaviour in the concrete joint of the two-layer ceiling elements, influences of cable penetrations in PVC pipes and different concrete grades need to be investigated in more detail. Similarly, there is no uniform

normative basis for the dimensioning and designing of suitable test specimens. While the fire behaviour of reinforced concrete composite slabs has already been extensively investigated (see, e.g. <sup>2</sup>), only a few sources on the fire behaviour of lattice girder plates can be found. Large-scale tests on composite slabs were carried out, for example, at the Technical University of Munich <sup>3</sup>. The test specimens exhibited good load-bearing properties after fire, but it was pointed out that the failure mechanisms of these composite specimens in a fire would need to be studied in more detail. Case studies such as in <sup>4</sup> essentially focused on investigating the residual load-bearing capacity of beam-type support structures and found that they exhibited little damage after a short fire duration, similar to the scenario chosen in this study. Existing investigation concepts for concrete mix designs with respect to their behaviour in a fire are well established (see, e.g.: <sup>5</sup>), but cost-effective alternative test specimens for the specific design of lattice girder plates are needed. For the identification of relevant influencing parameters, fire tests with small-sized plate-like test specimens were developed, carried out and subsequently analyzed. The following results and documentations are based on <sup>6</sup>.

## MATERIALS AND METHODS

A total of 24 plate-like concrete specimens were produced for the fire tests on small-format test specimens, of which 12 were cast in 2 layers. The parameters influencing the test were the concrete quality, its curing in the case of two-layer test specimens and different surface coatings in order to be able to investigate as wide a range of floor systems as possible. The dimensions of the test specimens were chosen large enough to allow meaningful test results to be obtained both for the investigation of the carbonation depth and for adhesive tensile strengths after exposure to fire. The selected dimensions can be taken from Figure 1.

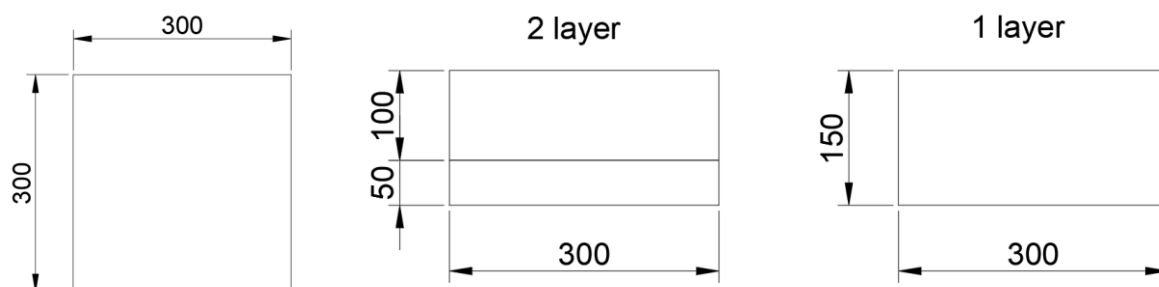


Figure 1 Dimensions of the concrete plates in mm

A total of three different concrete qualities (C25/30, C50/60, C35/45) were used for the test specimens. The recipes were produced with a maximum grain size of 16 mm and CEM I 42.5 N-SR 0 WT 27 and differed mainly in their w/c ratio.

BST 550 (yield strength 550 MPa) with a diameter of 6 mm was used for the reinforcement of the test specimens. In addition, for 6 test specimens, PVC empty pipes were attached to the structural reinforcement with cable ties in order to be able to investigate any negative effect of the pipes on the chloride load after the fire. The arrangement of the reinforcement and a typical layout of a latticed girder composite slab can be taken from Figure 2.

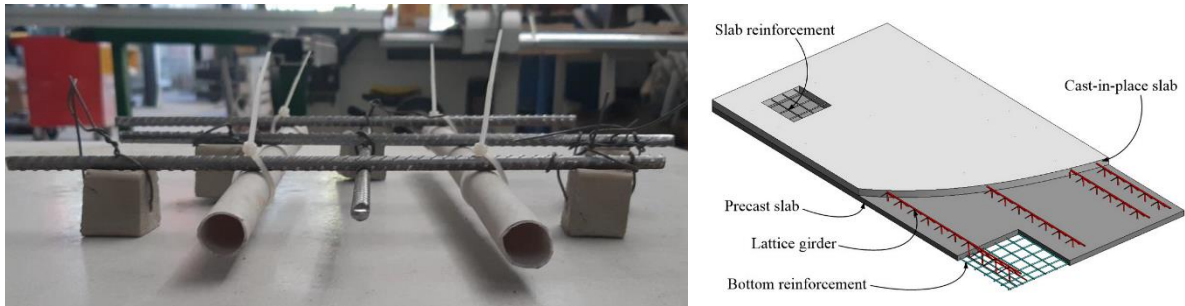


Figure 2 Reinforcement and PVC tube layout of the specimens (left), Latticed girder composite slabs (LGCS)<sup>7</sup> (right)

A total of 12 of the 24 test specimens were produced in two concreting sections to simulate the construction of a lattice slab. For this purpose, two types of surface finishing were selected between the concreting sections. 6 test specimens were made with a smooth joint and the remaining 6 were mechanically roughened in the fresh state after concreting (see Figure 3).



Figure 3 Surface preparation of the specimen

The test specimens and accompanying test specimens were stored under laboratory conditions at approx. 22°C.

In order to be able to reproduce the underside of a concrete slab, the test specimens were provided with surface coatings. For 6 of the test specimens, a fine lime plaster was used as a thin plaster mortar, and for another 6 specimens, an approx. 10 mm thick gypsum plasterboard surface was attached to the specimen with the aid of a gypsum-based binder (see Figure 4).



Figure 4 Lime-based thin bed mortar (left); Plasterboard (right)

For the determination of the compressive strengths, 3 cubes each with edge lengths of 15 cm were produced and tested to the test day (~ 60 days). An overview of the test constellations and the corresponding compressive strengths can be taken from Table 1.

Table 1 Test series overview

Test series – spec. no.	Mean compr. strength baseplate [MPa]	Mean compr. strength top concrete [MPa]	Type of plate	Interface preparation	Surface covering
S1-1	59,8	-	1 layer	no interf.	mortar
S1-2	59,8	-	1 layer	no interf.	plasterboard
S1-3	59,8	-	1 layer	no interf.	none
S2-1	59,8	-	1 layer	no interf.	mortar
S2-2	59,8	-	1 layer	no interf.	plasterboard
S2-3	59,8	-	1 layer	no interf.	concrete
S3-1	52,2	-	1 layer	no interf.	mortar
S3-2	52,2	-	1 layer	no interf.	plasterboard
S3-3	52,2	-	1 layer	no interf.	concrete
S4-1	52,2	-	1 layer	no interf.	mortar
S4-2	52,2	-	1 layer	no interf.	plasterboard
S4-3	52,2	-	1 layer	no interf.	concrete
S5-1	72,6	53,2	2 layer	flat	mortar
S5-2	72,6	53,2	2 layer	flat	plasterboard
S5-3	72,6	53,2	2 layer	flat	concrete
S6-1	72,6	53,2	2 layer	flat	mortar
S6-2	72,6	53,2	2 layer	flat	plasterboard
S6-3	72,6	53,2	2 layer	flat	concrete
S7-1	72,6	53,2	2 layer	roughened	mortar
S7-2	72,6	53,2	2 layer	roughened	plasterboard
S7-3	72,6	53,2	2 layer	roughened	concrete
S8-1	72,6	53,2	2 layer	roughened	mortar
S8-2	72,6	53,2	2 layer	roughened	plasterboard
S8-3	72,6	53,2	2 layer	roughened	concrete

The fire tests were carried out in cooperation with the Carinthian State Fire Brigade School in Klagenfurt. For this purpose, the test specimens were fired with a gas burner in a half-open structure. The duration of the fire was determined to be 30 minutes, since in Austria, in the

event of a fire, an average time of 10 to 15 minutes is assumed until the alarm is raised and an effective extinguishing attack is carried out after about 30 minutes. With the help of fireclay bricks, a combustion chamber with an opening on the rear side for a sufficient oxygen supply was constructed. The distance between the gas burners and the test bodies was approx. 8 cm on the whole length of the specimens. The surface temperature (front and back) of the concrete slabs was measured directly after the fire test and the subsequent extinguishing process using an infrared thermometer. Likewise, the temperature in the spaces between the slabs was measured at a distance of 1 cm from the flame in the area of the slab joints. The temperature in the joint could be monitored by means of a digital display panel during the test (see Figure 5 (3)). The fire load during the test averaged approx. 600 degrees Celsius.



*Figure 5 Experimental configuration (1); Burning specimen (2); Temperature probe position (3); Digital scoreboard (4)*

For the simulation of an extinguishing process, the test specimens were set up outside directly after 30 minutes and sprayed with water for 6 seconds using a hollow jet pipe. Similar to the extinguishing process in an interior room, the slab surfaces cooled down in a short time. The aim was to identify possible negative effects on the concrete and the composite joint.



*Figure 6 Extinguishing process with hollow jet pipe*

## **EXPERIMENTAL RESULTS**

The test specimens were exposed to a fire load simulating that of a fully burning interior. After 30 minutes of exposure to the fire load, the test specimens showed visible discoloration on the top of the specimen (see Figure 7).





Figure 7 Specimens after fire exposure: Thin board mortar (left); Mortar board (middle), Concrete (right)

After the extinguishing process, clear spalling was visible on the test specimens with lime plaster. The areas that were protected by direct flame exposure due to the support on the fireclay bricks did not show any damage. In the case of the test specimens with gypsum plasterboard, these were interspersed with crackle-like net cracks. The test specimens without an additional surface system showed no visible damage. For further analysis of the degree of damage, drill cores were taken from the test specimens. When grinding the cores, special attention was paid to ensure that only a very small amount of material was removed in order to preserve the outer layer of the surface exposed to the fire as far as possible. *Table 2* gives an overview of the average strength losses as a function of the surface system.

*Table 2 Compressive strength losses in [%]*

Surface material	Average reduction in compr. strength in %
mortar	-32,0
plasterboard	-20,5
none	-35,25

The lowest losses in compressive strength of 20.5 % were achieved by the gypsum plasterboards. Compared to the unprotected surfaces with 35.25 %, the test specimens with lime-cement plaster showed only slightly lower strength losses of 32.0 %.

The determination of carbonation after firing was carried out with an ordinary phenolphthalein solution, which reveals areas at fractures with a lower PH value than 9.5. The specimens examined showed consistent carbonation depths both on the side facing the fumigator and on the side away from the fumigator, ranging from 1.1 to a maximum of 4.08 mm (see Figure 8). The majority of the samples were in the range of about 2.5 mm. Therefore, in the case of a similar fire event, it can be assumed that the concrete carbonation can be neglected with regard to the corrosion protection of the reinforcement.



Figure 8 Carbonatisation depth example

For the chloride analysis, drill dust samples were taken at depths of 15 and 30 mm to the surface and analyzed according to [1]. According to [2], a risk of corrosion is assumed if chlorides exceed 0.6 M.-% of the cement content.

Table 3 gives an overview of the test results obtained. All samples were below the critical limit.

Table 3 chloride concentration in specimens after fire exposure

Series	Depth	M.-% of cement
1 to 2	0-15 mm	0,01
1 to 2	0-30 mm	0,09
3 to 4	0-15 mm	0,225
3 to 4	0-30 mm	0,255
5 to 8	0-15 mm	0,18
5 to 8	0-30 mm	0,06

Samples taken in the vicinity of the PVC pipes also showed no limit value violations. On closer inspection and opening of the samples with the aid of a drilling hammer, it was evident that the short fire duration in combination with the fire load was not sufficient to completely decompose the PVC pipes. Massive damage is clearly visible (see Figure 9), but an increased chloride input due to the hydrochloric acid produced during the disintegration of the PVC pipes cannot be assumed with this type of fire load and 30 minutes fire duration.



Figure 9 Damaged PVC tube



The test specimens were freed from the residues of the surface coatings using an angle grinder with steel brush attachment and then examined using a Freundl Easy M 2000 tensile adhesion tester, 0-15 KN. The feed rate was chosen to be 0.05 N/mm<sup>2</sup>. Table 4 gives an overview of the adhesive tensile strengths obtained.

*Table 4 mean adhesive tensile strength after fire exposure*

Series	Surface system	Mean adhesive tensile strength [N/mm <sup>2</sup> ]
1 to 2	mortar	1,52
1 to 2	plasterboard	1,65
1 to 2	plasterboard (longer mech. prep.)	2,71
3 to 4	concrete	1,37
3 to 4	plasterboard	1,94
3 to 4	plasterboard (longer mech. prep.)	3,01
5 to 8	concrete	2,27
5 to 8	mortar	1,83
5 to 8	plasterboard	1,85

Insufficient surface pretreatment of the test specimens reinforced with gypsum board resulted in adhesive tensile strengths of approx. 1.6 MPa and 1.94 MPa. A repetition of the tests after additional mechanical treatment of the surfaces resulted in adhesive tensile strengths averaging 2.71 MPa and 3.01 MPa, which can be attributed to slight damage to the first surface layer and residues of the binder on the surface. The other test specimens showed adhesive tensile strengths between 1.37 MPa for directly flamed concrete and 1.52 MPa for the specimens with thin-board mortar. In the event of damage, therefore, even a minor removal of the surfaces may be sufficient to enable any repair and reinforcement measures to be carried out.

In addition to the previous investigations, the structural reinforcement in selected test specimens was uncovered with the aid of a drilling impact hammer (see Figure 10) and examined for its tensile strength. No noticeable deviations from the reference tensile strengths were found in the investigated steel tensile strengths. All steel specimens exhibited a yield point of 548 to 566 MPa and maximum tensile strength of 644 to 666 MPa on average, depending on the surface treatment.



*Figure 10 Exposed reinforcement after fire test*

In the case of the two-layer boards, loud cracking noises were perceived during the test. Following the fire exposure, all 5 cm thick slabs detached from the rest of the test specimen in a shell-like manner. The mechanically roughened test specimens could also be separated

with little force. As shown in Figure 11, this can be explained by two mechanisms of action. Due to the uneven heating of the test specimens on one side, transverse forces act in the concrete joint. In addition, the heating of the concrete during the test creates a vapour pressure, which has a negative effect on the bond due to the structural change in the interface and ultimately leads to the detachment of the concrete. For future investigations, it is necessary to perform tests with defined varying roughnesses and also to investigate the adhesive tensile strengths in the bonded joint.

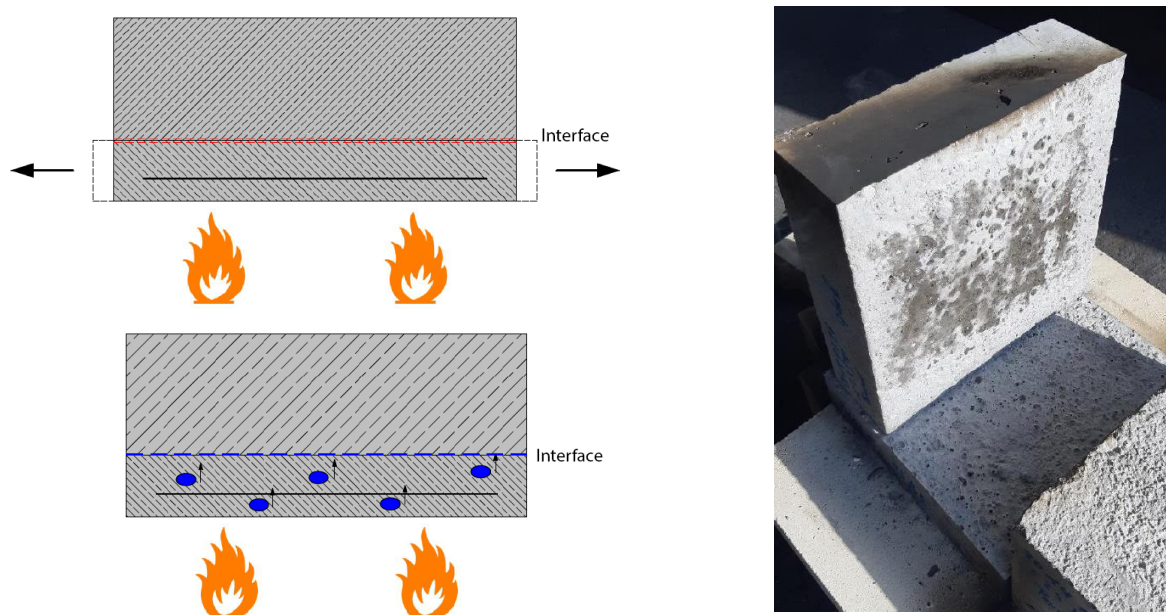


Figure 11 forces on the interface (left); separated plate after fire exposure (right)

## CONCLUSIONS

After the fire tests, the investigated two-layer test specimens showed different damage depending on their surface system. Further investigations showed that in the event of a fire, damage to ceiling systems with partly precast elements is to be expected even at low fire loads and temperatures.

- Even a short fire load of 30 minutes at moderate temperature resulted in significant damage to the concrete with respect to its compressive strength in the slab-type test specimens.
- The investigated carbonation depths were in an uncritical range for all test specimens after the fire test.
- Due to the low temperature exposure, the inserted PVC pipes were not completely decomposed and no elevated chloride concentrations could be detected.
- The tensile bond strengths investigated varied depending on the post-treatment of the specimens after the fire test. Complete and careful mechanical cleaning led to greatly improved tensile strengths.
- Due to the one-sided heat development and the resulting steam pressure, the test specimens produced in two concreting sections separated from each other. A bond in the field without connection reinforcement cannot be assumed.

## REFERENCES

1. "Richtlinien zur Brandschadensanierung," No. VDS2357:2014-06, 2014, p. 70.
2. Cameron, N. "The Behaviour and Design of Composite Floor Systems in Fire," 2003.
3. Stadler, M., Mensinger, M., Schaumann, P., et al. "MUNICH FIRE TESTS ON MEMBRANE ACTION," *Application of Structural Fire Design*, 2011, p. 6.
4. Srinivasan, P., Cinitha, A., Mohan, V., et al. "EVALUATION OF FIRE-DAMAGED CONCRETE STRUCTURES WITH A CASE," 2014, p. 8.
5. Hertz, K. D., and Sørensen, L. S. "Test method for spalling of fire exposed concrete," *Fire Safety Journal*, V. 40, No. 5, 2005, pp. 466–76.
6. Treffner, L. "Diploma thesis: Ermittlung des Bauteilverhaltens und der Sanierbarkeit von Betondecken nach einem Brand," 2019.
7. Zhang, X., Li, H., Liang, S., et al. "Experimental and Numerical Study of Lattice Girder Composite Slabs with Monolithic Joint," *Crystals*, V. 11, No. 2, 2021, p. 219.

# Influence of elevated temperature and different cooling regimes on mechanical and transport properties on High Strength Self-Compacting concrete

Pavan Kumar<sup>1\*</sup>, Umesh Kumar Sharma<sup>1</sup> & A. B. Danie Roy<sup>2</sup>

<sup>1</sup> Department of Civil Engineering, Indian Institute of Technology Roorkee, Roorkee, India

<sup>2</sup> Department of Civil Engineering, Thapar Institute of Engineering & Technology, Patiala, India

\* Corresponding author (pkumar61@ce.iitr.ac.in, Research Scholar, Department of Civil Engineering, Indian Institute of Technology Roorkee, Roorkee, Uttarakhand, India, 247667)

## ABSTRACT

Concrete is a complex material whose properties change when exposed to high temperatures, causing catastrophic failure or extensive damage. Fire weakens and deteriorates concrete, causing spalling of near-surface concrete layers. Concrete imperviousness is the first line of defence against any deterioration process and is directly related to spalling behavior at high temperatures. This study presents the effect of high temperature (i.e. 300 °C, 500 °C, and 800 °C) with different heating parameters and cooling regimes (normal and water quenching) on the mechanical and transport properties of high-strength self-compacting concrete (M60 grade) and compared the same with Normal Vibrated Concrete (NVC) at elevated temperatures. Compressive strength and non-destructive testing were used to assess the mechanical properties of the concrete, while water and air permeability tests were used to evaluate the transport properties. The specimens were exposed to 300°C, 500°C, and 800°C for two holding periods, i.e., 1 hour and 2 hours, and further compared the same with the specimens at room temperature (27 °C). All the specimens were cured for 28 days. The result observed that there was no significant effect between holding periods at high temperatures. However, it was discovered that water quenching was more detrimental to high-strength self-compacting and normal vibrated concrete than normal cooling. Furthermore, no spalling was observed in any specimens after high-temperature exposure.

**KEYWORD:** Elevated temperature, cooling regimes, mechanical and transport properties, HS-SCC

## INTRODUCTION

Nowadays, all over the world, fire accidents are one of the most frequent hazards. Fire has the great potential to damage buildings and other structures. There are many previous studies, that show that in the case of natural or even accidental fire, elevated temperatures can reach up to 1000°C [1,2]. All over the world, due to different reasons, many fire accidents are continuously happening. Therefore, it is a matter of serious concern for structural safety. Thus,

the transformations in concrete properties due to exposure to high temperatures must be understood [3].

Generally, concrete's fire performance is considered non-combustible and assumed as a thermal barrier, which prevents heat and fire expansion. The concrete structures generally perform well in the exposed temperature. However, concrete is a complex material, and its properties can alter seriously when exposed to elevated temperatures. Loss of strength, durability, and spalling are the principal effects on concrete at elevated temperatures. When exposed to heat, concrete responds to instantaneous physical changes like expansion and also undergoes various chemical transformations. This type of response is incredibly complex due to the non-uniformity property of the material. Concrete contains cement and aggregate elements, which may react to heating in various ways. However some of these are reversible after cooling, but others are non – reversible and may significantly deteriorate the concrete structure after exposed temperatures. One of the greatest complex and poorly understood behavioral characteristics in the reaction of concrete to elevated temperatures or fire is the 'explosive spalling', and this often frequently occurs only at high temperatures. If it becomes severe, spalling can deleteriously affect the strength of reinforced concrete structures. Karatus *et al* [4] studied the residual strength of steel fiber SCC at high temperatures. Some other researchers [5,6] also studied the mechanical properties of concrete at high temperatures and find useful results.

Currently, the construction technology has very advanced, and it demands variable concrete that is workable as well as durable so that the problems in the construction industry like remote casting, filling of enclosed spaces, and dense reinforcement can be easily solved. The advancement of self-compacting concrete (SCC) may be the solution to these aforementioned construction-related problems and other technological benefits. Self-consolidating concrete has the capability of high flowability, non-segregating property that can spread easily into dense places, fills the formwork, and dense reinforcement without any mechanical vibration; hence, SCC is a good option compared to normal vibrated concrete in those areas which are highly congested reinforcement and where the placement of concrete and compaction is difficult [7]. A well-designed SCC mix should be nonsegregated and has high deformability with excellent stability characteristics. In the current practice of modern construction, SCC plays a vital role in fulfilling the demand for modern architectural and complex, indeterminate structural structures having complex geometrical configurations. Self-compacting concrete has been used in various structures like bridges or even on pre-cast sections. Applications of SCC are increasing day by day over the world. Self-compacting concrete was - introduced in Japan in 1988 with the name "High-Performance Concrete" the additional development was carried out by many researchers (Okamura & Ouchi, 2003, Bartos & Grauers, 1999;) [8,9]. Self-compacted concrete is a good option where concrete placement and compaction are not easy.

## **MATERIALS AND METHODS**

### **Materials**

In this study, locally available material was used to prepare normal vibrated concrete (NVC) and self-compacted concrete. For the binding agent, Ordinary Portland cement (CEM-I) was used with natural river coarse sand, and the maximum nominal size of coarse aggregate was 12.5 mm for both normal vibrated and self-compacting concrete. In this study, the standard quality aggregate was used because the main focus was the behavior of SCC and NVC, so the aggregate thermal degradation was neglected, and PCE-based superplasticizer (BASF MasterGlenium 51) was used to get a higher slump value with a low w/c ratio. A viscosity

modifier agent (VMA), (BASF MasterMatrix 102) was also used. Material's physical properties are shown in Table 1.

*Table 1 Physical properties of the materials*

	Cement	Coarse aggregate	Fine aggregate	SP	VMA
Specific gravity	3.15	2.62	2.45	-	-
Water absorption (%)	-	1	1.49	-	-
Relative density	-	-	-	1.09	1.01

### Mix Design

The IS 10262:2019 was used for mix design of NVC, and the Nan-Su method for mix designing of SCC. The primary aim of the mix design of SCC is to select the optimum proportions of aggregate to produce highly compacted concrete, and the binders paste to fill into the aggregates' voids to confirm that the concrete so obtained desired SCC properties. In this method, the proportioning of coarse aggregates was done considering the optimum packing factor (PF) of aggregate. The trials were performed by adjusting the w/c ratio and the amount of VMA ad superplasticizer. Table 2 shows the mixed proportions of self-compacting concrete and normal vibrated concrete. The slump value for NVC was 120 mm.

*Table 2 Final mix proportions*

	Cement (OPC)	Coarse aggregate	Fine aggregates	Water	w/c ratio	SP	VMA
NVC	470 kg/m <sup>3</sup>	918.90 kg/m <sup>3</sup>	884.56 kg/m <sup>3</sup>	141 kg/m <sup>3</sup>	0.30	1.1 %	-
SCC	520 kg/m <sup>3</sup>	526.73 kg/m <sup>3</sup>	1116.24 kg/m <sup>3</sup>	135.20 kg/m <sup>3</sup>	0.26	1.5	0.025%

### Test on Fresh Properties of Self-Compacted Concrete

Four-measure characteristics can define the stability and filling ability of self-compacting concrete in its fresh state: flowability, viscosity, passing ability, and segregation. V funnel flow tests were performed to check the flow ability and segregation resistance ability, and an L box test was performed to satisfy the passing ability of concrete through congested openings.

### Slump Flow Test

A slump flow test was performed to ensure the flow criteria of concrete. This primary test generally specifies for all SCC as the first confirmation that the fresh concrete consistency fulfills the required parameter. As per EFNARC, concrete having a slump value of 550 mm to 850 mm endorse self-compaction ability. For this test, a baseplate is made from a flat plate with a plane area of 1000 mm x 1000 mm, a smooth and non-absorbent surface with a thickness of 3 mm, and a 300 and 500 mm marked diameter was used. After flowing the concrete, take an average of two diameters. In this study, the slump value of SCC is 690 mm. Figure 1 shows the flowability test of SCC.



Figure 1 Slump flow test



Figure 2 J-Ring test.

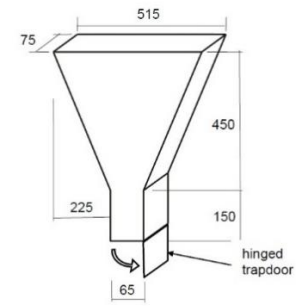


Figure 3 V-funnel test setup

### J-Ring test

The test was performed to investigate the filling ability and the passing ability of the SCC mix. It indicates the limited deformability due to the blocking of the reinforcement bar. The test was performed according to ASTM C1621. The J-Ring is a combination of the slump flow kind of test with the added complication, that the concrete is required to flow through an added cylindrical contraption, which has reinforcing bars and gaps in the bars. J-Ring flow is the average of the two diameters; the difference between slump value and J-Ring value indicates the filling ability of SCC. In this test, the value of this gap was 46 mm. Figure 2 suggests this test.

### V-Funnel Test

In this test, the time needed to flow concrete through the V-funnel apparatus represents the viscosity of SCC, a measure of the ability of segregation resistance. Generally, 12 - 14 liters of concrete were used in this test. A V-funnel apparatus with a standard dimension according to EFNARC (Figure 3) stands vertically on the ground. The time required for the full discharge of concrete through the V-funnel was noted. The recommended value is 6 – 12 sec. In this test, this value is 11 sec.

### L-Box Test

This method helps investigate the passing ability of SCC. For this test L-shaped mold with 3 three smooth bars was used (Figure 4), according to EFNARC. In this test the reached height of fresh SCC after passing through the specified gaps of steel bars and flowing within the fixed flow distance. With these heights, the blocking and passing behavior of SCC is calculated. For this study, this value is 0.9. (Figure 5).

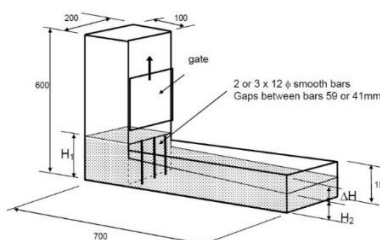


Figure 4 L-box



Figure 5 L-box test



Figure 6 Epoxy coating



Figure 7 Sorptivity test



### Test on Hardened Concrete

All ingredients were mixed well in the mixer and placed the SCC concrete in molds, and a plastic sheet covered the molds. After 24-h, the specimens were demolded and cured in fresh water at 27°C. After 28 days of water curing, the saturated specimens were removed from the water and put in the natural environment in the laboratory; their constant mass (0.5 – 1%) was achieved in a hot air oven.

The sorptivity test was performed on the concrete samples at fixed time intervals according to ASTM C1585 [10]. The sample size was 100 mm dia. and 50 mm height, cut from 100 × 200 mm cylinder. An average of three samples reading was used. Before the experiment, for constant weight, the samples were kept in an oven at 105 ± 5 °C until constant weight. The lateral area of sample surfaces was shielded with an epoxy coating (Figure 6), and the top surface was covered with a plastic sheet. The samples were placed in a plastic tray containing water. The time interval for measurement of weight of samples was 1, 5, 10, 20, 30, 60, 120, 180, 240, 300, 360, and 1440 min from the beginning of the experiment. The test setup is shown in Figure 7.

To investigate the compressive strength of concrete, 150 mm concrete cubes [4] were used. After 28 days of curing the specimens, the test was conducted because there was no addition of any SCM, so as per standard, 99% strength was achieved at 28 days of curing, and after 28 days of curing, strength gain is very low, which can be neglected. An average of three samples were tested at a constant loading rate according to IS – 516: 1959 using the 3000 kN compression testing machine.

The air permeability of concrete was determined by Torrent Permeability Tester (Figure 8). In this test, "vacuum is created inside the 2-chamber vacuum cell, which is sealed onto the concrete surface by means of a pair of concentric soft rings, creating two separate chambers. A vacuum pump creates a vacuum cell with the help of a vacuum pump. The principle of the device is a two-chamber vacuum cell with a pressure regulator which provides the airflow into the inner chamber oriented perpendicularly to the surface of the tested structure. The measurement results are the coefficient of air permeability and penetration length. The quality class of the concrete from the viewpoint of durability is given in Table 3." [11]. Concrete cubes of 150 mm are used to perform this test.

Table 3 Quality index for air permeability test

Quality of covercrete	Index	kT [ $10^{-16} \text{ m}^2$ ]
Very bad	5	> 10
Bad	4	1.0 – 10
Normal	3	0.1 – 01
Good	2	0.01 – 0.1
Very good	1	< 0.01

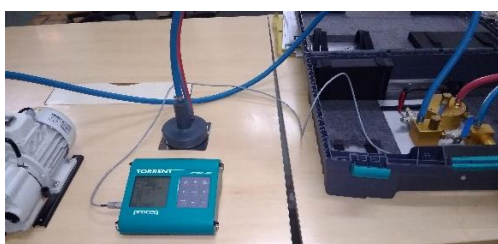


Figure 8 Torrent permeability tester



Figure 9 UPV test



Figure 10 Electric furnace

The UPV measurement was a non-destructive test and performed according to ASTM C597-16. The test was conducted on cube samples of 150 mm cube size after 28 days of curing at all elevated temperatures. A pair of 54 kHz transducers was used across the cube, one as the transmitter and the other as the receiver (Figure 9).

### Heating Regime and Cooling Pattern

With an electric furnace (Figure 10), the concrete specimens were heated up to four temperatures, i.e. room temperature (27°C), 300°C, 500°C, and 800°C. The heating rate was 5°C/min considered based on literature [12]. To ensure a uniform temperature throughout the specimens, two holding times of 60 minutes and 120 minutes and two cooling regimes of ambient cooling and sudden water quenching were used to simulate real possible cooling conditions; for water quenching, water was sprayed with normal water for  $5 \pm 2$  min [13] and placed in the same environment to cool down. Sprayed water for quenching was used to simulate fire-fighting phenomena.

## RESULTS AND DISCUSSION

### Sorptivity Test

Figure 11 and 12 shows the result of the sorptivity test of SCC and NVC. The initial rate of absorption for SCC at 300°C, 500°C, and 800°C for 1 hr and 2 hr holding periods was 0.0106, 0.0335, 0.0419 and 0.0143, 0.0338, 0.0460 for furnace cooling and same for water quenching was 0.0180, 0.0374, 0.0360 and 0.0218, 0.0328, 0.0360. For room temperature, this value was 0.0103.

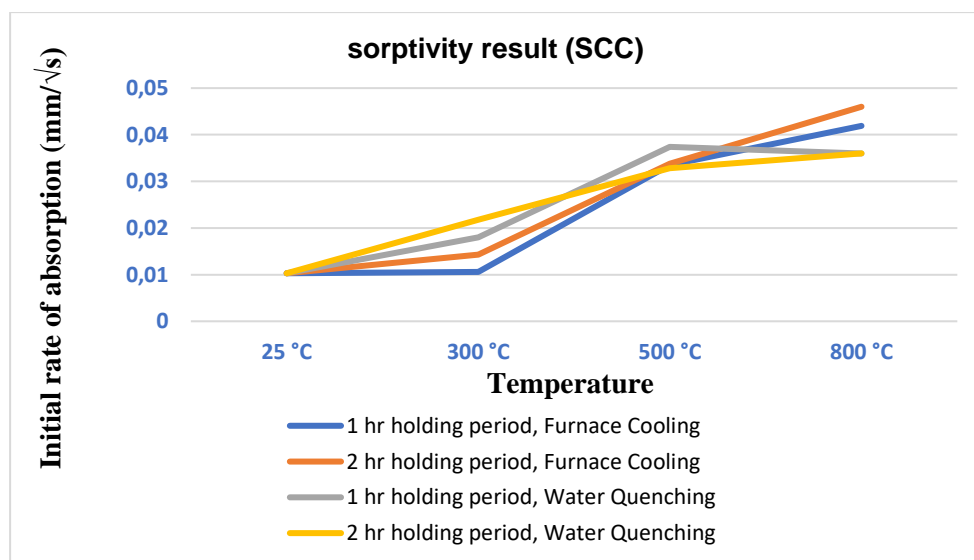


Figure 11 Sorptivity results of SCC

The initial rate of absorption for NVC at room temperature was 0.0112 and at 300°C, 500°C, and 800°C for furnace cooling at 1hr and 2 hr holding periods was 0.0123, 0.0355, 0.0525 and 0.0150, 0.0362, 0.0551 and same for water quenching was 0.0189, 0.0374, 0.0372 and 0.0225, 0.0329, 0.0361.

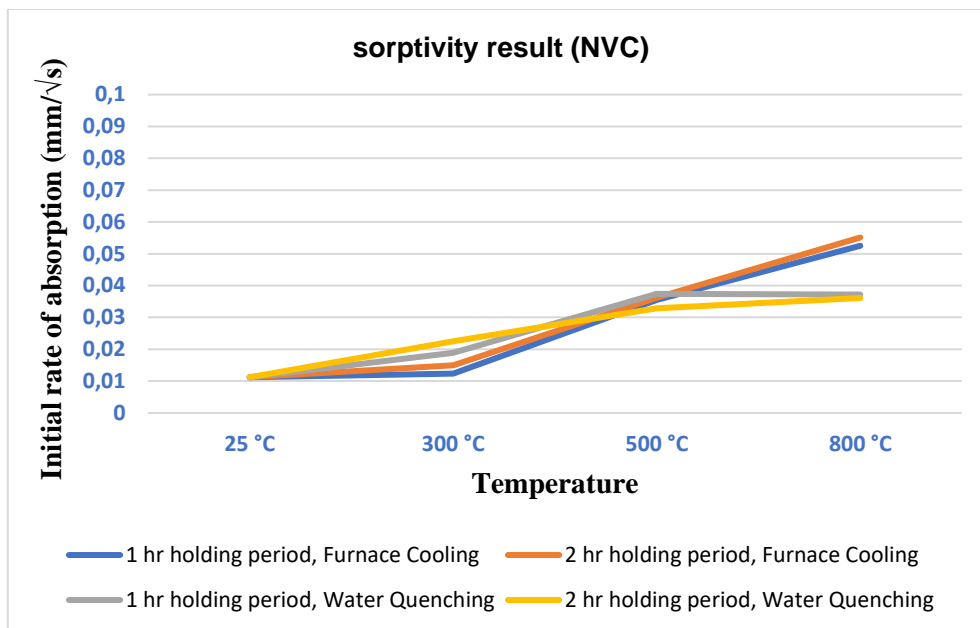


Figure 12 Sorptivity results of NVC

### Air Permeability Test

Figure 13 and 14 shows the result of air permeability of SCC and NVC. The coefficient of air permeability of SCC at 27°C was  $0.368 \times 10^{-16} \text{ m}^2$  and at 300°C for furnace cooling at 1 hr and 2 hr holding periods was  $3.517 \times 10^{-16} \text{ m}^2$  and for 1 hr water quenching, it was  $37.769$  and same for NVC was  $0.437, 0.833, 5.828$  and  $51.737 \times 10^{-16} \text{ m}^2$ .

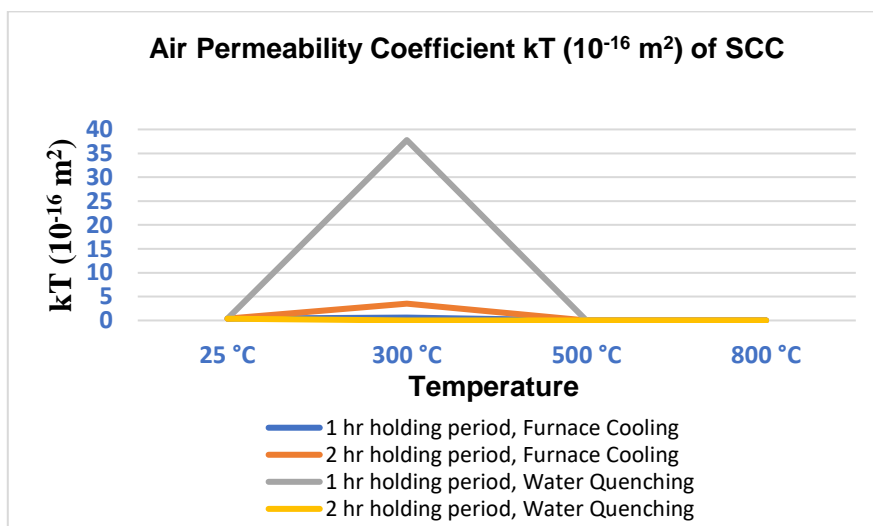


Figure 13 Air permeability coefficient of SCC

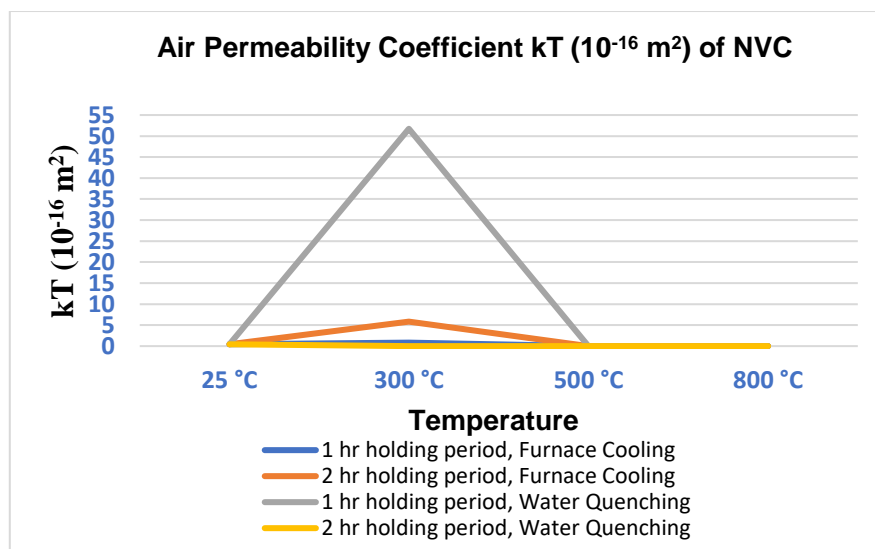


Figure 14 Air permeability coefficient of NVC

### Compressive Strength Test

It has been stated earlier, that the deterioration of mechanical properties of concrete at elevated temperatures is influenced by many factors. An increase in exposed temperature commonly causes a gradual loss of its mechanical strength. Variations of compressive strength values of SCC and NVC samples exposed to an elevated temperature at the 28 days of the curing period are shown in Figures 15 and 16. Tables 3 and 4 show the strength of SCC and NVC for all variables.

Table 3 Compressive strength of SCC

Temp	1 hr holding period, Furnace Cooling	2 hr holding period, Furnace Cooling	1 hr holding period, Water Quenching	2 hr holding period, Water Quenching
25 °C	69.36	69.36	69.36	69.36
300 °C	81.29	77.2	74.664	72.41
500 °C	59.11	56.423	50.623	46.727
800 °C	31.34	26.32	21.243	18.286

Table 4 Compressive strength of NVC

Temp	1 hr holding period, Furnace Cooling	2 hr holding period, Furnace Cooling	1 hr holding period, Water Quenching	2 hr holding period, Water Quenching
25 °C	68.85	68.85	68.85	68.85
300 °C	81.06	79.52	78.12	76.43
500 °C	59.86	56.45	53.38	48.1
800 °C	28.75	24.19	22	21.84

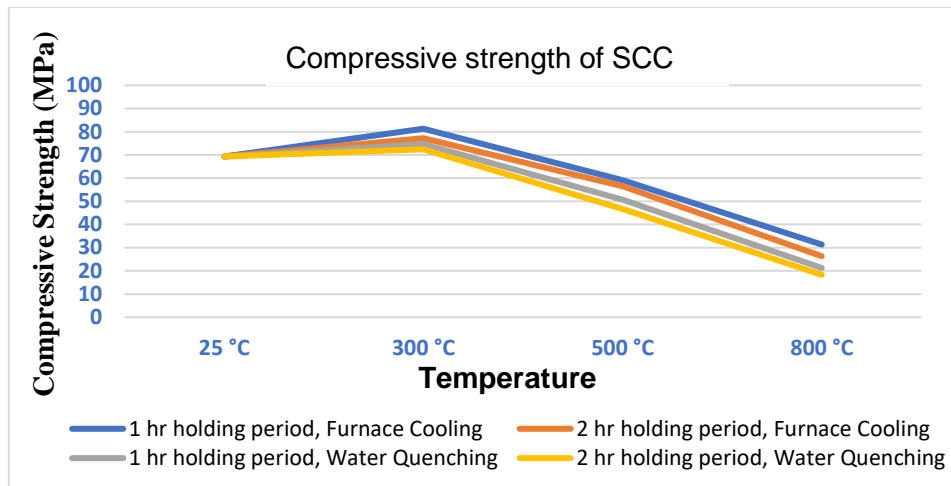


Figure 15 Compressive strength of SCC

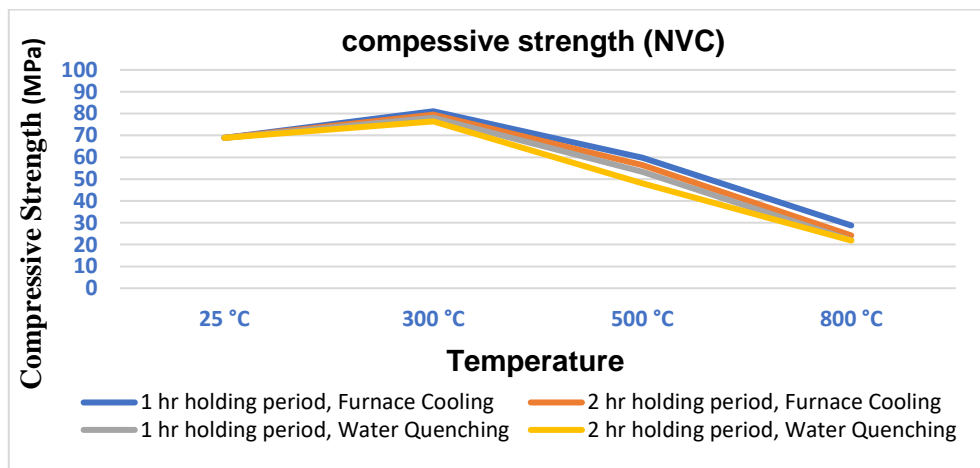


Figure 16 Compressive strength of NVC

### Ultrasonic Pulse Velocity Test

Figures 17 and 18 show the UPV values of SCC and NVC specimens at the temperature of 27°C, 300°C, and 500°C. At 800°C, UPV values were lowest due to severe deterioration of specimens. As shown in Figures 17 and 18, as the temperature increment, UPV values decrease progressively.

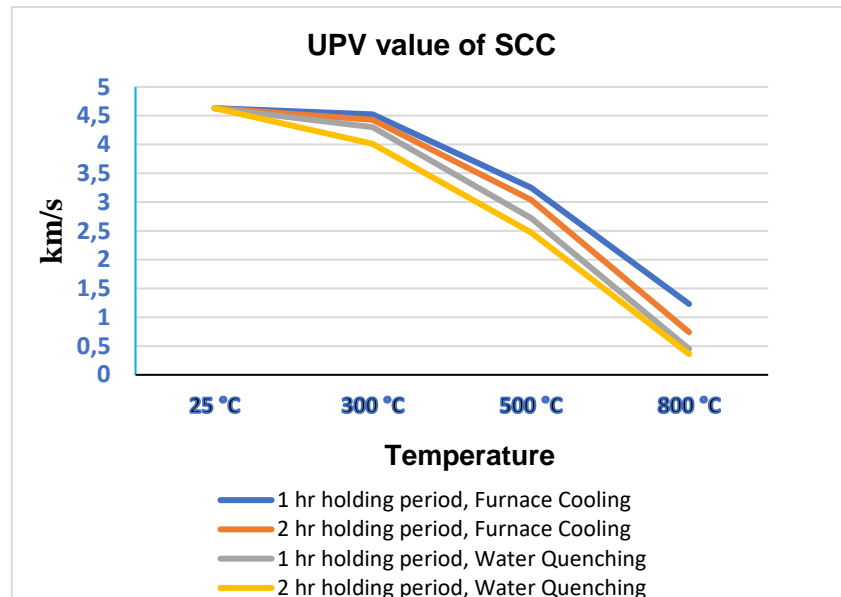


Figure 17 UPV values of SCC

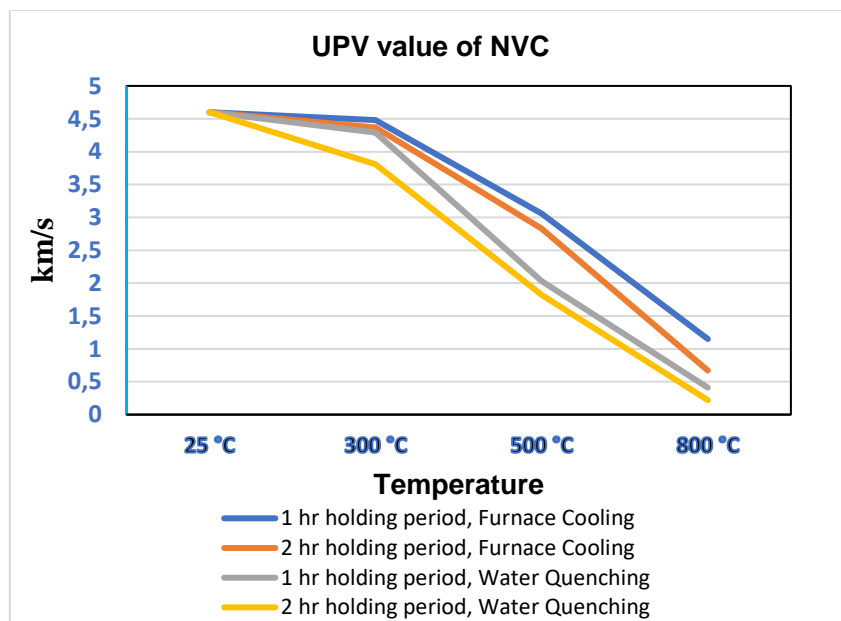


Figure 18 UPV values of NVC

## CONCLUSION

An experimental study was conducted to investigate the durability and mechanical properties of SCC and NVC exposure to elevated temperatures. Based on the results and discussions reported herein, we conclude that there is no significant effect of 300°C on the durability properties of both concrete; however, the compressive strength of both concrete was enhanced at this temperature. There is a considerable effect of 500°C, and concrete deteriorates very severely at 800°C. It was observed that there was no significant effect between holding periods at high temperatures. However, it was found that water quenching was more detrimental to high-strength self-compacting and normal vibrated concrete than normal cooling. Furthermore, no spalling was observed in any specimens after high-temperature exposure. The study also investigated that there was no noticeable effect between holding periods at high temperatures. However, it was observed that water quenching was more detrimental to high-strength self-compacting and normal vibrated concrete than normal cooling.

## REFERENCES

1. V.M. Roitman, Consideration of real fire conditions while calculating the fire resistance of building structures on the basis of the kinetic approach, *Fire Saf. J.* 16 (6) (1990) 433–442.
2. F. Wald, J. Chlouba, A. Uhlíř, P. Kallerova, M. Štujberová, Temperatures during fire tests on structure and its prediction according to Eurocodes, *Fir Saf. J.* 44 (1) (2009) 135–146.
3. Vasusmitha, R., and Rao D. P. S., 2012. Effect of Elevated Temperature on Mechanical Properties of High Strength Self Compacting Concrete, *International Journal of Engineering Research & Technology*, 1(8).
4. K. Mehmet, D. Murat, B. Ahmet, M. Mehzijd. High temperature effect on the mechanical behavior of steel fiber reinforced self-compacting concrete containing ground pumice powder. *fib Wiley, structural concrete*, 2019;20:1734-1749.
5. S. Ali, H. G. Saeed, T. Behzad. Residual strength and microstructure of fiber reinforced self-compacting concrete exposed to high temperatures. *Construction and Building Materials* 230 (2020) 116969.
6. P. Snahashish, H. R. Muhammad, A. R. Md. Effect of elevated temperature on residual strength of self compacted concrete. *Journal of Engineering Science* 11(2), 2020, 107-115.
7. Mathew, G., and Paul M. M., 2012. Mix design methodology for laterized self-compacting concrete and its behaviour at elevated temperature, *Construction and Building Materials*, 36, 104–109.
8. Okamura, H., and Ouchi M., 2003. Self-Compacting Concrete, *Journal of Advanced Concrete Technology*, 1(1), 5–15.
9. Bartos, P. J. M., and Grauers M., 1999. Self-compacting concrete, *Concrete*, 33(4), 9–13.
10. ASTM C1585-20, Standard Test Method for Measurement of Rate of Absorption of Water by Hydraulic-Cement Concretes, ASTM International, West Conshohocken, PA, 2020.
11. Torrent, R.J. (1992), A Two-Chamber Vacuum Cell for Measuring the Coefficient of Permeability to Air of the Concrete Cover on Site. *Materials and Structures*. Vol. 25, pp. 358–365.



12. Li Q. , Li. Z., Yuan G., Effects of elevated temperatures on properties of concrete containing ground granulated blast furnace slag as cementitious material. *Construction and Building Materials* 35 (2012) 687–692.
13. G.-F. Peng, S.-H. Bian, Z.-Q. Guo, J. Zhao, X.-L. Peng, Y.-C. Jiang, Effect of thermal shock due to rapid cooling on residual mechanical properties of fiber concrete exposed to high temperatures, *Constr. Build. Mater.* 22 (2008) 948–955, <http://dx.doi.org/10.1016/j.conbuildmat.2006.12.002>.

# Performance of limestone calcined clay cement (LC<sup>3</sup>) at high temperatures

Akshay Sharma<sup>1\*</sup>, Danie Roy A.B.<sup>2</sup>, & Prem Pal Bansal<sup>3</sup>  
<sup>1,2,3</sup> Thapar Institute of Engineering and Technology  
Patiala Punjab

\* Corresponding author (asharma\_phd19@thapar.edu,  
Research Scholar, Civil Engineering Department,  
Thapar Institute of Engineering & Technology, Patiala,  
Punjab. 147004, +91-8894298478)

## ABSTRACT

Concrete has become the most widely used indispensable material for the construction industry. However, due to its excessive use, much CO<sub>2</sub> is released during the manufacturing of the concrete and its constituent materials. Limestone Calcined Clay Cement (LC<sup>3</sup>) has emerged as one of the alternative binding materials for concrete. It is produced by blending its components into a homogenous blend. The sources of clay and limestone are available worldwide, and LC<sup>3</sup> is a feasible cheaper option for producing sustainable concrete. In LC<sup>3</sup>, around 50% of cement clinkers are replaced by additional cementitious materials like calcined clay, limestone, fly ash. In the present study, LC<sup>3</sup> was used as a replacement for normal OPC 53 cement. After heating the concrete samples at different temperature regimes, specimens were cooled and tested. The results of the mechanical properties testing show that quality and strength reduce with increased exposed temperature. When the temperature reached 400°C, noticeable cracks and colour changes appeared on the specimen surface.

**KEYWORD:** Heat, LC<sup>3</sup>, Concrete, High Temperature

## INTRODUCTION

Contributing to more than 5% of the globally produced CO<sub>2</sub>, Portland cement and its different types have raised a new concern for the construction industry to choose a more sustainable way to use energy and natural resources optimally and take care of carbon emissions to the environment [1]. This has led to the use of supplementary cementitious materials (SCMs) as a partial substitution of cement in the concrete mix, providing us with a new alternative of limestone calcined clay cement (LC<sup>3</sup>)[2,3]. LC<sup>3</sup> is a new type of low carbon binder that can reduce carbon dioxide emissions, proven to be a resource saver, cost-effective and equal in performance to that of Ordinary Portland Cement (OPC)[4]. In LC<sup>3</sup>, around 50-60% of the clinkers are replaced by SCMs (calcined clay, limestone, fly ash, gypsum), which are in abundance compared to Portland cement's normal constituents [5,6].

Numerous studies have been carried out to study the different properties of LC<sup>3</sup> based concrete. Dhandapani et al. [4,7] studied the mechanical and durability performance of concrete made with LC<sup>3</sup>. They found that apart from giving the same strength as that of concrete made by OPC, LC<sup>3</sup> provides better chloride ingress, gas permeability and capillary water absorption and comparable performance to FA30. Zhang et al. [1] used LC<sup>3</sup> based

engineered cementitious composites (ECC) to substitute OPC in ECC and reported that LC<sup>3</sup> based ECC had high early strength development but lower 28-day strength. They also found that LC<sup>3</sup> lead to reductions in CO<sub>2</sub> emissions. Besides improving the mechanical and durability properties, LC<sup>3</sup> contributes to microstructure improvement. Also, Shah et al., Yang et al. [8,9], reported that LC<sup>3</sup> has a better initial setting time and higher pore tortuosity. However, the performance of LC<sup>3</sup> paste under various temperature ranges of 10°C, 20°C, 40°C and 60°C was investigated by Avet et al. [10]; they found that though there is a significant difference in calcium, silica and aluminium content between LC<sup>3</sup> and OPC pastes, both are having the same progression of the water content.

Though concrete still has a vast area of applications, concrete performance is affected when exposed to extreme environments such as elevated temperatures and corrosive environments. Fire accidents in concrete structures lead to an elevation in temperature. Temperature can reach up to 1000°C (and above), causing deterring effects such as loss in strength [11][12], colour change [13], spalling of concrete [14], and changes at the microstructural level, dehydration and decomposition of bonds affecting the durability aspects. As a result, testing every new type of concrete for elevated temperatures is necessary.

This study aims to determine the performance of concrete when LC<sup>3</sup> partially replaces ordinary portland cement at various levels of percentages (10%, 20%, 30%), and samples are subjected to a temperature regime of normal room temperature 200°C, 400°C, 600°C, 800°C.

## EXPERIMENTAL PLAN

### Materials

Four concrete mixes with 18 (100mm x100mm x 100mm) cube samples were prepared using two types of cement: ordinary Portland cement (OPC)- 53 grade conforming to IS 269:2015[15], and limestone calcined clay cement (LC<sup>3</sup>) having physical properties as shown in Table 1. The coarse and fine aggregates were also locally procured, conforming IS 383: 2016 [16]. The coarse aggregates used had a nominal size of 10mm, and fine aggregates confirmed to Zone-II as prescribed in Table 9, IS 383:2016 [16]. While preparing the mix, potable water and super-plasticizer (polycarboxylic ether based, used at 1.2% of the binder) were used; the mix proportions for the concrete mix are shown in Table 2.

Table 1 Physical Properties of Cement used in the mix

S.No.	Property	OPC-53	LC <sup>3</sup>
1.	Specific Gravity	3.17	3.15
2.	Initial Setting Time	46 min.	38 min.
3.	Final Setting Time	365 min.	380 min.
4.	28-Day Cement Mortar Cube Strength	46MPa	43.64 MPa

Table 2 Mix Proportions used for preparing the mix

Designation	OPC-53 (kg/m <sup>3</sup> )	LC <sup>3</sup> (kg/m <sup>3</sup> )	Coarse Aggregates (kg/m <sup>3</sup> )	Fine Aggregates (kg/m <sup>3</sup> )	Water (kg/m <sup>3</sup> )	Super plasticizer
S1	544.73	-	913.24	909.50	163.42	1.2%
S2 (10% Replacement)	490.26	54.13				
S3 (20% Replacement)	435.78	108.26				
S4 (30% Replacement)	381.31	163.42				

### Test Procedures

After mixing of concrete, a slump cone test was performed to find the workability of the prepared mix. It was observed that for S1 mix, the slump was more than the mix with partial replacement of OPC with LC<sup>3</sup>. The results of slump cone test are shown in Figure 1[17].

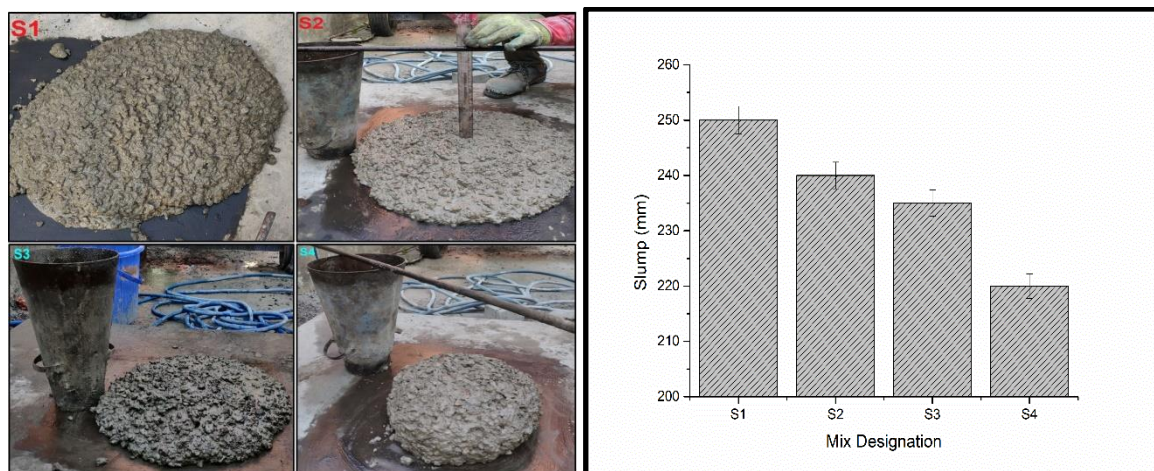


Figure 1 Slump cone test values for the mix.

Following casting, specimens were cured for 28 days in a temperature-controlled curing tank at a temperature of  $27 \pm 1^\circ\text{C}$ . The curing water was changed at an interval of every seven days. At 28 days of curing completion, three specimens of each mix were tested for 28-day strength; the rest, fifteen samples, were stored in the lab for rest 56 days. The specimens were weighed after completing the dormant period at 84-87 days. Samples were then kept at  $100^\circ\text{C}$  for 24 hours to pre-heat the samples and remove the surface evaporable water. For elevated temperature testing, samples were kept in a high temperature muffle furnace, operated at a range of  $200^\circ\text{C}$ ,  $400^\circ\text{C}$ ,  $600^\circ\text{C}$ , and  $800^\circ\text{C}$ , for a fixed period of 3-hour achieved at a heating rate of  $10^\circ\text{C}/\text{minute}$ . Then the samples were allowed to cool under atmospheric air. Again the samples were weighed for calculating the mass loss, rebound hammer Non Destructive Test (conforming to IS 13311-2:1992 [18]) was performed, and actual residual compressive strength was found by compressive testing (IS 516:1959 [19]) using an automatic compression testing machine of 3000kN capacity.

## Results & Discussion

### Color Change

The impact of elevated temperature on the colour change of the control and partially replaced mix is presented in Figure 2. For control mix S1, the significant colour change started to take place at 400°C, while for the other blends with partial replacement of OPC with LC<sup>3</sup>, a different trend was observed. The difference in the texture and composition of concrete and the resultant crystal destruction during the heating and cooling of concrete samples lead to a change in concrete color at higher temperatures [20]. For the S2 mix, the colour change occurred at 400°C, but this temperature range had minimal impact on S3 and S4. S3 and S4 had significant colour changes at 600°C. Up to 200°C normal greyish colour was observed. At 400°C, the colour changed from greyish to pink; at 600°C-800°C, the colour changed to whitish-grey[13,21].

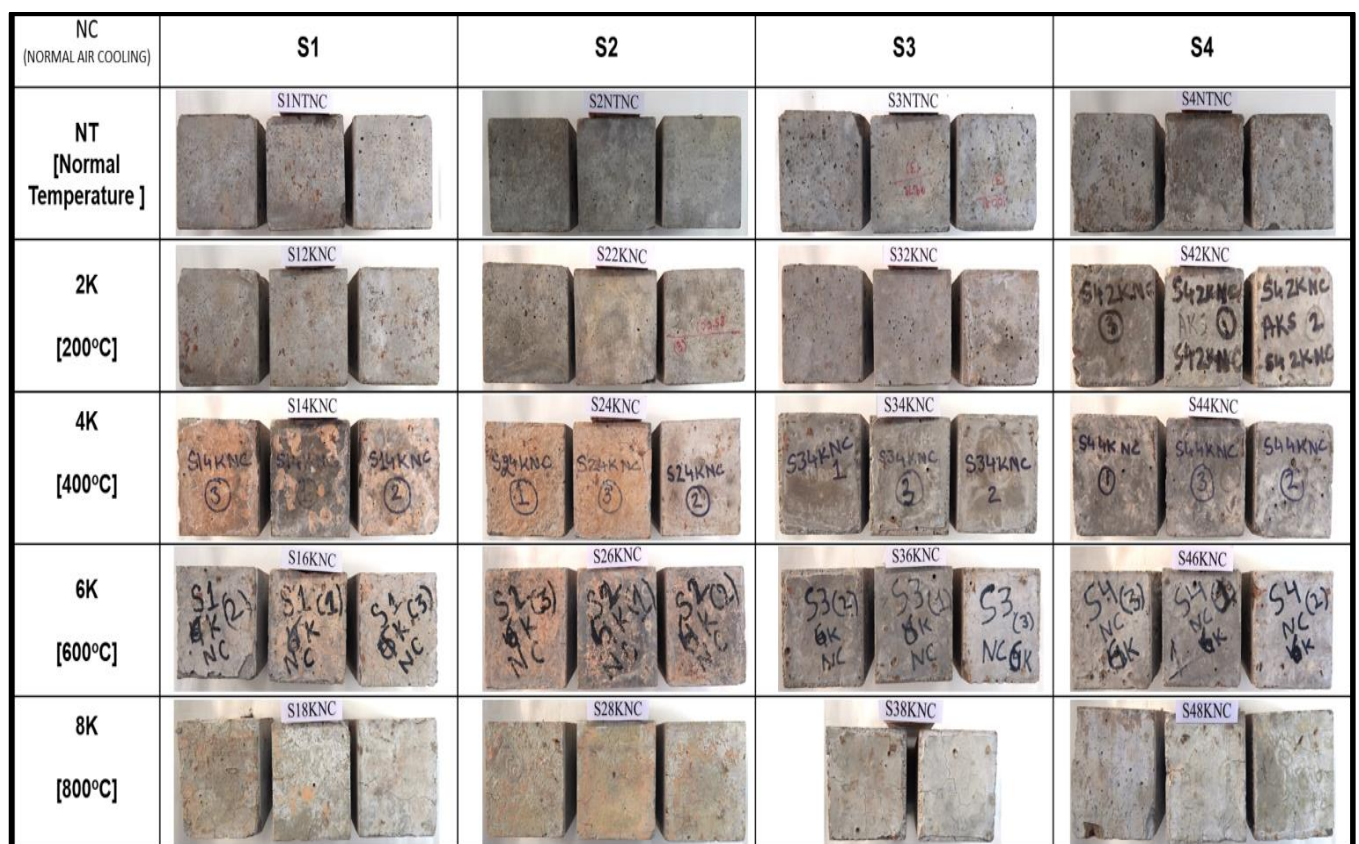


Figure 2 Color change in concrete

### Cracking & Spalling

In this study, thermal cracks were observed on the surface of the specimens, as shown in Figure 2. Visible thin hairline cracks started to appear at 400°C. Under elevated temperatures, concrete loses its strength due to the pore expansion caused by the high pressure of vaporization of the absorbed water, which may lead to explosive spalling. Corner spalling and visible dominant cracks appeared at 600°C, and honeycomb structure-like cracks appeared when the samples were subjected to 800°C. Explosive spalling occurred when the S3 mix samples were tested, and one of the specimens exploded inside the muffle furnace chamber. In the cooling stage, the ionized CaO formed by the decomposition of Ca(OH)<sub>2</sub> absorbs water



and becomes  $\text{Ca}(\text{OH})_2$  again, which results in the expansion of the concrete volume. The damage accumulated during the cooling process further reduces the residual strength, leading to further expansion of any cracks daily [20,22,23].

### Mass Loss

Figure 3 gives the average percentage mass loss of the specimens monitored before and after exposure to elevated temperature ranges. The mass loss percentage increases as the temperature increases. In the control mix S1, the mass loss was the highest for every temperature range (4.71% at 200°C, 5.09% at 400°C, 6.22% at 600°C and 7.49% at 800°C). While S3 and S4 mix had less mass loss at 600°C and 800°C, S2 follows the same trend as S1, but on the lower side, the loss of mass in this domain may correspond to the departure of free water contained in the capillary pores. When the temperature rises from 200 to 400°C, a significant increase in mass loss corresponding to the 4.93%-4.71% range of the initial mass can be observed for all mixes. Mass loss in this range is due to the release of both capillary and gel water. At higher temperatures, the mass loss could result from decomposition of aggregates, the release of  $\text{CO}_2$  and the sloughing off of the concrete surface [24]. At 800°C, a mass loss corresponding to 7.49%-8.32% of the initial mass was observed.

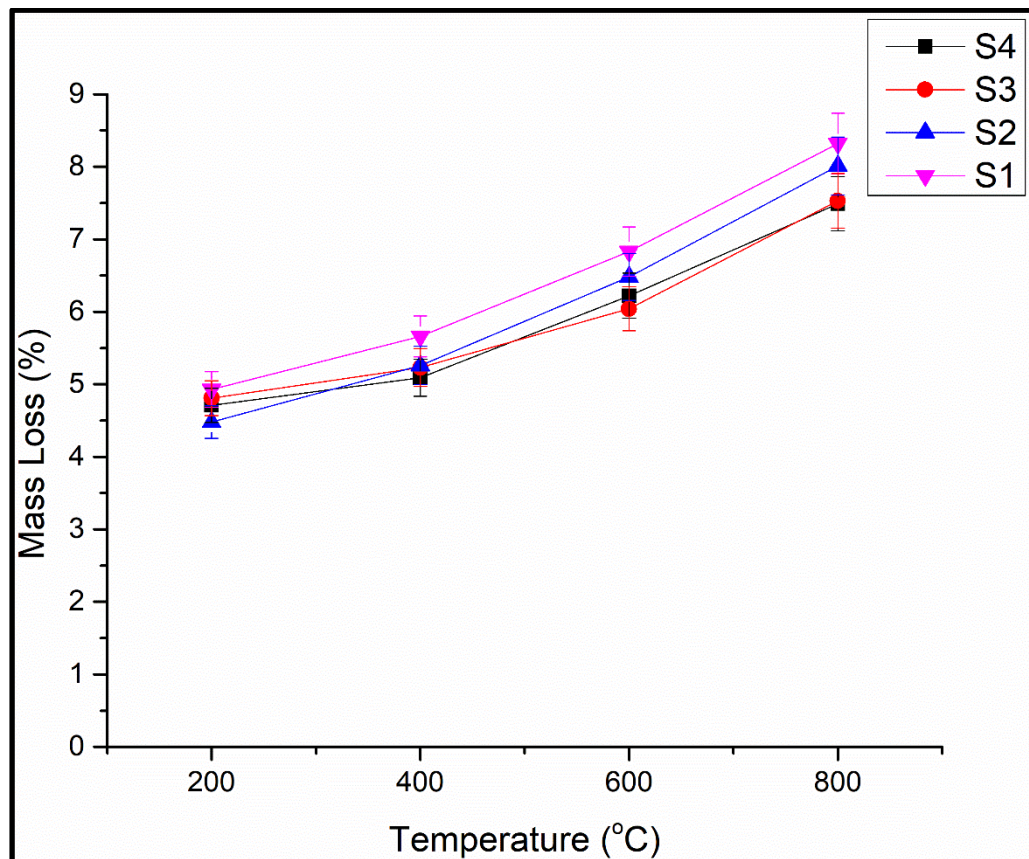


Figure 3 Percentage Mass loss of the various mixes when subjected to elevated temperatures.

## Residual Compressive Strength

### Non-Destructive Testing (Rebound Hammer Test)

On the completion of the heating process, a rebound hammer test was performed on the concrete specimens to estimate their compressive strength. Rebound hammer measures surface hardness, measured on a graduated scale in terms of rebound number, which then indicates the probable strength of the specimen corresponding to the chart between rebound number (R) and strength of concrete ( $\text{N/mm}^2$ ). Figure 4 shows the average residual strength of concrete mixes. It can be observed that under normal room temperature conditions, S3 ( $59.37 \text{ N/mm}^2$ ) and S2 ( $57.85 \text{ N/mm}^2$ ) had higher strength than S4 ( $51.82 \text{ N/mm}^2$ ) and S1 ( $51.12 \text{ N/mm}^2$ ). As the temperature increased, the surface hardness decreased, leading to a decrement in the residual compressive strength. At  $200^\circ\text{C}$ , S1, S3 and S2 ( $46.57 \text{ N/mm}^2$ ,  $46.22 \text{ N/mm}^2$  &  $46 \text{ N/mm}^2$ ) had less surface hardness than S4 ( $48.85 \text{ N/mm}^2$ ), while at  $400^\circ\text{C}$ , all the mixes performed equally well in the range of  $43.15 \text{ N/mm}^2 - 45.88 \text{ N/mm}^2$ . Under  $600^\circ\text{C}$ , a significant drop in residual strength can be observed where S2 ( $37.8 \text{ N/mm}^2$ ) leads the other three mixes (S1- $34.98 \text{ N/mm}^2$ , S3- $35.92 \text{ N/mm}^2$ , S4- $32.82 \text{ N/mm}^2$ ). But at the highest degree of exposure,  $800^\circ\text{C}$ , S2 ( $32.7 \text{ N/mm}^2$ ) and S3 ( $31.67 \text{ N/mm}^2$ ) had retained their surface hardness resulting in higher strength than S1 ( $30.5 \text{ N/mm}^2$ ) and S4 ( $30.5 \text{ N/mm}^2$ ) [25,26].

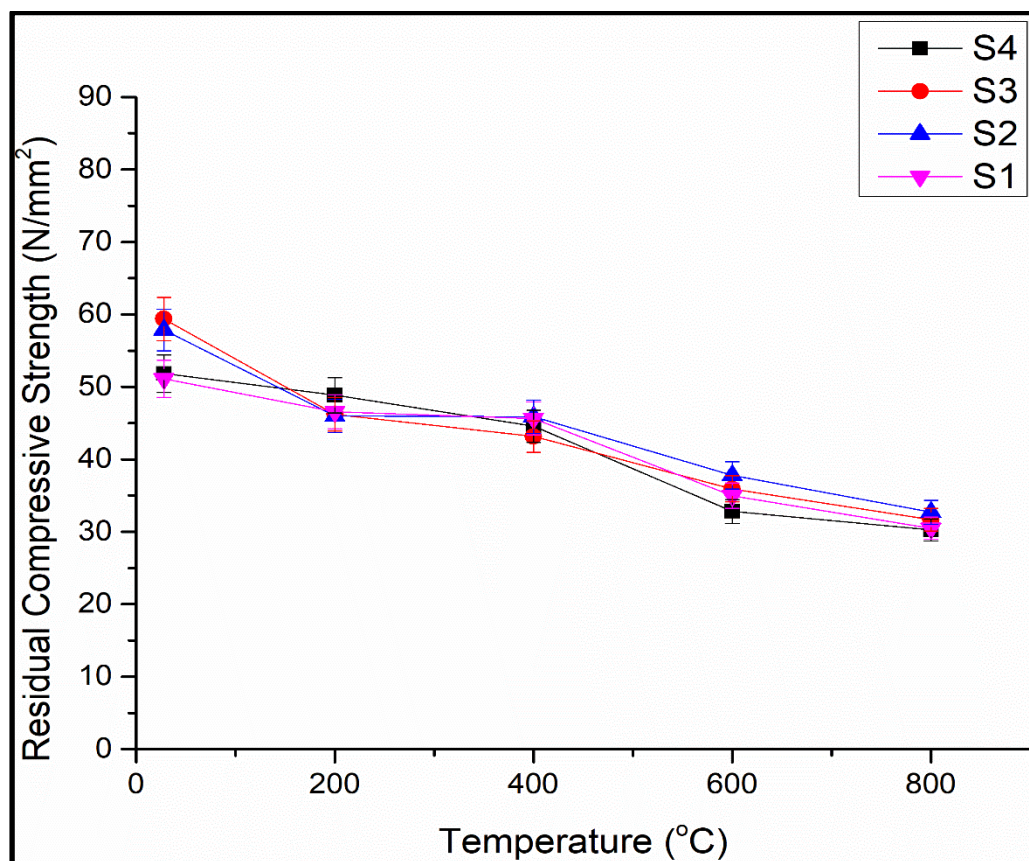


Figure 4 Residual compressive strength as measured from rebound hammer test.



## Compression Test

After the specimens were completely cooled down, compression testing on the specimen was performed as per IS 516:1959 and results, as shown in figure 5, were obtained. In ambient conditions, S3 (76.39 N/mm<sup>2</sup>) had the highest strength as compared to S1 (72.98 N/mm<sup>2</sup>), S3 (73.10 N/mm<sup>2</sup>) and S4 (67.64 N/mm<sup>2</sup>). On the contrary, to the result found during rebound hammer testing, the strength at 200°C was increased. The increase in strength may be because of the complete removal of water (moisture) from the interlayer of cement gel, which increases the bonding forces between the hydration products and the compressive strength. In figure 5, the critical change can be observed for S4 (79.3 N/mm<sup>2</sup>) and S3 (78.25 N/mm<sup>2</sup>), while minimal increment was there for S2 (75.97 N/mm<sup>2</sup>) and S1 (73.28 N/mm<sup>2</sup>) at 200°C [24]. At 400°C, S3 (80.63 N/mm<sup>2</sup>) and S4 (78.92 N/mm<sup>2</sup>) again showed an increase in strength as compared to S2 (73.37 N/mm<sup>2</sup>) and S1 (72.15 N/mm<sup>2</sup>), which had decrement patterns. The increase in compressive strength can be explained by the increased LC<sup>3</sup> content in S3 and S4. As LC<sup>3</sup> has a finer size than OPC-53, the water, which would have been used in the hydration of concrete, is not able to escape rapidly, thus leading to an increase in strength for S3 & S4, while for S1 & S2, water escaped, therefore, gain in strength is inhibited. At 600°C, all the mixes specimens found a decrement in strength (66.55 N/mm<sup>2</sup>, 65.36N/mm<sup>2</sup>, 63.75 N/mm<sup>2</sup>, 63.74 N/mm<sup>2</sup>). After final 800°C, S4 reached the bottom to 42.90 N/mm<sup>2</sup>, while S3 (48.43 N/mm<sup>2</sup>) & S2 47.4(N/mm<sup>2</sup>) outperformed S1 (45.77N/mm<sup>2</sup>). Thus, the internal pressure increases at high temperatures, damaging the internal structure. The extent of damage determines the micro-cracking inside the concrete structure leading to a decrease in strength and, ultimately, may lead to explosive spalling of concrete[27][28].

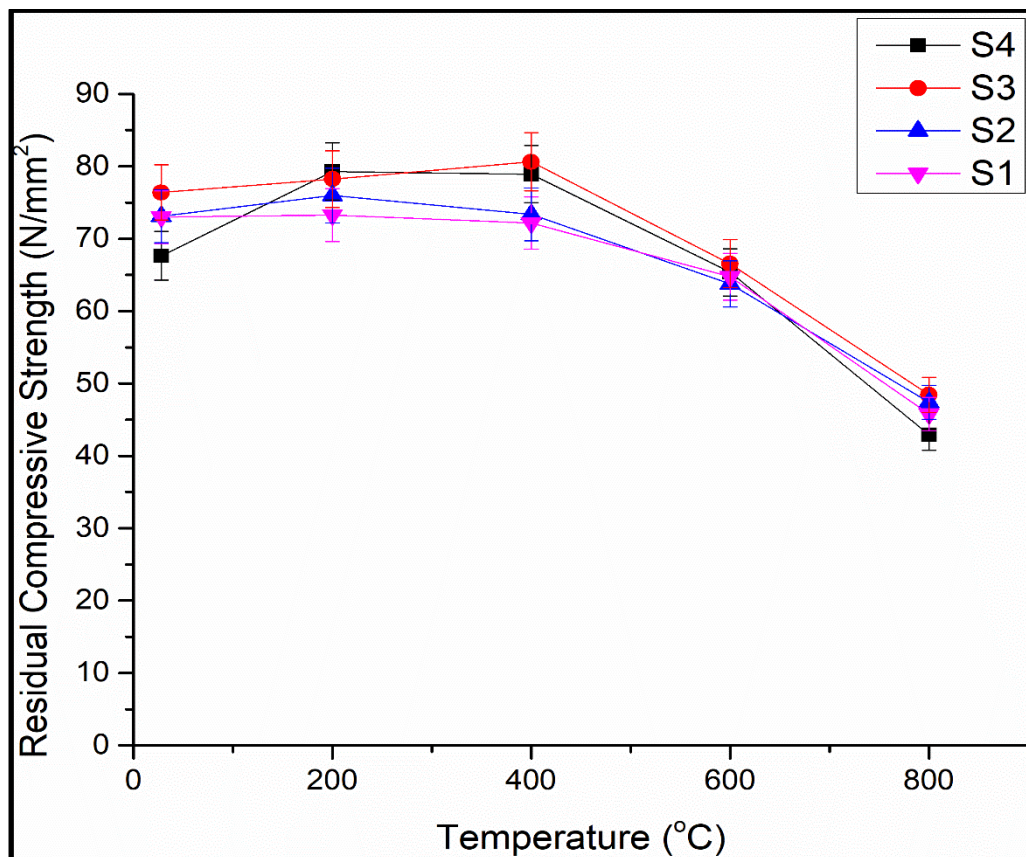


Figure 5 Residual compressive strength of the specimens after compression testing.

## Conclusion

This study presented the performance of limestone calcined clay cement (LC<sup>3</sup>) as a partial replacement of ordinary portland cement measured under high temperature. The following conclusions can be drawn from the results:

- (a) The residual compressive strength generally decreases with an increase in temperature, but depending upon the level of replacement by LC<sup>3</sup> (10%, 20%, 30%), the performance may vary at different temperatures (say 200°C-400°C-600°C-800°C).
- (b) The residual compressive strength found by non-destructive testing was less in magnitude than the ultimate compressive strength of the specimens, but both NDT and destructive testing followed an almost similar decrement trend.
- (c) For a constant water-cement ratio, the workability of the concrete mix decreases as the content of LC<sup>3</sup> increases. This is because LC<sup>3</sup> is finer cement than OPC, which means it has more reactivity and requires more water.
- (d) The percentage mass loss (4%-8%) increases with an increase in the temperature, LC<sup>3</sup> mixes have less mass loss at higher temperatures when compared to the OPC control mix.
- (e) At normal temperature, the compressive strength of the control mix is comparable to the mix with 10% LC<sup>3</sup>, the mix with 20% LC<sup>3</sup> performed better as compared to other mixes.
- (f) Explosive spalling was observed for the mix with 20% LC<sup>3</sup> at a heating temperature of 800°C.
- (g) 30% LC<sup>3</sup> mix has less percentage mass loss and performs well in the temperature range of 200°C-600°C, but has less residual compressive strength at 800°C.

## REFERENCES

1. D. Zhang, B. Jaworska, H. Zhu, K. Dahlquist, V.C. Li, Engineered Cementitious Composites (ECC) with limestone calcined clay cement (LC3), *Cem. Concr. Compos.* 114 (2020) 103766. <https://doi.org/10.1016/j.cemconcomp.2020.103766>.
2. R.S. Lin, Y. Han, X.Y. Wang, Macro-meso-micro experimental studies of calcined clay limestone cement (LC3) paste subjected to elevated temperature, *Cem. Concr. Compos.* 116 (2021) 103871. <https://doi.org/10.1016/j.cemconcomp.2020.103871>.
3. C. Baiano, E. Schiavo, C. Gerbaldi, F. Bella, G. Meligrana, G. Talarico, P. Maddalena, M. Pavone, A.B. Muñoz-García, Role of surface defects in CO<sub>2</sub> adsorption and activation on CuFeO<sub>2</sub> delafossite oxide, *Mol. Catal.* 496 (2020). <https://doi.org/10.1016/j.mcat.2020.111181>.
4. Y. Dhandapani, T. Sakthivel, M. Santhanam, R. Gettu, R.G. Pillai, Mechanical properties and durability performance of concretes with Limestone Calcined Clay Cement (LC3), *Cem. Concr. Res.* 107 (2018) 136–151. <https://doi.org/10.1016/j.cemconres.2018.02.005>.
5. S. Bishnoi, S. Maity, A. Mallik, S. Joseph, S. Krishnan, Pilot scale manufacture of limestone calcined clay cement : The Indian experience, *Indian Concr. J.* 88 (2014) 22–28.
6. A.C. Emmanuel, P. Haldar, S. Maity, S. Bishnoi, Second pilot production of limestone calcined clay cement in India: The experience, *Indian Concr. J.* 90 (2016) 57–63.
7. B. V. Vaasudevaa, Y. Dhandapani, M. Santhanam, Performance evaluation of limestone-calcined clay (LC2) combination as a cement substitute in concrete systems

- subjected to short-term heat curing, *Constr. Build. Mater.* 302 (2021) 124121. <https://doi.org/10.1016/j.conbuildmat.2021.124121>.
8. V. Shah, A. Parashar, G. Mishra, S. Medepalli, S. Krishnan, S. Bishnoi, Influence of cement replacement by limestone calcined clay pozzolan on the engineering properties of mortar and concrete, *Adv. Cem. Res.* 32 (2020) 101–111. <https://doi.org/10.1680/jadcr.18.00073>.
  9. P. Yang, Y. Dhandapani, M. Santhanam, N. Neithalath, Simulation of chloride diffusion in fly ash and limestone-calcined clay cement (LC3) concretes and the influence of damage on service-life, *Cem. Concr. Res.* 130 (2020) 106010. <https://doi.org/10.1016/j.cemconres.2020.106010>.
  10. F. Avet, K. Scrivener, Influence of pH on the chloride binding capacity of Limestone Calcined Clay Cements (LC3), *Cem. Concr. Res.* 131 (2020) 106031. <https://doi.org/10.1016/j.cemconres.2020.106031>.
  11. Q. Ma, R. Guo, Z. Zhao, Z. Lin, K. He, Mechanical properties of concrete at high temperature-A review, *Constr. Build. Mater.* (2015). <https://doi.org/10.1016/j.conbuildmat.2015.05.131>.
  12. V. Kodur, Properties of concrete at elevated temperatures, *ISRN Civ. Eng.* 2014 (2014). <https://doi.org/10.1155/2014/468510>.
  13. M.H. Osman, N.N. Sarbini, I.S. Ibrahim, C.K. Ma, M. Ismail, M.F. Mohd, A case study on the structural assessment of fire damaged building, *IOP Conf. Ser. Mater. Sci. Eng.* 271 (2017). <https://doi.org/10.1088/1757-899X/271/1/012100>.
  14. B.L. György, É. Lublőy, Fire: Structural and Material Consequences, *Zb. Rad. Građevinskog Fak.* 33 (2017) 37–44. <https://doi.org/10.14415/konferencijagfs2017.003>.
  15. Bureau of Indian Standards, Ordinary Portland Cement —, IS 269 2015 (Reaffirmed 2020). Bureau of (2020) 1–10.
  16. Bureau of Indian Standards, Coarse and Fine Aggregate for Concrete Specification, IS 383 2016. Bureau of (2016) 1–18.
  17. Bureau of Indian Standards, Fresh Concrete- Methods of Sampling , Testing and Analysis, IS 1199 (PART 2) 2018. Bureau of (2018) 1–20.
  18. Bureau of Indian Standards, Non-Destructive Testing of Concrete- Methods of Test Part 2 - Rebound Hammer, IS 13311 (PART 2 ) 1992 Reaffirmed 2018. Bureau of (2018) 1–5.
  19. Bureau of Indian Standards, Methods of Tests for Strength of Concrete., IS 516-1959. Bureau of (2018) 1–30.
  20. A.B.D. Roy, U.K. Sharma, P. Bhargava, Confinement strengthening of heat-damaged reinforced concrete columns, *Mag. Concr. Res.* 68 (2016) 291–304. <https://doi.org/10.1680/macrc.15.00078>.
  21. I. Hager, Colour Change in Heated Concrete, *Fire Technol.* 50 (2014) 945–958. <https://doi.org/10.1007/s10694-012-0320-7>.
  22. A. Roy, U. Sharma, P. Bhargava, Strengthening of heat damaged reinforced concrete short columns, *J. Struct. Fire Eng.* (2014).
  23. N. Yermak, P. Pliya, A.-L. Beaucour, A. Simon, A. Noumowé, Influence of steel and/or polypropylene fibres on the behaviour of concrete at high temperature: Spalling, transfer and mechanical properties, *Constr. Build. Mater.* 132 (2017) 240–250. <https://doi.org/https://doi.org/10.1016/j.conbuildmat.2016.11.120>.
  24. S. Hachemi, Evaluating residual mechanical and physical properties of thermally damaged concrete, in: 2015.
  25. Chirag Ajmera, Dr. Ashok R. Mundhada, Effect of High Temperatures on Concrete/ RCC: A Review, *Int. J. Eng. Res.* V7 (2018) 18–22. <https://doi.org/10.17577/ijertv7is030036>.
  26. R. Wheatley, N. Gibbin, M. De Melo, M. González-Quesada, K. Harwood, Assessment and repair of a fire-damaged pre-stressed concrete bridge, *Forensic Eng. Informing Futur. with Lessons from Past - Proc. 5th Int. Conf. Forensic Eng.* (2013) 115–124. <https://doi.org/10.1680/feng.58224.115>.

27. S.N.R. Shah, F.W. Akashah, P. Shafigh, Performance of High Strength Concrete Subjected to Elevated Temperatures: A Review, *Fire Technol.* 55 (2019) 1571–1597. <https://doi.org/10.1007/s10694-018-0791-2>.
28. D. Cree, M. Green, A. Noumowé, Residual strength of concrete containing recycled materials after exposure to fire: A review, *Constr. Build. Mater.* 45 (2013) 208–223. <https://doi.org/10.1016/j.conbuildmat.2013.04.005>.